

Transformation of phenolic contaminants and dissolved organic matter by manganese oxides

By

Emma Leigh Leverich Trainer

A dissertation submitted in partial fulfillment of
the requirements for the degree of

Doctor of Philosophy

(Environmental Chemistry and Technology Program)

at the

UNIVERSITY OF WISCONSIN-MADISON

2021

Date of final oral examination: 05/13/2021

The dissertation is approved by the following members of the Final Oral Committee:

Christina K. Remucal, Associate Professor, Civil and Environmental Engineering
Matthew Ginder-Vogel, Associate Professor, Civil and Environmental Engineering
Haoran Wei, Assistant Professor, Civil and Environmental Engineering
James P. Hurley, Professor, Civil and Environmental Engineering
Joel A. Pedersen, Professor, Soil Science

Abstract

Transformation of phenolic contaminants and dissolved organic matter by manganese oxides

By

Emma Leigh Leverich Trainer

Doctor of Philosophy - Environmental Chemistry and Technology Program

University of Wisconsin-Madison

Associate Professor Christina K. Remucal
Associate Professor Matthew Ginder-Vogel

Manganese(IV) oxides are ubiquitous, highly redox active minerals formed through natural processes and as byproducts in engineered systems, including drinking water treatment and acid mine drainage remediation. These solids can oxidize inorganic and organic compounds, including phenolic compounds, which impact ecosystems and human health and are an environmental justice concern. The degradation of phenols by manganese oxides occurs through a series of potential rate-limiting steps, including sorption of the organic molecule to the manganese surface and sequential electron transfers. While these potential rate-limiting oxidation mechanisms have been identified, previous research focuses on either transformation within the manganese solid or single compound transformations and product formation. This dissertation is the product of three studies investigating this oxidation mechanism under increasingly complex reaction conditions. In each study, we pair aqueous and solid-phase

characterization techniques to understand what drives reactivity differences across phenols and dissolved organic matter.

Across 29 phenolic compounds ranging from simple model phenols to complex contaminants, we observe both electron transfer- and sorption-limited oxidation mechanisms. Reclaimed oxides collected from drinking water treatment and acid mine drainage remediation systems oxidize all tested phenols and the reaction mechanism and relative oxidation rates are inconsistent between a synthetic manganese oxide (δ -MnO₂) and these reclaimed minerals. The oxidation mechanism depends on the phenol structure as well as the surface area, surface charge, and iron content of manganese oxide materials. Furthermore, quantitative structure activity relationships do not predict the rate or mechanism of phenol oxidation for *ortho*-substituted compounds or complex contaminants, limiting their efficacy at predicting reactivity in this system.

When four phenols are reacted in varying mixtures, the oxidation mechanism with δ -MnO₂ predicts whether oxidation rates are enhanced or inhibited. Electron transfer-limited phenols (i.e., triclosan, bisphenol A, resorcinol) have inhibited pseudo-first-order oxidation rates in mixtures attributed to competitive intermolecular interactions occurring at or near the manganese surface. In contrast, 4,4'-biphenol, a sorption-limited compound, has enhanced oxidation rates in mixtures due to indirect oxidation by phenoxy radical products of electron transfer-limited phenols in solution.

Phenolic moieties in dissolved organic matter (DOM) also react with manganese oxides which uniquely transform DOM from 29 diverse whole waters. Bulk characterizations of these transformations are not all consistent with oxidation reactions, but a subset of waters analyzed by high-resolution mass spectrometry all form molecular formulas attributable to phenol oxidation

by MnO_2 . Most reactive formulas in each sample are lignin- and tannin-like formulas, but the products are diverse, indicating that multiple transformation reactions occur in dissolved organic carbon pools in addition to oxidation of phenolic moieties.

Acknowledgements

While this dissertation is the cumulative product of my own hard work and learning experiences, I would not have progressed this far in my education and my career without the constant support of those around me. Not only have I learned an immense amount about research, academia, and environmental chemistry, but I've also learned important lessons in supportive mentorship, symbiotic collaboration, and unwavering dedication. I once heard a project be described as the business version of "The Circle of Life" from *The Lion King* and I cannot think of a truer metaphor for graduate school than the academic "Circle of Life".

First and foremost, this project would not have been possible without those who came before and paved the way for my success. To my advisors, Matt Ginder-Vogel and Christy Remucal, you have inspired and driven me to produce the best science I can. Thank you for knowing when to push me to learn new techniques or produce better writing, when to trust me as I jump down an analytic rabbit hole, and when to support me during the many hurdles of the past five years. Matt, thank you for always thinking of the big picture, suggesting new instrumental analyses, and championing for the correct grammatical use of however. Christy, thank you for your eye for detail, prioritizing the story of the data, and crazy quick editing. You've both contributed so much to my research and make a great advisory team; I strive to mirror your informative and supportive mentoring styles in my own career.

To my committee members, I appreciate you for taking the time to evaluate my progress along the way and to bring your own expertise to my research. To Greeshma Gadikota, Tim Bertram, and Haoran Wei, thank you for your feedback and perspectives on my research as members of my preliminary or defense committees. Joel Pedersen, thank you for your hard questions and keen eye for detail in organic chemistry. I appreciate you attending each of my

seminars and your reliable constructive criticisms over the years. To Jim Hurley, thank you for being a reader and serving on my defense committee. More importantly, thank you for always listening to the students and continuously improving the EC&T program based on our outspoken feedback.

The academic “Circle of Life” also depends on great colleagues and mutual collaborations. To Chris Worley, Sue Pustina, and James Lazarcik, thank you for keeping the building operational and supporting my research endeavors. James, you were especially helpful in trusting and building my instrumental knowledge and experience. Thank you for always pointing out ways to improve my analyses and knowing I’ll want to understand all the mechanical and analytical details of instrumentation during our trainings. I enjoyed our hours talking science and troubleshooting data in front of the HPLCs, ICPs, fluorimeter, and BET and greatly appreciated your flexibility and student prioritization when everything changed due to COVID-19.

To everyone at WSEL and in the EC&T program, thank you for offering endless advice, support, friendship, and food. I would especially like to thank Beth Tomaszewski, Sarah Balgooyen, Lily Schacht, and AnnaBeth Thomas for the constant discussions of geoscience, research frustrations, and life. You made our many synchrotron trips enjoyable, taught me the power of trail mix and bunny friends snacks, and mentored me in the non-academic aspects of graduate school.

In addition to those who contributed academically to this dissertation, I have to thank my friends and family who kept me sane and got me to this point in my life. You all are my support system and I love each and every one of you for the late night talks, unlimited understanding, and crazy adventures. To Devon Bulman, Sarah Balgooyen, and Stephanie Berg, I’m so glad we

found each other during graduate school. SJB, you started as my mentor and quickly became a friend. Thank you for teaching me all about Mn, putting up with my sleep deprived antics on way too many beam trips, and letting me be the last one to leave every party. Devon, thank you for your deep advice and contagious energy. Steph, thank you for always finishing my beer and making us mojitos or gin and tonics. Thank you for unconsciously keeping the same timeline as me throughout grad school. I'm still amazed that we managed to prelim, submit every paper, and now defend within a few weeks of one another; it has definitely been a blessing to go through these milestones with you. To Gina Falada and Tasman Grout, without you two I would've graduated from Grinnell as a Sociology and Tech. Studies major which would've made this PhD in Environmental Chemistry and Technology much more difficult. I owe so much of my personal development and life choices to you both; thank you for always being there for me whether we're roommates or live across the world, and for understanding me better than I understand myself some days.

To my family, you all are the reason I never gave up on my dream of graduating with a PhD. Mom, you taught me to be independent and confident in myself. Your ability to go to graduate school and write a master's thesis with three young kids proved to me at a young age that I could succeed in my academic and career aspirations if I worked hard enough and dreamed big enough. To the Trainer family, thank you for embracing me as one of your own. Laura, thank you for doing everything possible to let me focus on this thesis as our lives were uprooted during COVID-19. To Evan, Nicole, Sam, and Alec, thank you for pushing me to work harder when I slack off and to take breaks when I work too hard, as only siblings can do.

Finally, to my husband Austin, I will forever be grateful that you followed me unconditionally as I moved for graduate school. Thank you for being my biggest supporter, for

making me dinner and buying me coffee during my all-nighters, for keeping me grounded, for listening while I excitedly rambled about instrumentation or ranted about long days in lab, for always reminding me to back-up my work, and for agreeing to get a cat. I love the life we built together during this time and cannot wait to see what the next chapter brings for us.

In memory of Tasman Grout and Shawn Trainer.

Table of Contents

ABSTRACT.....	I
ACKNOWLEDGEMENTS	IV
LIST OF FIGURES	XI
LIST OF TABLES.....	XVII
LIST OF SYMBOLS AND ABBREVIATIONS	XXI
CHAPTER 1	1
1.1 MOTIVATION.....	1
1.2 MANGANESE OXIDE SOURCES	1
1.3 MANGANESE OXIDE REACTIVITY.....	3
1.4 PHENOLIC CONTAMINANTS	4
1.5 OXIDATION OF PHENOLS BY MANGANESE OXIDES	6
1.6 PHENOL REACTIVITY	8
1.6 DISSOLVED ORGANIC MATTER.....	9
1.7 APPLICATION OF RESEARCH FOR WATER TREATMENT	9
1.8 RESEARCH NEEDS.....	10
1.9 RESEARCH OBJECTIVES	12
1.10 REFERENCES	16
CHAPTER 2.....	27
2.1 COLLABORATION AND PUBLISHING INFORMATION	27
2.2 ABSTRACT.....	28
2.3 INTRODUCTION.....	29
2.4 EXPERIMENTAL	31
2.4.1 <i>Materials</i>	31
2.4.2 <i>Solid characterization</i>	32
2.4.3 <i>Kinetic reactions</i>	32
2.4.4 <i>Kinetic modeling</i>	33
2.4.5 <i>Quantitative structure activity relationships</i>	34
2.5 RESULTS AND DISCUSSION	34
2.5.1 <i>Kinetics and mechanisms of oxidation by δ-MnO₂</i>	34
2.5.2 <i>Phenol degradation by reclaimed manganese oxides</i>	37
2.5.3 <i>QSAR analysis for synthetic and reclaimed Mn oxides</i>	45
2.5.4 <i>Assessment of quantitative structure activity relationships</i>	52
2.6 CONCLUSIONS	54
2.7 ACKNOWLEDGEMENTS.....	57
2.8 SUPPORTING INFORMATION	57
2.9 REFERENCES	58
CHAPTER 3.....	63
3.1 COLLABORATION INFORMATION	63
3.2 ABSTRACT.....	63
3.3 INTRODUCTION.....	64
3.4 MATERIALS AND METHODS	67
3.4.1 <i>Materials</i>	67
3.4.2 <i>δ-MnO₂ synthesis and characterization</i>	67
3.4.3 <i>Kinetic reactions</i>	68

3.5 RESULTS AND DISCUSSION	69
3.5.1 <i>Phenol reactivity</i>	70
3.5.2 <i>Impact of mixtures on electron transfer-limited phenols</i>	74
3.5.3 <i>Impacts of mixtures on a sorption-limited phenol</i>	78
3.6 ENVIRONMENTAL IMPLICATIONS	83
3.7 ACKNOWLEDGEMENTS	85
3.8 SUPPORTING INFORMATION	85
3.9 REFERENCES	86
CHAPTER 4.....	91
4.1 COLLABORATION INFORMATION	91
4.2 ABSTRACT	92
4.3 INTRODUCTIONS	92
4.4 MATERIALS AND METHODS	95
4.4.1 <i>Materials</i>	95
4.4.2 <i>Sampling</i>	95
4.4.3 <i>Reactions</i>	96
4.4.4 <i>Mass spectrometry analysis</i>	97
4.5 RESULTS AND DISCUSSION	98
4.5.1 <i>Bulk DOM and Mn oxide transformation</i>	98
4.5.2 <i>Impact of DOM composition and water chemistry on reactivity</i>	102
4.5.3 <i>Molecular transformations analyzed by FT-ICR MS</i>	104
4.5.4 <i>Oxidation product formulas</i>	107
4.5.5 <i>Molecular reactivity trends</i>	110
4.6 ENVIRONMENTAL IMPLICATIONS	111
4.7 ACKNOWLEDGEMENTS	112
4.8 SUPPORTING INFORMATION	113
4.9 REFERENCES	114
CHAPTER 5.....	120
5.1 SUMMARY OF FINDINGS	120
5.2 DIRECTIONS FOR FUTURE RESEARCH	123
5.3 IMPLICATIONS FOR ENVIRONMENTAL JUSTICE	124
5.3.1 <i>Environmental injustice in the United States</i>	124
5.3.2 <i>Manganese contamination</i>	126
5.3.3 <i>Phenol contamination</i>	127
5.3.4 <i>Implications of this research</i>	129
5.4 REFERENCES	130
APPENDIX A.....	135
A.1. MATERIALS	135
A.2. SOLID CHARACTERIZATION	139
A.3. BUFFER SELECTION AND CONTROLS	142
A.3.1. <i>Sodium acetate buffer</i>	142
A.3.2. <i>Control reactions of solids and phenols</i>	142
A.4. ANALYTICAL METHODS	144
A.4.1. <i>Phenol quantification</i>	144
A.4.2. <i>Observed rate constants</i>	144
A.5. SORPTION VALIDATION	150

A.6. KINETIC MODELING	152
A.7. QUANTITATIVE STRUCTURE ACTIVITY RELATIONSHIP DATA	155
A.8. QSAR RESIDUALS AND VALIDATION	170
A.9. REFERENCES	187
APPENDIX B	190
B.1. MATERIALS	190
B.2. MANGANESE OXIDE COMPOSITION	191
B.3. PHENOL CONCENTRATION QUANTIFICATION	193
B.4. OBSERVED RATE CONSTANTS	194
B.5. SORPTION AND MECHANISM DETERMINATION	195
B.6. EFFECT OF <i>TERT</i> -BUTANOL	197
B.7. REFERENCES	199
APPENDIX C	200
C1. MATERIALS	200
C.2. SAMPLING AND WATER CHEMISTRY	201
<i>C.3.1. Sampling</i>	<i>201</i>
<i>C.2.2 Water chemistry</i>	<i>202</i>
C.3. 50-HOUR KINETIC TRANSFORMATIONS	210
C.4. 28-DAY BULK TRANSFORMATIONS	214
C.5. MASS SPECTROMETRY	220
<i>C.5.1. Sample preparation</i>	<i>220</i>
<i>C.5.2 FT-ICR MS Analysis</i>	<i>220</i>
C.6. LINEAR CORRELATIONS	223
C.7. MOLECULAR TRANSFORMATIONS	228
C.8. REFERENCES	237

List of Figures

Figure 1.1. Layer structure of Mn(III/IV) phyllophanates.....	2
Figure 1.2. General phenol structure, where R indicates a substituent group, and example chlorophenol isomers.....	5
Figure 1.3. Reaction mechanism and rate-limiting steps of phenol oxidation by manganese(III/IV) oxides.....	6
Figure 2.1. Kinetic data and pseudo-first-order rate fittings for (a) triclosan and (b) 4,4'-dihydroxybiphenyl based on quenched and filtered samples.....	34
Figure 2.2. X-ray diffraction patterns of δ -MnO ₂ , drinking water treatment (DWT), and acid mine drainage (AMD) solids.....	38
Figure 2.3. Initial pseudo-first-order log <i>k</i> values for reactions of 15 phenolic compounds with δ -MnO ₂ , drinking water treatment solids, and acid mine drainage remediation solids. Filled points are electron transfer-limited and hollow points are sorption-limited. Error bars indicate the standard deviation of triplicate data.....	40
Figure 2.4. The log of the quenched pseudo-first-order rate constant of 29 target phenolic compounds reacted with δ -MnO ₂ normalized to the rate constant of 4-chlorophenol versus (a) sum of the tabulated Hammett constants, (b) first phenolic pK _a , (c) energy of the highest occupied molecular orbital, and (d) corrected oxidation energy of the first electron transfer. Error bars indicate the standard deviation of triplicate data. Filled data points indicate electron transfer-limited mechanisms and hollow data points indicate sorption-limited reaction mechanism. Regression values are for the simple <i>meta</i> - and <i>para</i> -substituted phenols; regression values for all lines are given in Table B.9 . Experiments were conducted with 10 μ M phenol and 15 mg/L δ -MnO ₂ in 10 mM acetate at pH 5.5.....	46
Figure 2.5. Quantitative structure-activity relationships for 15 phenols reacted with drinking water treatment and acid mine drainage remediation reclaimed solids and 29 phenols reacted with δ -MnO ₂ , all normalized to 15 mg-Mn L ⁻¹ . Plots show the log of the quenched rate constant normalized to the rate constant of 4-chlorophenol versus (a) sum of the tabulated Hammett constants and (b) corrected oxidation energy of the first electron transfer. Error bars indicate standard deviation of triplicate measurements. Filled data points indicate electron transfer-limited mechanisms and hollow data points indicate sorption-limited reaction mechanism. Lines indicate regression fits through each solid. Regression values for all 15 phenols with each manganese oxide are given in Table B.11	47

Figure 2.6. Quantitative structure-activity relationships for literature normalized rate constants of phenols and anilines reacted with synthetic manganese oxides and reactions from this study with δ -MnO₂. The log of the average observed rate constant normalized to the rate constant of 4-chlorophenol or 4-chloroaniline is plotted against (a) sum of Hammett constants and (b) oxidation energy of the first electron transfer. Error bars indicate the standard deviation of triplicate measurements. Filled data points indicate *meta*- or *para*-substitution, partially filled points indicate *ortho*-substitution, and hollow points indicate complex compounds. Given regression values are for the simple *meta*- and *para*-substituted compounds; regression values for all lines are provided in **Table B.10**.....49

Figure 2.7. Average residuals of Hammett constant, pK_a, E_{HOMO}, E_{ox,corr.} (or E_{ox}) based QSAR models developed with either all compounds or only simple *meta*- and *para*-substituted compounds, using data from this study or compiled from literature. Error bars indicate one standard deviation. Residual values for each QSAR model are given in **Table B.15** for this study and **Table B.16** for literature data.....52

Figure 3.1. Pseudo-first-order oxidation rates (a) and maximum percent sorption (b) versus initial concentration of resorcinol, bisphenol A, triclosan, and 4,4'-biphenol reacted with δ -MnO₂ at pH 5.5. Error bars are ± 1 standard deviation of triplicate reactors; the 10% line in plot b indicates the cutoff for sorption-limited (< 10% sorption) or electron transfer-limited (> 10% sorption) oxidation mechanisms.....71

Figure 3.2. (a) Pseudo-first-order oxidation rates and (b) maximum percent sorption of resorcinol, bisphenol A, triclosan, and 4,4'-biphenol reacted with δ -MnO₂ at pH 5.5 in isolation or in mixture solutions with other phenolic contaminants. Error bars are ± 1 standard deviation of triplicate reactors; the 10% line in plot b indicates the cutoff for sorption-limited (< 10% sorption) or electron transfer-limited (> 10% sorption) oxidation mechanisms.....73

Figure 3.3. Plots of (a) pseudo-first-order oxidation rates and (b) maximum percent sorption of 4,4'-biphenol reacted with δ -MnO₂ with 2 mM *tert*-butanol in solution versus without *tert*-butanol. Each point is either an isolated reaction or mixture of 4,4'-biphenol with one or three other phenols in solution. Error bars are ± 1 standard deviation of triplicate reactors.....78

Figure 4.1. Percent changes in (a) [DOC], specific UV absorbance (SUVA₂₅₄), and E₂:E₃; (b) aqueous Mn(II/III) and average manganese oxidation number; and (c) weighted averages of H:C, O:C, DBE, and MW determined using high-resolution mass spectrometry following 50-hour reactions of DOM with acid birnessite (3:4 C:Mn molar ratio, pH 7). Average changes across all waters are included as the final point on each plot. Error bars represent (a) standard deviation of triplicate measurements and (b) standard deviation of triplicate Mn(II/III) measurements and AMON linear combination fitting method error described by Manceau et al.....97

Figure 4.2. van Krevelen diagrams showing changes in St. Louis River (R6; a, b, and c) and Western Lake Superior Sanitary District effluent (WW1; d, e, and f) DOM formulas after 50-hour reactions with acid birnessite. Panels (a) and (d) show matched phenol oxidation and hydrogen abstraction products, panels (b) and (e) are formulas which decrease in intensity during reaction, and panels (c) and (f) show formulas which increase in intensity during reaction. The overlaid boxes indicate (1) protein-like, (2) lignin-like, and (3) tannin-like formulas. van Krevelen diagrams for the other 11 waters are in **Figures C.11 – C.14**.....107

Figure A.1. Scanning electron microscopy images of (a) drinking water treatment solids and (b) acid mine drainage remediation solids.....138

Figure A.2. Percent sorption and loss for (a) triclosan and (b) 4,4'-dihydroxybiphenyl. Error bars indicate standard deviation of triplicate data.....142

Figure A.3. Experimental and modeled concentrations of triclosan versus time. The kinetic model fit for k' and k'' determination is shown.....150

Figure A.4. E_{ox} values versus oxidation potentials reported by Pavitt et al. for phenolic compounds ($n = 15$) calculated using the M06-2x theory. The linear regression shown was used to calculate $E_{ox,corr}$ values.....153

Figure A.5. QSAR plots of normalized pseudo-first-order rate constants from literature and δ -MnO₂ reactions in this study versus (a) pK_a values of the speciated (e.g., phenol versus phenolate) compounds and (b) energy of the highest occupied molecular. Filled data points indicate *meta*- or *para*-substitution, *ortho*-substituted compounds are partially filled, and complex compounds are indicated by hollow points. Error bars indicate the standard deviation of triplicate measurements. Given regression values are for the simple *meta*- and *para*-compounds; regressions values for all lines are given in **Table A.10**.....154

Figure A.6. Quantitative structure-activity relationships for 15 phenols reacted with drinking water treatment and acid mine drainage remediation reclaimed solids and 29 phenols reacted with δ -MnO₂, all normalized to 15 mg-Mn L⁻¹. Plots show the log of the average observed quenched rate constant normalized to the rate constant of 4-chlorophenol versus (a) first phenolic pK_a and (b) energy of the highest occupied molecular orbital. Error bars indicate the standard deviation of triplicate measurements. Filled data points indicate electron transfer-limited mechanisms and hollow data points indicate sorption-limited reaction mechanism. Lines indicate regression fits for all 15 phenols reacted with each manganese oxide; regressions values are given in **Table A.11**.....155

Figure A.7. Percent of initial triclosan concentration (a) sorbed to solid surface and (b) oxidized over the first 10 hours of reaction with δ -MnO₂, DWT solids, and AMD solids. Error bars represent the standard deviation of triplicate measurements.....165

Figure A.8. Comparison of log k for DWT and AMD solids with δ -MnO₂ reacted with 15 phenols. Error bars indicate the standard deviation of triplicate measurements.....166

Figure A.9. Plots of residuals versus independent QSAR descriptors for this study (a through d) and literature data (e through h). Residuals were calculated for QSAR relationships including either the simple (*meta*-, *para*-) or all compounds.....177

Figure A.10. Plots of residuals versus independent QSAR descriptors for drinking water treatment (DWT) and acid mine drainage (AMD) solids. Residuals were calculated for QSAR relationships calculated for both the individual solids and all solids.....178

Figure A.11. Residual normality plots of the calculated residuals versus probability (P) of each residual for QSAR relationships including using only simple *meta*- and *para*-substituted compounds or all compounds. Plots (a) through (d) show data from only this study and plots (e) through (h) show the data for the larger literature data set.....179

Figure A.12. Residual normality plots of the calculated residuals versus probability of each residual for QSAR relationships including using only a single manganese oxide or all solids. Plots (a) through (d) show data for drinking water treatment (DWT) solids and plots (e) through (h) show the data for the acid mine drainage (AMD) solids data.....180

Figure A.13. Residuals of each QSAR for phenols reacted with drinking water treatment solids (DWT) versus the residuals for phenols reacted with acid mine drainage solids (AMD).....181

Figure B.1. X-ray diffraction spectra of synthesized δ -MnO₂ starting material, buffered control reacted for 14 days in 10 mM pH 5.5 sodium acetate, and *tert*-butanol control reacted for 14 days in 2 mM *tert*-butanol and 10 mM pH 5.5 sodium acetate.....189

Figure B.2. Plots of (a) pseudo-first-order oxidation rates and (b) maximum percent sorption of triclosan, bisphenol A, and resorcinol reacted with δ -MnO₂ with 2 mM *tert*-butanol in solution versus without *tert*-butanol. Each point is either an isolated reaction or mixture with one or three other phenols in solution. Error bars are ± 1 standard deviation of triplicate reactors.....195

Figure C.1. Maps of sampling locations, color coded by water type. **Table C.1** lists the full name and coordinates for each sampling site.....201

Figure C.2. Time series plots of bulk changes in (a) DOC, (b) SUVA₂₅₄, (c) E₂:E₃, and (d) AMON. Error bars represent (a-c) standard deviation of triplicate measurements and (d) XANES and linear combination fitting method error as determined by Manceau et al.....210

Figure C.3. Percent changes in (a) DOC, SUVA₂₅₄, and E₂:E₃; and (b) aqueous Mn(II/III) and AMON after 28-day reactions. Error bars represent (a) standard deviation of triplicate measurements and (b) standard deviation of triplicate Mn(II/III) measurements and AMON linear combination fitting method error as determined by Manceau et al.....212

Figure C.4. Percent changes in (a) DOC, SUVA₂₅₄, and E₂:E₃; and (b) aqueous Mn(II/III) and AMON after 28-day reactions. Error bars represent (a) standard deviation of triplicate measurements and (b) standard deviation of triplicate Mn(II/III) measurements and AMON linear combination fitting method error as determined by Manceau et al.....213

Figure C.5. Average manganese oxidation number of particles formed after reactions of MnO₂ in the initial filtrate. AMON values and error are calculated by linear combination fitting.....214

Figure C.6. Net Mn reduction of acid birnessite after 50-hour or 28-day reactions with DOM. Net Mn reduction is calculated as the difference between the starting AMON (3.74) and a mass balance after reaction, using the measured solid AMON and the concentrations and average AMON (2.64) of filtrate Mn(II/III). AMON values and Mn(II/III) concentrations are given in **Figure 3.1** and **Figure C.3**.....215

Figure C.7. Changes in bulk UV-vis measurements versus molecular FT-ICR measurements which represent changes in organic matter (a) aromaticity, H:C_w and DBE_w versus SUVA₂₅₄, and (b) molecular weight, MW_w versus E₂:E₃.....223

Figure C.8. Principal component analysis (PCA) plots of (a) control relative formula intensities and (b) relative formula intensities of both control and treated waters. The variance explained by PC1 and PC2, respectively, is (a) 77.6% and 11.4% and (b) 77.6% and 11.7%.....226

Figure C.9. Linear distances between control and treated waters on PCA plot (**Figure C.8b**). Distances are a proxy for extent of reaction.....226

Figure C.10. H:C versus O:C van Krevelen plots of matched CHO formulas in control waters. Overlaid boxes indicate (1) protein-like, (2) lignin-like, and (3) tannin-like formulas. Sample name is indicated in each panel.....228

Figure C.11. H:C versus O:C van Krevelen plots of oxidation product formulas formed from 50-hour reactions with acid birnessite. Overlaid boxes indicate (1) protein-like, (2) lignin-like, and (3) tannin-like formulas. Sample name is indicated in each panel.....229

Figure C.12. H:C versus O:C van Krevelen plots of formulas present only in the control samples or only in the reacted samples. Overlaid boxes indicate (1) protein-like, (2) lignin-like, and (3) tannin-like formulas. Sample name is indicated in each panel.....230

Figure C.13. H:C versus O:C van Krevelen plots of formulas matched in both control and treated samples which decrease in intensity after reacting 50 hours with acid birnessite. Overlaid boxes indicate (1) protein-like, (2) lignin-like, and (3) tannin-like formulas. Sample name is indicated in each panel.....231

Figure C.14. H:C versus O:C van Krevelen plots of formulas matched in both control and treated samples which increase in intensity after reacting 50 hours with acid birnessite. Overlaid boxes indicate (1) protein-like, (2) lignin-like, and (3) tannin-like formulas. Sample name is indicated in each panel.....232

List of Tables

Table 2.1. Solid phase characteristics of δ -MnO ₂ , DWT, and AMD solids.....	39
Table 3.1. Chemical structure, contaminant class, and rate-limiting step of oxidation by δ -MnO ₂ of each phenolic contaminant.....	68
Table 4.1. Schematic of tested phenol oxidation pathways and expected molecular changes for each reaction.....	105
Table A.1. Sources and purity of phenols.....	134
Table A.2. Structures of phenols shown at pH 5.5. Gray cells are simple (i.e., <i>meta</i> - and <i>para</i> -substituted phenols), red cells are <i>ortho</i> -substituted phenols, and blue cells are complex phenols.....	135
Table A.3. Percent elemental composition (wt:wt) of metals and cations analyzed by ICP-OES for bulk solids extracted in 6 M HCl. N.D. indicates the element was below detection limits.....	138
Table A.4. Average manganese oxidation number determined by XANES for manganese oxide starting materials and following 10-day equilibration in 10 mM pH 5.5 sodium acetate buffer without any organic reductants.....	140
Table A.5. HPLC parameters for parent compound detection. The aqueous mobile phase was 10% v:v acetonitrile, 0.1% v:v formic acid at pH 2.5.....	143
Table A.6. Quenched and filtered pseudo-first-order rate constants for 29 phenolic compounds reacted with δ -MnO ₂ and 15 phenols reacted with AMD and DWT reclaimed solids. The time for which the initial pseudo-first-order rate constants were determined and the observed rate-limiting step (RLS) for each reaction are included.....	144
Table A.7. Modeled k' and k'' , respective R ² values, and pseudo-first-order $k''*C_0$ values for 29 phenols reacted with δ -MnO ₂	151
Table A.8. Calculated phenol descriptor data including QSAR Hammett constants (σ) predicted pK _a values, E _{HOMO} , and E _{ox,corr.} , as well as the pK _a corrected distribution ratio for the compound in octanol versus water (log D _{ow}), and partitioning coefficients for soil organic carbon to water (log K _{oc}) and octanol to water (log K _{ow}).....	156
Table A.9. Regression statistics for QSAR descriptors versus normalized observed initial rate constants of 29 phenols reacted with δ -MnO ₂ (Figure 2.4) calculated for 95% confidence interval. Gray values indicate p < 0.005; bold values are p < 0.05.....	157

Table A.10. Regression statistics for QSAR descriptors versus normalized literature rate constants and reactions of 29 phenols with δ -MnO ₂ (Figure 2.6 ; Figure A.5) calculated for 95% confidence interval. Literature data available in Table A.12 . Gray values indicate $p < 0.005$; bold values are $p < 0.05$	158
Table A.11. Regression statistics for QSAR descriptors versus normalized observed initial rate constants of 15 phenols reacted with δ -MnO ₂ , drinking water treatment solids, and acid mine drainage remediation solids (Figure 2.5 ; Figure A.6) calculated for 95% confidence interval. Gray values indicate $p < 0.005$; bold values are $p < 0.05$	159
Table A.12. Literature data sources and reported reaction conditions.....	160
Table A.13. Literature QSAR descriptors. Log (k/k_{4-Cl}) values calculated based on reported loss rates (Table A.12). Hammett constants, pK _a values, E _{HOMO} and E _{ox} values determined in this study.....	163
Table A.14. Observed oxidation rate-limiting step for phenols reacted with δ -MnO ₂ , DWT, and AMD solids.....	166
Table A.15. Residual values calculated against the <i>meta</i> - and <i>para</i> -substituted and all compound QSARs developed with data from this study. QSAR linear regressions provided in Table A.9	172
Table A.16. Residual values calculated against the <i>meta</i> - and <i>para</i> -substituted and all compound QSARs developed with data from this study and compiled from literature. QSAR linear regressions provided in Table A.10	173
Table A.17. Residual values calculated against the individual solid and all three solids QSARs, developed with data from this study. QSAR linear regressions provided in Table A.11	176
Table A.18. QSAR validation based on structural substitutions using data from this study (with δ -MnO ₂) and literature. Gray values fall within the accepted ranges for that measure.....	182
Table A.19. QSAR validation measures using data from this study with three manganese oxides (i.e., δ -MnO ₂ and two reclaimed solids). Gray values fall within the accepted ranges for that measure.....	183
Table B.1. Average manganese oxidation number (AMON) and Brauner-Emmett-Teller N ₂ surface area of Mn reacted in sodium acetate buffered control solutions with and without varying concentrations of <i>tert</i> -butanol in solution. Reported error is the standard deviation of replicate measurements.....	189

Table B.2. HPLC Parameters for compound detection for individual phenols and mixtures. The aqueous mobile phase A was 10% acetonitrile, and 0.1% formic acid at pH 2.5. Acetonitrile was the organic mobile phase.....190

Table B.3. Average pseudo-first-order rate constants (hr^{-1}) for each phenol at initial concentrations of 10, 20 and 40 μM with no competing phenolic compounds in solution. Rate constants are the average of multiple time ranges and triplicate solutions; error is ± 1 standard deviation.....191

Table B.4. Average pseudo-first-order rate constants (hr^{-1}) for each phenol with competing phenolic compounds in solution, listed at the top of each column. Rate constants are the average of multiple time ranges and triplicate solutions; error is ± 1 standard deviation.....191

Table B.5. *Tert*-butanol quenched average pseudo-first-order rate constants (hr^{-1}) for each phenol with competing phenolic compounds in solution, listed at the top of each column. Rate constants are the average of multiple time ranges and triplicate solutions; error is ± 1 standard deviation.....192

Table B.6. Average maximum percent sorption for each phenol at initial concentrations of 10, 20 and 40 μM with no competing compounds in solution. Percent sorption values are the average of triplicate reactions; error is ± 1 standard deviation. Cells with no fill are electron transfer-limited; gray cells indicate reactions are sorption-limited.....192

Table B.7. Average maximum percent sorption for each phenol with competing phenolic compounds in solution, listed at the top of each column. Percent sorption values are the average of triplicate reactions; error is ± 1 standard deviation. Cells with no fill are electron transfer-limited; gray cells indicate reactions are sorption-limited.....193

Table B.8. *Tert*-butanol quenched average maximum percent sorption for each phenol with competing phenolic compounds in solution, listed at the top of each column. Percent sorption values are the average of triplicate reactions; error is ± 1 standard deviation. Cells with no fill are electron transfer-limited; gray cells indicate reactions are sorption-limited.....193

Table B.9. Structure-activity and partitioning constants for resorcinol, bisphenol A, triclosan, and 4,4'-biphenol. Constants include the acid dissociation constant (pK_a), energy of the highest occupied molecular orbital (E_{HOMO}), oxidation potential (E_{ox}), log of the octanol:water partitioning coefficient ($\log K_{\text{ow}}$) and the pH adjusted value ($\log D_{\text{ow}}$), and the log of the organic carbon:water partitioning coefficient ($\log K_{\text{oc}}$). Sources for each constant are given in subscript following the column heading.....193

Table C.1. Sampling site coordinates and sample collection dates. Abbreviations correspond to bogs (B), eutrophic lakes (E), mesotrophic lakes (M), oligotrophic lakes (O), rivers (R), and wastewater effluent or wastewater-impacted sites (WW).....202

Table C.2. [DOC], alkalinity, SUVA ₂₅₄ , and E ₂ :E ₃ of filtered samples. Reported error is the standard deviation of triplicate measurements. N/A indicates data that is unavailable.....	203
Table C.3. Initial anion concentrations of filtered grab samples measured by ion chromatography. St. Louis River Estuary values (R5-R9, E5-E7, WW1, O5) include those reported by Berg et al. Reported error is standard deviation of triplicate measurements.....	204
Table C.4. Initial cation concentrations of filtered grab samples measured by ICP-OES. St. Louis River Estuary values include those reported by Berg et al. using the same samples. Reported error is the standard deviation of triplicate measurements.....	205
Table C.5. Samples included in each phase of this study as marked by an X.....	206
Table C.6. Percent change in measured DOM characteristics during reaction with MnO ₂ . Values which increase during reaction are shaded green while decreases are shaded red; lighter colors indicate changes less than 2% in either direction. Gray boxes mark unavailable data.....	216
Table C.7. Linear correlation statistics between various initial bulk characteristics, absolute changes in AMON and Mn(II/III), and percent changes in bulk characteristics from 50-hour reactions with MnO ₂ . Both absolute delta values and percent changes were calculated as the final value minus the initial value. Slope (m) and intercept (b) are reported for a line of the form $y = mx + b$. p-values from 2-tailed t-tests are reported and cells are shaded for significant t-test results ($p < 0.05$). X-variables are listed in first row and y-variables in first column of table.....	219
Table C.8. Linear correlation statistics based on control molecular dissolved organic matter characteristics or extent of reaction values with absolute changes (delta) or percent changes measured after 50-hour reactions with MnO ₂ . Both absolute delta values and percent changes were calculated as the final value minus the initial value. Slope (m) and intercept (b) are reported for a line of the form $y = mx + b$. p-values from 2-tailed t-tests are reported and cells are shaded for significant results ($p < 0.05$). X-variables are listed in first row and y-variables in first column of table.....	222
Table C.9. Number of matched formulas and percent of total formulas for control and treated waters reacted with acid birnessite for 50 hours.....	224
Table C.10. Average weighted values for control and treated waters after reaction with acid birnessite for 50 hours.....	225
Table C.11. Number of matched oxidized product formulas in each sample.....	227

List of Symbols and Abbreviations

MnO ₂	manganese oxide
δ	delta
α	alpha
β	beta
γ	gamma
AMON	aqueous manganese oxidation number
AOS	average oxidation state
DWT	drinking water treatment solids
AMD	acid mine drainage remediation solids
QSAR	quantitative structure activity relationship
LFER	linear free energy relationship
DOM	dissolved organic matter
XAS	X-ray absorption spectroscopy
XANES	X-ray absorption near-edge spectroscopy
Q-XANES	quick scanning X-ray absorption near-edge spectroscopy
XRD	X-ray diffraction
SEM	scanning electron microscopy
BET	Brunauer–Emmett–Teller surface area
BPA	bisphenol A
E1	estrone
E2	17β-estradiol
DHBP	4,4'-dihydroxybiphenyl, 4,4'-biphenol
HPLC	high-performance liquid chromatography
<i>k</i>	rate constant
<i>k'</i>	modeled rate constant for electron transfer-limited mechanism
<i>k''</i>	modeled rate constant for sorption-limited mechanism
<i>C</i>	phenol concentration
<i>C</i> ₀	initial (time = 0 hour) concentration
<i>C</i> _e	equilibrium concentration
<i>S</i> _{rxn}	modeled concentration of mineral surface sites
p <i>K</i> _a	acid dissociation constant
<i>K</i> _{ow}	octanol:water partitioning coefficient
<i>D</i> _{ow}	<i>K</i> _{ow} pH adjusted
<i>K</i> _{oc}	organic carbon:water partitioning coefficient
σ	Hammett constant
<i>E</i> _{HOMO}	energy of the highest occupied molecular orbital
<i>E</i> _{ox}	energy of first oxidative electron transfer
<i>E</i> _{ox,corr.}	corrected energy of first oxidative electron transfer
<i>V</i>	volts
eV	electronvolt
SHE	standard hydrogen electrode
pH _{pzc}	point of zero charge of a mineral
[Mn]	concentration of aqueous manganese

MnCO ₃	rhodochrosite
·OH	hydroxyl radical
CO ₃ · ⁻	carbonate radical
NTL-LTER	Northern Temperate Lakes Lon-Term Ecological Research
NaHCO ₃	sodium bicarbonate
UV	ultraviolet light
[DOC]	concentration of dissolved organic carbon
FT-ICR MS	Fourier-transform ion cyclotron resonance mass spectrometry
SUVA ₂₅₄	ratio of specific UV absorbance at 254 nm and dissolved organic carbon concentration
E ₂ :E ₃	ratio of UV absorbance at 250 nm divided by absorbance at 365 nm
MW	molecular weight
MW _w	relative intensity weighted molecular weight
H:C _w	relative intensity weighted hydrogen to carbon ratio
O:C _w	relative intensity weighted oxygen to carbon ratio
DBE _w	relative intensity weighted double bond equivalents
PCA	principal component analysis
Δ	delta, indicates change

Chapter 1

Introduction

1.1 Motivation

Manganese oxides are ubiquitous, highly redox active minerals that can oxidize phenolic compounds and are commonly considered for passive *in situ* water treatment systems. The reaction between manganese oxides and phenols is well understood for simple model phenols, but there is limited understanding of the reaction for complex phenols and diverse mixtures, including for phenolic moieties present in dissolved organic matter. This dissertation is the culmination of work investigating the mechanism of phenol oxidation by manganese oxides. We examine (1) the impact of phenol structure on oxidation rates and mechanisms with three manganese oxide materials, (2) changes in both reaction mechanism and rate due to competition among four phenols (i.e., resorcinol, triclosan, bisphenol A, and 4,4'-biphenol), and (3) reactions of manganese oxides with dissolved organic matter (DOM). This dissertation combines high-resolution solid-phase and aqueous analytical techniques with kinetic and mechanistic investigations to illuminate how these environmental variables alter the phenolic oxidation mechanism.

1.2 Manganese oxide sources

Manganese (Mn) is the fifth most abundant trace element and is commonly found in the +2, +3, and +4 oxidation states, although +5 through +7 also exist.¹⁻³ Mn(II) and Mn(III) are

environmentally relevant as dissolved species in natural waters or in Mn(II) carbonate minerals (e.g., rhodochrosite, MnCO_3), while Mn(III) and Mn(IV) are ubiquitous in soils and sediments as manganese (hydr)oxides (e.g., MnO_2 , MnOOH).¹⁻⁷ Among these Mn(III/IV) minerals, birnessite-like minerals are formed both abiotically in natural waters and biotically by Mn-oxidizing fungi and bacteria.^{1-4,8-25} Birnessite minerals are highly redox active phylломanganates formed by layers of MnO_6 octahedra with vacant sites and Mn^{2+} and Mn^{3+} substituted centers (**Figure 1.1**).^{2-4,8} These layers are separated by water and interlayer cations, which can impact the reactivity of these minerals.^{3,4,8,26} Acid birnessite and $\delta\text{-MnO}_2$ are sodium-substituted Mn(IV) synthetic analogues of biogenic birnessite and are commonly used in controlled laboratory experiments.^{3,4} The general layer structure of these phylломanganate solids is shown in **Figure 1.1**; deviations from this structure alter the reactive properties of the mineral as discussed further in subsection 1.3.

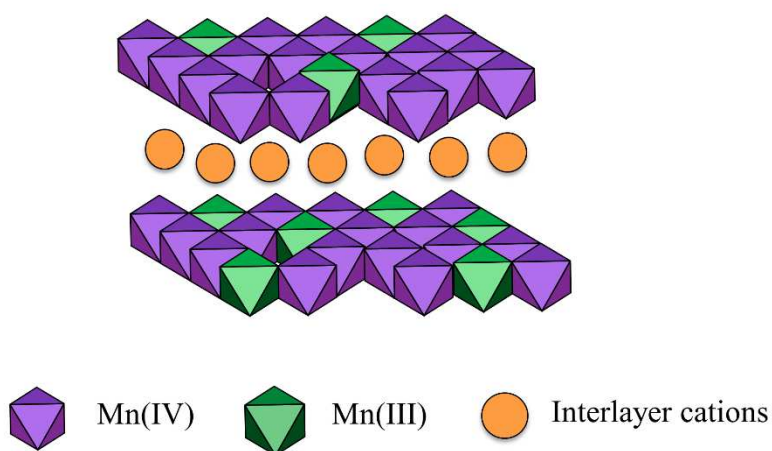


Figure 1.1. Layer structure of Mn(III/IV) phylломanganates.

Aside from abiotic, biogenic, and synthetic minerals, manganese oxides also form as byproducts of engineered remediation systems. Two key examples are drinking water treatment and acid mine drainage remediation. Aqueous manganese and iron (Fe) concentrations are regulated by secondary standards for drinking water due to implications for both color and taste.²⁷⁻³⁰ As a result, drinking water utilities with high aqueous Mn and Fe filter out these metals prior to distribution. Well 29 in Madison, Wisconsin removes these metals using greensand filter media which is engineered from glauconite to remove manganese, iron, sulfates, and other inorganic contaminants by oxidation and ion exchange.^{27,31,32} During greensand-based water filtration, iron-substituted manganese oxides form on the filter media and these solids are then reduced back to their aqueous form or disposed of as solid sludge.^{32,33}

Manganese oxides are also formed as a byproduct of acid mine drainage remediation systems. Acid mine drainage is the low pH runoff from mining operations and is contaminated with high levels of sulfate, iron, manganese, and other metals. To remove the toxic concentrations of metals from these streams, passive acid mine drainage remediation sites run the contaminated waters over a series of packed beds, ponds, and aerobic wetlands which sequentially remove metals.^{34,35} Manganese and iron are precipitated on oxic limestone beds as the last step of these sequential treatments and, as with greensand filtered manganese oxides, must be disposed of to regenerate the limestone media.³³⁻³⁶

1.3 Manganese oxide reactivity

Many structural properties of manganese oxides alter the reactivity of these solids. Reactions occur at surface or vacancy sites in the mineral^{3,5,20,25,26,37-42} and the structure and reduction potential of manganese oxides are largely linked to their average oxidation state

(AOS), which is also described as average manganese oxidation number (AMON).^{4,5,8,19,25,33,43-46} As a result, surface area,^{4,38,42,44,46,47} crystallinity,^{2,3,20,33,41,44,48-50} vacancies,^{39,41,42,45,51} inner-layer cation content,²⁶ Mn(III) content,^{45,50,52-55} and impurities of other trace metals^{4,6,16-19,33,40,42,56-58} all affect the reactivity of manganese oxides with inorganic and organic compounds. As the two synthetic Mn(IV) minerals included in this dissertation are synthetic analogues of biogenic sodium birnessite and both have AMONs around 3.75 – 3.95, differences in the initial reactivity of δ -MnO₂ and acid birnessite are attributed primarily to surface area, which is proportional to number of surface sites, and to crystallinity differences.^{3,4,8,43,46} However, reclaimed oxides such as those from Well 29 or acid mine drainage remediation sites have significantly lower reactivities than these synthetic minerals due to coprecipitated impurities (e.g., Fe) in the mineral structure, differing surface charges, lower surface areas, and inconsistencies in vacancy sites and inner-layer cations.

1.4 Phenolic contaminants

Phenols are a common organic compound class characterized by an aromatic hydroxyl group (**Figure 1.2**) substituted by a range of heteroatoms, aliphatic carbon chains, aromatic or aliphatic rings, and organic functional groups (e.g., carboxylic acids). These substitutions may occur at the *meta*-, *ortho*-, or *para*- positions on the aromatic ring, altering the physiochemical properties of structural isomers through orbital interactions, resonance stability, and intermolecular bonding.^{33,59-62} The wide variety of phenol structures gives these compounds properties which are manufactured for use as pesticides,^{4,63} plastic additives,^{45,64-66} antibacterial agents,^{4,67-72} surfactants,^{4,64,73} pharmaceuticals,^{65,74-81} flame retardants,^{4,82-85} and antioxidants.⁴

These compounds are detected in stormwater and agricultural runoff, landfill leachates, industrial waste, and wastewater effluents which contaminate soils and surface waters.^{47,63,66,76,79,81,84,86-94}

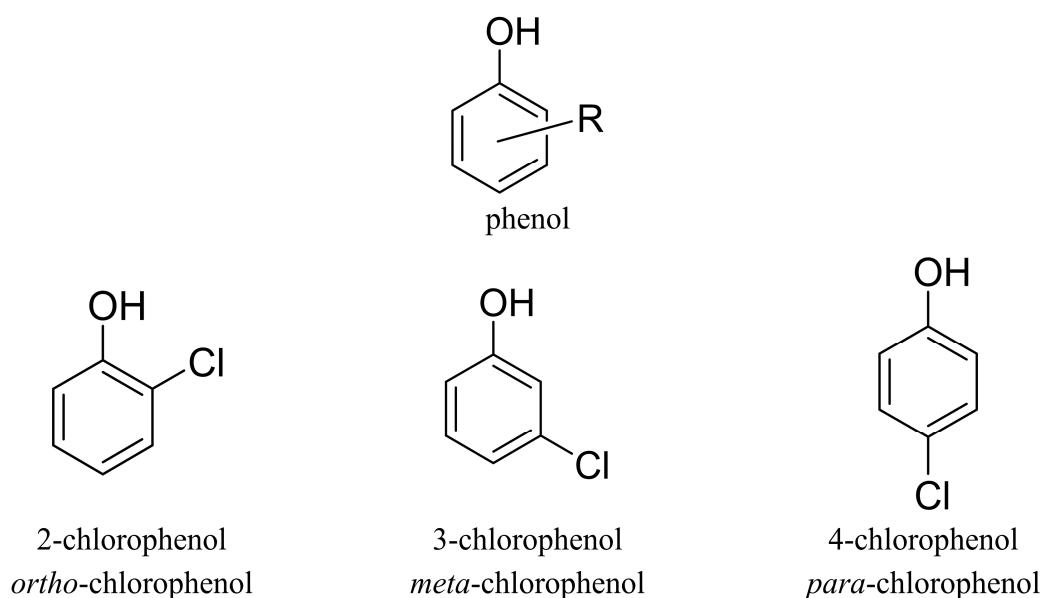


Figure 1.2. General phenol structure, where R indicates a substituent group, and example chlorophenol isomers.

Many phenolic contaminants have adverse effects on human and ecosystem health. For example, endocrine disrupting compounds, including bisphenol A (BPA), triclosan, alkylphenol surfactants, brominated flame retardants, and estrogenic compounds (e.g., estrogen, 17 β -estradiol) have well documented health effects.^{4,54,64,71,72,85,88,93,95-99} These compounds bioconcentrate in organisms and interfere with estrogen and androgen hormone production by either blocking or enhancing natural hormone signals, causing cells to produce more or less of the hormone, respectively. The resulting imbalance in hormone levels affects reproductive, cardiovascular, and immune responses.^{64,95-97,99} In humans, this causes developmental

impairment, decreased reproductivity, or cancer while fish may change sex, potentially stopping reproduction within an entire fish population.^{64,71,72,93,95-99} Non-endocrine disrupting phenols may also be toxic or alter ecosystems in other ways, such as pesticides (e.g., pentachlorophenol) and piscicides (e.g., 3-trifluoromethyl-4-nitrophenol) unintentionally destroying non-targeted species or antibacterial agents (e.g., triclosan) triggering the emergence and spread of resistant genes.^{4,63,78,81,84,86,93,100,101}

1.5 Oxidation of phenols by manganese oxides

Due to the high redox activity of manganese oxides, these minerals play an important role in contaminant degradation, partitioning, and fate.^{1,4} In particular, manganese oxides can transform organic contaminants with phenol and aniline functional groups through oxidation.^{4,6,33,44,46,50,58,61,68,69,84,86,102-116} This work focuses on phenolic compounds to determine how structural differences and solution complexities alter the mechanism and rates of oxidation, although these results may also help describe aniline degradation and both functional groups may be present in dissolved organic matter matrices. The oxidation of phenols by manganese oxides is well studied for simply substituted compounds such as phenol, chlorophenols, and hydroxyphenols.^{4,6,57,61,102,108,109,111-113,117}

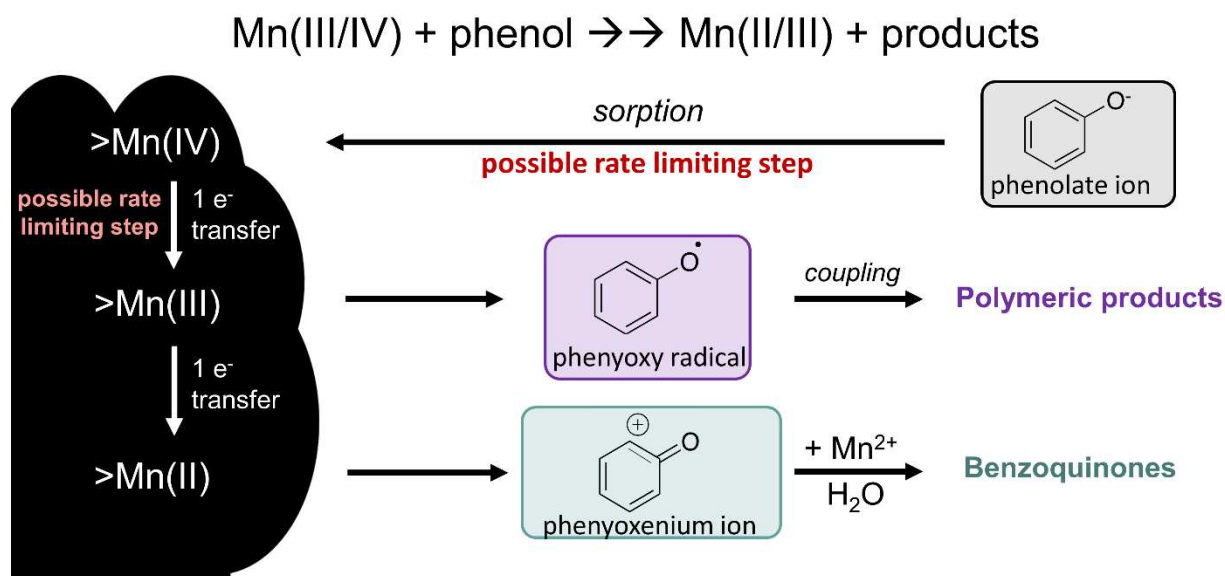


Figure 1.3. Reaction mechanism and rate-limiting steps of phenol oxidation by manganese(III/IV) oxides.

In this mechanism, the phenolic compound first loses the phenolic hydrogen to form a phenolate ion, diffuses to the Mn surface, and forms a precursor complex with an available Mn(IV) surface site.^{4,7,33,46,105,109,113,118} This process is referred to as sorption throughout this thesis and it includes all steps leading to the formation of the precursor complex. Once the phenol is sorbed to the Mn surface, a first one-electron transfer occurs, forming an oxidized phenoxy radical product and reduced Mn(III) surface site. Following the first electron transfer, the phenoxy radical product may either diffuse from the surface and undergo radical coupling to form hydroquinone-like products or the phenoxy radical may undergo a second one-electron transfer on the Mn surface to form an oxidized quinone-like product and reduced Mn(II) center (**Figure 1.3**).^{4,7,33,46,105,109,113,118}

The rate of this overall reaction is pseudo-first-order, meaning that the initial oxidation rate is only dependent on the concentration of phenol in solution; however, this oxidation rate slows and is no longer pseudo-first-order as the reaction proceeds due to surface loading, pH changes, and mineral reduction.^{4,33,46,68,103,105} While any step of this oxidation reaction may be

rate limiting, there is evidence that the processes of sorption,^{4,7,33,46,68,113} and the first electron transfer are the most common rate limiting steps.^{4,7,33,46,68,113}

1.6 Phenol reactivity

The structural diversity of phenolic compounds not only affects their use in manufactured products, but also their reactivity with manganese oxides. Studies comparing the reactivity of model phenols (e.g., phenol, 4-chlorophenol, 4-nitrophenol, catechol) reacted with manganese oxides demonstrate clear functional group dependence as *para*-substituted halogens and alkyl groups have slightly different inductive or resonance effects on the stability of, and thus reactivity of, the phenolic carbon.^{4,61,109,113} These molecular differences are highlighted by quantitative structure activity relationships (QSARs) or linear free energy relationships (LFERs), which are used to visualize and quantify how the oxidation rate of these model phenols depends on physiochemical measurements. Common variables in QSARs describe either the inductive effects of the functional group (e.g., Hammett constants; acid dissociation constants, pK_a) or the reaction and oxidation potential of the molecule as modeled using density functional theory, including energy of the highest occupied molecular orbital (i.e., E_{HOMO}) and energy of the first electron oxidation (i.e., E_{ox}).^{59-62,94,116,119,120}

In addition to these reactivity studies with common model phenols, previous studies report a wide range of oxidation rates for phenolic contaminants (e.g., BPA, triclosan) reacted with manganese oxides.^{4,61} It is difficult to compare observed oxidation rates across studies as the reactivity of both manganese oxides and phenols depend strongly on reaction conditions, including the manganese oxide material, pH and buffer compound, initial concentrations, and temperature.⁴ There is a lack of comprehensive studies applying foundational QSAR modeling

techniques and consistent reaction conditions to investigate the reactivity of a range of structures from model phenols to complex, multiring contaminants. Thus, further information about structural dependency of this reaction and further insights into the oxidation mechanism is limited for these contaminants of environmental concern.

1.6 Dissolved organic matter

Another ubiquitous component of natural waters which may impact the degradation of phenolic contaminants by manganese oxides is dissolved organic matter (DOM). Dissolved organic matter is a mixture of thousands of carbon-, hydrogen-, and oxygen-containing molecules that differ widely in heteroatom content (e.g., nitrogen, sulfur), aromaticity, molecular weight, and redox properties.¹²¹⁻¹⁴² The source and physiochemical processing of DOM impacts DOM composition; microbially-derived lake DOM is commonly less aromatic and lower in molecular weight than DOM from terrestrial rivers or bogs. DOM is also present in wastewater effluent alongside phenolic contaminants and this effluent DOM is relatively low in molecular weight and aromaticity; however, wastewater effluents can be very diverse and contain a greater percentage of heteroatom formulas, which alter the reactivity of wastewater DOM compared to DOM from natural sources.^{121,123,126,128,132,134-141,143-147}

1.7 Application of research for water treatment

This research aims to extend our current mechanistic understanding of phenol oxidation by manganese oxides to more complex reaction conditions to better predict phenolic contaminant fate in engineered and natural waters. Phenolic contaminants are detected in most surface waters at low concentrations and in wastewater effluents and stormwater runoff at higher

concentrations. Many of these contaminants are not efficiently degraded or removed by current water treatment techniques and manganese oxides are a potential solution. Simulated and pilot studies implementing manganese oxide materials into stormwater treatment systems show promising results on the implementation of manganese oxides for contaminant removal.^{47,63,84,86,87,100,148} However, there is a disconnect between controlled, mechanistic studies and these pilot treatments. The results of this research help to connect these research approaches and expand upon fundamental understandings of how phenol oxidation occurs in complex matrices.

1.8 Research needs

The field of organic compound oxidation by manganese oxides has transformed and evolved since initial studies investigating the reductive dissolution of manganese under high organic loads in the 1980s.^{7,52,58,109,113,118} Recent studies branch to focus on either specific manganese oxide structural changes (e.g., crystallinity changes, interlayer cations, Mn reactions within the layer structure)^{20,37,38,41,43,44,49,50,56,86,149,150} or loss rates and product formation of organic contaminants.^{45,46,67,69,70,83,103,104,106,108,112,151-158} However, these studies rarely bridge oxidation kinetics with high-resolution mineral characterizations and phenol-focused studies usually include less than five compounds. Because these reactions are highly sensitive to changes in mineral structure, reaction pH, and initial concentrations,⁴ it is difficult to directly connect changes in the manganese oxide with organic studies or to identify structural predictors of phenolic contaminant reactivity.

Additionally, there is a lack of research investigating how oxidation rates and mechanisms change for mixtures of phenolic compounds compared to these single phenol reactions. Phenolic mixtures are prevalent in both surface waters and potential treatment systems (e.g., stormwater runoff, wastewater). Many phenolic compounds also have potential oxidation products which are also phenols; for example, 4-hydroxycumyl alcohol is an identified oxidation product of bisphenol A^{105,152} and 4-hydroquinone and 2,4-dichlorophenol are known oxidation products of triclosan.⁶⁹ As these parent phenols are oxidized to their phenolic products, these parent and product phenols then may interact, altering the oxidation of both compounds. Potential interactions, such as competitive sorption to surface sites and electrostatic interactions, may enhance or inhibit sorption to the Mn surface and overall oxidation rates. Furthermore, it is well established that mixtures of endocrine disrupting phenols have additive, antagonistic, and synergistic effects on mice and fish which can either enhance or inhibit hormone disruption based on the specific phenol mixture tested.^{64,97,99,159} Therefore, it is imperative to understand how these phenol mixtures alter oxidation by manganese oxides to better predict and tailor degradation in treatment systems.

There is also a knowledge gap concerning the impact of dissolved organic matter on this reaction despite its prevalence throughout natural and wastewaters. Interactions between DOM and manganese oxides may alter DOM composition and reactivity in the subsurface or compete with target contaminants in treatment systems. The most commonly studied aspects of this reaction are changes in DOM sorption linked to Mn structure^{43,160,161}, including comparisons between multiple Mn oxides reacted with DOM isolates and/or model compounds.^{40,162} Whole water DOM is rarely included in studies with manganese oxides, but instead used to understand interactions with dissolved trace metals (e.g., Fe, Al).¹⁶³⁻¹⁶⁵ Furthermore, changes in DOM

composition are typically attributed to oxidation based on the transformation of small organic acids or reduction of manganese oxides.^{123,127,129} However, there is a lack of molecular proof that DOM is oxidized in these reactions with manganese oxides, making it difficult to predict composition and reactivity changes to DOM in natural and engineered systems.

1.9 Research objectives

The aim of this dissertation is to address these identified research needs by determining (1) how phenol and manganese structures alter the rates and mechanisms of oxidation by reacting a suite of phenolic compounds ranging in structural complexity with δ -MnO₂ and two reclaimed minerals, (2) what effect mixtures of phenolic contaminants have on oxidation rates and mechanisms and what interactions cause these changes in oxidation, and (3) how manganese oxides transform dissolved organic matter whether or not MnO₂ oxidizes the phenolic moieties within DOM.

In Chapter 2, we quantify oxidation rates and determine the rate-limiting step for 29 phenolic compounds reacted with δ -MnO₂, as well as 15 phenols oxidized by reclaimed drinking water treatment (DWT) and acid mine drainage remediation (AMD) solids. By combining aqueous kinetic measurements with solid-phase manganese characterizations, we determine that both electron transfer-limited and sorption-limited oxidation reactions occur within the suite of 29 phenols and the mechanism depends on both the structure of the phenol as well as the manganese oxide surface area, surface charge, and iron content. This kinetic data also demonstrates the potential to reclaim byproduct manganese oxides from DWT and AMD systems for treatment of wastewater effluent or stormwater runoff, providing a cost- and energy-effective alternative to synthetic manganese oxides. From these oxidation results, we assess the

efficacy of quantitative structure activity relationships and find that the reactivity of *ortho*-substituted and complex phenols is not predicted by these linear relationships despite good fits for *meta*- and *para*-substituted simple phenols. By conducting kinetic measurements and reaction modeling on a diverse set of phenols reacted with both synthetic and reclaimed manganese oxides, we are able to connect oxidation rates and mechanisms to specific phenolic substituents and differences between manganese oxides to elucidate which characteristics drive reactivity in these reactions.

In Chapter 3, we investigate the effect of phenol mixtures on the oxidation rates and mechanisms determined in Chapter 2. For this study, we chose four target contaminants with varying structures and which encompass both electron transfer-limited and sorption-limited reaction mechanisms. The four contaminants are bisphenol A, triclosan, resorcinol, and 4,4'-biphenol, which are an endocrine disruptor, antimicrobial, pharmaceutical, and antioxidant, respectively. Of the four compounds, bisphenol A, triclosan, and resorcinol are all electron transfer-limited and react relatively quickly in isolated reactions with δ -MnO₂. In mixtures, these three phenols are all inhibited with lower levels of sorption to the Mn surface and slower pseudo-first-order oxidation kinetics, which is consistent with competitive intermolecular interactions. Conversely, 4,4'-biphenol is sorption-limited with δ -MnO₂ and has orders of magnitude lower pseudo-first-order oxidation rates than the other three compounds. In solutions with other phenols, 4,4'-biphenol reacts faster than it does in isolation. We tested for the mechanism of this oxidation enhancement by repeating all mixture and control reactions in the presence of *tert*-butanol, a non-specific radical quencher.^{49,91,166-170} With *tert*-butanol, rates of 4,4'-biphenol oxidation decreased relative to the non-quenched analogues suggesting that indirect oxidation by phenoxy radical intermediates enhance 4,4'-biphenol oxidation in contaminant mixtures. This

study is the first to determine oxidation rate and mechanism changes in multi-contaminant solutions and suggests that the oxidation mechanism of these phenols with manganese oxides not only impacts the degradation rate in isolated solutions, but also influences whether oxidation of these phenols is enhanced or inhibited in contaminated mixtures.

In Chapter 4, we use acid birnessite, a more crystalline MnO_2 mineral, to transform a variety of whole water dissolved organic matter samples. Acid birnessite was used in place of δ - MnO_2 to ensure mineral changes did not affect the MnO_2 reactivity over the course of longer 28 day reactions as δ - MnO_2 changes after about 4 – 5 days following synthesis. These whole waters were collected from oligotrophic lakes, eutrophic lakes, bogs, rivers, and wastewater effluents around Wisconsin and Minnesota and they were characterized to ensure they varied in aromaticity, carbon concentration, and molecular weight. Reactions with MnO_2 (50-hour and 28-day) were carbon normalized to control for differences resulting from inconsistent C:Mn ratios; changes observed for 50-hour reactions were consistent with longer term results. Bulk measurements of aromaticity, dissolved organic carbon, and molecular weight changes were inconsistent across the 29 waters as were high-resolution Fourier transform-ion cyclotron resonance mass spectrometry characteristics such as H:C and double bond equivalence values, which are related to aromaticity of the DOM pool, and O:C which measures the oxidation state of the DOM. Many of these characterizations changed opposite of the expected direction for oxidation (e.g., O:C decreased instead of increased). However, oxidation products were identified in all 14 waters analyzed by FT-ICR MS. Analysis of the reactive molecular formulas in each samples indicates that the same lignin- and tannin-like formulas react in each water to form a variety of transformation products, suggesting that oxidation is not the only transformation to occur in DOM reacted with MnO_2 .

1.10 References

1. Borch, T.; Kretzschmar, R.; Kappler, A.; Van Cappellen, P.; Ginder-Vogel, M.; Voegelin, A.; Campbell, K., Biogeochemical redox processes and their impact on contaminant dynamics. *Environ. Sci. Technol.* **2010**, *44*, (1), 15-23.
2. Tebo, B. M.; Bargar, J. R.; Clement, B. G.; Dick, G. J.; Murray, K. J.; Parker, D.; Verity, R.; Webb, S. M., Biogenic manganese oxides: Properties and mechanisms of formation. *Annu. Rev. Earth Planet. Sci.* **2004**, *32*, (1), 287-328.
3. Post, J. E., Manganese oxide minerals: Crystal structures and economic and environmental significance. *Proc. Natl. Acad. Sci. U.S.A.* **1999**, *96*, (7), 3447-3454.
4. Remucal, C. K.; Ginder-Vogel, M., A critical review of the reactivity of manganese oxides with organic contaminants. *Environ. Sci. Process. Impacts* **2014**, *16*, (6), 1247-1266.
5. Manceau, A.; Marcus, M. A.; Grangeon, S., Determination of Mn valence states in mixed-valent manganates by XANES spectroscopy. *Am. Mineral.* **2012**, *97*, (5-6), 816-827.
6. Pizzigallo, M. D. R.; Ruggiero, P.; Crecchio, C.; Mininni, R., Manganese and iron-oxides as reactants for oxidation of chlorophenols. *Soil Sci. Soc. Am. J.* **1995**, *59*, (2), 444-452.
7. Stone, A. T.; Morgan, J. J., Reduction and dissolution of manganese(III) and manganese(IV) oxides by organics. 1. Reaction with hydroquinone. *Environ. Sci. Technol.* **1984**, *18*, (6), 450-456.
8. Elzinga, E. J., ⁵⁴Mn radiotracers demonstrate continuous dissolution and reprecipitation of vernadite (δ -MnO₂) during interaction with aqueous Mn(II). *Environ. Sci. Technol.* **2016**, *50*, (16), 8670-8677.
9. Estes, E. R.; Andeer, P. F.; Nordlund, D.; Wankel, S. D.; Hansel, C. M., Biogenic manganese oxides as reservoirs of organic carbon and proteins in terrestrial and marine environments. *Geobiology* **2016**, *15*, (1), 158-172.
10. Villalobos, M.; Toner, B.; Bargar, J.; Sposito, G., Characterization of the manganese oxide produced by *Pseudomonas putida* strain MnB1. *Geochim. Cosmochim. Acta* **2003**, *67*, (14), 2649-2662.
11. Learman, D. R.; Hansel, C. M., Comparative proteomics of Mn(II)-oxidizing and non-oxidizing *Roseobacter* clade bacteria reveal an operative manganese transport system but minimal Mn(II)-induced expression of manganese oxidation and antioxidant enzymes. *Environ. Microbiol. Rep.* **2014**, *6*, (5), 501-509.
12. Learman, D. R.; Voelker, B. M.; Madden, A. S.; Hansel, C. M., Constraints on superoxide mediated formation of manganese oxides. *Front. Microbiol.* **2013**, *4*, 262.
13. Santelli, C. M.; Webb, S. M.; Dohnalkova, A. C.; Hansel, C. M., Diversity of Mn oxides produced by Mn(II)-oxidizing fungi. *Geochim. Cosmochim. Acta* **2011**, *75*, (10), 2762-2776.
14. Learman, D. R.; Voelker, B. M.; Vazquez-Rodriguez, A. I.; Hansel, C. M., Formation of manganese oxides by bacterially generated superoxide. *Nature Geoscience* **2011**, *4*, (2), 95-98.
15. Tang, Y.; Zeiner, C. A.; Santelli, C. M.; Hansel, C. M., Fungal oxidative dissolution of the Mn(II)-bearing mineral rhodochrosite and the role of metabolites in manganese oxide formation. *Environ. Microbiol.* **2013**, *15*, (4), 1063-1077.

16. Taujale, S.; Zhang, H., Impact of interactions between metal oxides to oxidative reactivity of manganese dioxide. *Environ. Sci. Technol.* **2012**, *46*, (5), 2764-2771.
17. Wang, Z.; Giammar, D. E., Metal contaminant oxidation mediated by manganese redox cycling in subsurface environment. In *Advances in the Environmental Biogeochemistry of Manganese Oxides*, Feng, X.; Li, W.; Zhu, M.; Sparks, D. L., eds. American Chemical Society: Washington, D.C., 2015; Vol. 1197, pp 29-50.
18. Miyata, N.; Tani, Y.; Sakata, M.; Iwahori, K., Microbial manganese oxide formation and interaction with toxic metal ions. *J. Biosci. Bioeng.* **2007**, *104*, (1), 1-8.
19. Duckworth, O. W.; Rivera, N. A.; Gardner, T. G.; Andrews, M. Y.; Santelli, C. M.; Polizzotto, M. L., Morphology, structure, and metal binding mechanisms of biogenic manganese oxides in a superfund site treatment system. *Environ. Sci. Process. Impacts* **2017**, *19*, (1), 50-58.
20. Zhang, T.; Liu, L.; Tan, W.; Suib, S. L.; Qiu, G.; Liu, F., Photochemical formation and transformation of birnessite: Effects of cations on micromorphology and crystal structure. *Environ. Sci. Technol.* **2018**, *52*, (12), 6864-6871.
21. Johnson, J. E.; Savalia, P.; Davis, R.; Kocar, B. D.; Webb, S. M.; Nealson, K. H.; Fischer, W. W., Real-time manganese phase dynamics during biological and abiotic manganese oxide reduction. *Environ. Sci. Technol.* **2016**, *50*, (8), 4248-4258.
22. Toner, B.; Fakra, S.; Villalobos, M.; Warwick, T.; Sposito, G., Spatially resolved characterization of biogenic manganese oxide production within a bacterial biofilm. *Appl. Environ. Microbiol.* **2005**, *71*, (3), 1300-1310.
23. Murray, J. W., The surface chemistry of hydrous manganese dioxide. *J. Colloid Interf. Sci.* **1974**, *46*, (3), 357-371.
24. McKenzie, R. M., The synthesis of birnessite, cryptomelane, and some other oxides and hydroxides of manganese. *Mineral. Mag.* **1971**, *38*, 493-502.
25. Ilton, E. S.; Post, J. E.; Heaney, P. J.; Ling, F. T.; Kerisit, S. N., XPS determination of Mn oxidation states in Mn (hydr)oxides. *Appl. Surf. Sci.* **2016**, *366*, 475-485.
26. Balgooyen, S.; Remucal, C. K.; Ginder-Vogel, M., Identifying the mechanisms of cation inhibition of phenol oxidation by acid birnessite. *J. Environ. Qual.* **2020**, *49*, (6), 1644-1654.
27. Schlenker, T.; Hausbeck, J.; Sorsa, K., Manganese in Madison's drinking water. *J. Environ. Health* **2008**, *71*, (5), 12-16.
28. Tobiason, J. E.; Bazilio, A.; Goodwill, J.; Mai, X.; Nguyen, C., Manganese removal from drinking water sources. *Curr. Pollut. Rep.* **2016**, *2*, (3), 168-177.
29. Environmental Protection Agency, National primary drinking water regulations. In National Service Center for Environmental Publications: 2021.
30. Gillispie, E. C.; Austin, R. E.; Rivera, N. A.; Bolich, R.; Duckworth, O. W.; Bradley, P.; Amoozegar, A.; Hesterberg, D.; Polizzotto, M. L., Soil weathering as an engine for manganese contamination of well water. *Environ. Sci. Technol.* **2016**, *50*, (18), 9963-9971.
31. Madison Water Utility. *2006 manganese monitoring report*; Madison Water Utility: Madison, WI, 2007.
32. Madison Water Utility; EarthTech, Inc. *Well 29 pilot study report*; Madison, WI, 2007.
33. Trainer, E. L.; Ginder-Vogel, M.; Remucal, C. K., Organic structure and solid characteristics determine reactivity of phenolic compounds with synthetic and reclaimed manganese oxides. *Environ. Sci. Water Res. Technol.* **2020**, *6*, (3), 540-553.

34. Bussiere, B., Acid mine drainage from abandoned mine sites: Problematic and reclamation approaches. In *Advances in Environmental Geotechnics*, 2010; pp 111-125.
35. Skousen, J.; Zipper, C. E.; Rose, A.; Ziemkiewicz, P. F.; Nairn, R.; McDonald, L. M.; Kleinmann, R. L., Review of passive systems for acid mine drainage treatment. *Mine Water Environ.* **2016**, *36*, (1), 133-153.
36. Tan, H.; Zhang, G. X.; Heaney, P. J.; Webb, S. M.; Burgos, W. D., Characterization of manganese oxide precipitates from appalachian coal mine drainage treatment systems. *Appl. Geochem.* **2010**, *25*, (3), 389-399.
37. Essington, M. E.; Vergeer, K. A., Adsorption of antimonate, phosphate, and sulfate by manganese dioxide: Competitive effects and surface complexation modeling. *Soil Sci. Soc. Am. J.* **2015**, *79*, (3), 803-814.
38. Pena, J.; Bargar, J. R.; Sposito, G., Copper sorption by the edge surfaces of synthetic birnessite nanoparticles. *Chem. Geol.* **2015**, *396*, 196-207.
39. Wang, Y.; Benkaddour, S.; Marafatto, F. F.; Pena, J., Diffusion- and pH-dependent reactivity of layer-type MnO₂: Reactions at particle edges versus vacancy sites. *Environ. Sci. Technol.* **2018**, *52*, (6), 3476-3485.
40. Chorover, J.; Amistadi, M. K., Reaction of forest floor organic matter at goethite, birnessite and smectite surfaces. *Geochim. Cosmochim. Acta* **2001**, *65*, (1), 95-109.
41. Zhao, H.; Zhu, M.; Li, W.; Elzinga, E. J.; Villalobos, M.; Liu, F.; Zhang, J.; Feng, X.; Sparks, D. L., Redox reactions between Mn(II) and hexagonal birnessite change its layer symmetry. *Environ. Sci. Technol.* **2016**, *50*, (4), 1750-1758.
42. van Genuchten, C. M.; Pena, J., Sorption selectivity of birnessite particle edges: A d-PDF analysis of Cd(II) and Pb(II) sorption by delta-MnO₂ and ferrihydrite. *Environ. Sci. Process. Impacts* **2016**, *18*, (8), 1030-1041.
43. Ma, D.; Wu, J.; Yang, P.; Zhu, M., Coupled manganese redox cycling and organic carbon degradation on mineral surfaces. *Environ. Sci. Technol.* **2020**, *54*, (14), 8801-8810.
44. Huang, J.; Zhong, S.; Dai, Y.; Liu, C. C.; Zhang, H., Effect of MnO₂ phase structure on the oxidative reactivity toward bisphenol A degradation. *Environ. Sci. Technol.* **2018**, *52*, (19), 11309-11318.
45. Balgooyen, S.; Alaimo, P. J.; Remucal, C. K.; Ginder-Vogel, M., Structural transformation of MnO₂ during the oxidation of bisphenol A. *Environ. Sci. Technol.* **2017**, *51*, (11), 6053-6062.
46. Shaikh, N.; Zhang, H.; Rasamani, K.; Artyushkova, K.; Ali, A. S.; Cerrato, J. M., Reaction of bisphenol A with synthetic and commercial MnO_{x(s)}: Spectroscopic and kinetic study. *Environ. Sci. Process. Impacts* **2018**, *20*, (7), 1046-1055.
47. Okaikue-Woodi, F. E. K.; Cherukumilli, K.; Ray, J. R., A critical review of contaminant removal by conventional and emerging media for urban stormwater treatment in the United States. *Water Res.* **2020**, *187*.
48. Wang, Z.; Lee, S. W.; Catalano, J. G.; Lezama-Pacheco, J. S.; Bargar, J. R.; Tebo, B. M.; Giammar, D. E., Adsorption of uranium(VI) to manganese oxides: X-ray absorption spectroscopy and surface complexation modeling. *Environ. Sci. Technol.* **2013**, *47*, (2), 850-858.
49. Huang, J.; Dai, Y.; Singewald, K.; Liu, C.-C.; Saxena, S.; Zhang, H., Effects of MnO₂ of different structures on activation of peroxydisulfate for bisphenol A degradation under acidic conditions. *Chem. Eng. J.* **2019**, *370*, 906-915.

50. Charbonnet, J. A.; Duan, Y.; van Genuchten, C. M.; Sedlak, D. L., Regenerated manganese-oxide coated sands: The role of mineral phase in organic contaminant reactivity. *Environ. Sci. Technol.* **2021**, *55*, (8), 5282-5290.
51. Balgooyen, S.; Campagnola, G.; Remucal, C. K.; Ginder-Vogel, M. Impact of bisphenol A influent concentration and reaction time on MnO₂ transformation in a stirred flow reactor. *Environ. Sci. Process. Impacts* **2019**, *21*, (1), 19-27.
52. Wang, Y.; Stone, A. T., Reaction of Mn(III,IV) (hydr)oxides with oxalic acid, glyoxylic acid, phosphonoformic acid, and structurally-related organic compounds. *Geochim. Cosmochim. Acta* **2006**, *70*, (17), 4477-4490.
53. Nico; Zasoski, Mn(III) center availability as a rate controlling factor in the oxidation of phenol and sulfide on δ -MnO₂. *Environ. Sci. Technol.* **2001**, *35*.
54. Wang, X.; Xiang, W.; Wang, S.; Ge, J.; Qu, R.; Wang, Z., Oxidative oligomerization of phenolic endocrine disrupting chemicals mediated by Mn(III)-L complexes and the role of phenoxyl radicals in the enhanced removal: Experimental and theoretical studies. *Environ. Sci. Technol.* **2020**, *54*, (3), 1573-1582.
55. Hu, E.; Zhang, Y.; Wu, S.; Wu, J.; Liang, L.; He, F., Role of dissolved Mn(III) in transformation of organic contaminants: Non-oxidative versus oxidative mechanisms. *Water Res.* **2017**, *111*, 234-243.
56. Yin, H.; Feng, X.; Qiu, G.; Tan, W.; Liu, F., Characterization of co-doped birnessites and application for removal of lead and arsenite. *J. Hazard Mater.* **2011**, *188*, (1-3), 341-349.
57. Lehmann, R. G.; Cheng, H. H.; Harsh, J. B., Oxidation of phenolic acids by soil iron and manganese oxides. *Soil Sci. Soc. Am. J.* **1987**, *51*, (2), 352-356.
58. Klausen, J.; Haderlein, S. B.; Schwarzenbach, R. P., Oxidation of substituted anilines by aqueous MnO₂: Effect of co-solutes on initial and quasi-steady-state kinetics. *Environ. Sci. Technol.* **1997**, *31*, (9), 2642-2649.
59. Schwarzenbach, R. P.; Gschwend, P. M.; Imboden, Organic acids and bases: Acidity constant and partitioning behavior. In *Environmental Organic Chemistry*, 2nd ed.; John Wiley & Sons, Inc.: Hoboken, New Jersey, 2003; 245-274.
60. Tratnyek, P. G.; Weber, E. J.; Schwarzenbach, R. P., Quantitative structure-activity relationships for chemical reductions of organic contaminants. *Environ. Toxicol. Chem.* **2003**, *22*, (8), 1733-1742.
61. Pavitt, A. S.; Bylaska, E. J.; Tratnyek, P. G., Oxidation potentials of phenols and anilines: Correlation analysis of electrochemical and theoretical values. *Environ. Sci. Process. Impacts* **2017**, *19*, (3), 339-349.
62. Arnold, W. A.; Oueis, Y.; O'Connor, M.; Rinaman, J. E.; Taggart, M. G.; McCarthy, R. E.; Foster, K. A.; Latch, D. E., QSARs for phenols and phenolates: Oxidation potential as a predictor of reaction rate constants with photochemically produced oxidants. *Environ. Sci. Process. Impacts* **2017**, *19*, (3), 324-338.
63. Wolfand, J. M.; Seller, C.; Bell, C. D.; Cho, Y. M.; Oetjen, K.; Hogue, T. S.; Luthy, R. G., Occurrence of urban-use pesticides and management with enhanced stormwater control measures at the watershed scale. *Environ. Sci. Technol.* **2019**.
64. Bonefeld-Jorgensen, E. C.; Long, M.; Hofmeister, M. V.; Vinggaard, A. M., Endocrine-disrupting potential of bisphenol A, bisphenol A dimethacrylate, 4-*n*-nonylphenol, and 4-*n*-octylphenol *in vitro*: New data and a brief review. *Environ. Health Perspect. Suppl. 1*, 69-76.

65. Bexfield, L. M.; Toccalino, P. L.; Belitz, K.; Foreman, W. T.; Furlong, E. T., Hormones and pharmaceuticals in groundwater used as a source of drinking water across the United States. *Environ. Sci. Technol.* **2019**, *53*, (6), 2950-2960.
66. Baldwin, A. K.; Corsi, S. R.; Mason, S. A., Plastic debris in 29 Great Lakes tributaries: Relations to watershed attributes and hydrology. *Environ. Sci. Technol.* **2016**, *50*, (19), 10377-10385.
67. Liu, C. S.; Zhang, L. J.; Li, F. B.; Wang, Y.; Gao, Y.; Li, X. Z.; Cao, W. D.; Feng, C. H.; Dong, J.; Sun, L. N., Dependence of sulfadiazine oxidative degradation on physicochemical properties of manganese dioxides. *Industr. Eng. Chem. Res.* **2009**, *48*, (23), 10408-10413.
68. Zhang, H.; Chen, W. R.; Huang, C. H., Kinetic modeling of oxidation of antibacterial agents by manganese oxide. *Environ. Sci. Technol.* **2008**, *42*, (15), 5548-5554.
69. Zhang, H.; Huang, C. H., Oxidative transformation of triclosan and chlorophene by manganese oxides. *Environ. Sci. Technol.* **2003**, *37*, (11), 2421-2430.
70. Ding, J.; Su, M.; Wu, C.; Lin, K., Transformation of triclosan to 2,8-dichlorodibenzo-*p*-dioxin by iron and manganese oxides under near dry conditions. *Chemosphere* **2015**, *133*, 41-46.
71. Olaniyan, L. W.; Mkwetshana, N.; Okoh, A. I., Triclosan in water, implications for human and environmental health. *Springerplus* **2016**, *5*, (1), 1639.
72. Dann, A. B.; Hontela, A., Triclosan: Environmental exposure, toxicity and mechanisms of action. *J. Appl. Toxicol.* **2011**, *31*, (4), 285-311.
73. Krop, H.; de Voogt, P.; Eschauzier, C.; Droge, S., Sorption of surfactants onto sediment at environmentally relevant concentrations: Independent-mode as unifying concept. *Environ. Sci. Process. Impacts* **2020**, *22*, (5), 1266-1286.
74. Forrez, I.; Carballa, M.; Fink, G.; Wick, A.; Hennebel, T.; Vanhaecke, L.; Ternes, T.; Boon, N.; Verstraete, W., Biogenic metals for the oxidative and reductive removal of pharmaceuticals, biocides and iodinated contrast media in a polishing membrane bioreactor. *Water Res.* **2011**, *45*, (4), 1763-1773.
75. Liu, W.; Langenhoff, A. A. M.; Sutton, N. B.; Rijnaarts, H. H. M., Biological regeneration of manganese(IV) and iron(III) for anaerobic metal oxide-mediated removal of pharmaceuticals from water. *Chemosphere* **2018**, *208*, 122-130.
76. Bulloch, D. N.; Nelson, E. D.; Carr, S. A.; Wissman, C. R.; Armstrong, J. L.; Schlenk, D.; Larive, C. K., Occurrence of halogenated transformation products of selected pharmaceuticals and personal care products in secondary and tertiary treated wastewaters from southern California. *Environ. Sci. Technol.* **2015**, *49*, (4), 2044-2051.
77. Yang, Y.; Ok, Y. S.; Kim, K. H.; Kwon, E. E.; Tsang, Y. F., Occurrences and removal of pharmaceuticals and personal care products (PPCPs) in drinking water and water/sewage treatment plants: A review. *Sci. Total Environ.* **2017**, *596-597*, 303-320.
78. Gottschall, N.; Topp, E.; Metcalfe, C.; Edwards, M.; Payne, M.; Kleywegt, S.; Russell, P.; Lapen, D. R., Pharmaceutical and personal care products in groundwater, subsurface drainage, soil, and wheat grain, following a high single application of municipal biosolids to a field. *Chemosphere* **2012**, *87*, (2), 194-203.
79. Oulton, R. L.; Kohn, T.; Cwiertny, D. M., Pharmaceuticals and personal care products in effluent matrices: A survey of transformation and removal during wastewater treatment and implications for wastewater management. *J. Environ. Monit.* **2010**, *12*, (11), 1956-1978.

80. Boreen, A. L.; Arnold, W. A.; McNeill, K., Photodegradation of pharmaceuticals in the aquatic environment: A review. *Aquat. Sci.* **2003**, *65*, (4), 320-341.
81. Thomaidis, N. S.; Gago-Ferrero, P.; Ort, C.; Maragou, N. C.; Alygizakis, N. A.; Borova, V. L.; Dasenaki, M. E., Reflection of socioeconomic changes in wastewater: Licit and illicit drug use patterns. *Environ. Sci. Technol.* **2016**, *50*, (18), 10065-10072.
82. Covaci, A.; Voorspoels, S.; Abdallah, M. A.; Geens, T.; Harrad, S.; Law, R. J., Analytical and environmental aspects of the flame retardant tetrabromobisphenol-A and its derivatives. *J. Chromatogr. A.* **2009**, *1216*, (3), 346-363.
83. Liu, A.; Shi, J.; Qu, G.; Hu, L.; Ma, Q.; Song, M.; Jing, C.; Jiang, G., Identification of emerging brominated chemicals as the transformation products of tetrabromobisphenol A (TBBPA) derivatives in soil. *Environ. Sci. Technol.* **2017**, *51*, (10), 5434-5444.
84. Grebel, J. E.; Charbonnet, J. A.; Sedlak, D. L., Oxidation of organic contaminants by manganese oxide geomedia for passive urban stormwater treatment systems. *Water Res.* **2016**, *88*, 481-491.
85. Han, W.; Wang, S.; Huang, H.; Luo, L.; Zhang, S., Simultaneous determination of brominated phenols in soils. *J. Environ. Sci. (China)* **2013**, *25*, (11), 2306-2312.
86. Charbonnet, J. A.; Duan, Y.; van Genuchten, C. M.; Sedlak, D. L., Chemical regeneration of manganese oxide-coated sand for oxidation of organic stormwater contaminants. *Environ. Sci. Technol.* **2018**, *52*, (18), 10728-10736.
87. Grebel, J. E.; Mohanty, S. K.; Torkelson, A. A.; Boehm, A. B.; Higgins, C. P.; Maxwell, R. M.; Nelson, K. L.; Sedlak, D. L., Engineered infiltration systems for urban stormwater reclamation. *Environ. Eng. Sci.* **2013**, *30*, (8), 437-454.
88. Bina, B.; Mohammadi, F.; Amin, M. M.; Pourzamani, H. R.; Yavari, Z., Determination of 4-nonylphenol and 4-tert-octylphenol compounds in various types of wastewater and their removal rates in different treatment processes in nine wastewater treatment plants of Iran. *Chin. J. Chem. Eng.* **2018**, *26*, (1), 183-190.
89. Kalscheur, K. N.; Penskar, R. R.; Daley, A. D.; Pechauer, S. M.; Kelly, J. J.; Peterson, C. G.; Gray, K. A., Effects of anthropogenic inputs on the organic quality of urbanized streams. *Water Res.* **2012**, *46*, (8), 2515-2524.
90. Butler, E.; Whelan, M. J.; Sakrabani, R.; van Egmond, R., Fate of triclosan in field soils receiving sewage sludge. *Environ. Pollut.* **2012**, *167*, 101-109.
91. Shahamat, Y. D.; Farzadkia, M.; Nasserli, S.; Mahvi, A. H.; Gholami, M.; Esrafil, A., Magnetic heterogeneous catalytic ozonation: A new removal method for phenol in industrial wastewater. *J. Env. Health Sci. Eng.* **2014**, *12*, (50).
92. Heidler, J.; Halden, R. U., Mass balance assessment of triclosan removal during conventional sewage treatment. *Chemosphere* **2007**, *66*, (2), 362-369.
93. Montes-Grajales, D.; Fennix-Agudelo, M.; Miranda-Castro, W., Occurrence of personal care products as emerging chemicals of concern in water resources: A review. *Sci. Total Environ.* **2017**, *595*, 601-614.
94. Lee, Y.; von Gunten, U., Quantitative structure-activity relationships (QSARs) for the transformation of organic micropollutants during oxidative water treatment. *Water Res.* **2012**, *46*, (19), 6177-6195.
95. Feng, Y.; Zhang, P.; Zhang, Z.; Shi, J.; Jiao, Z.; Shao, B., Endocrine disrupting effects of triclosan on the placenta in pregnant rats. *PLoS One* **2016**, *11*, (5).

96. Li, Z.; Zhang, H.; Gibson, M.; Li, J., An evaluation on combination effects of phenolic endocrine disruptors by estrogen receptor binding assay. *Toxicol. In Vitro* **2012**, *26*, (6), 769-774.
97. Pollock, T.; Weaver, R. E.; Ghasemi, R.; deCatanzaro, D., A mixture of five endocrine-disrupting chemicals modulates concentrations of bisphenol A and estradiol in mice. *Chemosphere* **2018**, *193*, 321-328.
98. Wu, Q.; Lam, J. C. W.; Kwok, K. Y.; Tsui, M. M. P.; Lam, P. K. S., Occurrence and fate of endogenous steroid hormones, alkylphenol ethoxylates, bisphenol A and phthalates in municipal sewage treatment systems. *J. Environ. Sci. (China)* **2017**, *61*, 49-58.
99. Toft, G.; Baatrup, E., Sexual characteristics are altered by 4-*tert*-octylphenol and 17 β -estradiol in the adult male guppy (*Poecilia reticulata*). *Ecotoxicol. Environ. Saf.* **2001**, *48*, (1), 76-84.
100. Luthy, R.; Sedlak, D. L. *Enhanced removal of nutrients and trace organic contaminants in pilot-scale stormwater treatment systems*; Water Research Foundation; Water Environment & Reuse Foundation; U.S. Environmental Protection Agency: U.S.A., 2017.
101. Zhang, Y.; Zhu, H.; Szewzyk, U.; Lübbecke, S.; Uwe Geissen, S., Removal of emerging organic contaminants with a pilot-scale biofilter packed with natural manganese oxides. *Chem. Eng. J.* **2017**, *317*, 454-460.
102. Park, J. W.; Dec, J.; Kim, J. E.; Bollag, J. M., Effect of humic constituents on the transformation of chlorinated phenols and anilines in the presence of oxidoreductive enzymes or birnessite. *Environ. Sci. Technol.* **1999**, *33*, (12), 2028-2034.
103. Lin, K.; Liu, W.; Gan, J., Reaction of tetrabromobisphenol A (TBBPA) with manganese dioxide: Kinetics, products, and pathways. *Environ. Sci. Technol.* **2009**, *43*, (12), 4480-4486.
104. Shaikh, N.; Taujale, S.; Zhang, H.; Artyushkova, K.; Ali, A. S.; Cerrato, J. M., Spectroscopic investigation of interfacial interaction of manganese oxide with triclosan, aniline, and phenol. *Environ. Sci. Technol.* **2016**, *50*, (20), 10978-10987.
105. Balgooyen, S.; Campagnola, G.; Remucal, C. K.; Ginder-Vogel, M., Impact of bisphenol A influent concentration and reaction time on MnO₂ transformation in a stirred flow reactor. *Environ. Sci. Process. Impacts* **2019**, *21*, (1), 19-27.
106. Chirkst, D. E.; Cheremisina, O. V.; Sulimova, M. A.; Kuzhaeva, A. A.; Zgonnik, P. V., Kinetics of oxidation of phenol with manganese dioxide. *Russian J. Gen. Chem.* **2011**, *81*, (4), 704-709.
107. Balgooyen, S. Manganese oxide structure and transformation during oxidation of phenolic contaminants. University of Wisconsin-Madison, 2019.
108. Ukrainczyk, L.; McBride, M. B., Oxidation and dechlorination of chlorophenols in dilute aqueous suspensions of manganese oxides - reaction products. *Environ. Toxicol. Chem.* **1993**, *12*, (11), 2015-2022.
109. Ulrich, H. J.; Stone, A. T., Oxidation of chlorophenols adsorbed to manganese oxide surfaces. *Environ. Sci. Technol.* **1989**, *23*, (4), 421-428.
110. Ukrainczyk, L.; McBride, M. B., Oxidation of phenol in acidic aqueous suspensions of manganese oxides. *Clays Clay Miner.* **1992**, *40*, (2), 157-166.
111. Chang Chien, S. W.; Chen, H. L.; Wang, M. C.; Seshaiyah, K., Oxidative degradation and associated mineralization of catechol, hydroquinone and resorcinol catalyzed by birnessite. *Chemosphere* **2009**, *74*, (8), 1125-1133.

112. Zhao, L.; Yu, Z.; Peng, P.; Huang, W.; Dong, Y., Oxidative transformation of tetrachlorophenols and trichlorophenols by manganese dioxide. *Environ. Toxicol. Chem.* **2009**, *28*, (6), 1120-1129.
113. Stone, A. T., Reductive dissolution of manganese(III/IV) oxides by substituted phenols. *Environ. Sci. Technol.* **1987**, *21*, (10), 979-988.
114. Tran, T. H.; Labanowski, J.; Gallard, H., Adsorption and transformation of the anthelmintic drug niclosamide by manganese oxide. *Chemosphere* **2018**, *201*, 425-431.
115. Laha, S.; Luthy, R. G., Oxidation of aniline and other primary aromatic amines by manganese dioxide. *Environ. Sci. Technol.* **1990**, *24*, (3), 363-373.
116. Salter-Blanc, A. J.; Bylaska, E. J.; Lyon, M. A.; Ness, S. C.; Tratnyek, P. G., Structure-activity relationships for rates of aromatic amine oxidation by manganese dioxide. *Environ. Sci. Technol.* **2016**, *50*, (10), 5094-5102.
117. Makino, T.; Takahashi, Y.; Sakurai, Y.; Nanzyo, M., Influence of soil chemical properties on adsorption and oxidation of phenolic acids in soil suspension. *Soil Sci. Plant Nutr.* **1996**, *42*, (4), 867-879.
118. Stone, A. T.; Morgan, J. J., Reduction and dissolution of manganese(III) and manganese(IV) oxides by organics: 2. Survey of the reactivity of organics. *Environ. Sci. Technol.* **1984**, *18*, (8), 617-24.
119. Canonica, S.; Tratnyek, P. G., Quantitative structure-activity relationships for oxidation reactions of organic chemicals in water. *Environ. Toxicol. Chem.* **2003**, *22*, (8), 1743-1754.
120. Colon, D.; Weber, E. J.; Baughman, G., Sediment-associated reactions of aromatic amines 2. QSAR development. *Environ. Sci. Technol.* **2002**, *36*, 2443-2450.
121. Zhang, S.; Gutierrez, L.; Niu, X. Z.; Qi, F.; Croue, J. P., The characteristics of organic matter influence its interfacial interactions with MnO₂ and catalytic oxidation processes. *Chemosphere* **2018**, *209*, 950-959.
122. Ding, Y.; Shi, Z.; Ye, Q.; Liang, Y.; Liu, M.; Dang, Z.; Wang, Y.; Liu, C., Chemodiversity of soil dissolved organic matter. *Environ. Sci. Technol.* **2020**, *54*, (10), 6174-6184.
123. Polubesova, T.; Chefetz, B., DOM-affected transformation of contaminants on mineral surfaces: A review. *Crit. Rev. Environ. Sci. Technol.* **2014**, *44*, (3), 223-254.
124. Subdiaga, E.; Orsetti, S.; Haderlein, S. B., Effects of sorption on redox properties of natural organic matter. *Environ. Sci. Technol.* **2019**, *53*, (24), 14319-14328.
125. Walpen, N.; Getzinger, G. J.; Schroth, M. H.; Sander, M., Electron-donating phenolic and electron-accepting quinone moieties in peat dissolved organic matter: Quantities and redox transformations in the context of peat biogeochemistry. *Environ. Sci. Technol.* **2018**, *52*, (9), 5236-5245.
126. McKay, G., Emerging investigator series: Critical review of photophysical models for the optical and photochemical properties of dissolved organic matter. *Environ. Sci. Process. Impacts* **2020**, *22*, (5), 1139-1165.
127. Stuckey, J. W.; Goodwin, C.; Wang, J.; Kaplan, L. A.; Vidal-Esquivel, P.; Beebe, T. P., Jr.; Sparks, D. L., Impacts of hydrous manganese oxide on the retention and lability of dissolved organic matter. *Geochem. Trans.* **2018**, *19*, (1), 6.
128. Aiken, G. R.; Hsu-Kim, H.; Ryan, J. N., Influence of dissolved organic matter on the environmental fate of metals, nanoparticles, and colloids. *Environ. Sci. Technol.* **2011**, *45*, (8), 3196-201.

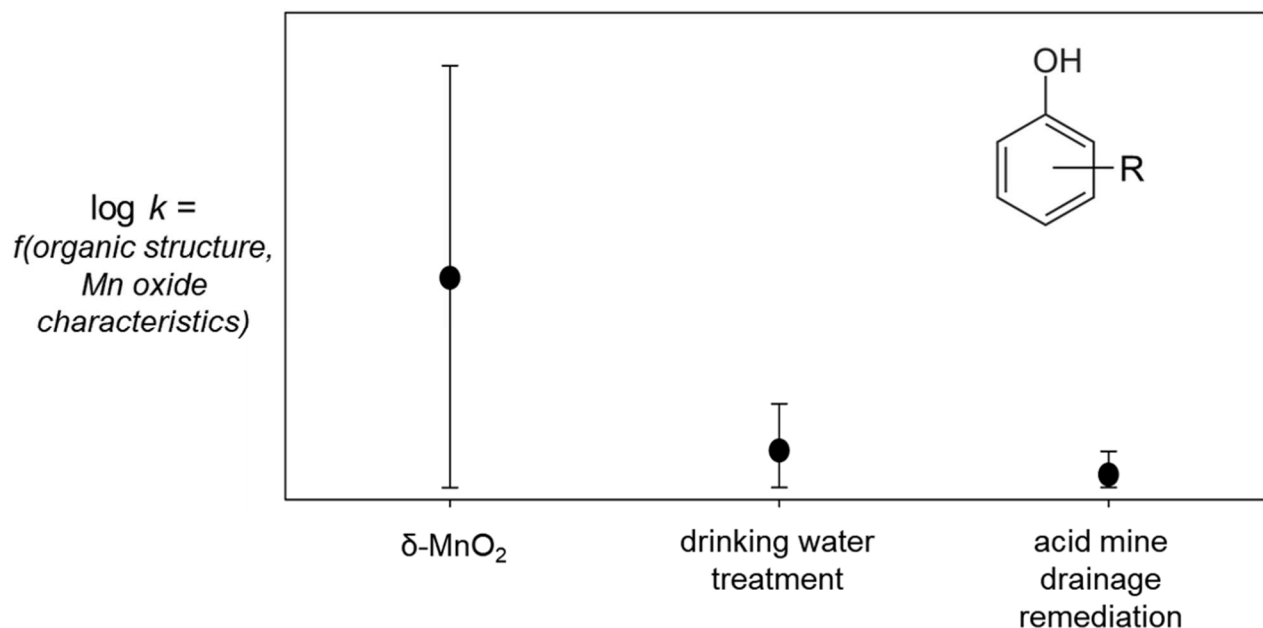
129. Taujale, S.; Baratta, L. R.; Huang, J.; Zhang, H., Interactions in ternary mixtures of MnO₂, Al₂O₃, and natural organic matter (NOM) and the impact on MnO₂ oxidative reactivity. *Environ. Sci. Technol.* **2016**, *50*, (5), 2345-2353.
130. Philippe, A.; Schaumann, G. E., Interactions of dissolved organic matter with natural and engineered inorganic colloids: A review. *Environ. Sci. Technol.* **2014**, *48*, (16), 8946-8962.
131. Hawkes, J. A.; D'Andrilli, J.; Agar, J. N.; Barrow, M. P.; Berg, S. M.; Catalán, N.; Chen, H.; Chu, R. K.; Cole, R. B.; Dittmar, T.; Gavard, R.; Gleixner, G.; Hatcher, P. G.; He, C.; Hess, N. J.; Hutchins, R. H. S.; Ijaz, A.; Jones, H. E.; Kew, W.; Khaksari, M.; Palacio Lozano, D. C.; Lv, J.; Mazzoleni, L. R.; Noriega-Ortega, B. E.; Osterholz, H.; Radoman, N.; Remucal, C. K.; Schmitt, N. D.; Schum, S. K.; Shi, Q.; Simon, C.; Singer, G.; Sleighter, R. L.; Stubbins, A.; Thomas, M. J.; Tolic, N.; Zhang, S.; Zito, P.; Podgorski, D. C., An international laboratory comparison of dissolved organic matter composition by high resolution mass spectrometry: Are we getting the same answer? *Limnol. Oceanogr. Methods* **2020**, *18*, (6), 235-258.
132. Wagner, S.; Riedel, T.; Niggemann, J.; Vahatalo, A. V.; Dittmar, T.; Jaffe, R., Linking the molecular signature of heteroatomic dissolved organic matter to watershed characteristics in world rivers. *Environ. Sci. Technol.* **2015**, *49*, (23), 13798-13806.
133. Zhang, Y.; Yue, D.; Wang, X.; Song, W., Mechanism of oxidation and catalysis of organic matter abiotic humification in the presence of MnO₂. *J. Environ. Sci. (China)* **2019**, *77*, 167-173.
134. Nebbioso, A.; Piccolo, A., Molecular characterization of dissolved organic matter (DOM): A critical review. *Anal. Bioanal. Chem.* **2013**, *405*, (1), 109-124.
135. Maizel, A. C.; Remucal, C. K., Molecular composition and photochemical reactivity of size-fractionated dissolved organic matter. *Environ. Sci. Technol.* **2017**, *51*, (4), 2113-2123.
136. Hansen, A. M.; Kraus, T. E. C.; Pellerin, B. A.; Fleck, J. A.; Downing, B. D.; Bergamaschi, B. A., Optical properties of dissolved organic matter (DOM): Effects of biological and photolytic degradation. *Limnol. Oceanogr.* **2016**, *61*, (3), 1015-1032.
137. Chen, M.; Hur, J., Pre-treatments, characteristics, and biogeochemical dynamics of dissolved organic matter in sediments: A review. *Water Res.* **2015**, *79*, 10-25.
138. Dittmar, T., Reasons behind the long-term stability of dissolved organic matter. In *Biogeochemistry of Marine Dissolved Organic Matter*, 2015; 369-388.
139. Maizel, A. C.; Li, J.; Remucal, C. K., Relationships between dissolved organic matter composition and photochemistry in lakes of diverse trophic status. *Environ. Sci. Technol.* **2017**, *51*, (17), 9624-9632.
140. Minor, E. C.; Swenson, M. M.; Mattson, B. M.; Oyler, A. R., Structural characterization of dissolved organic matter: A review of current techniques for isolation and analysis. *Environ. Sci. Process. Impacts* **2014**, *16*, (9), 2064-2079.
141. Williams, C. J.; Yamashita, Y.; Wilson, H. F.; Jaffé, R.; Xenopoulos, M. A., Unraveling the role of land use and microbial activity in shaping dissolved organic matter characteristics in stream ecosystems. *Limnol. Oceanogr.* **2010**, *55*, (3), 1159-1171.
142. Lin, H.; Guo, L., Variations in colloidal DOM composition with molecular weight within individual water samples as characterized by flow field-flow fractionation and EEM-parafac analysis. *Environ. Sci. Technol.* **2020**, *54*, (3), 1657-1667.

143. Maizel, A. C.; Remucal, C. K., The effect of advanced secondary municipal wastewater treatment on the molecular composition of dissolved organic matter. *Water Res.* **2017**, *122*, 42-52.
144. Wilson, H. F.; Xenopoulos, M. A., Effects of agricultural land use on the composition of fluvial dissolved organic matter. *Nature Geoscience* **2008**, *2*, (1), 37-41.
145. Fimmen, R. L.; Cory, R. M.; Chin, Y.-P.; Trouts, T. D.; McKnight, D. M., Probing the oxidation–reduction properties of terrestrially and microbially derived dissolved organic matter. *Geochim. Cosmochim. Acta* **2007**, *71*, (12), 3003-3015.
146. Berg, S. M.; Whiting, Q. T.; Herrli, J. A.; Winkels, R.; Wammer, K. H.; Remucal, C. K., The role of dissolved organic matter composition in determining photochemical reactivity at the molecular level. *Environ. Sci. Technol.* **2019**, *53*, (20), 11725-11734.
147. Gucker, B.; Silva, R. C. S.; Graeber, D.; Monteiro, J. A. F.; Boechat, I. G., Urbanization and agriculture increase exports and differentially alter elemental stoichiometry of dissolved organic matter (DOM) from tropical catchments. *Sci. Total Environ.* **2016**, *550*, 785-792.
148. Charbonnet, J. A.; Duan, Y.; Sedlak, D. L., The use of manganese oxide-coated sand for the removal of trace metal ions from stormwater. *Environ. Sci. Water Res. Technol.* **2020**, *6*, (3), 593-603.
149. Pena, J.; Kwon, K. D.; Refson, K.; Bargar, J. R.; Sposito, G., Mechanisms of nickel sorption by a bacteriogenic birnessite. *Geochim. Cosmochim. Acta* **2010**, *74*, (11), 3076-3089.
150. Wang, Q.; Yang, P.; Zhu, M., Structural transformation of birnessite by fulvic acid under anoxic conditions. *Environ. Sci. Technol.* **2018**, *52*, (4), 1844-1853.
151. Forrez, I.; Carballa, M.; Verbeken, K.; Vanhaecke, L.; Ternes, T.; Boon, N.; Verstraete, W., Diclofenac oxidation by biogenic manganese oxides. *Environ. Sci. Technol.* **2010**, *44*, (9), 3449-54.
152. Im, J.; Prevatte, C. W.; Campagna, S. R.; Loffler, F. E., Identification of 4-hydroxycumyl alcohol as the major MnO₂-mediated bisphenol A transformation product and evaluation of its environmental fate. *Environ. Sci. Technol.* **2015**, *49*, (10), 6214-6221.
153. Rubert, K.; Pedersen, J. A., Kinetics of oxytetracycline reaction with a hydrous manganese oxide. *Environ. Sci. Technol.* **2006**, *40*, (23), 7216-7221.
154. Khatiwada, R.; Olivares, C.; Abrell, L.; Root, R. A.; Sierra-Alvarez, R.; Field, J. A.; Chorover, J., Oxidation of reduced daughter products from 2,4-dinitroanisole (DNAN) by Mn(IV) and Fe(III) oxides. *Chemosphere* **2018**, *201*, 790-798.
155. Lin, K.; Liu, W.; Gant, J., Oxidative removal of bisphenol A by manganese dioxide: Efficacy, products, and pathways. *Environ. Sci. Technol.* **2009**, *43*, (10), 3860-3864.
156. Lin, K.; Peng, Y.; Huang, X.; Ding, J., Transformation of bisphenol A by manganese oxide-coated sand. *Environ. Sci. Pollut. Res. Int.* **2013**, *20*, (3), 1461-1467.
157. Gao, J.; Hedman, C.; Liu, C.; Guo, T.; Pedersen, J. A., Transformation of sulfamethazine by manganese oxide in aqueous solution. *Environ. Sci. Technol.* **2012**, *46*, (5), 2642-2651.
158. Kekes, T.; Nika, M.-C.; Tsopeles, F.; Thomaidis, N. S.; Tzia, C., Use of δ -manganese dioxide for the removal of acetaminophen from aquatic environment: Kinetic – thermodynamic analysis and transformation products identification. *J. Environ. Chem. Eng.* **2020**, *8*, (6).

159. Pollock, T.; Mantella, L.; Reali, V.; deCatanzaro, D., Influence of tetrabromobisphenol A, with or without concurrent triclosan, upon bisphenol A and estradiol concentrations in mice. *Environ. Health Perspect.* **2017**, *125*, (8).
160. Li, Q.; Xie, L.; Jiang, Y.; Fortner, J. D.; Yu, K.; Liao, P.; Liu, C., Formation and stability of NOM-Mn(III) colloids in aquatic environments. *Water Res.* **2019**, *149*, 190-201.
161. Huangfu, X.; Jiang, J.; Ma, J.; Liu, Y.; Yang, J., Aggregation kinetics of manganese dioxide colloids in aqueous solution: Influence of humic substances and biomacromolecules. *Environ. Sci. Technol.* **2013**, *47*, (18), 10285-10292.
162. Allard, S.; Gutierrez, L.; Fontaine, C.; Croue, J. P.; Gallard, H., Organic matter interactions with natural manganese oxide and synthetic birnessite. *Sci. Total Environ.* **2017**, *583*, 487-495.
163. Graham, M. C.; Gavin, K. G.; Kirika, A.; Farmer, J. G., Processes controlling manganese distributions and associations in organic-rich freshwater aquatic systems: The example of Loch Bradan, Scotland. *Sci. Total Environ.* **2012**, *424*, 239-250.
164. Komada, T.; Burdige, D. J.; Li, H. L.; Magen, C.; Chanton, J. P.; Cada, A. K., Organic matter cycling across the sulfate-methane transition zone of the Santa Barbara basin, California borderland. *Geochim. Cosmochim. Acta* **2016**, *176*, 259-278.
165. Poulin, B. A.; Ryan, J. N.; Nagy, K. L.; Stubbins, A.; Dittmar, T.; Orem, W.; Krabbenhoft, D. P.; Aiken, G. R., Spatial dependence of reduced sulfur in Everglades dissolved organic matter controlled by sulfate enrichment. *Environ. Sci. Technol.* **2017**, *51*, (7), 3630-3639.
166. Gao, J.; Duan, X.; O'Shea, K.; Dionysiou, D. D., Degradation and transformation of bisphenol A in UV/sodium percarbonate: Dual role of carbonate radical anion. *Water Res.* **2020**, *171*.
167. Liu, J.; An, F.; Li, M.; Yang, L.; Wan, J.; Zhang, S., Efficient degradation of 2,4-dichlorophenol on activation of peroxymonosulfate mediated by MnO₂. *Bull. Environ. Contam. Toxicol.* **2021**.
168. Zhang, P.; Zhang, G.; Dong, J.; Fan, M.; Zeng, G., Bisphenol A oxidative removal by ferrate (Fe(VI)) under a weak acidic condition. *Sep. Purif. Technol.* **2012**, *84*, 46-51.
169. Zhou, K.; Zhang, J.; Xiao, Y.; Zhao, Z.; Zhang, M.; Wang, L.; Zhang, X.; Zhou, C., High-efficiency adsorption of and competition between phenol and hydroquinone in aqueous solution on highly cationic amino-poly(vinylamine)-functionalized GO-(o-MWCNTs) magnetic nanohybrids. *Chem. Eng. J.* **2020**, *389*.
170. Zou, S.; Zhang, B.; Yan, N.; Zhang, C.; Xu, H.; Zhang, Y.; Rittmann, B. E., Competition for molecular oxygen and electron donor between phenol and quinoline during their simultaneous biodegradation. *Process Biochem.* **2018**, *70*, 136-143.

Chapter 2

Organic structure and solid characteristics determine reactivity of phenolic compounds with synthetic and reclaimed manganese oxides



2.1 Collaboration and publishing information

This chapter was completed by Emma L. Trainer, Matthew Ginder-Vogel, and Christina K. Remucal. E. L. Trainer completed all laboratory experiments and data analyses. E. L. Trainer, M. Ginder-Vogel, and C.K. Remucal wrote the manuscript. This chapter is published in *Environmental Science: Water Research and Technology* **2020**, 6, 540-553.

2.2 Abstract

Manganese (Mn) oxides have been proposed for in situ treatment of organic (e.g., phenolic) contaminants, although little is known about the reactivity of reclaimed solids that might be used as alternatives to synthetic oxides. In this study, we investigate the impacts of phenol substituents and manganese oxide properties (e.g., surface area, iron substitution) on the kinetics and mechanism of this reaction. Reclaimed solids from acid mine drainage and drinking water treatment systems contain Mn(IV) and are capable of oxidizing phenolic contaminants, although their reactivity is 1–3 orders of magnitude slower than that of synthetic δ -MnO₂. Both electron transfer-limited and sorption-limited mechanisms occur in 29 phenols reacted with the three manganese oxide materials. This finding contrasts with the common assumption that the first one-electron transfer from the phenol to the manganese oxide is rate-limiting. The occurrence of both mechanisms has implications for the rates and products of phenol oxidation. Interestingly, the mechanism for a given phenol changes between solids. We attribute this observed mechanism shift primarily to phenolic substituent effects, with influences from the pH_{pzc} , surface area, and iron substitution of the manganese oxide materials. In addition, we investigate the predictive utility of quantitative structure–activity relationships, as these models have not been tested using complex reactants and non-synthetic manganese oxides. In-depth analysis and external validation measures indicate these common QSAR models are ineffective at predicting the behavior of complex contaminants or reactions with non-synthetic manganese oxides, and therefore have limited application for predicting contaminant oxidation by manganese oxides in environmental and engineered systems.

2.3 Introduction

Manganese (Mn) oxides (e.g., MnO_2) are ubiquitous, strong oxidants that control the fate of redox active inorganic (e.g., arsenic) and organic (e.g., anilines, phenols) contaminants¹⁻¹¹ in surface waters^{1,3} and soils.^{1,2,9,12-15} Mn oxides form naturally and are also generated as byproducts in water treatment systems that use pyrolusite filters to remove dissolved Mn and iron (Fe), as well as in acid mine drainage remediation systems that precipitate Mn on passive limestone or coir fiber beds.¹⁶⁻¹⁸ Mn oxides may coprecipitate with Fe and other non-Mn species (e.g., Zn, Al, silica) or comprise a fraction of a heterogeneous mixture, as in the case of natural soils. As a result, Mn oxides exhibit a wide range of characteristics (e.g., surface area, Mn oxidation state) that alter their reactivity compared to synthetic materials.^{2,4,7,19-21} Contaminants that react with Mn oxides are present in many anthropogenic systems that discharge to natural environments, where they are typically recalcitrant and often threaten ecosystem and human health.^{1,22-26} Therefore, Mn oxides have been proposed for passive, *in situ* treatment of contaminated waters. Such applications are particularly attractive for reclaimed solids as inexpensive alternatives for the treatment of phenolic contaminants in wastewater effluents, landfill leachates, or stormwater basins. However, there is a lack of research bridging well-controlled, microscopic studies with *in situ* macroscopic investigations.

Phenols react with manganese oxides through a series of one-electron transfers, first forming a phenoxy radical which can either desorb from the manganese surface reaction site and couple to form a polymeric product or undergo a second one-electron transfer to form benzoquinone-like products.^{1,6} This reaction has two potential rate-limiting steps: sorption of the phenolate ion to the manganese reaction site or the first one-electron transfer.^{1,6,27,28} The overall reaction mechanism, identified by the rate-limiting step, dictates both the rate of reaction and

final oxidation products (i.e., benzoquinone or polymeric products).^{1,29-31} The influence of reclaimed Mn oxide characteristics (e.g., surface area, Fe content) on the rates and mechanism of phenol oxidation are unknown.

The oxidation of organic compounds by Mn oxides is frequently investigated with a limited set of simple phenols and well-characterized synthetic manganese oxides (e.g., δ -MnO₂).^{6,11,27,31-41} These highly controlled studies then use quantitative structure activity relationships (QSARs) to describe trends in the reactivity of Mn(III/IV) oxides with anilines^{1,35,36,38} and phenols.^{1,6,42} QSARs are simple, linear models relating descriptive molecular parameters and structural properties to reactivity to predict reaction rate constants of related compounds. However, previous studies applying these linear models to predict organic oxidation rates by manganese oxides do not test the applicability in complex environmental systems. Notably, the acceptance of QSAR models is not grounded in external validation techniques, but rather on basic linear regression statistics. Importantly, there is a lack of data for isomeric sets of phenols (i.e., *ortho*-, *meta*-, and *para*-), complex phenols (e.g., triclosan, 17 β -estradiol), and non-synthetic manganese oxides.

In this study, phenols ranging in complexity from simple model compounds to complex contaminants and metabolites are reacted with synthetic δ -MnO₂ and two reclaimed manganese oxides to investigate how organic structural properties and solid phase characteristics mechanistically alter reactivity. In addition, we assess whether QSARs are a reliable enough predictive tool to overcome the complexities expected in environmental systems to which such QSAR models may be applied. To do this, we first compare the oxidation rates and rate-limiting steps of 29 phenols reacted with δ -MnO₂ and verify the results with kinetic models. Second, we react selected phenols with two reclaimed Mn oxides to determine the impact of Mn structural

changes on reactivity and oxidative mechanism. Finally, we construct QSARs using general and specific structural descriptors to assess their utility as a predictive tool for complex contaminants using external validation measures. This work combines complementary aqueous and solid-phase analyses to demonstrate how both complex contaminants and non-synthetic solids mechanistically alter phenol degradation by manganese oxides, with implications for oxidation rates and products. In addition, we show that previous literature QSARs built for this system have little predictive utility outside of simple, well-controlled laboratory studies.

2.4 Experimental

2.4.1 Materials

Commercial chemicals were used as received (**Appendix A.1.1**). Phenol stock solutions were prepared in methanol and stored at 4 °C. Ultrapure water was supplied by a Milli-Q water purification system maintained at 18.2 MΩ·cm.

δ-MnO₂ was synthesized by a modified Murray method (**Appendix A.1.2**).⁴³ Drinking water treatment (DWT) solids were collected from a Mn removal system at Well 29 in Madison, WI, operated by Madison Water Utility. Acid mine drainage (AMD) remediation solids were collected by Hedin Environmental from a passive limestone Mn removal bed in western Pennsylvania.¹⁶ Both reclaimed solids were pre-equilibrated in pH 5.5 10 mM sodium acetate buffer over four days at 4 °C to remove carbonate phases and stabilize the solution pH prior to reaction with phenols.

2.4.2 Solid characterization

δ -MnO₂, DWT, and AMD starting materials were characterized to determine average manganese oxidation number (AMON) by X-ray absorption near edge spectroscopy (Mn K edge; 6532 eV).⁴⁴ Specific surface area was determined by Brunauer–Emmett–Teller measurements (Quantachrome Autosorb-1, nitrogen adsorbate; 30 °C). The solids were also characterized by X-ray diffraction (Rigaku Rapid II, Mo K α source; $\lambda = 0.7093$ Å) and scanning electron microscopy (LEO 1530, Schottky-type field-emission electron source). Sodium (δ -MnO₂) or trace metal (DWT and AMD solids) content was quantified by dissolution in HCl followed by inductively coupled plasma-optical emission spectrometry (ICP-OES; Perkin Elmer 4300). The pH of zero charge values (pH_{pzc}) were determined by rapid potentiometric titration.^{45,46} Details are provided in **Appendix A.2**.

2.4.3 Kinetic reactions

Triplicate batch reactions of each target phenol (10 μ M; <0.1% methanol) and Mn oxides (15 mg-Mn/L) were conducted in pH 5.5 10 mM sodium acetate buffer. Experiments with 4-*n*-nonylphenol used a concentration of 1 μ M with 1.5 mg-Mn/L due to its lower solubility.⁴⁷ All experiments were conducted in the dark. This pH and buffer were selected for several reasons. Although pH 5.5 is low for most natural waters, it is relevant for AMD systems. More importantly, this pH is below the phenolic acid dissociation constant (pK_a) of all 29 phenols (**Table A.8**) so that the speciation of the phenolic functional group is constant. Furthermore, this lower pH value is also correlated with faster oxidation kinetics, enabling rate determination of less reactive solids.^{1,6,11,32} Finally, unlike Good's buffers and phosphate,^{1,30,32,35,48,49} sodium acetate does not reduce or complex δ -MnO₂ (**Appendix A.3**).

The reactors were continuously stirred for up to ten days. Two aliquots were collected at each timepoint to quantify the parent phenol concentration of filtered (0.2 μM PTFE) and quenched (5:1 ascorbic acid:Mn molar ratio) samples. Filtering removes all solids from the filtered aliquots, including any sorbed parent phenol. In contrast, the Mn oxide and all sorbed species are dissolved into solution in the acid quenched aliquots. Organic compound concentrations were quantified by high performance liquid chromatography (HPLC) and used to calculate initial pseudo-first-order rate constants (**Appendix A.4**). The sorbed fraction of the parent compounds was calculated at each timepoint as the difference between the total dissolved (i.e., quenched) and aqueous (i.e., filtered) concentrations. Compounds with observed maximum sorption <10% or with error greater than the average measured sorption were classified as having reaction rates that were sorption-limited, as discussed in **Appendix A.5**. The phenols with a maximum observed percent sorption >10% were classified as undergoing electron transfer-limited reactions.

Fifteen phenols with oxidation rates limited by either electron transfer or sorption and that represent a range of structural complexity were selected for experiments with DWT and AMD solids. Solids were added at a Mn normalized concentration of 15 mg-Mn L⁻¹. Quenched aliquots were subsequently filtered through 0.2 μm PTFE filters to remove residual solids prior to analysis.

2.4.4 Kinetic modeling

Calculated rate constants for the electron transfer-limited and sorption-limited reaction pathways (k' and k'' , respectively) were fit to quenched experimental data, as described previously.²⁸ The calculated pseudo-first-order rate constant (k' or k'' multiplied by the initial

concentration) that gave a higher R^2 fit to the experimental loss curve was selected for each compound and compared to observed pseudo-first-order rate constants for phenolic oxidation by δ -MnO₂. Details are provided in **Appendix A.6**.

2.4.5 Quantitative structure activity relationships

Hammett constants (σ) were summed from tabulated substituent group values.⁵⁰⁻⁵³ These constants were only available for sixteen phenols to avoid the assumption that *ortho*-substitutions are adequately described by *para*-substituted values. Acid dissociation constants were calculated using ChemAxxon software;⁵⁴ the lowest predicted phenolic pK_a values were used.

Theoretical molecular calculations were computed with NWChem EMSL Arrows online API service⁵⁵ using density functional theory, 6-311++G(2d,2p) basis, M06-2x cross correlation, and COSMO-SMD solvation theory.^{38,42} Energy of the highest occupied molecular orbital (E_{HOMO}) values were calculated for each phenol species at pH 5.5. Oxidation energy of the first electron transfer (E_{ox}) was determined for the loss of the first electron from the parent phenol and corrected (E_{ox,corr.}) to values reported by Pavitt et al.⁴² (**Appendix A.7; Figure A.4**).⁵⁶ All pseudo-first-order rate constants were normalized to 4-chlorophenol to enable cross-study comparison. Normalized literature pseudo-first-order rate constants and QSAR descriptors were calculated in the same manner (**Table A.12**).

2.5 Results and discussion

2.5.1 Kinetics and mechanisms of oxidation by δ -MnO₂

We investigate the influence of increasingly complex organic structure on reaction rates and oxidation mechanism by reacting 29 phenols with δ -MnO₂. These phenols include a range of

functional group placements (i.e., *ortho*-, *meta*-, or *para*-substitutions, including three isomeric sets), electron-withdrawing versus electron-donating substituents, and structural complexity (Table A.2). Initial pseudo-first-order rate constants are fit to both total and dissolved kinetic data (i.e., quenched and filtered samples; Table A.6). Percent sorption is calculated to experimentally determine the observed rate-limiting step (Appendix A.5).

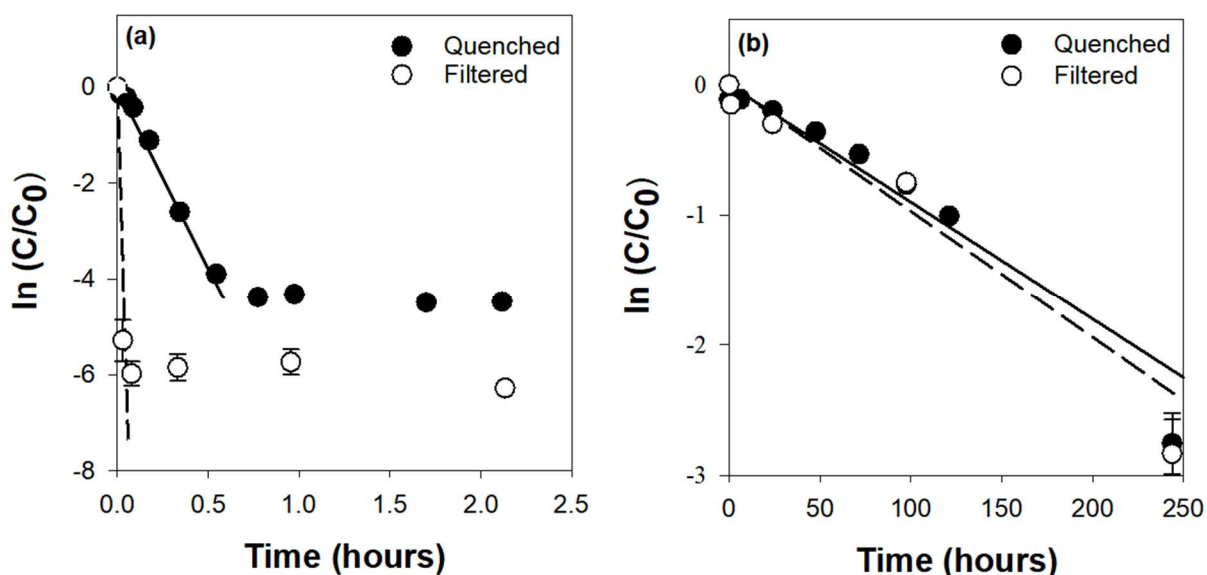


Figure 2.1. Kinetic data and pseudo-first-order rate fittings for (a) triclosan and (b) 4,4'-dihydroxybiphenyl based on quenched and filtered samples.

Sixteen compounds (e.g., triclosan; **Figure 2.1a**) rapidly sorb to δ -MnO₂ over the initial reaction period and have a maximum observed percent sorption >13%. The degradation rates of these compounds, determined from quenched reactions, are on average 5 times slower than their removal rate from solution, indicating that sorption of these phenolic compounds to the mineral surface is more rapid than the first one-electron transfer.^{1,6,27,28} These compounds are rapidly removed from solution by sorption to the treatment media (δ -MnO₂), while overall degradation of the parent compound is limited by the rate of electron transfer with the Mn oxide. In contrast,

degradation of the remaining thirteen phenols is sorption-limited since they show no evidence of accumulation on the manganese surface (**Table A.6**).^{1,6,27,28} For these compounds (e.g., 4,4'-dihydroxybiphenyl, **Figure 2.1b**), the measured sorbed concentration is <8% and the average ratio of filtered to quenched rate constants is 1, indicating that the total removal rate equals the rate of oxidation. Thus, these thirteen species are degraded at the same rate as they partition to the manganese surface, so the observed removal from solution is attributable to oxidation.

The rate-limiting step was also investigated by fitting the data with a previously developed kinetic model from Zhang et al.²⁸ Modeled rate-limiting steps agree with the observed rate-limiting step for 24 of the 29 phenols. 4-Cresol, 2-chlorophenol, and 4-*n*-nonylphenol are experimentally determined to be electron transfer-limited but are better fit by the modeled sorption-limited $k'' \cdot C_0$ (**Appendix A.6**). The opposite trend is observed for 2-nitrophenol and 4,4'-dihydroxybiphenyl. In the cases where the model and experimental rates disagree, minimal differences between the R^2 fit of modeled electron transfer-limited (i.e., k') and sorption-limited (i.e., $k'' \cdot C_0$) rate constants are observed (i.e., difference in R^2 ranging between 8.7×10^{-6} and 4.7×10^{-2} ; **Table A.7**). This mechanistic model supports the 10% sorption cutoff used in this study and the occurrence of both rate-limiting steps within the suite of 29 phenols reacted with δ -MnO₂ (**Appendix A.5**).

Compounds with larger observed rate constants (i.e., faster oxidation kinetics) are overall fit better by k' and are electron transfer-limited, while phenols with smaller observed rate constants are better fit by $k'' \cdot C_0$ and are sorption-limited (**Table A.7**). Interestingly, isomeric differences in the rate-limiting step occur for chlorophenols, but not for nitrophenols or hydroxybenzoates. For example, 3-chlorophenol is sorption-limited, while 2- and 4-chlorophenol are electron transfer-limited. While each of these isomeric substitutions (i.e., COO⁻, NO₂, Cl) are

electron withdrawing, halogens have unique interactions (e.g., orbital overlap) with the aromatic pi-bond system which may explain why chlorophenols exhibit isomeric effects not demonstrated by the nitro- or carboxylate-substituted phenol isomers. Previous studies also report isomeric effects for chlorophenols (i.e., primarily that *meta*-chlorophenols react slower than *ortho*- or *para*-chlorophenols) and that reaction rates for all studied chlorophenols increased with increased sorption to MnO₂ surfaces,^{11,57} which we attribute here to the differences in the reaction mechanism between these isomers. However, there are no clear trends in substituent group effects on oxidation mechanism within the overall dataset. Similarly, there are no trends with the analyzed partitioning and structural properties of each compound, including the distribution ratio between octanol and water (log D_{ow}), solubility, organic carbon partitioning coefficient (log K_{oc}), or van der Waals' volume (**Table A.8**).

The occurrence of both electron transfer- and sorption-limited mechanisms within the 29 phenols reacted with δ-MnO₂ illustrates that contaminant structure controls both the mechanism and degradation kinetics when reacted with a given oxidant. This observation disagrees with the commonly accepted mechanism in which the rate of phenolic compound oxidation by manganese oxides is electron transfer-limited.^{1,6,27,28} Although evaluation of the oxidation products of the large number of phenols is beyond the scope of this study, the divergence in rate-limiting steps suggests that the relative importance of benzoquinone and polymeric degradation products will also vary across the studied phenols.

2.5.2 Phenol degradation by reclaimed manganese oxides

Manganese oxides that form naturally (e.g., Mn rich soils or biogenic solids) or in engineered systems are potential alternatives to synthetic minerals for passive *in situ* contaminant

treatment systems. Natural and reclaimed solids are often impure, heterogenous phases containing manganese, iron, and/or other trace metals. They differ from δ -MnO₂ in crystallinity, bulk surface area and charge, and heteroatom interactions.^{1,2,5-9,13,21} Therefore, these oxides likely interact with organic contaminants differently than commonly studied synthetic materials. However, it is not clear which solid-phase characteristics have the greatest impact on contaminant degradation or how the phenol oxidation mechanisms change across manganese oxide materials as the only studies comparing these factors across Mn oxides use synthetic materials.^{27,34}

To determine whether organic structure or solid characteristics control reactivity, we compare the degradation rates and mechanisms of fifteen selected phenols reacted with δ -MnO₂ and reclaimed manganese oxides from drinking water treatment and acid mine drainage remediation systems. The selected phenols vary in reactivity, identified reaction mechanisms with δ -MnO₂, and substitution. The fifteen phenols include contaminants (e.g., estrone, bisphenol A, and triclosan) and the full isomeric set of chlorophenols (**Table A.14**). The three solids (i.e., δ -MnO₂, AMD, and DWT) are normalized in reactions to 15 mg-Mn L⁻¹ and represent a range of bulk composition and structural properties (**Appendix A.2**).^{1,2,5-9,13,14,21}

δ -MnO₂ is a poorly crystalline layered mineral; it is a well-characterized, highly reactive proxy for birnessite.^{1,32,34,43,58} In contrast, the AMD and DWT solids are heterogenous (**Figure A.1**) and contain 0.2 and 42.9 weight % Fe, respectively, along with other trace metal impurities (e.g., up to 7.9 wt % Al; **Table A.3**). The bulk composition of AMD solids also includes crystalline phases (e.g., quartz, silica; **Figure 2.2**). The surfaces of these materials highlight the variation between synthetic and non-synthetic materials. δ -MnO₂ has a higher N₂-BET surface area than DWT or AMD solids (191, 22, and 6 m² g⁻¹, respectively). In contrast, the DWT and

AMD solids have higher average pH_{pzc} values than $\delta\text{-MnO}_2$ (9.9 and 6.2 versus 2.2, respectively), corresponding to differences in the net surface charge at the reaction pH of 5.5. All three solids in this study have AMON values around 3.8 (**Table 2.1**), so reactivity differences are indicative of bulk composition and surface characteristics, rather than Mn oxidation state.^{1,5-7,34,58}

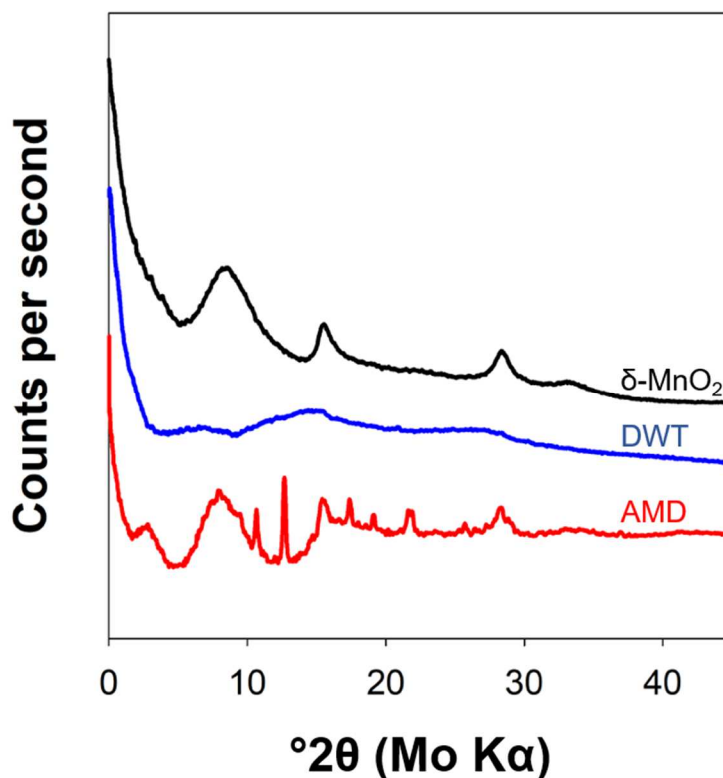


Figure 2.2. X-ray diffraction patterns of $\delta\text{-MnO}_2$, drinking water treatment (DWT), and acid mine drainage (AMD) solids.

Based on the surface areas of the reclaimed oxides, these materials are expected to be less reactive than $\delta\text{-MnO}_2$. Measurable oxidation did occur for each of the fifteen phenolic compounds when exposed to the reclaimed solids, demonstrating the potential for natural and reclaimed solid reuse for passive *in situ* treatment applications. Overall, DWT solids are 1 – 2 orders of magnitude less reactive and AMD solids are 1 – 3 orders of magnitude less reactive than $\delta\text{-MnO}_2$ (**Figure 2.3**; **Table A.6**). For example, the quenched, pseudo-first-order oxidation

rate constant for estrone is 6.0 hour^{-1} with $\delta\text{-MnO}_2$, 0.09 hour^{-1} with DWT solids, and 0.01 hour^{-1} with AMD solids.

Table 2.1. Solid phase characteristics of $\delta\text{-MnO}_2$, DWT, and AMD solids.

	% Mn	% Fe	Average Mn oxidation number	Surface area ($\text{m}^2 \text{ g}^{-1}$)	Point of zero charge	Surface charge at pH 5.5
$\delta\text{-MnO}_2$	63 ± 6	0 ± 0	3.8 ± 0.2	191	2.19 ± 0.06	Negative
DWT	8.7 ± 0.8	43 ± 2	3.82 ± 0.04	22	9.9 ± 0.2	Positive
AMD	42.8 ± 0.8	0.2 ± 0.2	3.79 ± 0.04	6	6.2 ± 0.3	Circumneutral

These observed rate constants are of similar magnitude to other studies comparing synthetic and natural soil Mn and Fe oxides. For example, one study reports 1 – 2 orders of magnitude lower percent loss for six phenolic acids reacted with Mn- and Fe-rich Palouse soil compared to MnO_2 and $\text{Fe}(\text{OH})_3$.⁵⁹ Similarly, catechol degrades at a rate of 0.04 to 1.8 hr^{-1} with four Mn- and Fe-containing soils at pH 8 compared to about 0.1 hr^{-1} with a commercial Mn(IV) oxide.⁶⁰ These soil rates include microbial influences (e.g., re-oxidation of reduced Mn and direct microbial catechol degradation), which may explain the ten-fold faster rates of some soils compared to commercial Mn(IV). Another study reports equal rates of diclofenac oxidation (0.2 hr^{-1}) for a biogenic manganese oxide and $\delta\text{-MnO}_2$ at pH 4.7.⁶¹ While these studies do not directly assess the reactivity of reclaimed materials and include a small number of target compounds, the results for biogenic and natural soil Mn oxides are similar to our finding that the reclaimed oxides degrade phenols 1 – 3 orders of magnitude slower than $\delta\text{-MnO}_2$ without additional microbial influences.

The rate-limiting step is different between the three different manganese oxides for twelve of the fifteen phenols (**Figure 2.3; Table A.14**). For example, 4,4'-dihydroxybiphenyl, 4-*tert*-octylphenol, 3-chlorophenol, and 3-nitrophenol are sorption-limited with δ -MnO₂ and electron transfer-limited with both reclaimed solids. In contrast, eight phenols (e.g., triclosan, phenol, 2-chlorophenol) switch from an electron transfer-limited reaction with δ -MnO₂ to a sorption-limited reaction with one or both reclaimed solids. The rate-limiting step does not change for the three remaining phenols; 4-nitrocatechol and 4-chlorophenol remain electron transfer-limited and 2-nitrophenol remains sorption-limited across the three solids. There are no clear trends in reaction mechanism with phenolic structure across the three solids.

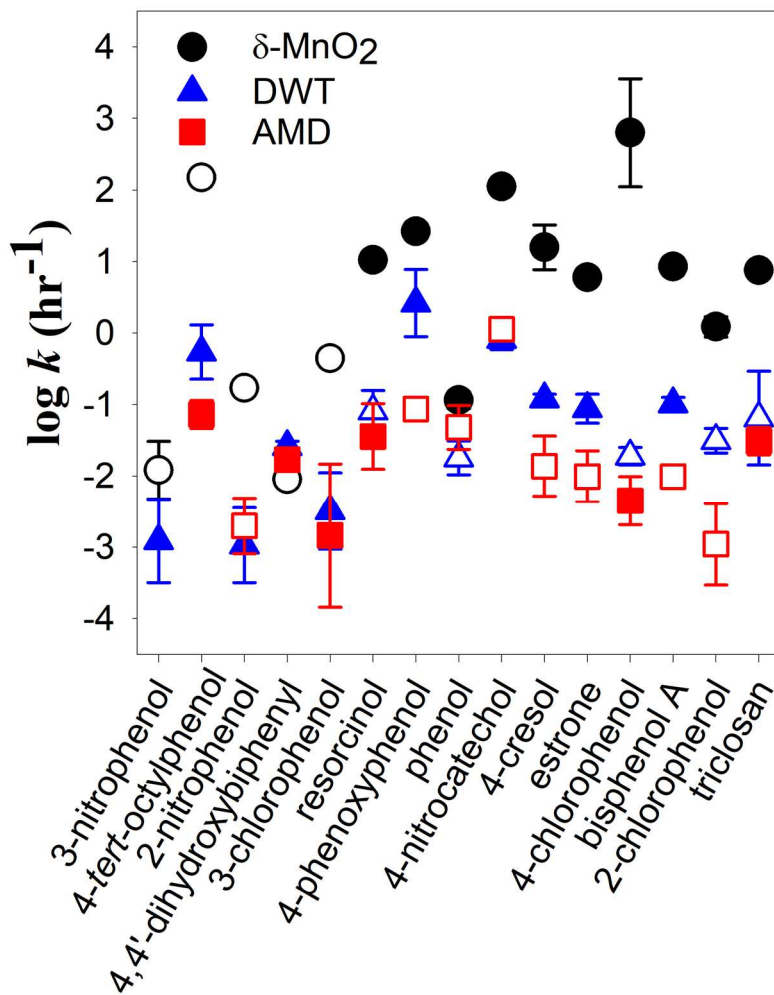


Figure 2.3. Initial pseudo-first-order log k values for reactions of 15 phenolic compounds with $\delta\text{-MnO}_2$, drinking water treatment solids, and acid mine drainage remediation solids. Filled points are electron transfer-limited and hollow points are sorption-limited. Error bars indicate the standard deviation of triplicate data.

The changes in reaction mechanism cannot be explained by a single parameter related to either the organic compound structure (e.g., isomeric substitution, partitioning coefficients; **Table A.8**) or Mn oxide surface chemistry (e.g., surface area, pH_{pzc} ; **Table 2.1**). Instead, the variability in rate-limiting steps implies that unique interactions between each individual pair of solid and organic-phase reactants influence the relative sorption and electron transfer kinetics controlling the rate-limiting process. For example, although 2- and 4-chlorophenol are both electron transfer-limited with $\delta\text{-MnO}_2$, the differences in *ortho*- and *para*-substitution cause

these compounds to react differently with the reclaimed solids. The reaction of 2-chlorophenol is sorption-limited and 4-chlorophenol is electron transfer-limited with both AMD and DWT solids. While this may be attributed to the unique inductive and steric hindrance effects of 2-chlorophenol, these effects do not explain why triclosan, phenol, and resorcinol share the same rate limitation pattern (**Figure 2.3**). This is a novel result overlooked by research on a single contaminant or single solid which suggest simple explanations for shifts in observed mechanisms.^{27,28,34,39} Past work identifies AMON,^{27,34,62,63} surface area,^{34,62,63} or pH_{pzc} ^{34,63} as the dominant reactivity-controlling characteristics of synthetic manganese oxides with limited sets of organic compounds, while our study demonstrates that organic structure must also be considered.

Since the rate-limiting step is both compound- and solid-dependent, we analyze the relative number of sorption-limited and electron transfer-limited reactions with each Mn oxide (**Figure 2.3**) to identify which solid characteristics are most important. With $\delta\text{-MnO}_2$, 11 of the 15 phenols are electron transfer-limited, despite electrostatic repulsion of the phenolate anion ($\text{pH}_{\text{pzc}} = 2.2$; **Table 2.1**). Thus, the relatively fast sorption kinetics are likely due to the high surface area of $\delta\text{-MnO}_2$ ($191 \text{ m}^2 \text{ g}^{-1}$). In contrast, only six phenols are electron transfer-limited with AMD solids even though the circumneutral net surface charge ($\text{pH}_{\text{pzc}} = 6.2$) should be more attractive toward the phenolate anion than $\delta\text{-MnO}_2$. The reactive surface area of AMD solids ($6 \text{ m}^2 \text{ g}^{-1}$) is 30 times smaller than that of $\delta\text{-MnO}_2$, which may explain the shift towards sorption-limited kinetics despite increased electrostatic attraction. AMD solids also contain incorporated crystalline phases (e.g., quartz, silica; **Figure 2.2**) and trace metal impurities (e.g., Zn, Ni; **Table A.3**), which decrease the concentration of available manganese surface sites and further slow the relative sorption rate.

Ten phenols are electron transfer-limited with DWT solids. Although the relatively low surface area ($22 \text{ m}^2 \text{ g}^{-1}$) is similar to AMD solids, the large Fe content and resulting high pH_{pzc} (i.e., 9.9; **Table 2.1**) enhance sorption to the bulk surface. Fe surface sites have a higher sorption potential and lower oxidation potential than Mn, so phenolic compounds may favorably sorb to these Fe surface sites without undergoing oxidation by $\text{Fe}^{2,5,10,13,14,41,64}$. This change in surface chemistry favors sorption and shifts organic oxidation by the bulk solid towards an electron transfer-limited mechanism.

In summary, electrostatic interactions, surface area, and the presence of impurities control general reactivity and influence the rate-limiting step across the Mn oxides. Bulk characteristics (e.g., elemental composition, crystallinity) appear to have a larger effect on the rate of the first one-electron transfer, while the surface characteristics (e.g., surface area, pH_{pzc}) influence the rate of sorption. These properties also relate to the decrease in kinetics observed between $\delta\text{-MnO}_2$ and the reclaimed solids because each of the selected 15 phenols are 1 – 3 orders of magnitude less reactive with DWT and AMD solids than with $\delta\text{-MnO}_2$. The reclaimed solids have a lower Mn content, higher Fe and impurity content, smaller surface area, and larger pH_{pzc} values than $\delta\text{-MnO}_2$. Additionally, the DWT solids are generally more reactive than the AMD solids (**Figure 2.3**), which implies that larger surface area and/or lower crystallinity may be the primary driver of the observed oxidation rate trends between the three solids. Although the role of organic compound structure cannot be linked to a specific structural descriptor, it contributes to some of the variability in reactivity, as discussed below.

2.5.3 QSAR analysis for synthetic and reclaimed Mn oxides

To assess the extent to which organic structure controls reactivity across the three studied Mn oxides, we analyze differences between structural groups and solid oxidants using quantitative structure activity relationships. Linear QSARs relating normalized rate constants to organic structural properties are successful at predicting the reactivity of *meta*- and *para*-substituted phenols and anilines with synthetic manganese oxides,^{1,6,36,38,42,65} yet their utility outside of reactions between synthetic Mn oxides and simply substituted model compounds is untested. We evaluate the strength of QSARs with 27 phenols; hydroquinone and 2,5-dihydroxybenzoate are excluded from QSAR development due to indeterminable quenched rate constants (**Appendix A.4**). The 27 phenols are separated into three groups. The first group includes *meta*- and *para*-substituted phenols, which are commonly studied and for which structural descriptors are readily available. The second group includes *ortho*-substituted phenols, which are more difficult to accurately describe with general molecular descriptors (e.g., Hammett constants) due to intramolecular interactions and steric hinderance.^{6,38,65} *Ortho*-substituted compounds are less common in mechanistic studies of phenol oxidation by manganese oxides and studies that include these compounds typically focus on substituted chlorophenols.^{6,11,31,37} The final group includes complex phenols, which are also difficult to predict by molecular descriptors as they contain multiple aromatic rings or large, branched functional groups. These phenols are not typically included in multi-compound reactivity studies but are common environmental contaminants.^{1,6,11,36-38}

General molecular descriptors used in the development of QSARs include Hammett constants (σ) and pK_a values.^{36,50-53,65} Hammett constants are available for sixteen compounds, while predicted pK_a values are calculated for all 27 phenols. Electron-withdrawing substituents

(denoted by positive σ and correspondingly low pK_a) decrease electron density on the phenolic moiety, making the phenol group less susceptible to oxidation.^{36,38,50,65} Thus, phenolic oxidation rates are expected to increase with decreasing Hammett constants and increasing pK_a .^{36,38,51,65} QSARs developed with Hammett constants and pK_a values for δ -MnO₂ follow the expected trends (**Figures 2.4a** and **2.4b**), although the goodness of the fit (R^2 and p-values) of the linear relationship decreases as phenol complexity increases (**Table A.9**). QSARs developed with Hammett constants inherently select for simple compounds due to the lack of tabulated values for complex substituents, therefore Hammett constants are not a realistic descriptor to predict complex contaminant reactivity, despite the strong linear regression ($p = 0.00022$ for *meta*- and *para*-phenols; **Figure 2.4a**). The pK_a -dependent QSAR also fails to accurately account for complex substituents. Although the regressions are significant at $p < 0.05$, the linear relationship contains visible scatter even for *meta*- and *para*-substituted compounds (**Figure 2.4b**; **Table A.9**).

Unlike general structural properties determined from substituent groups, the energy of the highest occupied molecular orbital (E_{HOMO}) and corrected one-electron oxidation potential ($E_{ox,corr.}$) values are calculated for the molecule of interest and account for intramolecular interactions not explained by Hammett constants and pK_a values. This study uses NWChem's open source API⁵⁵ to calculate E_{HOMO} and E_{ox} values for 24 and 23 phenols, respectively. This computational database is an ideal tool for molecular contaminant fate predictions than traditional software due to its increased accessibility, but it does not currently contain all 27 species. E_{HOMO} is related to the inverse of ionization potential, so compounds with larger values will lose an electron more easily and have faster oxidation rate constants.^{38,65} The strong linear regression (**Figure 2.4c**; $p = 1.3 \times 10^{-5}$ for *meta*- and *para*-substituted phenols) follows the

expected positive trend. In contrast, higher $E_{\text{ox,corr.}}$ is significantly correlated with lower oxidation rate constants (**Figure 2.4d**; **Table A.9**) as the increasing energy required for oxidation of the first electron slows reaction rates with Mn oxides.^{36,38,42,56,65} This correlation is not as strong as the correlation of E_{HOMO} or Hammett constants for *meta*- and *para*-substituted compounds ($p = 0.0004$). However, $E_{\text{ox,corr.}}$ is the best descriptor for modeling complex phenols based on the availability of data and low p-value ($p = 0.0082$ for all phenols; **Table A.9**).

These linear regression results are expected based on literature model trends and first principles of phenol oxidation. However, without identifying the rate-limiting steps of each reaction, studies cannot delve further into the structural and mechanistic trends present in these QSAR models. Qualitatively, all four descriptors illustrate the clear separation between the faster electron transfer-limited reactions and the slower sorption-limited reactions with $\delta\text{-MnO}_2$. As a result, in these well-controlled investigations of phenol oxidation by synthetic $\delta\text{-MnO}_2$, simple QSARs illuminate the influence of substituent effects on the rate-limiting steps of reaction. Phenols that are sorption-limited with $\delta\text{-MnO}_2$, and thus have lower observed rate constants, are those with high Hammett constants, low pK_a values, low E_{HOMO} values, and high $E_{\text{ox,corr.}}$ values. Thus, the sorption-limited compounds have electron-withdrawing substituents, have less electron density on the phenolic group, and have greater oxidation potential energies. The relationship between the rate-limiting step and the observed pseudo-first-order rate constants suggests that organic structure is a major factor influencing the reaction mechanism with $\delta\text{-MnO}_2$.

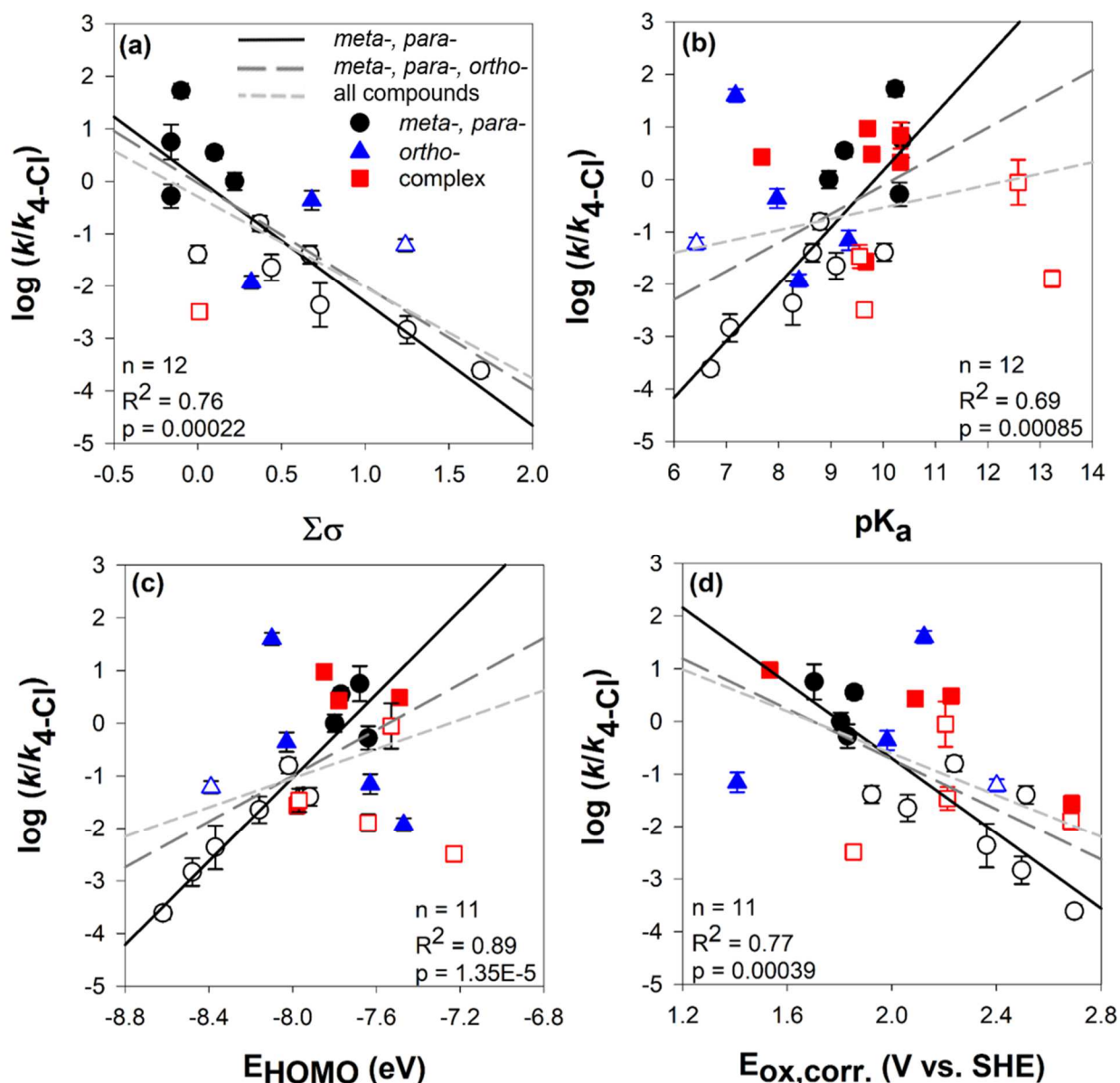


Figure 2.4. The log of the quenched pseudo-first-order rate constant of 29 target phenolic compounds reacted with δ -MnO₂ normalized to the rate constant of 4-chlorophenol versus (a) sum of the tabulated Hammett constants, (b) first phenolic pK_a , (c) energy of the highest occupied molecular orbital, and (d) corrected oxidation energy of the first electron transfer. Error bars indicate the standard deviation of triplicate data. Filled data points indicate electron transfer-limited mechanisms and hollow data points indicate sorption-limited reaction mechanism. Regression values are for the simple *meta*- and *para*-substituted phenols; regression values for all lines are given in **Table A.9**. Experiments were conducted with 10 μ M phenol and 15 mg/L δ -MnO₂ in 10 mM acetate at pH 5.5.

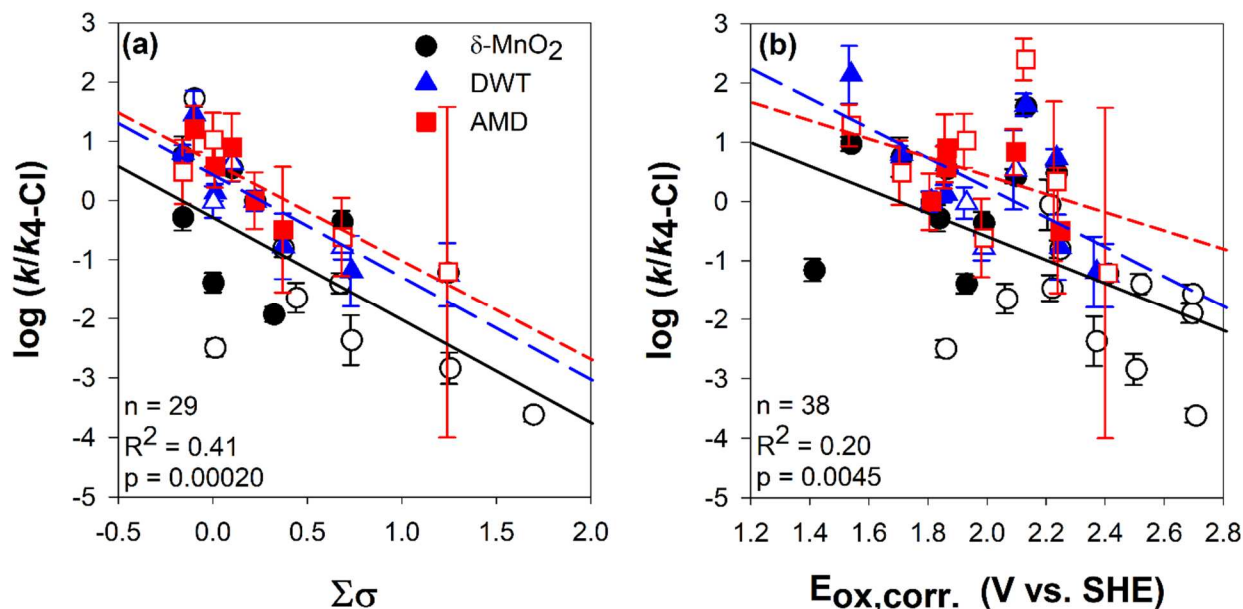


Figure 2.5. Quantitative structure activity relationships for 15 phenols reacted with drinking water treatment and acid mine drainage remediation reclaimed solids and 29 phenols reacted with δ -MnO₂, all normalized to 15 mg-Mn L⁻¹. Plots show the log of the quenched rate constant normalized to the rate constant of 4-chlorophenol versus (a) sum of the tabulated Hammett constants and (b) corrected oxidation energy of the first electron transfer. Error bars indicate standard deviation of triplicate measurements. Filled data points indicate electron transfer-limited mechanisms and hollow data points indicate sorption-limited reaction mechanism. Lines indicate regression fits through each solid. Regression values for all 15 phenols with each manganese oxide are given in **Table A.11**.

Furthermore, increasing compound complexity results in deviations away from the strong linear relationship developed for simple *meta*- and *para*-substituted compounds (**Figure 2.4**). Although the QSAR correlations remain significant in all cases except for E_{HOMO} , the addition of *ortho*-substituted and complex phenols lowers the R^2 39 – 85% and increases p-values by 1 – 3 orders of magnitude compared to *meta*- and *para*-substituted phenols reacted with δ -MnO₂ (**Table A.9**). While QSARs previously developed using simple phenols or anilines reacted with δ -MnO₂ result in strong correlations and support the utility of these relationships,^{36,38,42,65} our dataset developed with structurally varied phenols shows that QSARs are ineffective for *ortho*-

substituted and complex phenols. While the limited utility of QSARs for complex phenols is generally assumed, this assumption has not been previously tested in the Mn oxide literature.

QSAR plots constructed based on the kinetics of AMD and DWT solids (**Figure 2.5**) show the same linear trends as observed for δ -MnO₂. This result is unexpected given the orders of magnitude rate differences and mechanism shifts between the investigated manganese oxides. The linear relationships are less significant than with δ -MnO₂, with only Hammett constants ($p = 0.0002$) and $E_{\text{ox,corr}}$ ($p = 0.0045$; **Table A.11**) giving significant linear correlations across all solids. Unlike the QSAR trends for the 27 phenols reacted with δ -MnO₂, the separation between electron transfer-limited and sorption-limited relative rate constants is not distinctive in DWT and AMD solids (**Figure 2.5**). The lack of a distinct separation between electron transfer- and sorption-limited rate constants highlight how the two reclaimed solids behave differently than synthetic δ -MnO₂ beyond the 1 – 3 orders of magnitude rate differences. This indicates that structural properties are important determinants of the reaction mechanism across Mn oxides and, importantly, that synthetic oxides may not predict the reactivity of reclaimed solids. However, the inconsistent shifts in the rate-limiting step between the three solids for each of the 15 phenols (**Table A.14**), as well as the consistent QSAR trends with structural descriptors (**Figure 2.5**), suggests that organic structure may have a greater influence on oxidation rates and overall reactivity than Mn oxide characteristics.

The ability of QSARs to predict reactivity of substituted phenols and anilines with synthetic manganese oxides is further tested by constructing QSARs using literature rate constants (**Figures 2.6 and A.5**).^{6,11,36-38} Despite differences in reaction conditions (**Table A.12**), $\log k$ values normalized to the rate constant for 4-chlorophenol enable cross-study comparison. The resulting QSARs follow the same trends as our experimental data, with stronger correlations

due to the larger data set ($n = 69$ versus 27). For example, p -values are 2 – 40 times higher when considering QSARs developed using all compounds as compared to only *meta*- and *para*-substituted compounds for Hammett constants, E_{HOMO} , and E_{ox} . Despite this improvement, the scatter is pronounced with structural complexity in QSARs constructed using literature data. The pK_{a} QSAR statistics do not show the same trend because QSARs were developed using both aniline and phenol species (**Figure A.5a**). Separating this relationship by anilines versus phenols results in p -values of 2.7×10^{-4} and 7.5×10^{-2} , respectively (**Table A.10**).

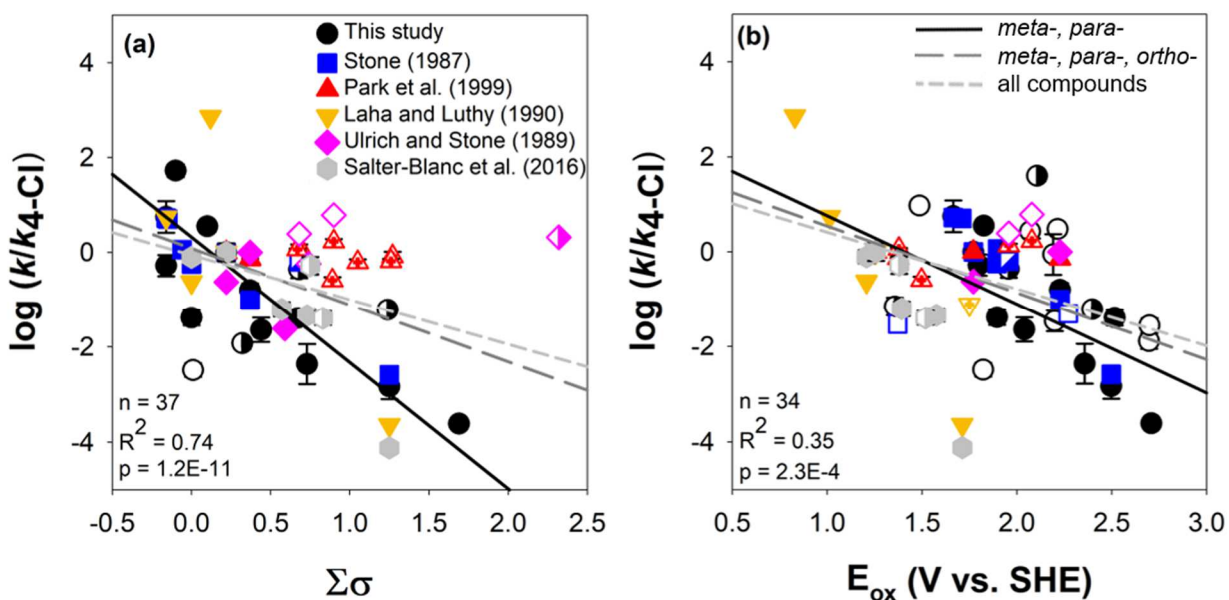


Figure 2.6. Quantitative structure activity relationships for literature normalized rate constants of phenols and anilines reacted with synthetic manganese oxides^{6,11,36-38} and reactions from this study with $\delta\text{-MnO}_2$. The log of the average observed rate constant normalized to the rate constant of 4-chlorophenol or 4-chloroaniline is plotted against (a) sum of Hammett constants and (b) oxidation energy of the first electron transfer. Error bars indicate the standard deviation of triplicate measurements. Filled data points indicate *meta*- or *para*-substitution, partially filled points indicate *ortho*-substitution, and hollow points indicate complex compounds. Given regression values are for the simple *meta*- and *para*-substituted compounds; regression values for all lines are provided in **Table A.10**.

2.5.4 Assessment of quantitative structure activity relationships

The QSAR plots (**Figures 2.4 – 2.6**) show significant linear relationships that follow the expected trends based on first principles and literature relationships.^{38,42,56,64,65} In spite of significant p-values, it is apparent that the QSARs are scattered with the inclusion of more complex compounds; average R^2 values decrease from 0.78 for *meta*- and *para*-compounds reacted with δ -MnO₂ to 0.26 when *ortho*- and complex compounds are included. These observations directly contrast the strong linear regression statistics presented in the existing literature examining phenol and aniline oxidation by Mn oxides^{1,36,38,42,56,64,65} and suggest that organic structure may impact the predictive utility of these models. However, linear regressions are not enough to test these qualitative results as R^2 values only measure how closely the data falls to the trendline and p-values test the probability that the linear correlation is random.

Thus, we investigate the structure-dependent systematic deviations and the validity of QSAR models in order to quantify the qualitative observations described above and to test whether organic structural complexities directly influence the observed non-linearity of these QSARs. First, to test the impact of organic structure on the observed scatter, we analyze the residuals for both the simple (*meta*-, *para*-dependent or individual solid) and the all-encompassing (all phenols or all solids) regression lines for QSARs constructed using the three solids and literature data (**Figures 2.4 – 2.6; Appendix A.8**). Plotting the normalized log k residuals for each compound against independent descriptor parameters shows that the residuals are not randomly distributed for any tested QSAR model, but instead follow clear linear or funnel-shaped trends (**Figures A.9 and A.10**). The bimodal ‘s’ shaped distributions of the normality plots (**Figures A.11 and A.12**) further support the observed non-random residual distributions and suggest that non-linear descriptors may fit the data better.⁶⁶ In addition, the log

k terms for each organic compound are consistently overpredicted (negative residuals) or underpredicted (positive residuals) by a similar magnitude, regardless of which QSAR model is used (**Figures 2.7** and **A.13**). This result suggests that organic structure directly influences not only reactivity, but also the predictive ability of QSARs, although there is no clear trend with substitution (i.e., simple, *ortho*-, or complex) across the residual distribution (**Figure 2.7**). These residual analyses showing the non-random error distribution and systematic over- and underprediction of normalized reaction rates illustrate the problematic nature of relying on linear QSARs for modeling contaminant reactivity.

Second, we test the validity of the structural descriptors (e.g., Hammett constants) for predicting reactivity and the cross-application of these models using external validation methods (**Appendix A.8**). While residual analyses demonstrate the systematic error in predicting contaminant reactivity by QSARs, we use validation statistics (e.g., R^2_{pred} , r_m^2) to quantify the data variability and compare test and training data subsets to investigate if these QSARs can be applied across compound type, studies, or Mn oxides.⁶⁷⁻⁶⁹ All combinations of test-training subsets (e.g., this study versus literature and randomized) return results outside the accepted range except for a Hammett constant descriptor case for which the relationship is inapplicable to complex contaminants lacking tabulated constants (**Table A.18**). More importantly, QSARs developed using *meta*- and *para*-substituted phenols do not accurately predict the reactivity of *ortho*- and complex phenols (**Table A.18**), supporting our conclusion that the behavior of commonly studied simple phenols cannot be used to predict oxidation rates of complex contaminants due to the strong influence of organic structure. Similarly, the rate constants for δ -MnO₂ are not predictive of the oxidation rate constants with the two reclaimed materials (**Table**

A.19), demonstrating that commonly collected δ -MnO₂ kinetic data cannot be extended to predict oxidation rates by non-synthetic materials.

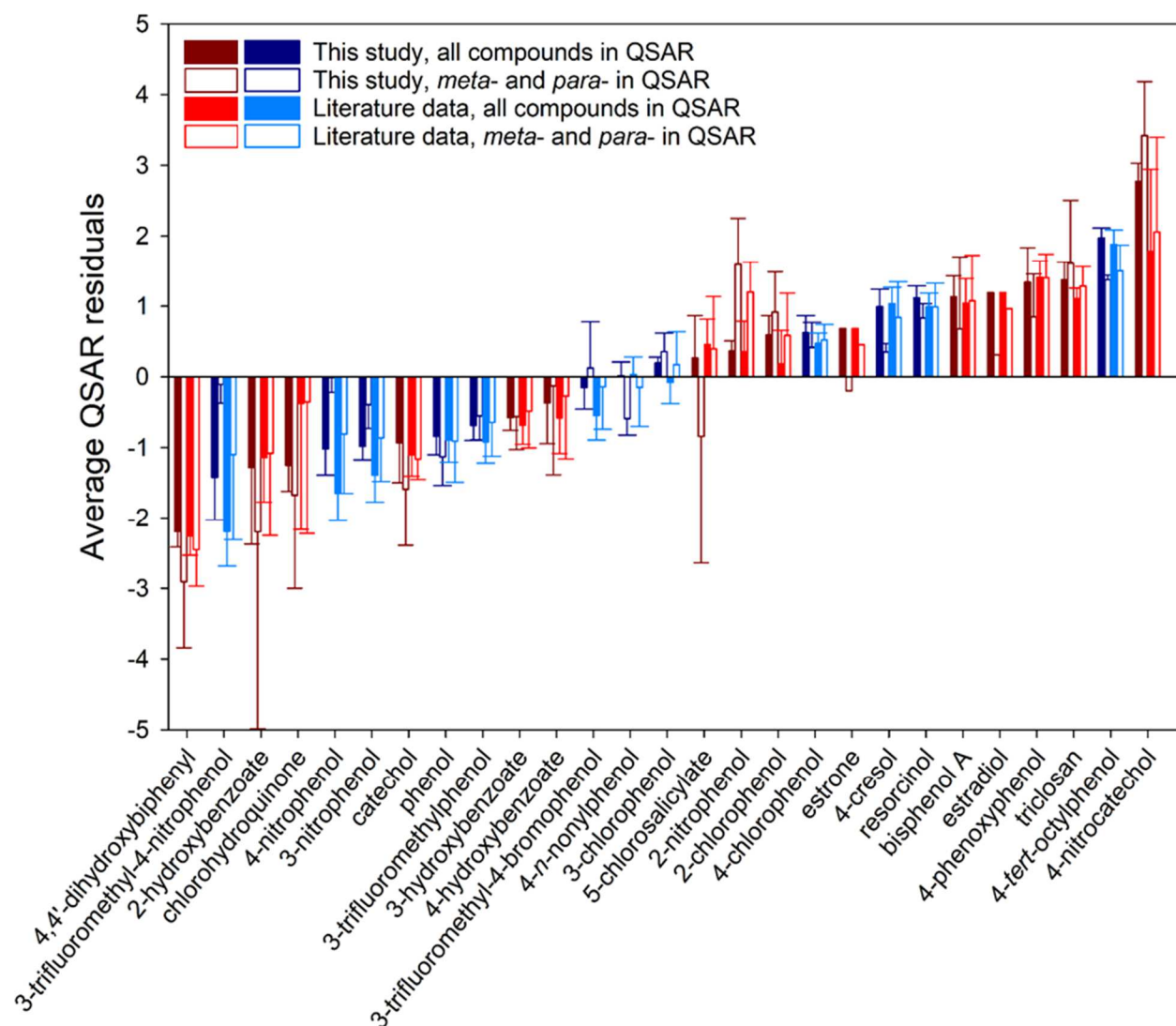


Figure 2.7. Average residuals of Hammett constant, pK_a , E_{HOMO} , $E_{ox,corr.}$ (or E_{ox}) based QSAR models developed with either all compounds or only simple *meta*- and *para*-substituted compounds, using data from this study or compiled from literature. Error bars indicate one standard deviation. Residual values for each QSAR model are given in **Table A.15** for this study and **Table A.16** for literature data.

2.6 Conclusions

This study provides evidence that both sorption-limited and electron transfer-limited reaction mechanisms are observed across a wide range of phenols reacted with δ -MnO₂. The

studied phenols are also oxidized by both drinking water treatment and acid mine drainage reclaimed manganese oxides, although the rate-limiting steps of reaction changes as a result of both solid-phase and organic structural characteristics. These results indicate that reclaimed Mn-containing oxide materials could potentially be applied as an alternative to synthetic materials for the *in situ* degradation of organic contaminants. By analyzing the degradation mechanism for a suite of phenols with three different solid phase oxidants, this study provides the first coupled solid and aqueous-phase insight into the complex interactions that govern both degradation rate and mechanism. We identify organic structure as the primary mechanism determinant and observe that solid characteristics (e.g., iron content, surface area) also influence the relative sorption and electron transfer rates.

The mechanism by which each contaminant degrades with any given manganese oxide has implications for the *in situ* processes and rates of removal. Electron transfer-limited reactions result in relatively fast physical removal by sorption to the solid species, potentially followed by slower chemical transformation. In contrast, sorption-limited reactions are relatively slow. Since both mechanisms may occur in applied systems targeting multiple contaminants, the rates and extent of total contaminant removal from waters (e.g., by both physical sorption and chemical transformation) will differ from the rate and extent of contaminant degradation. In addition, the phenol oxidation products will differ between electron transfer-limited and sorption-limited removal pathways (i.e., polymers versus benzoquinones, respectively), which has implications for both the toxicity and environmental fate of the transformation products in treated waters.^{1,6,27,28} Thus, both mechanisms need to be considered to accurately predict contaminant fate, removal rates, and product formation in manganese oxide treatment systems.

Furthermore, we demonstrate that QSARs are ineffective for predicting the reactivity of *ortho*-substituted or complex structures (e.g., multiple aromatic rings), including contaminants of environmental concern. While QSARs constructed to evaluate Mn oxide reactivity are acknowledged for their predictive strength,^{36,38,42,65} the oxidation of complex organic structures (i.e., those of key contaminants and metabolites identified in natural water systems) and reclaimed solids does not follow the same linear regressions. QSAR prediction models constructed using previously identified descriptor constants (e.g., pK_a and E_{HOMO})^{38,42} have limited validity and non-random error distributions indicate these common linear models are not a good predictor of observed rate constants for the oxidation of organic species by manganese oxides. Polyparameter or non-linear relationships built to incorporate multiple descriptors, data transformation, or much larger datasets may improve the error distributions, validity, and fit of such QSAR models.^{64,67-69} However, these empirical strategies are ineffective for the prediction of environmental systems as they move away from the first principles that ground linear QSARs in well supported theory and may not apply across reaction conditions. In addition, constructing a large enough dataset that spans reaction conditions, rate-limiting processes, and oxidant characteristics to potentially overcome these challenges is infeasible without dedicated data sharing platforms like those available for environmental toxicology.

The oxidation kinetics, QSAR predictive power, and environmental implications (e.g., organic product formation) of the system depend on the unique interactions between contaminant structure and Mn oxides. Solution conditions (e.g., pH, dissolved organic matter concentration and composition) are expected to further influence the kinetics of organic contaminant oxidation by manganese oxides and warrant continued studies in increasingly complex matrices. This study highlights the necessity for studies investigating both the aqueous organic and solid phases in-

depth and calls for a departure from reliance on QSARs along with the adoption of standardized model validation procedures.

2.7 Acknowledgements

Funding was provided by the Wisconsin Groundwater Coordinating Council and the National Science Foundation (CBET 1509879). Any opinions, findings, and conclusions or recommendations expressed in this material are those of the authors and do not necessarily reflect the views of the National Science Foundation. We acknowledge the Madison Water Utility and Robert Hedin for assistance with sample collection, Keerthana Sreenivasan for laboratory assistance, and Andrew M. Graham (Grinnell College) for helpful discussions. X-ray absorption spectroscopy was conducted at Sector 10 of the Advanced Photon Source at Argonne National Laboratory. MRCAT operations are supported by the Department of Energy and MRCAT member institutions. This research used resources of the Advanced Photon Source, a U.S. Department of Energy (DOE) Office of Science User Facility operated for the DOE Office of Science by Argonne National Laboratory under Contract No. DE-AC02-06CH11357.

2.8 Supporting information

Additional details pertaining to analytical methods, kinetic modeling, additional data, and quantitative structure activity relationship validation can be found in Appendix A.

2.9 References

1. C. K. Remucal and M. Ginder-Vogel, A critical review of the reactivity of manganese oxides with organic contaminants, *Environ. Sci. Processes Impacts*, **2014**, *16*, 1247-1266.
2. O. W. Duckworth, N. A. Rivera, T. G. Gardner, M. Y. Andrews, C. M. Santelli and M. L. Polizzotto, Morphology, structure, and metal binding mechanisms of biogenic manganese oxides in a superfund site treatment system, *Environ. Sci. Processes Impacts*, **2017**, *19*, 50-58.
3. J. E. Grebel, J. A. Charbonnet and D. L. Sedlak, Oxidation of organic contaminants by manganese oxide geomedia for passive urban stormwater treatment systems, *Water Res.*, **2016**, *88*, 481-491.
4. J. Pena, K. D. Kwon, K. Refson, J. R. Bargar and G. Sposito, Mechanisms of nickel sorption by a bacteriogenic birnessite, *Geochim. Cosmochim. Acta*, **2010**, *74*, 3076-3089.
5. J. E. Post, Manganese oxide minerals: Crystal structures and economic and environmental significance, *Proc. Natl. Acad. Sci. U.S.A.*, **1999**, *96*, 3447-3454.
6. A. T. Stone, Reductive dissolution of manganese(III/IV) oxides by substituted phenols, *Environ. Sci. Technol.*, **1987**, *21*, 979-988.
7. B. M. Tebo, J. R. Bargar, B. G. Clement, G. J. Dick, K. J. Murray, D. Parker, R. Verity and S. M. Webb, Biogenic manganese oxides: Properties and mechanisms of formation, *Ann. Rev. Earth Planet. Sci.*, **2004**, *32*, 287-328.
8. M. Villalobos, B. Toner, J. Bargar and G. Sposito, Characterization of the manganese oxide produced by *Pseudomonas putida* strain MnB1, *Geochim. Cosmochim. Acta*, **2003**, *67*, 2649-2662.
9. Z. Wang and D. E. Giammar, in *Advances in the Environmental Biogeochemistry of Manganese Oxides*, eds. X. Feng, W. Li, M. Zhu and D. L. Sparks, American Chemical Society, Washington, D.C., **2015**, vol. 1197, ch. 2, pp. 29-50.
10. T. Borch, R. Kretzschmar, A. Kappler, P. Van Cappellen, M. Ginder-Vogel, A. Voegelin and K. Campbell, Biogeochemical redox processes and their impact on contaminant dynamics, *Environ. Sci. Technol.*, **2010**, *44*, 15-23.
11. H. J. Ulrich and A. T. Stone, Oxidation of chlorophenols adsorbed to manganese oxide surfaces, *Environ. Sci. Technol.*, **1989**, *23*, 421-428.
12. C. Li, B. Zhang, T. Ertunc, A. Schaeffer and R. Ji, Birnessite-induced binding of phenolic monomers to soil humic substances and nature of the bound residues, *Environ. Sci. Technol.*, **2012**, *46*, 8843-8850.
13. H. Li, L. S. Lee, D. G. Schulze and C. A. Guest, Role of soil manganese in the oxidation of aromatic amines, *Environ. Sci. Technol.*, **2003**, *37*, 2686-2693.
14. T. Makino, Y. Takahashi, Y. Sakurai and M. Nanzyo, Influence of soil chemical properties on adsorption and oxidation of phenolic acids in soil suspension, *J. Soil Sci. Plant Nutr.*, **1996**, *42*, 867-879.
15. L. Schacht and M. Ginder-Vogel, Arsenite depletion by manganese oxides: A case study on the limitations of observed first order rate constants, *Soil Systems*, **2018**, *2*, 39.
16. R. Hedin, T. Weaver, N. Wolfe and G. Watzlaf, presented in part at the 35th Annual National Association of Abandoned Mine Land Programs Conference, Daniels, West Virginia, **2013**.

17. J. Skousen, C. E. Zipper, A. Rose, P. F. Ziemkiewicz, R. Nairn, L. M. McDonald and R. L. Kleinmann, Review of passive systems for acid mine drainage treatment, *Mine Water Environ.*, **2016**, *36*, 133-153.
18. A. Reghuvaran, Biochemical aspects and formation of phenolic compounds by coir pith degraded by *Pleurotus sajor caju*, *J. Toxicol. Environ. Health Sci.*, 2012, **4**, 29-36.
19. E. R. Estes, P. F. Andeer, D. Nordlund, S. D. Wankel and C. M. Hansel, Biogenic manganese oxides as reservoirs of organic carbon and proteins in terrestrial and marine environments, *Geobiology*, **2017**, *15*, 158-172.
20. I. Forrez, M. Carballa, G. Fink, A. Wick, T. Hennebel, L. Vanhaecke, T. Ternes, N. Boon and W. Verstraete, Biogenic metals for the oxidative and reductive removal of pharmaceuticals, biocides and iodinated contrast media in a polishing membrane bioreactor, *Water Res.*, **2011**, *45*, 1763-1773.
21. C. M. Santelli, S. M. Webb, A. C. Dohnalkova and C. M. Hansel, Diversity of Mn oxides produced by Mn(II)-oxidizing fungi, *Geochim. Cosmochim. Acta*, **2011**, *75*, 2762-2776.
22. E. C. Bonfeld-Jorgensen, M. Long, M. V. Hofmeister and A. M. Vinggaard, Endocrine-disrupting potential of bisphenol A, bisphenol A dimethacrylate, 4-*n*-nonylphenol, and 4-*n*-octylphenol in vitro: New data and a brief review, *Environ. Health Perspect.*, **2007**, *115*, 69-76.
23. D. Lu, C. Feng, D. Wang, Y. Lin, H. S. Ip, J. She, Q. Xu, C. Wu, G. Wang and Z. Zhou, Analysis of twenty phenolic compounds in human urine: Hydrochloric acid hydrolysis, solid-phase extraction based on K₂CO₃-treated silica, and gas chromatography tandem mass spectrometry, *Anal. Bioanal. Chem.*, **2015**, *407*, 4131-4141.
24. D. Montes-Grajales, M. Fennix-Agudelo and W. Miranda-Castro, Occurrence of personal care products as emerging chemicals of concern in water resources: A review, *Sci. Total Environ.*, **2017**, *595*, 601-614.
25. T. Pollock, R. E. Weaver, R. Ghasemi and D. deCatanzaro, A mixture of five endocrine-disrupting chemicals modulates concentrations of bisphenol A and estradiol in mice, *Chemosphere*, **2018**, *193*, 321-328.
26. M. L. Davi and F. Gnudi, Phenolic compounds in surface water, *Water Res.*, **1999**, *33*, 3213-3219.
27. N. Shaikh, H. Zhang, K. Rasamani, K. Artyushkova, A. S. Ali and J. M. Cerrato, Reaction of bisphenol A with synthetic and commercial MnO_{x(s)}: Spectroscopic and kinetic study, *Environ. Sci. Processes Impacts*, **2018**, *20*, 1046-1055.
28. H. Zhang, W. R. Chen and C. H. Huang, Kinetic modeling of oxidation of antibacterial agents by manganese oxide, *Environ. Sci. Technol.*, **2009**, *42*, 5548-5554.
29. K. Lin, W. Liu and J. Gant, Oxidative removal of bisphenol A by manganese dioxide: Efficacy, products, and pathways, *Environ. Sci. Technol.*, **2009**, *43*, 3860-3864.
30. K. Rubert and J. A. Pedersen, Kinetics of oxytetracycline reaction with a hydrous manganese oxide, *Environ. Sci. Technol.*, **2006**, *40*, 7216-7221.
31. L. Ukrainczyk and M. B. McBride, Oxidation and dechlorination of chlorophenols in dilute aqueous suspensions of manganese oxides - reaction products, *Environ. Toxicol. Chem.*, **1993**, *12*, 2015-2022.
32. S. Balgooyen, P. J. Alaimo, C. K. Remucal and M. Ginder-Vogel, Structural transformation of MnO₂ during the oxidation of bisphenol A, *Environ. Sci. Technol.*, **2017**, *51*, 6053-6062.

33. S. Balgooyen, G. Campagnola, C. K. Remucal and M. Ginder-Vogel, Impact of bisphenol A influent concentration and reaction time on MnO₂ transformation in a stirred flow reactor, *Environ. Sci. Processes Impacts*, **2019**, *21*, 19-27.
34. J. Huang, S. Zhong, Y. Dai, C. C. Liu and H. Zhang, Effect of MnO₂ phase structure on the oxidative reactivity toward bisphenol A degradation, *Environ. Sci. Technol.*, **2018**, *52*, 11309-11318.
35. J. Klausen, S. B. Haderlein and R. P. Schwarzenbach, Oxidation of substituted anilines by aqueous MnO₂: Effect of co-solutes on initial and quasi-steady-state kinetics, *Environ. Sci. Technol.*, **1997**, *31*, 2642-2649.
36. S. Laha and R. G. Luthy, Oxidation of aniline and other primary aromatic amines by manganese dioxide, *Environ. Sci. Technol.*, **1990**, *24*, 363-373.
37. J. W. Park, J. Dec, J. E. Kim and J. M. Bollag, Effect of humic constituents on the transformation of chlorinated phenols and anilines in the presence of oxidoreductive enzymes or birnessite, *Environ. Sci. Technol.*, **1999**, *33*, 2028-2034.
38. A. J. Salter-Blanc, E. J. Bylaska, M. A. Lyon, S. C. Ness and P. G. Tratnyek, Structure-activity relationships for rates of aromatic amine oxidation by manganese dioxide, *Environ. Sci. Technol.*, **2016**, *50*, 5094-5102.
39. N. Shaikh, S. Taujale, H. Zhang, K. Artyushkova, A. S. Ali and J. M. Cerrato, Spectroscopic investigation of interfacial interaction of manganese oxide with triclosan, aniline, and phenol, *Environ. Sci. Technol.*, **2016**, *50*, 10978-10987.
40. H. Zhang and C. H. Huang, Oxidative transformation of triclosan and chlorophene by manganese oxides, *Environ. Sci. Technol.*, **2003**, *37*, 2421-2430.
41. M. D. R. Pizzigallo, P. Ruggiero, C. Crecchio and R. Mininni, Manganese and iron-oxides as reactants for oxidation of chlorophenols, *Soil Sci. Soc. Am. J.*, **1995**, *59*, 444-452.
42. A. S. Pavitt, E. J. Bylaska and P. G. Tratnyek, Oxidation potentials of phenols and anilines: Correlation analysis of electrochemical and theoretical values, *Environ. Sci. Processes Impacts*, **2017**, *19*, 339-349.
43. J. W. Murray, The surface chemistry of hydrous manganese dioxide, *J. Colloid Interface Sci.*, **1974**, *46*, 357-371.
44. A. Manceau, M. A. Marcus and S. Grangeon, Determination of Mn valence states in mixed-valent manganates by XANES spectroscopy, *Am. Mineral.*, **2012**, *97*, 816-827.
45. M. Kosmulski, Isoelectric points and points of zero charge of metal (hydr)oxides: 50 years after Parks' review, *Adv. Colloid Interface Sci.*, **2016**, *238*, 1-61.
46. T. Mahmood, M. T. Saddique, A. Naeem, P. Westerhoff, S. Mustafa and A. Alum, Comparison of different methods for the point of zero charge determination of NiO, *Ind. Eng. Chem. Res.*, **2011**, *50*, 10017-10023.
47. *CRC Handbook of Chemistry and Physics*, CRC Press LLC, Boca Raton, FL 95th edn., **2014-2015**.
48. S. C. Ying, B. D. Kocar, S. D. Griffis and S. Fendorf, Competitive microbially and Mn oxide mediated redox processes controlling arsenic speciation and partitioning, *Environ. Sci. Technol.*, **2011**, *45*, 5572-5579.
49. W. S. Yao and F. J. Millero, Adsorption of phosphate on manganese dioxide in seawater, *Environ. Sci. Technol.*, **1996**, *30*, 536-541.
50. C. Hansch, A. Leo and R. W. Taft, A survey of Hammett substituent constants and resonance and field parameters, *Chem. Review*, **1991**, *91*, 165-195.

51. R. P. Schwarzenbach, P. M. Gschwend and Imboden, in *Environmental Organic Chemistry*, John Wiley & Sons, Inc., Hoboken, New Jersey, 2nd edn., **2003**, ch. 8, pp. 245-274.
52. G. B. Barlin and D. D. Perrin, Prediction of the strengths of organic acids, *Quarterly Reviews, Chemical Society*, **1966**, 75-101.
53. J. Clark and D. D. Perrin, Prediction of the strengths of organic bases, *Quarterly Reviews, Chemical Society*, **1964**, 295-320.
54. M. Swain, Chemicalize.org, *J. Chem. Inf. Model.*, **2012**, 52, 613-615.
55. M. Valiev, E. J. Bylaska, N. Govind, K. Kowalski, T. P. Straatsma, H. J. J. Van Dam, D. Wang, J. Nieplocha, E. Apra, T. L. Windus and W. de Jong, NWChem: A comprehensive and scalable open-source solution for large scale molecular simulations, *Comput. Phys. Commun.*, **2010**, 181, 1477-1489.
56. W. A. Arnold, Y. Oueis, M. O'Connor, J. E. Rinaman, M. G. Taggart, R. E. McCarthy, K. A. Foster and D. E. Latch, QSARs for phenols and phenolates: Oxidation potential as a predictor of reaction rate constants with photochemically produced oxidants, *Environ. Sci. Processes Impacts*, **2017**, 19, 324-338.
57. L. Zhao, Z. Yu, P. Peng, W. Huang and Y. Dong, Oxidative transformation of tetrachlorophenols and trichlorophenols by manganese dioxide, *Environ. Toxicol. Chem.*, **2009**, 28, 1120-1129.
58. Y. Wang, S. Benkaddour, F. F. Marafatto and J. Pena, Diffusion- and pH-dependent reactivity of layer-type MnO₂: Reactions at particle edges versus vacancy sites, *Environ. Sci. Technol.*, **2018**, 52, 3476-3485.
59. R. G. Lehmann, H. H. Cheng and J. B. Harsh, Oxidation of phenolic acids by soil iron and manganese oxides, *Soil Sci. Soc. Am. J.*, **1987**, 51, 352-356.
60. M. L. Colarieti, G. Toscano, M. R. Ardi and G. Greco, Jr., Abiotic oxidation of catechol by soil metal oxides, *J. Hazard. Mater.*, **2006**, 134, 161-168.
61. I. Forrez, M. Carballa, K. Verbeken, L. Vanhaecke, T. Ternes, N. Boon and W. Verstraete, Diclofenac oxidation by biogenic manganese oxides, *Environ. Sci. Technol.*, **2010**, 44, 3449-3454.
62. J. Dong, Z. LiJia, L. Hui, L. ChengShuai, G. YuanXue and S. LiNa, The oxidative degradation of 2-mercaptobenzothiazole by different manganese dioxides, *Fresenius Environmental Bulletin*, **2010**, 19, 1615-1622.
63. C. S. Liu, L. J. Zhang, F. B. Li, Y. Wang, Y. Gao, X. Z. Li, W. D. Cao, C. H. Feng, J. Dong and L. N. Sun, Dependence of sulfadiazine oxidative degradation on physicochemical properties of manganese dioxides, *Ind. Eng. Chem. Res.*, **2009**, 48, 10408-10413.
64. D. Colon, E. J. Weber and G. Baughman, Sediment-associated reactions of aromatic amines 2. QSAR development, *Environ. Sci. Technol.*, **2002**, 36, 2443-2450.
65. P. G. Tratnyek, E. J. Weber and R. P. Schwarzenbach, Quantitative structure-activity relationships for chemical reductions of organic contaminants, *Environ. Toxicol. Chem.*, **2003**, 22, 1733-1742.
66. J. L. Devore, *Probability & Statistics for Engineering and the Sciences*, Brooks/Cole, Boston, MA, 8th edn., **2012**.
67. N. Frimayanti, M. L. Yam, H. B. Lee, R. Othman, S. M. Zain and N. A. Rahman, Validation of quantitative structure-activity relationship (QSAR) model for photosensitizer activity prediction, *Int. J. Mol. Sci.*, **2011**, 12, 8626-8644.

68. P. Gramatica, On the development and validation of QSAR models, *Methods Mol. Biol.*, **2013**, *930*, 499-526.
69. R. Veerasamy, H. Rajak, A. Jain, S. Sivadasan, C. P. Varghese and R. K. Agrawal, Validation of QSAR models - strategies and importance, *Int. J. Drug Des. Discov.*, **2011**, *2*, 511-519.

Chapter 3

Enhancement and inhibition of oxidation rates in mixtures of phenolic compounds reacted with manganese oxides

3.1 Collaboration information

This chapter was completed by Emma L. Trainer, Matthew Ginder-Vogel, and Christina K. Remucal. E. L. Trainer completed all laboratory experiments and data analyses. E. L. Trainer, M. Ginder-Vogel, and C. K. Remucal wrote the manuscript. This chapter is in preparation to submit to a peer-reviewed journal.

3.2 Abstract

Phenolic compounds are ubiquitous across natural and engineered waters where they can be oxidized by manganese oxides in the subsurface or in passive treatments of contaminated streams such as stormwater runoff and wastewater effluent. These surface waters, stormwater runoff, and wastewater effluents contain a mixture of phenolic compounds, and toxicology studies indicate that mixtures of endocrine-disrupting phenolic contaminants have additive, synergistic, and antagonistic effects on hormone levels in mice and fish. However, the effects of such mixtures on phenol oxidation by manganese oxides is not well understood. This study addresses this knowledge gap by determining pseudo-first-order oxidation rates and oxidation mechanisms for four phenols reacted in varying mixtures with δ -MnO₂. Oxidation rates of electron transfer-limited phenols (i.e., triclosan, resorcinol, bisphenol A) are inhibited in all mixtures up to 56 times relative to isolated reactions. In addition, the extent of sorption of these

phenols also decreases and resorcinol and bisphenol A become sorption-limited in some mixtures. These inhibitory results are consistent with competition between phenols occurring near the Mn surface. In contrast, sorption-limited 4,4'-biphenol oxidation rates are enhanced in all mixtures. Analogous reactions with *tert*-butanol indicate that this rate enhancement is driven by indirect oxidation and transformation through radical reactions, likely from phenoxy radical products of electron transfer-limited phenols in solution. These findings demonstrate that mixtures have a large impact on oxidation of phenols by manganese oxides as electron transfer-limited phenols are inhibited due to competition interactions and sorption-limited phenols have enhanced oxidation rates due to indirect oxidation by radicals.

3.3 Introduction

Phenolic compounds are abundant in surface waters and encompass a variety of contaminant classes, including antimicrobial agents (e.g., triclosan), antioxidants (4,4'-biphenol), estrogenic endocrine disruptors (e.g., bisphenol A), and pharmaceuticals (e.g., resorcinol; **Table 3.1**).¹⁻⁴ Many of these anthropogenic contaminants are released to surface waters in wastewater effluent, runoff, landfill leachates, and other waste streams.³⁻¹² In surface waters, these phenolic contaminants impact ecological and human health and may have toxicological effects, including endocrine disruption and bioaccumulation.^{5,11-17} Contaminants are frequently present as mixtures in the environment, which influences both their toxicological effects and removal efficiency in water treatment processes.

Toxicological effects (e.g., estrogen production or inhibition) of phenolic contaminants are dependent on not only contaminant dose, but competition between multiple contaminants.^{13,16-18} In many cases, multi-contaminant exposure increases estrogen production

through additive and/or multiplicative effects compared to single contaminant exposure. For example, exposure to both triclosan and tetrabromobisphenol A increases bisphenol A and natural estrogen (17β -estradiol; E2) release in female mice.^{16,17} Similarly, a study of nonylphenol, octylphenol, bisphenol A (BPA), and 2,4-dichlorophenol exposure effects on E2 receptor binding assays found the effect of each phenolic contaminant on receptor binding affinity ranked BPA > octylphenol > nonylphenol > 2,4-dichlorophenol in individual assays. However, in both equipotent and environmentally relevant concentration ratios, multi-contaminant mixtures were antagonistic due to competitive ligand receptor binding.¹⁸ These studies indicate the importance of understanding the environmental fate and behavior of contaminant mixtures, as toxicological effects are not adequately predicted by single-contaminant studies.

Phenolic contaminants are degraded in natural systems by manganese (Mn) oxides, which are ubiquitous and highly redox active.^{1,2,19-22} These naturally occurring minerals are also formed as byproducts of engineered systems (e.g., drinking water treatment, acid mine drainage remediation) or synthetically manufactured and may be applied in passive *in-situ* treatment systems for organic contaminants.^{2,3,6,10,23-26} δ -MnO₂, a synthetic proxy for biogenic birnessite,²⁶ readily oxidizes many phenolic contaminants of interest including estrogens, BPA, and other endocrine disruptors with demonstrated toxicological effects.^{1,2,9,21,27-31} The oxidation of these phenols by Mn oxides occurs through two stepwise electron transfer reactions and may be rate-limited by either sorption of the contaminant to the Mn surface or the first electron transfer.^{1,2,31,32} The rate limiting step of oxidation depends on both phenolic contaminant structure and Mn oxide characteristics in isolated batch reactions,² but the influence of competing contaminants in solution on the mechanism and rate of oxidation are unknown.

Competition is an important factor not only for predicting toxicological effects and degradation of parent contaminant compounds, but also for understanding the competition between parent contaminants and their oxidation products. This interaction is especially important for cases in which either the parent compound or product is more toxic than the other (e.g., chlorophenol products of triclosan oxidation).^{14,27,33-36} Competition between parent compounds and their products has been suggested in previous studies to explain decreases in oxidation rates or sorption as the reaction proceeds.²⁷ Other research investigates the treatment of contaminant mixtures in applied environmental systems such as simulated stormwater columns^{3,6-8} or wastewater.^{4,5,37} However, these studies rarely report oxidation rates and the impact of mechanistic changes or compound-specific effects have not been examined in these competitive solutions.

This study investigates the effect of mixtures on the initial kinetics and rate-limiting steps of phenol oxidation by δ -MnO₂. We react four phenols with differing toxicological effects, functional groups, and rates and mechanisms of oxidation with Mn oxides² in isolation and in mixtures to determine how oxidative mechanism and structural effects alter phenol oxidation in the presence of other compounds. To account for potential indirect oxidation by phenoxy radical products, experiments are conducted in the presence and absence of a non-specific radical quencher, *tert*-butanol. From these reactions, we (1) analyze changes in the initial pseudo-first-order rate constants and rate-limiting steps of each phenol in varying mixtures, (2) compare changes across the four contaminants to determine if mixtures affect oxidation mechanisms and rates of these phenols universally, and (3) examine how *tert*-butanol alters these results to provide insight into the interactive mechanisms at play in these mixture reactions. Our work suggests that mixtures do not affect phenolic contaminants universally as more reactive, electron

transfer-limited compounds are subject to a varying degree of competition for sorption sites while less reactive, sorption-limited phenols have enhanced oxidation kinetics in mixtures.

3.4 Materials and methods

3.4.1 Materials

Commercial chemicals were used as received. Ultrapure water was supplied by a Milli-Q water purification system maintained at 18.2 M Ω -cm. Bisphenol A, triclosan, resorcinol and 4,4'-biphenol stock solutions (5 mM) were prepared in methanol and stored at 4 °C. Further details are provided in Supporting Information (**Appendix B.1**).

3.4.2 δ -MnO₂ synthesis and characterization

δ -MnO₂ was synthesized by adding Mn(NO₃)₂ dropwise (1 mL min⁻¹) into a mixture of KMnO₄ and NaOH at a molar ratio of 3:2:4 Mn^{II}:Mn^{VII}:OH⁻, as reported previously.^{2,38,39} The slurry solution stirred for 20 hours and solids were removed by centrifuge washing at 2500 rpm for 15 minutes in decreasing volumes of Milli-Q water for three rounds, followed by two centrifuge washings in the pH 5.5 10 mM sodium acetate buffer solution. Reactions were started within 2 days of δ -MnO₂ synthesis to minimize mineral aging effects.

The average manganese oxidation number (AMON) of the δ -MnO₂ starting material was determined by oxalate titration^{2,40,41} and verified by X-ray absorption near edge spectroscopy (Mn K edge; 6532 eV).⁴² Aqueous manganese, as well as solid-phase sodium content, were quantified by inductively coupled plasma-optical emission spectrometry (ICP-OES; Perkin Elmer 4300). Specific surface area was determined by Brunauer–Emmett–Teller measurements

(Quantachrome Autosorb-1, nitrogen adsorbate; 30 °C). Data from manganese oxide characterization are presented in **Appendix B.2**.

3.4.3 Kinetic reactions

Resorcinol, bisphenol A, triclosan, and 4,4'-biphenol were reacted with δ -MnO₂ (15 mg-Mn/L) in triplicate batch reactions. Reactions of isolated compounds with δ -MnO₂ were done at concentrations of 10, 20 and 40 μ M (<0.1% MeOH) to test for concentration effects of each phenol and to serve as controls for mixture reactions. The four phenols were also reacted with δ -MnO₂ in each possible paired combination (10 μ M each, 20 μ M total organics) and in a mixture of all four phenols (10 μ M each, 40 μ M total organics). All reactions were conducted in pH 5.5 10 mM sodium acetate buffer which does not alter the reactivity of δ -MnO₂ with phenols;² pH changed less than 0.5 units during reactions. Rates of phenol oxidation by manganese oxides are pH dependent,^{1,20,43} these four chosen compounds react with δ -MnO₂ at pH 5.5 on a timescale of hours to days. Reactors were continuously stirred for up to 7 days in the dark to prevent photochemical degradation.

The 10 μ M isolated reactions, paired reactions, and mixture of all four phenols with δ -MnO₂ were repeated in the presence of 2 mM *tert*-butanol, a non-specific radical quencher,⁴⁴⁻⁵⁰ to determine the effect of product phenoxy radicals on oxidation rates and mechanisms. δ -MnO₂ characteristics were verified in the presence of *tert*-butanol and ascorbic acid in the absence of phenolic contaminants to ensure differences in sorption and oxidation rates in the presence of *tert*-butanol were not attributable to changes in δ -MnO₂ (**Appendix B.2**).

Two aliquots collected at each timepoint from triplicate reactors were filtered (0.2 μ M PTFE syringe filters) and quenched (5:1 ascorbic acid:Mn molar ratio) aqueous and total phenol

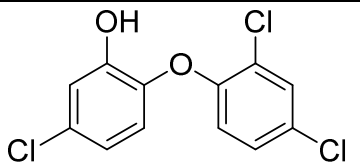
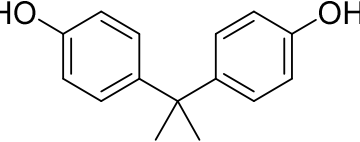
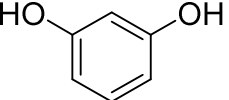
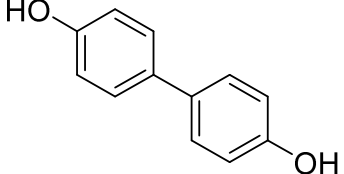
concentrations, respectively. Phenol concentrations were quantified by high performance liquid chromatography (**Appendix B.3**). Ascorbic acid quenched aliquots, in which the δ -MnO₂ is dissolved to released sorbed organics, were used to calculate initial pseudo-first-order rate constants. Phenol concentrations in filtered aliquots were subtracted from quenched aliquots to determine the fraction of each compound which sorbed to the Mn surface at each timepoint. Phenols with observed maximum sorption <10%, or with error greater than the average measured sorption, were designated sorption-limited, as validated previously.² Compounds with a maximum observed percent sorption >10% were classified as electron transfer-limited.

3.5 Results and discussion

It is well established that manganese oxides degrade phenolic contaminants;^{1, 2,31} however, the effects of phenol mixtures on oxidation by manganese oxides is not understood and may lead to enhanced or inhibited reaction rates. To determine the effects of a mixture of four known phenolic contaminants (resorcinol, 4,4'-biphenol, bisphenol A, and triclosan), we analyze the oxidation of these compounds with δ -MnO₂ alone, in pairs, and in mixtures of all four phenols. These compounds include an antimicrobial agent, pharmaceutical, antioxidant, and hormone disruptor (**Table 3.1**). Furthermore, resorcinol, triclosan, and bisphenol A are all electron transfer-limited and 4,4'-biphenol is sorption-limited with δ -MnO₂ based on previous reactions under similar reaction conditions.² Since the rate and extent of sorption play a large role in determining the overall rate and mechanism of phenol oxidation,² we hypothesize that all four phenols will have slower pseudo-first-order oxidation rates and less sorption due to competition effects in mixtures. Furthermore, we expect that these competition effects will

impact the oxidation of slower reacting and more sorption-limited phenols (e.g., 4,4'-biphenol) to a greater extent than the more reactive phenols (e.g., resorcinol) in solution.

Table 3.1. Chemical structure, contaminant class, and rate-limiting step of oxidation by δ -MnO₂ of each phenolic contaminant.

Phenol	Structure	Contaminant class	Rate limiting step
triclosan		antimicrobial	Electron transfer-limited
bisphenol A		endocrine disruptor	Electron transfer-limited
resorcinol		pharmaceutical	Electron transfer-limited
4,4'-biphenol		antioxidant	Sorption-limited

3.5.1 Phenol reactivity

Overall, the pseudo-first-order phenol oxidation rates rank resorcinol > bisphenol A > triclosan >> 4,4'-biphenol in isolated reactions with δ -MnO₂ (**Figures 3.1** and **3.2**). As in previous studies,² resorcinol, BPA, and triclosan are all electron transfer-limited with δ -MnO₂ as these compounds readily form precursor complexes with the Mn surface. 4,4'-Biphenol is sorption-limited, causing the orders of magnitude lower oxidation rate compared to the other three phenols (**Figures 3.1** and **3.2**).

Quantitative structure activity constants help explain the observed reactivity trends across these four phenols. Energy of the highest occupied molecular orbital (E_{HOMO}) and oxidation potential (E_{ox}) describe the susceptibility of each compound to oxidation, electron abstraction, or reaction. Higher energy of the highest occupied molecular orbital values indicate the molecule can lose an electron more favorably and thus will have higher oxidation rates; conversely, higher oxidation potentials indicate the molecule takes more energy to oxidize and thus has lower oxidation rates. These trends are corroborated by surveys of these reactivity constants versus phenol oxidation rates and mechanisms.^{2,51,52} E_{HOMO} values trend 4,4'-biphenol < bisphenol A < resorcinol ~ triclosan which agrees with the general order of pseudo-first-order oxidation rates in isolated reactions here and in previous studies, as triclosan and BPA have very similar oxidation rates.^{2,51,53,54} E_{ox} constants do not agree with these oxidation rates as 4,4'-biphenol and resorcinol have nearly equal E_{ox} values of 1.82 and 1.83 V vs. SHE, respectively, while triclosan has an E_{ox} of 2.07 V vs. SHE and bisphenol has the largest E_{ox} value of 2.22 V vs. SHE. Among these four phenols, 4,4'-biphenol has both the lowest E_{ox} value and lowest oxidation rate and thus E_{ox} does not predict isolated reaction rates among these four phenols.

Partitioning coefficients including acidity constants (pK_a), octanol:water partitioning (K_{ow}) and organic carbon:water partitioning (K_{oc}), which is a proxy for solid:water partitioning, help predict sorption behavior in single phenol reactions. pK_a values are similar for 4,4'-biphenol, bisphenol A, and resorcinol at 9.64, 9.78, and 9.26, respectively, while triclosan has a pK_a of 7.68. These values are not predictive of either reaction rates or sorption of these phenols in isolation with $\delta\text{-MnO}_2$ as bisphenol A and triclosan have the greatest sorption (90-100%; **Figure 3.1**), followed by resorcinol and then 4,4'-biphenol. Octanol:water and organic carbon:water constants (K_{ow} and K_{oc} , respectively) trend similarly across the four phenols as K_{ow}

increases from resorcinol < 4,4'-biphenol < bisphenol A < triclosan and K_{oc} increases from resorcinol < 4,4'-biphenol < triclosan ~ bisphenol A (**Table B.9**). These constants indicate that resorcinol is polar and preferentially partitions to water over non-polar solvents or organic carbon, which acts as a proxy for most solids whereas bisphenol A and triclosan partition relatively more to solvents and solids. These constants agree with the relative order of sorption to the Mn surface which trend 4,4'-biphenol < resorcinol << triclosan ~ bisphenol A.

In addition to 10 μM isolated reactions of each phenol with $\delta\text{-MnO}_2$, we analyze the sorption and oxidation rate for initial concentrations of 20 and 40 μM of each compound with $\delta\text{-MnO}_2$ to confirm that changes in pseudo-first-order rate and sorption are the result of mixture effects rather than difference in the total organic load in solution. These concentrations correspond to the total initial organic concentration in isolated reactions, paired mixtures, and all a combination of all four phenols in solution, respectively.

Initial concentration does not impact the rate or mechanism of oxidation for resorcinol, bisphenol A, or triclosan which are all electron transfer-limited and relatively reactive compounds (**Figure 3.1**). However, initial concentration influences the oxidation of 4,4'-biphenol by $\delta\text{-MnO}_2$. 4,4'-Biphenol oxidation rates increase from 3.1×10^{-3} to $7.2 \times 10^{-3} \text{ hr}^{-1}$ and sorption increases from $28 \pm 29\%$ to $56 \pm 32\%$ with increasing initial phenol concentration. This increase indicates a mechanism change from sorption-limited at initial concentrations of 10 and 20 μM , due to the large error and observed kinetic behavior, to electron transfer-limited at 40 μM . Notably, 4,4'-biphenol is also the only compound in this study which is sorption-limited at 10 and 20 μM concentrations. All three other phenols are electron transfer-limited across the range of concentrations with less than 20% changes in the pseudo-first-order oxidation rates.

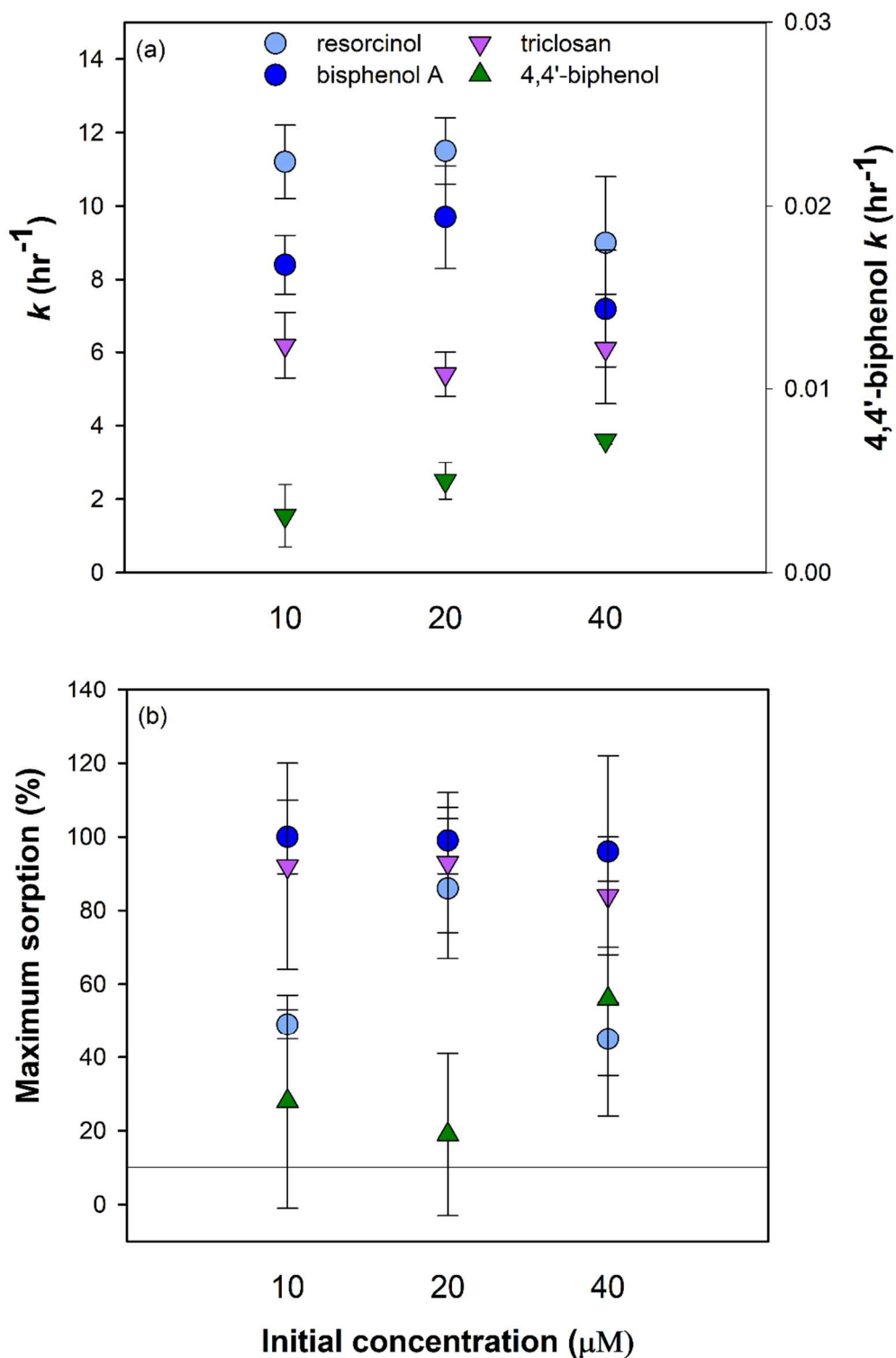


Figure 3.1. Pseudo-first-order oxidation rates (a) and maximum percent sorption (b) versus initial concentration of resorcinol, bisphenol A, triclosan, and 4,4'-biphenol reacted with $\delta\text{-MnO}_2$ at pH 5.5. Error bars are ± 1 standard deviation of triplicate reactors; the 10% line in plot b indicates the cutoff for sorption-limited (< 10% sorption) or electron transfer-limited (> 10% sorption) oxidation mechanisms.

Despite the increase in oxidation rates between 10 and 40 μM of 4,4'-biphenol (**Figure 3.1**), the differences in both oxidation rate and extent of sorption are less than those observed in the mixture solutions described below. Therefore, the lack of concentration effects affirms that changes in pseudo-first-order oxidation rates, sorption, and reaction mechanism are not the result of changes in the organic load, but instead are the effect of contaminant mixtures.

3.5.2 Impact of mixtures on electron transfer-limited phenols

Plotting the pseudo-first-order oxidation rates of these phenolic contaminants in mixtures shows differences across the phenols compared to their relative 10 μM isolated controls with $\delta\text{-MnO}_2$. The three phenols which are electron transfer-limited (i.e., triclosan, bisphenol A, and resorcinol) have similar decreases in both oxidation rates and sorption as a result of mixture effects. Triclosan is oxidized at rates of 4.8, 6.7, and 2.74 times slower with BPA, 4,4'-biphenol, and resorcinol, respectively, compared to the 10 μM isolated triclosan control, with decreases in sorption up to 47% in these mixtures (**Figure 3.2**). Triclosan is electron transfer-limited in all reactions and the decreases in rate and sorption support potential competition interactions between compounds for Mn surface sites.

Similar to triclosan, bisphenol A and resorcinol have minor changes in sorption and oxidation rates consistent with competition in these mixture solutions (**Figure 3.2**). BPA oxidation is 2 – 4 times slower in solution with triclosan and 4,4'-biphenol and 8.4 times slower in solution with all four phenols, while BPA sorption in these reactions decreases by up to 25%. The oxidation rate of resorcinol also decreases in all mixtures compared to the 10 μM control (**Figure 3.2**). Triclosan, 4,4'-biphenol and mixtures of all four phenols together result in 10 – 50 times lower oxidation rates of resorcinol and 2 – 3 times lower sorption.

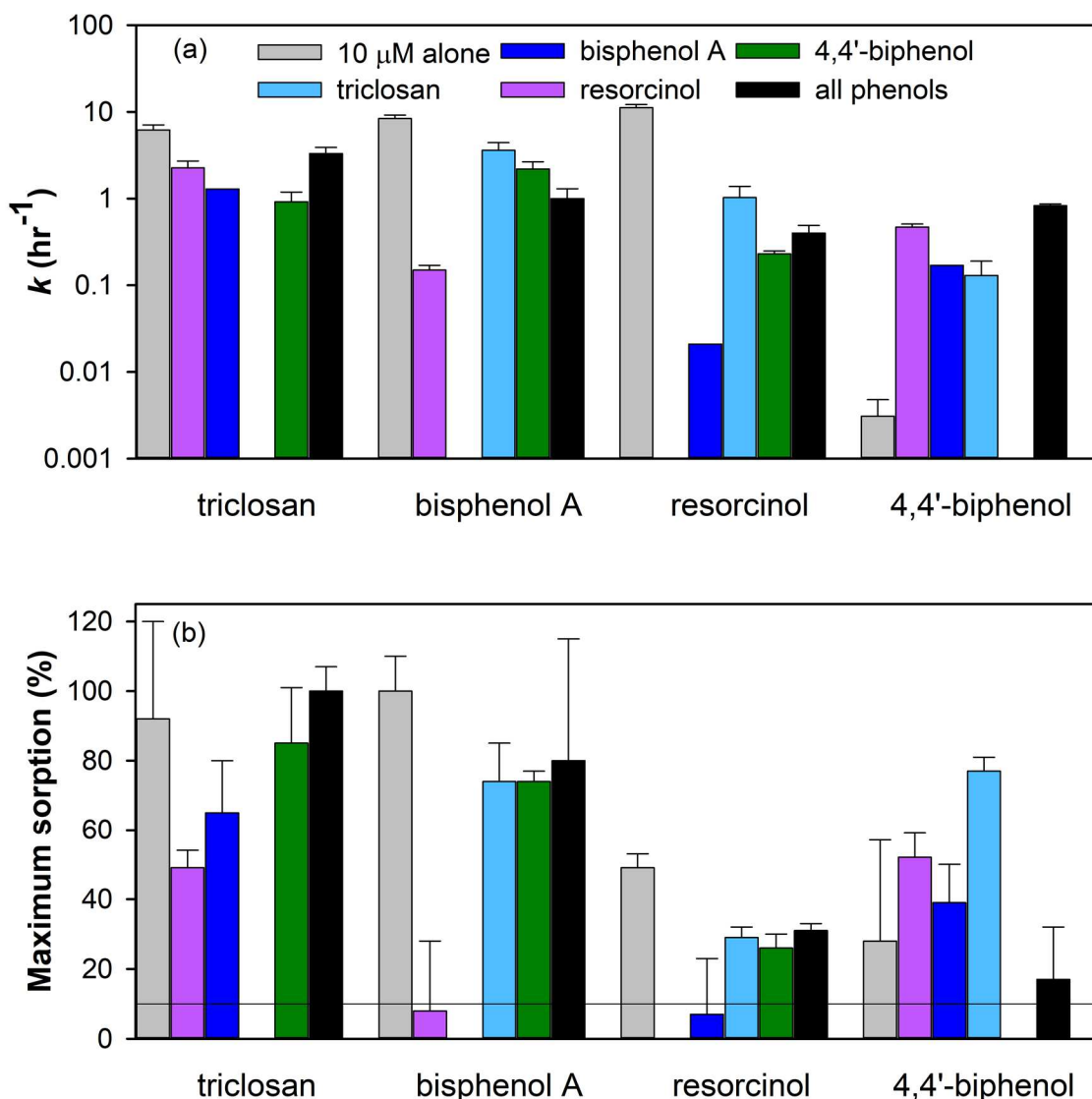


Figure 3.2. (a) Pseudo-first-order oxidation rates and (b) maximum percent sorption of resorcinol, bisphenol A, triclosan, and 4,4'-biphenol reacted with δ -MnO₂ at pH 5.5 in isolation or in mixture solutions with other phenolic contaminants. Error bars are ± 1 standard deviation of triplicate reactors; the 10% line in plot b indicates the cutoff for sorption-limited (< 10% sorption) or electron transfer-limited (> 10% sorption) oxidation mechanisms.

Interestingly, the pseudo-first-order oxidation rate of BPA is 56 times lower in solution with resorcinol, and sorption is also much lower (8% versus 100%) in this mixture. The lower extent of sorption correlates to a mechanism change as BPA is sorption-limited in solution with resorcinol but remains electron-transfer limited in all other mixtures (**Figure 3.2**). The oxidation rate of resorcinol in this mixture with BPA is three orders of magnitude lower than in isolated

solutions and resorcinol sorption is 7 times lower, dropping from 49 to 7%. As with BPA, resorcinol becomes sorption-limited rather than electron transfer-limited in this particular mixture.

These common changes in resorcinol and BPA in solution together indicate that resorcinol does not outcompete BPA, as would be expected based on the faster isolated kinetics of resorcinol than BPA, but rather both molecules are inhibited when in solution with δ -MnO₂ together. Both compounds become sorption-limited in solution with one another with decreased oxidation rates, suggesting that resorcinol and BPA react nearly simultaneously with δ -MnO₂ and block surface sites by filling those sites, electrostatic interactions, pi-pi orbital interactions, intermolecular bonding, and/or physical blocking of available sites. Because the extent of sorption is so low for both molecules (15% combined) compared to isolated reactions or other mixtures analyzed in this study, it is likely that electrostatic interactions and/or physical blocking of unfilled surface sites prevents sorption of these contaminants as δ -MnO₂ has a great enough concentration of surface sites to support 100% sorption of compounds in reactions with the same initial organic load (**Figure 3.2**).

These results suggest that phenolic contaminants which are electron transfer-limited with δ -MnO₂ are inhibited in mixtures due to competition interactions which limit sorption to the Mn surface and subsequently decrease oxidation rates. The extent of inhibition is not predicted by either extent of sorption or pseudo-first-order oxidation rates in isolated studies as bisphenol A has the greatest percent sorption to δ -MnO₂ and resorcinol has the highest pseudo-first-order rate constants in isolated systems. Oxidation rates of these two phenols are inhibited by mixtures with one another to the extent that they both become sorption-limited, while triclosan, which has

neither the greatest sorption nor fastest oxidation, remains electron transfer-limited in all mixtures.

Other physiochemical properties may predict these differences as triclosan has a much lower pK_a and higher $\log K_{ow}$ than the other compounds. These values indicate that triclosan is more negatively charged than the other phenols at the reaction pH and that it is more likely to partition to an organic phase than the aqueous buffer. As δ -MnO₂ has a point of zero charge around 2,^{1,2,26} it is negatively charged at the reaction pH of 5.5 suggesting the phenols with higher pK_a values will have more favorable electrostatic interactions with the negatively charged surface than triclosan.. The other three phenols have nearly equal first pK_a values and thus similar charges in these reactions which may enhance their competitive electrostatic interactions with each other compared to triclosan (e.g., resorcinol and BPA).

The higher $\log K_{ow}$ of triclosan may also help combat competitive interactions with other phenols as it has more favorable partitioning to organic phases (e.g., a hydrophobic, organic-loaded Mn surface) than aqueous solution. In contrast to triclosan's $\log K_{ow}$ of 4.76, resorcinol has a $\log K_{ow}$ value of 0.93 which indicates that resorcinol will likely remain in aqueous solution rather than partition to an organic phase. Similarly, resorcinol has the lowest $\log K_{oc}$ among the four phenols (**Table B.9**), again suggesting preferential partitioning to the aqueous buffer solution. These low partitioning constants help explain why resorcinol is outcompeted by triclosan and bisphenol A in solution since it most strongly partitions to the aqueous buffer. However, the same partitioning trends do not apply for bisphenol A despite the similar sorption and oxidation rate inhibitions between bisphenol A and resorcinol in mixtures.

These partitioning constants highlight the confounding factors impacting competition among these electron transfer-limited phenols in mixtures. Since oxidation rates in these

reactions depend on both precursor complex formation and reactivity with δ -MnO₂, predicting the outcome of these competitive interactions is complicated and depends on charge, oxidation potential, and partitioning behavior among other factors. However, the three, electron transfer-limited phenols showcased here each had varying physiochemical constants and reactivity in isolated solutions, yet all three are inhibited to some extent by all tested mixture combinations. Thus, these results are likely relevant for other phenolic contaminants which are electron transfer-limited under these conditions, such as chlorophenols, 4-nonylphenol, estrone and 17 β -estradiol.²

3.5.3 Impacts of mixtures on a sorption-limited phenol

Unlike the other three phenols which are all electron transfer-limited in isolated reactions and have decreased rates of oxidation and extent of sorption in mixtures, 4,4'-biphenol is sorption-limited with δ -MnO₂ and oxidizes faster with other phenols in solution compared to controls (**Figure 3.2**). With all three other phenolic contaminants, the pseudo-first-order oxidation rates of 4,4'-biphenol are an order of magnitude faster. Furthermore, 4,4'-biphenol sorbs 2-4 times more in paired mixtures than in isolation and is electron transfer-limited in these reactions rather than sorption-limited. The increased sorption in the presence of other compounds is in the range of higher concentration 4,4'-biphenol controls with δ -MnO₂, ranging from 19 – 56%, with the exception of the paired mixture with triclosan in which 77% of 4,4'-biphenol sorbs to the Mn surface. The shift from sorption-limited to electron transfer-limited oxidation of 4,4-biphenol in these mixtures may result from greater organic loading, since 40 μ M 4,4'-biphenol is also electron transfer-limited in isolate concentration controls (**Figure 3.1**); however, changes in the oxidation rate are not explained by the higher organic concentration.

These results indicate that 4,4'-biphenol oxidation is not inhibited by competition as the electron transfer-limited phenols are, but instead that another mechanism enhanced 4,4'-biphenol oxidation in these mixtures. One mechanism which may explain the enhanced oxidation rates without increased sorption in paired 4,4'-biphenol mixtures compared to high concentration controls is indirect oxidation by phenoxy radicals. As other compounds are oxidized by δ -MnO₂, they form a phenoxy radical as the product of the first electron transfer, which may remain sorbed to the Mn surface, undergo a second electron transfer, or diffuse from the surface and react in solution.^{1,2,21,31} When these radicals desorb, they are commonly thought to undergo radical coupling with other phenoxy radicals to form hydroquinone-like products.^{1,2,31} However, they may instead react with 4,4'-biphenol in solution, indirectly oxidizing this typically sorption-limited contaminant. This potential mechanism is further supported by the difference in rate limiting mechanisms between these compounds, as electron transfer-limited compounds quickly complex with the Mn surface, then undergo only one electron transfer as their overall oxidation rate is limited by the rate of the first electron transfer. In contrast, sorption-limited compounds form complexes with the Mn surface much slower before quickly undergoing both one electron transfer steps in succession to form a quinone-like product at the Mn surface site.^{1,2,31,32}

This mechanistic difference is supported by previous studies identifying phenolic oxidation products under varying reaction conditions. Balgooyen et. al.²⁷ demonstrated that polymeric product formation from BPA oxidation is not dependent on influent concentration despite changes in BPA oxidation rate and δ -MnO₂ reduction, suggesting that single-electron transfer reactions (i.e., electron transfer-limited reactions) are linked to radical coupled polymeric product formation compared to other oxidation products. Similarly, studies of triclosan and chlorophene oxidation by manganese oxides link fast, electron transfer-limited

reaction mechanisms with the formation of radical coupled dimer products identified by mass spectroscopy.⁴³

Based on evidence from these previous studies, resorcinol, bisphenol A, and triclosan are all likely to undergo only one electron transfer at the Mn surface, forming a phenoxy radical, as they are all electron transfer-limited in solution with 4,4'-biphenol. Thus, all three of these other contaminants may indirectly oxidize 4,4'-biphenol, enhancing the rate of 4,4'-biphenol degradation in contaminant slurries than is predicted by isolated experiments.

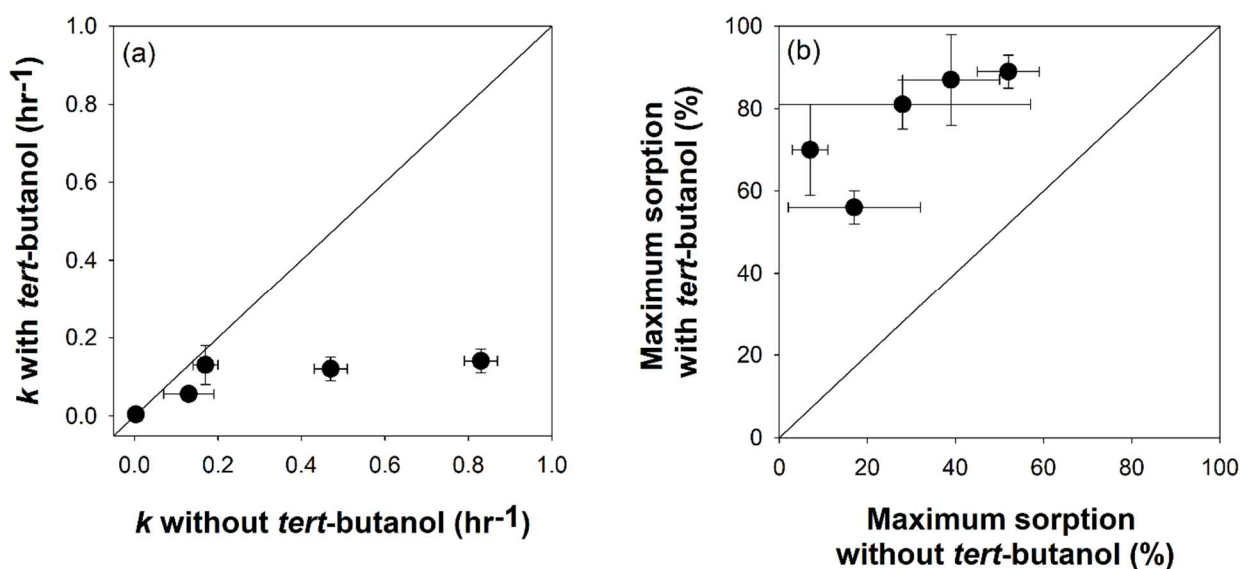


Figure 3.3. Plots of (a) pseudo-first-order oxidation rates and (b) maximum percent sorption of 4,4'-biphenol reacted with δ -MnO₂ with 2 mM *tert*-butanol in solution versus without *tert*-butanol. Each point is either an isolated reaction or mixture of 4,4'-biphenol with one or three other phenols in solution. Error bars are ± 1 standard deviation of triplicate reactors.

To test for the possible effects of indirect oxidation by radical production in these mixtures with sorption-limited 4,4'-biphenol, we repeated isolated 10 μM , paired mixtures, and combinations of all 4 phenol reactions in the presence of *tert*-butanol, a non-specific radical quencher.⁴⁴⁻⁵⁰ With the radical quencher in solution, triclosan, resorcinol, and bisphenol A had little change in reactivity in isolation or mixtures (**Section B.6**) while 4,4'-biphenol is again a

clear outlier in *tert*-butanol quenched mixtures. Sorption of 4,4'-biphenol to the δ -MnO₂ surface increases from $29 \pm 28\%$ to $81 \pm 6\%$ in unquenched and quenched 10 μ M controls, respectively, indicating that the presence of *tert*-butanol causes a shift from sorption-limited to electron transfer-limited oxidation mechanisms in the isolated solution (**Figure 3.3**). Strangely, the percent sorption increase in the 10 μ M isolated controls is not accompanied by a change in the pseudo-first-order oxidation rate, but may result from the greater organic load when 2 mM *tert*-butanol is in solution as with the 40 μ M concentration control.

4,4'-Biphenol oxidation rates and sorption do not change uniformly in all mixtures quenched by *tert*-butanol (**Figure 3.3**). In mixtures with both triclosan and BPA, 4,4'-biphenol pseudo-first-order oxidation rates in the presence of *tert*-butanol are similar to those without the radical quencher, while rates in the presence of resorcinol and all three other phenols decrease compared to the non-quenched analogues. Specifically, 4,4'-biphenol oxidation rates decrease from $0.47 \pm 0.04 \text{ hr}^{-1}$ to $0.12 \pm 0.03 \text{ hr}^{-1}$ with the addition of *tert*-butanol in paired mixtures with resorcinol (**Table B.5**). These rate changes are accompanied by more sorption to the Mn surface, ranging from 56 – 89% in the various mixtures, which is similar to the enhanced sorption of 81% observed in the *tert*-butanol quenched control. Since the extent of sorption is similar in quenched isolated controls and mixture solutions, we assume the presence of *tert*-butanol alone influences 4,4'-biphenol sorption to a greater extent than mixture effects in these quenched reactions. Furthermore, despite the increase in sorption in solutions containing both 4,4'-biphenol and resorcinol in the presence of *tert*-butanol, the oxidation rate is less than the unquenched reaction which had lower extents of sorption. The disconnect between increased sorption and decreased reaction rates in the presence of *tert*-butanol suggests that the oxidation of 4,4'-biphenol in these reactions is not dependent on the rates of sorption and electron transfer alone, but rather another

mechanism is at play. Since the oxidation rates decrease with a non-specific radical quencher in solution, this data supports our theory of indirect oxidation by oxidized resorcinol phenoxy radicals.

In addition to this direct evidence of radical-based indirect oxidation of 4,4'-biphenol in this system, phenolic contaminant oxidation by various radicals occurs in similar treatment systems. For example, rates of phenol oxidation and overall phenol removal by catalytic ozonation in wastewaters is diminished in the presence of *tert*-butanol, suggesting radical reactions dominate the degradation mechanism in the system.⁴⁶ Similarly, 2,4-dichlorophenol is also indirectly degraded by sulfate radicals produced in the peroxymonosulfate activation of α -, β -, or γ -MnO₂ as indicated by *tert*-butanol quenched controls.⁴⁵ Bisphenol A is degraded by •OH and •CO₃ in UV/sodium percarbonate and UV/H₂O₂ advanced oxidation processes⁴⁴ and alternative, radical-based mechanisms in oxidation by ferrate(VI)⁴⁸ as evidenced by decreased reaction rates and lower degradation in the presence of *tert*-butanol. However, when *tert*-butanol is added to reactions of BPA with peroxymonosulfate-activated δ -MnO₂, reaction rates do not significantly changed suggesting δ -MnO₂ rather than sulfate or hydroxyl radicals accounts for 94.5% of BPA oxidation by δ -MnO₂ under acidic conditions.⁴⁷

While these results are specific to phenolic contaminants in other oxidation-based treatment systems, they each support our findings. BPA degradation by peroxymonosulfate-activated δ -MnO₂ under acidic conditions does not depend on the presence of *tert*-butanol and thus is not dominated by indirect radical oxidation, which agrees with our findings for electron transfer-limited phenols which are affected by intermolecular competition interactions. Furthermore, the studies which demonstrate radical-mediated oxidation of phenolic contaminants point to decreased oxidation in the presence of *tert*-butanol as we observe for sorption-limited

4,4'-biphenol but not the other three, electron transfer-limited, phenols despite identical reaction conditions. Thus, this work demonstrates that intermolecular competition interactions such as physical blocking, electrostatic interactions, and intermolecular bonding (e.g., hydrogen bonding) inhibit oxidation of phenols which are electron transfer-limited in isolated reactions with δ -MnO₂. Furthermore, we provide evidence that sorption-limited 4,4'-biphenol oxidation is enhanced under these reaction conditions due to indirect oxidation by phenoxy radicals which are quenched in the presence of *tert*-butanol.

3.6 Environmental implications

Depending on the phenolic contaminant of interest, oxidation by Mn oxides may be either enhanced or inhibited by mixture effects. In general, electron transfer-limited contaminants, including resorcinol, BPA, and triclosan, have inhibited oxidation in mixtures due to competitive interactions with other compounds. In contrast, slow reacting and sorption-limited phenols such as 4,4'-biphenol are oxidized faster in mixtures. Our evidence suggests this increase in pseudo-first-order oxidation rates results from indirect oxidation by phenoxy radical products of other contaminants in solution. This is supported by observed product dependency on oxidation mechanisms in previous studies as well as decreases in oxidation rates despite increased sorption and mechanism changes in the presence of *tert*-butanol here. Product identification from mixtures with sorption-limited phenolic contaminants indirectly oxidized by manganese oxides is necessary to confirm this oxidation enhancement pathway. However, this is the first evidence of indirect oxidation in mixtures of phenolic contaminants by δ -MnO₂ and highlights the importance of extending mechanistic and kinetic studies to understand complex mixture dynamics.

In addition to furthering our understanding of phenol oxidation mechanisms and kinetics with manganese oxides, this study complements toxicological studies which demonstrate additive, multiplicative, and antagonistic effects of endocrine-disrupting phenolic contaminants in mice and fish, as both oxidation and hormone disruption processes are impacted by the mixture.^{16-18,55,56} Together, this research suggests that contaminated waste streams or natural waters which have mixtures of phenolic contaminants with toxicological effects^{3-5,57-59} may oxidize slower than expected with manganese oxides due to competition effects between electron transfer-limited compounds or have increased degradation resulting from indirect oxidation pathways in addition to altered uptake or hormone disruption behavior from the mixture.

Changes in pseudo-first-order oxidation rates are also accompanied by changes in sorption to the Mn surface in these multi-contaminant solutions, altering physical removal in treatment systems along with mechanisms of chemical degradation. These results are especially relevant for stormwater, wastewater, and landfill leachate which are primary candidates for treatment by manganese oxides, oxide-coated sands, or filter materials and contain a wide array of phenolic contaminants.^{1,3,4,6-8,25,37,59-62} Electron transfer-limited contaminants, which generally have higher oxidation rates with synthetic and reclaimed manganese oxides,^{2,32} will oxidize slower and sorb less than in isolated solutions, reducing both physical removal such as filtration by reactive media and chemical degradation treatments. In contrast, typically slow reacting sorption-limited contaminants will have increased oxidative degradation in solutions treated with manganese oxides. Indirect oxidation of these contaminants by phenoxy radical products of other phenols will also require less manganese surface site availability and less recharge of the reactive oxide media as indirect oxidation does not reduce the Mn surface, potentially making treatment

media longer-lasting and more effective overall for streams contaminated with compounds which undergo indirect oxidation.

3.7 Acknowledgements

Funding was provided by NSF (CBET 1509879 and CBET 1944464). Any opinions, findings, and conclusions or recommendations expressed in this material are those of the authors and do not necessarily reflect the views of the National Science Foundation. X-ray absorption spectroscopy was conducted at Sector 10 of the Advanced Photon Source, a U.S. Department of Energy (DOE) Office of Science User Facility operated for the DOE Office of Science by Argonne National Laboratory under Contract No. DE-AC02-06CH11357. MRCAT operations are supported by the Department of Energy and MRCAT member institutions.

3.8 Supporting information

Additional details on analytical methods, observed rate constants, and reactions of electron transfer-limited compounds with *tert*-butanol can be found in Appendix B.

3.9 References

1. Remucal, C. K.; Ginder-Vogel, M., A critical review of the reactivity of manganese oxides with organic contaminants. *Environ. Sci. Process. Impacts*, **2014**, *16*, (6), 1247-1266.
2. Trainer, E. L.; Ginder-Vogel, M.; Remucal, C. K., Organic structure and solid characteristics determine reactivity of phenolic compounds with synthetic and reclaimed manganese oxides. *Environ. Sci. Water Res. Technol.* **2020**, *6*, (3), 540-553.
3. Charbonnet, J. A.; Duan, Y.; van Genuchten, C. M.; Sedlak, D. L., Chemical regeneration of manganese oxide-coated sand for oxidation of organic stormwater contaminants. *Environ. Sci. Technol.* **2018**, *52*, (18), 10728-10736.
4. Yang, Y.; Ok, Y. S.; Kim, K. H.; Kwon, E. E.; Tsang, Y. F., Occurrences and removal of pharmaceuticals and personal care products (PPCPs) in drinking water and water/sewage treatment plants: A review. *Sci. Total Environ.* **2017**, *596-597*, 303-320.
5. Wu, Q.; Lam, J. C. W.; Kwok, K. Y.; Tsui, M. M. P.; Lam, P. K. S., Occurrence and fate of endogenous steroid hormones, alkylphenol ethoxylates, bisphenol A and phthalates in municipal sewage treatment systems. *J. Environ. Sci. (China)*, **2017**, *61*, 49-58.
6. Grebel, J. E.; Charbonnet, J. A.; Sedlak, D. L., Oxidation of organic contaminants by manganese oxide geomedia for passive urban stormwater treatment systems. *Water Res.*, **2016**, *88*, 481-491.
7. Luthy, R.; Sedlak, D. L. *Enhanced removal of nutrients and trace organic contaminants in pilot-scale stormwater treatment systems*; Water Research Foundation; Water Environment & Reuse Foundation; U.S. Environmental Protection Agency: U.S.A., 2017.
8. Okaikue-Woodi, F. E. K.; Cherukumilli, K.; Ray, J. R., A critical review of contaminant removal by conventional and emerging media for urban stormwater treatment in the United States. *Water Res.*, **2020**, *187*, 116434.
9. Zhang, H.; Chen, W. R.; Huang, C. H., Kinetic modeling of oxidation of antibacterial agents by manganese oxide. *Environ. Sci. Technol.* **2008**, *42*, (15), 5548-5554.
10. Zhang, Y.; Zhu, H.; Szewzyk, U.; Lübbecke, S.; Uwe Geissen, S., Removal of emerging organic contaminants with a pilot-scale biofilter packed with natural manganese oxides. *Chem. Eng. J.* **2017**, *317*, 454-460.
11. Bexfield, L. M.; Toccalino, P. L.; Belitz, K.; Foreman, W. T.; Furlong, E. T., Hormones and pharmaceuticals in groundwater used as a source of drinking water across the United States. *Environ. Sci. Technol.*, **2019**, *53*, (6), 2950-2960.
12. Bulloch, D. N.; Nelson, E. D.; Carr, S. A.; Wissman, C. R.; Armstrong, J. L.; Schlenk, D.; Larive, C. K., Occurrence of halogenated transformation products of selected pharmaceuticals and personal care products in secondary and tertiary treated wastewaters from southern California. *Environ. Sci. Technol.*, **2015**, *49*, (4), 2044-51.
13. Bonefeld-Jorgensen, E. C.; Long, M.; Hofmeister, M. V.; Vinggaard, A. M., Endocrine-disrupting potential of bisphenol A, bisphenol A dimethacrylate, 4-*n*-nonylphenol, and 4-*n*-octylphenol in vitro: New data and a brief review. *Environ. Health Perspect.*, **2007**, *115 Suppl. 1*, 69-76.
14. Covaci, A.; Voorspoels, S.; Abdallah, M. A.; Geens, T.; Harrad, S.; Law, R. J., Analytical and environmental aspects of the flame retardant tetrabromobisphenol-A and its derivatives. *J. Chromatogr. A.*, **2009**, *1216*, (3), 346-63.

15. Feng, Y.; Zhang, P.; Zhang, Z.; Shi, J.; Jiao, Z.; Shao, B., Endocrine disrupting effects of triclosan on the placenta in pregnant rats. *PLoS One*, **2016**, *11*, (5).
16. Pollock, T.; Mantella, L.; Reali, V.; deCatanzaro, D., Influence of tetrabromobisphenol A, with or without concurrent triclosan, upon bisphenol A and estradiol concentrations in mice. *Environ. Health Perspect.*, **2017**, *125*, (8).
17. Pollock, T.; Weaver, R. E.; Ghasemi, R.; deCatanzaro, D., A mixture of five endocrine-disrupting chemicals modulates concentrations of bisphenol A and estradiol in mice. *Chemosphere*, **2018**, *193*, 321-328.
18. Li, Z.; Zhang, H.; Gibson, M.; Li, J., An evaluation on combination effects of phenolic endocrine disruptors by estrogen receptor binding assay. *Toxicol. In Vitro*, **2012**, *26*, (6), 769-774.
19. Pizzigallo, M. D. R.; Ruggiero, P.; Crecchio, C.; Mininni, R., Manganese and iron-oxides as reactants for oxidation of chlorophenols. *Soil Sci. Soc. Am. J.*, **1995**, *59*, (2), 444-452.
20. Stone, A. T., Reductive dissolution of manganese(III/IV) oxides by substituted phenols. *Environ. Sci. Technol.*, **1987**, *21*, (10), 979-988.
21. Ulrich, H. J.; Stone, A. T., Oxidation of chlorophenols adsorbed to manganese oxide surfaces. *Environ. Sci. Technol.*, **1989**, *23*, (4), 421-428.
22. Borch, T.; Kretzschmar, R.; Kappler, A.; Van Cappellen, P.; Ginder-Vogel, M.; Voegelin, A.; Campbell, K., Biogeochemical redox processes and their impact on contaminant dynamics. *Environ. Sci. Technol.*, **2010**, *44*, (1), 15-23.
23. Skousen, J.; Zipper, C. E.; Rose, A.; Ziemkiewicz, P. F.; Nairn, R.; McDonald, L. M.; Kleinmann, R. L., Review of passive systems for acid mine drainage treatment. *Mine Water Environ.*, **2016**, *36*, (1), 133-153.
24. Liu, W.; Langenhoff, A. A. M.; Sutton, N. B.; Rijnaarts, H. H. M., Biological regeneration of manganese(IV) and iron(III) for anaerobic metal oxide-mediated removal of pharmaceuticals from water. *Chemosphere*, **2018**, *208*, 122-130.
25. Grebel, J. E.; Mohanty, S. K.; Torkelson, A. A.; Boehm, A. B.; Higgins, C. P.; Maxwell, R. M.; Nelson, K. L.; Sedlak, D. L., Engineered infiltration systems for urban stormwater reclamation. *Environ. Eng. Sci.*, **2013**, *30*, (8), 437-454.
26. Post, J. E., Manganese oxide minerals: Crystal structures and economic and environmental significance. *Proc. Natl. Acad. Sci. U.S.A.*, **1999**, *96*, (7), 3447-3454.
27. Balgooyen, S.; Campagnola, G.; Remucal, C. K.; Ginder-Vogel, M., Impact of bisphenol A influent concentration and reaction time on MnO₂ transformation in a stirred flow reactor. *Environ. Sci. Process. Impacts*, **2019**, *21*, (1), 19-27.
28. Park, J. W.; Dec, J.; Kim, J. E.; Bollag, J. M., Effect of humic constituents on the transformation of chlorinated phenols and anilines in the presence of oxidoreductive enzymes or birnessite. *Environ. Sci. Technol.*, **1999**, *33*, (12), 2028-2034.
29. Zhao, L.; Yu, Z.; Peng, P.; Huang, W.; Dong, Y., Oxidative transformation of tetrachlorophenols and trichlorophenols by manganese dioxide. *Environ. Toxicol. Chem.* **2009**, *28*, (6), 1120-9.
30. Shaikh, N.; Taujale, S.; Zhang, H.; Artyushkova, K.; Ali, A. S.; Cerrato, J. M., Spectroscopic investigation of interfacial interaction of manganese oxide with triclosan, aniline, and phenol. *Environ. Sci. Technol.*, **2016**, *50*, (20), 10978-10987.
31. Stone, A. T.; Morgan, J. J., Reduction and dissolution of manganese(III) and manganese(IV) oxides by organics: 2. Survey of the reactivity of organics. *Environ. Sci. Technol.*, **1984**, *18*, (8), 617-24.

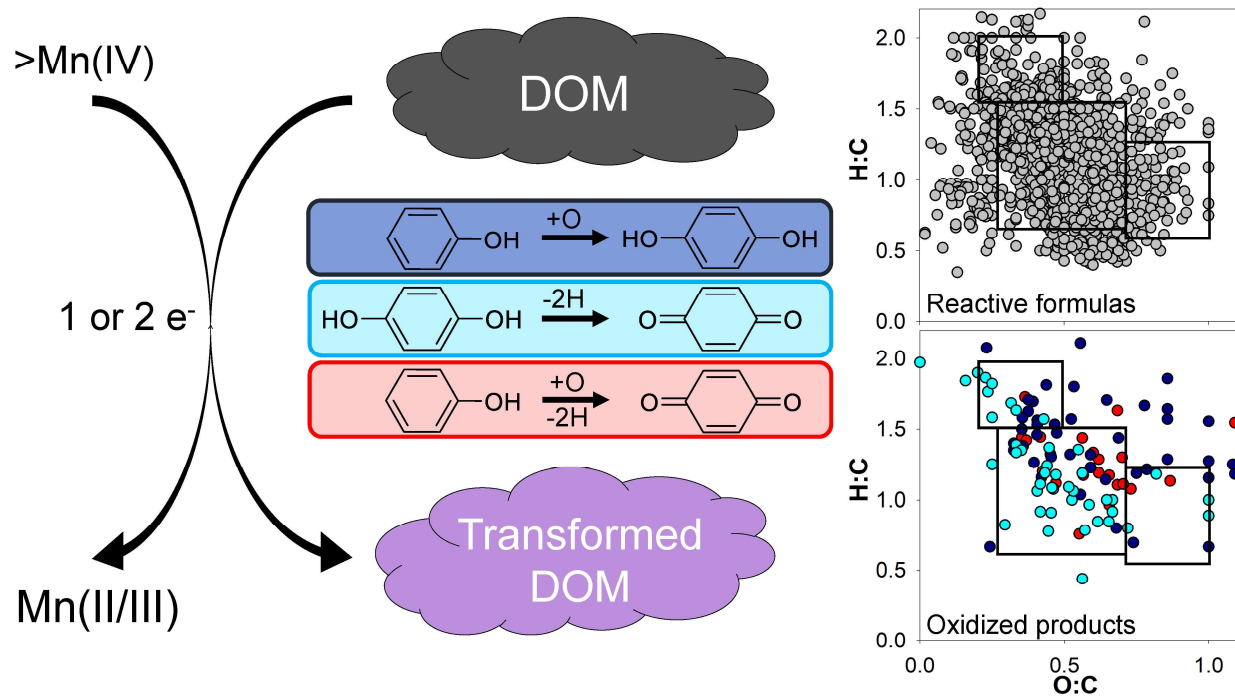
32. Shaikh, N.; Zhang, H.; Rasamani, K.; Artyushkova, K.; Ali, A. S.; Cerrato, J. M., Reaction of bisphenol A with synthetic and commercial $MnO_{x(s)}$: Spectroscopic and kinetic study. *Environ. Sci. Process. Impacts*, **2018**, *20*, (7), 1046-1055.
33. Ding, J.; Su, M.; Wu, C.; Lin, K., Transformation of triclosan to 2,8-dichlorodibenzo-*p*-dioxin by iron and manganese oxides under near dry conditions. *Chemosphere*, **2015**, *133*, 41-46.
34. Jiang, L.; Gu, Y.; Guo, H.; Liu, L.; Chen, J., Efficient removal of 17 α -ethinylestradiol (EE2) from water using freshly formed Fe–Mn binary oxide. *RSC Advances*, **2017**, *7*, (38), 23802-23811.
35. Liu, A.; Shi, J.; Qu, G.; Hu, L.; Ma, Q.; Song, M.; Jing, C.; Jiang, G., Identification of emerging brominated chemicals as the transformation products of tetrabromobisphenol A (TBBPA) derivatives in soil. *Environ. Sci. Technol.*, **2017**, *51*, (10), 5434-5444.
36. Im, J.; Prevatte, C. W.; Campagna, S. R.; Loffler, F. E., Identification of 4-hydroxycumyl alcohol as the major MnO_2 -mediated bisphenol a transformation product and evaluation of its environmental fate. *Environ. Sci. Technol.*, **2015**, *49*, (10), 6214-6221.
37. Bina, B.; Mohammadi, F.; Amin, M. M.; Pourzamani, H. R.; Yavari, Z., Determination of 4-nonylphenol and 4-*tert*-octylphenol compounds in various types of wastewater and their removal rates in different treatment processes in nine wastewater treatment plants of iran. *Chin. J. Chem. Eng.*, **2018**, *26*, (1), 183-190.
38. Murray, J. W., The surface chemistry of hydrous manganese dioxide. *J. Colloid Interf. Sci.*, **1974**, *46*, (3), 357-371.
39. Balgooyen, S.; Alaimo, P. J.; Remucal, C. K.; Ginder-Vogel, M., Structural transformation of MnO_2 during the oxidation of bisphenol A. *Environ. Sci. Technol.*, **2017**, *51*, (11), 6053-6062.
40. Fowler, R. M.; Bright, H. Standardization of permanganate solutions with sodium oxalate. *J. Res. Natl. Bur. Stand.*, **1935**, *15*.
41. Ohlweiler, O. A.; Schneider, A. M. H., Standardization of potassium permanganate by titration of sodium oxalate in presence of perchloric acid and manganese(II) sulfate. *Anal. Chim. Acta*, **1972**, *58*, 477-480.
42. Manceau, A.; Marcus, M. A.; Grangeon, S., Determination of Mn valence states in mixed-valent manganates by XANES spectroscopy. *Am. Mineral.*, **2012**, *97*, (5-6), 816-827.
43. Zhang, H.; Huang, C. H., Oxidative transformation of triclosan and chlorophene by manganese oxides. *Environ. Sci. Technol.*, **2003**, *37*, (11), 2421-2430.
44. Gao, J.; Duan, X.; O'Shea, K.; Dionysiou, D. D., Degradation and transformation of bisphenol A in UV/sodium percarbonate: Dual role of carbonate radical anion. *Water Res.*, **2020**, *171*.
45. Liu, J.; An, F.; Li, M.; Yang, L.; Wan, J.; Zhang, S., Efficient degradation of 2,4-dichlorophenol on activation of peroxymonosulfate mediated by MnO_2 . *Bull. Environ. Contam. Toxicol.*, **2021**.
46. Shahamat, Y. D.; Farzadkia, M.; Nasserli, S.; Mahvi, A. H.; Gholami, M.; Esrafil, A., Magnetic heterogeneous catalytic ozonation: A new removal method for phenol in industrial wastewater. *J. Env. Health Sci. Eng.*, **2014**, *12*, (50).
47. Huang, J.; Dai, Y.; Singewald, K.; Liu, C.-C.; Saxena, S.; Zhang, H., Effects of MnO_2 of different structures on activation of peroxymonosulfate for bisphenol A degradation under acidic conditions. *Chem. Eng. J.*, **2019**, *370*, 906-915.

48. Zhang, P.; Zhang, G.; Dong, J.; Fan, M.; Zeng, G., Bisphenol A oxidative removal by ferrate (Fe(VI)) under a weak acidic condition. *Sep. Purif. Technol.*, **2012**, *84*, 46-51.
49. Zhou, K.; Zhang, J.; Xiao, Y.; Zhao, Z.; Zhang, M.; Wang, L.; Zhang, X.; Zhou, C., High-efficiency adsorption of and competition between phenol and hydroquinone in aqueous solution on highly cationic amino-poly(vinylamine)-functionalized GO-(o-MWCNTs) magnetic nanohybrids. *Chem. Eng. J.*, **2020**, *389*.
50. Zou, S.; Zhang, B.; Yan, N.; Zhang, C.; Xu, H.; Zhang, Y.; Rittmann, B. E., Competition for molecular oxygen and electron donor between phenol and quinoline during their simultaneous biodegradation. *Process Biochem.*, **2018**, *70*, 136-143.
51. Pavitt, A. S.; Bylaska, E. J.; Tratnyek, P. G., Oxidation potentials of phenols and anilines: Correlation analysis of electrochemical and theoretical values. *Environ. Sci. Process. Impacts*, **2017**, *19*, (3), 339-349.
52. Arnold, W. A.; Oueis, Y.; O'Connor, M.; Rinaman, J. E.; Taggart, M. G.; McCarthy, R. E.; Foster, K. A.; Latch, D. E., Qsars for phenols and phenolates: Oxidation potential as a predictor of reaction rate constants with photochemically produced oxidants. *Environ. Sci. Process. Impacts*, **2017**, *19*, (3), 324-338.
53. Canonica, S.; Tratnyek, P. G., Quantitative structure-activity relationships for oxidation reactions of organic chemicals in water. *Environ. Toxicol. Chem.*, **2003**, *22*, (8), 1743-1754.
54. Salter-Blanc, A. J.; Bylaska, E. J.; Lyon, M. A.; Ness, S. C.; Tratnyek, P. G., Structure-activity relationships for rates of aromatic amine oxidation by manganese dioxide. *Environ. Sci. Technol.*, **2016**, *50*, (10), 5094-5102.
55. Ruczynska, W.; Szlinder-Richert, J.; Nermer, T., The occurrence and distribution of nonylphenols and nonylphenol ethoxylates in different species of fish. *Environ. Sci. Process. Impacts*, **2020**, *22*, (4), 1057-1070.
56. Toft, G.; Baatrup, E., Sexual characteristics are altered by 4-*tert*-octylphenol and 17 β -estradiol in the adult male guppy (*Poecilia reticulata*). *Ecotoxicol. Environ. Saf.*, **2001**, *48*, (1), 76-84.
57. Lu, D.; Feng, C.; Wang, D.; Lin, Y.; Ip, H. S.; She, J.; Xu, Q.; Wu, C.; Wang, G.; Zhou, Z., Analysis of twenty phenolic compounds in human urine: Hydrochloric acid hydrolysis, solid-phase extraction based on K₂CO₃-treated silica, and gas chromatography tandem mass spectrometry. *Anal. Bioanal. Chem.*, **2015**, *407*, (14), 4131-4141.
58. Drewes, J. E.; Letzel, T., Chemicals of emerging concern and their transformation products in the aqueous environment. In *Assessing transformation products of chemicals by non-target and suspect screening – strategies and workflows volume 1*, **2016**; pp 3-9.
59. Thomaidis, N. S.; Gago-Ferrero, P.; Ort, C.; Maragou, N. C.; Alygizakis, N. A.; Borova, V. L.; Dasenaki, M. E., Reflection of socioeconomic changes in wastewater: Licit and illicit drug use patterns. *Environ. Sci. Technol.*, **2016**, *50*, (18), 10065-10072.
60. Wolfand, J. M.; Seller, C.; Bell, C. D.; Cho, Y. M.; Oetjen, K.; Hogue, T. S.; Luthy, R. G., Occurrence of urban-use pesticides and management with enhanced stormwater control measures at the watershed scale. *Environ. Sci. Technol.*, **2019**.
61. Montes-Grajales, D.; Fennix-Agudelo, M.; Miranda-Castro, W., Occurrence of personal care products as emerging chemicals of concern in water resources: A review. *Sci. Total Environ.*, **2017**, *595*, 601-614.

62. Oulton, R. L.; Kohn, T.; Cwiertny, D. M., Pharmaceuticals and personal care products in effluent matrices: A survey of transformation and removal during wastewater treatment and implications for wastewater management. *J. Environ. Monit.*, **2010**, *12*, (11), 1956-1978.

Chapter 4

Selective reactivity and oxidation of dissolved organic matter by manganese oxides



4.1 Collaboration information

This chapter was completed by Emma L. Trainer, Matthew Ginder-Vogel, and Christina K. Remucal. E. L. Trainer completed all laboratory experiments and data analyses. E. L. Trainer, M. Ginder-Vogel, and C. K. Remucal wrote the manuscript. This chapter is in review at a journal.

4.2 Abstract

Dissolved organic matter (DOM) varies widely across natural and engineered systems, but little is known about the influence of DOM composition on its reactivity with manganese oxides. Here, we investigate bulk and molecular transformations of 30 diverse DOM samples after reaction with acid birnessite, a strong oxidant that may react with DOM in soils or engineered treatment systems. The reaction of DOM with acid birnessite reduces Mn and forms DOM that is generally more aliphatic and lower in molecular weight, but the extent of reaction is linked to water type (e.g., wastewater, rivers) and highly aromatic DOM undergoes greater changes. Despite the variability in reactivity due to DOM composition, products attributable to the oxidation of phenolic precursors are identified in waters analyzed by high-resolution mass spectrometry. The number of matched product formulas correlates significantly with indicators of DOM aromaticity, such as double-bond equivalents ($p = 2.43 \times 10^{-4}$). At the molecular level, highly aromatic, lignin-like carbon reacts selectively with acid birnessite in all samples despite the variability in initial DOM composition, resulting in the formation of a wide range of products. These findings demonstrate that DOM oxidation occurs in all tested waters, but also suggest that the reactivity and overall transformation of DOM by acid birnessite is composition-dependent and linked to DOM source and initial aromaticity.

4.3 Introductions

Dissolved organic matter (DOM) is a complex mixture of thousands of individual molecules containing carbon, hydrogen, oxygen, and heteroatoms (e.g., nitrogen, sulfur).¹⁻³ DOM is heterogeneous across natural and engineered waters with differing reactive functional groups, molecular weights, and aromaticity.^{2,4-9} DOM source (e.g., allochthonous versus

autochthonous) and extent of environmental processing alter its composition,^{5,10-13} with implications for bioavailability, contaminant mobility,^{4,9,14-17} photochemical transformation,^{5,8,18} and reactivity with oxidants (e.g., chlorine).^{12,13,19-22}

Metal oxides comprised of manganese(III/IV), hereafter referred to as manganese (Mn) oxides, are ubiquitous, redox active minerals that react with inorganic²³⁻²⁵ and organic compounds,²⁶⁻³³ including DOM.^{27,31,34-38} The reactivity of DOM with Mn oxides has important implications for DOM composition in the subsurface. Additionally, DOM may compete with target contaminants in treatment oxidation systems using Mn oxides. However, the heterogeneous nature of DOM complicates our understanding of its reactivity with Mn oxides. There are many possible transformation pathways for the various functional groups within DOM (e.g., phenols). Sorption and oxidation are the most widely considered reactions due to the sorption capacity and strong oxidation potential of naturally-occurring birnessite minerals (i.e., MnO₂).^{23,27,34,36,39,40} After sorption to the Mn surface, phenols may be oxidized via one- or two-electron transfer reactions to produce either hydroquinone- or quinone-like oxidation products, while Mn(IV) reaction sites are reduced to Mn(III) or Mn(II) centers, respectively. The oxidized organic carbon molecule and reduced Mn cation may remain sorbed to the Mn mineral surface or desorb into solution.^{27,29,30}

Each of these reaction steps between DOM and Mn oxides may alter the DOM pool and solid-phase Mn oxide chemistry. Sorption may fractionate DOM as molecules with higher aromaticity or molecular weight may be more likely to sorb.^{18,41,42} If electron transfer and product desorption then occurs, transformed organic products will shift the average DOM composition towards more oxidized carbon while releasing reduced Mn(II/III) cations. As

Mn(II/III) cations are released into solution, ligand stabilization of aqueous Mn can further fractionate DOM by forming non-filter passing organic matter-Mn(II/III) colloids.^{31,34,37}

Despite the possibility for DOM fractionation and multiple reaction mechanisms, there are a lack of studies comparing transformations across different DOM sources to determine how composition influences reactivity with Mn oxides. Most research on this system focuses either on the changes in Mn structure and DOM sorption^{35,36,43} or on comparing multiple Mn oxides reacted with DOM isolates and/or model compounds.^{34,44} Studies that include whole water DOM commonly seek to understand interactions with dissolved trace metals (e.g., Fe, Al).⁴⁵⁻⁴⁷ Due to the nature of these studies, changes in organic carbon are typically attributed to oxidation based on evidence of Mn reduction or small organic acid product formation.^{16,37,38} However, these studies do not provide conclusive proof that DOM oxidation occurs, therefore it is challenging to apply their results to more complex systems or diverse DOM sources.

This study examines how DOM composition influences reactivity with MnO₂ and evaluates the extent of its oxidation across a range of DOM sources. We combine bulk DOM analyses (e.g., UV-vis measurements) with high-resolution mass spectrometry and X-ray absorption near edge spectroscopy (XANES) to decouple sorption and oxidative mechanisms and link specific molecular transformations to potential bulk predictors of DOM reactivity. Our results demonstrate that (1) DOM reactivity and transformation by acid birnessite is dependent on DOM composition and correlates most strongly with measures of aromaticity; (2) oxidation occurs across diverse waters and wastewater effluents reacted with acid birnessite; (3) high-resolution mass spectrometry is necessary to confirm the production of oxidized products; and (4) although reactivity is dependent on DOM composition, the same lignin-like, highly aromatic formulas react in each water to form various transformation products.

4.4 Materials and methods

4.4.1 Materials

All chemicals were commercially available and used as received. Acid birnessite was synthesized as described previously.^{26,48} For more information, see **Appendix C.1**.

4.4.2 Sampling

Thirty water samples were collected from sites across Wisconsin and Minnesota between 2017 and 2019 (**Appendix C.2**). All waters were filtered (0.22 μm nylon) within 24 hours of collection and stored in amber glass bottles at 4 °C. Waters were re-filtered prior to reactions.

Wastewater samples were collected from two separate sanitation districts. WW1 is final effluent treated by disinfection and dechlorination. Samples from the second treatment plant include secondary effluent (WW2), final effluent after UV disinfection (WW3), and a sample immediately downstream of effluent release (WW4).

Water bodies included rivers (R), bogs (B), or lakes; lakes were categorized by their trophic status as oligotrophic (O), mesotrophic (M), or eutrophic (E).^{18,49,50} Surface grab samples were collected at least 1 m from shore. Waters from the Madison, WI area include R1-R4 from the Yahara River and Badfish Creek and lakes E1-E3. Waters collected from rural Wisconsin include M1-M2 and E4, as well as O1 – O4, B1 – B2, and M3; the latter seven lakes are core sites in the North Temperate Lakes-Long Term Ecological Research (NTL-LTER) program.⁵¹ Samples R5-R8 were collected from the St. Louis River in MN, along with E5-E7 and O5 sampled from the barrier peninsula separating Superior Bay and Lake Superior, respectively (**Table C.1; Figure C.1**).

4.4.3 Reactions

This study includes three sets of reactions: a kinetic study of WW1 transformation to determine reaction timing (**Appendix C.3**), examination of Mn and bulk DOM changes in 30 unique waters reacted with acid birnessite for 50 hours and 28 days (**Appendix C.4**), and molecular characterizations of 14 waters preceding and following 50-hour reactions with acid birnessite (**Table C.5**).

Reactions were buffered by 10 mM NaHCO_3^- in addition to initial alkalinity at $\text{pH } 7.0 \pm 0.5$. Carbonate buffer was chosen for its minimal interactions with both Mn oxides³⁰ and organic carbon quantification, as well the ubiquity of carbonate in natural waters.⁵² All reactions were conducted in sealed sacrificial reactors with no headspace to prevent atmospheric exchange of CO_2 ; pH remained within 0.5 pH units of initial values after experiments.

Waters with $[\text{DOC}]$ above 9 mg-C L^{-1} were diluted to $9.0 \pm 0.4 \text{ mg-C L}^{-1}$ (0.75 mM C) and reacted with 90 mg L^{-1} acid birnessite (1.05 mM Mn). Waters with lower $[\text{DOC}]$ were reacted with a proportional concentration of acid birnessite to preserve the 3:4 C:Mn molar ratio. Reactors were stirred at 350 rpm under dark conditions. After 50 hours and 28 days, sacrificial reactors were filtered ($0.22 \text{ }\mu\text{m}$ nylon) to remove particulate Mn. Filtered particulate manganese was air dried at room temperature ($22 \pm 2 \text{ }^\circ\text{C}$) for solid-phase analysis. Analogous control experiments were conducted in the absence of acid birnessite to determine DOM stability.

Filtered particulate average manganese oxidation number (AMON) was measured by quick scanning X-ray Absorption Near-Edge Structure spectroscopy (Q-XANES) and the resulting spectra were analyzed using linear combination fitting.⁵³ Filtrates were analyzed for $[\text{DOC}]$, SUVA_{254} , $\text{E}_2:\text{E}_3$, and aqueous Mn(II/III) concentrations as described above.

4.4.4 Mass spectrometry analysis

The molecular composition of DOM in 14 waters was analyzed before and after reaction with acid birnessite by Fourier transform-ion cyclotron resonance mass spectrometry (FT-ICR MS; Bruker Solarix XR 12T). These waters (**Table C.5**) were selected to represent a range of water types and DOM composition. Organic matter was extracted from filtrates (250 mL) by solid phase extraction (Agilent PPL).⁵⁴ Following negative electrospray ionization and FT-ICR MS analysis from 200-1000 m/z , m/z ions were converted to neutral masses, calibrated using common DOM formulas, and assigned formulas in R.^{5,12,13} Formula matches using the boundaries of $C_{1-180}^{13}C_{0-1}H_{1-140}O_{0-80}N_{0-1}S_{0-1}$ were required to be within <0.5 ppm mass error and fall within a homologous series (O vs. CH_4 or $+CH_2$).⁵⁵ Details on sample preparation, analysis by FT-ICR MS, formula matching, and calculations are provided in **Appendix C.5**.

Following formula matching, relative intensities were calculated for each assigned m/z peak by dividing the absolute peak intensity by the total intensity of all identified formulas within each sample. Weighted averages of H:C, O:C, molecular weight, and double bond equivalents ($H:C_w$, $O:C_w$, MW_w , and DBE_w) were calculated using relative intensity.^{5,8,12,13,18,56} Samples were grouped by principal component analysis (PCA) using the relative intensities of identified formulas in each sample or the change in relative formula intensities from the control to the treated waters (**Appendix C.5.2**).

Further analysis of FT-ICR MS results was based on relative intensity changes and formula presence/absence between the control and treated samples.¹³ Oxidation products were identified using expected mass changes for the oxidation of phenolic moieties to quinone-type products (i.e., -1H, -2H, +1O, +1O/-2H). Possible product masses were determined for each

matched formula in control samples then cross checked against the matched formulas in control and treated samples to identify unique products.

4.5 Results and Discussion

4.5.1 Bulk DOM and Mn oxide transformation

To investigate the influence of DOM composition on reactivity, we reacted acid birnessite with 30 waters ranging in DOM composition (**Table C.2**) and chemistry (**Tables C.3** and **C.4**).^{5,56,57} These variations are the result of environment-specific factors, including differences in organic matter source, extent of environmental processing, and waterbody type (**Appendix C.2**). Studies of DOM isolates, model compounds, and single DOM samples reacted with Mn oxides provide contradictory results. For instance, some studies report little sorption to the Mn oxide surface,⁴⁴ while others report extensive sorption and fractionation,^{34,36,37,39,58,59} with varying transformation products^{16,36} and extent of reductive Mn oxide dissolution.^{16,29,35,39,59-61} Based on these results, DOM composition is expected to influence the extent and manner of bulk DOM changes among the 30 waters. Specifically, we hypothesize that aromatic DOM from bogs and rivers will have greater changes in [DOC], SUVA₂₅₄, E₂:E₃, and Mn chemistry than less aromatic, microbially-processed lakes because aromatic moieties (e.g., phenols) have greater sorption capacities and can be redox active.

To test this hypothesis, changes in [DOC], SUVA₂₅₄, E₂:E₃, AMON, and aqueous [Mn] are analyzed for the first 50 hours of reaction, based on initial kinetic experiments up to 50 hours with WW1 (**Appendix C.3**). These reactions were repeated for 28 days to quantify long-term transformation of bulk DOM and Mn; general trends discussed here are the same for the 50-hour and 28-day reactions (**Appendix C.4**).

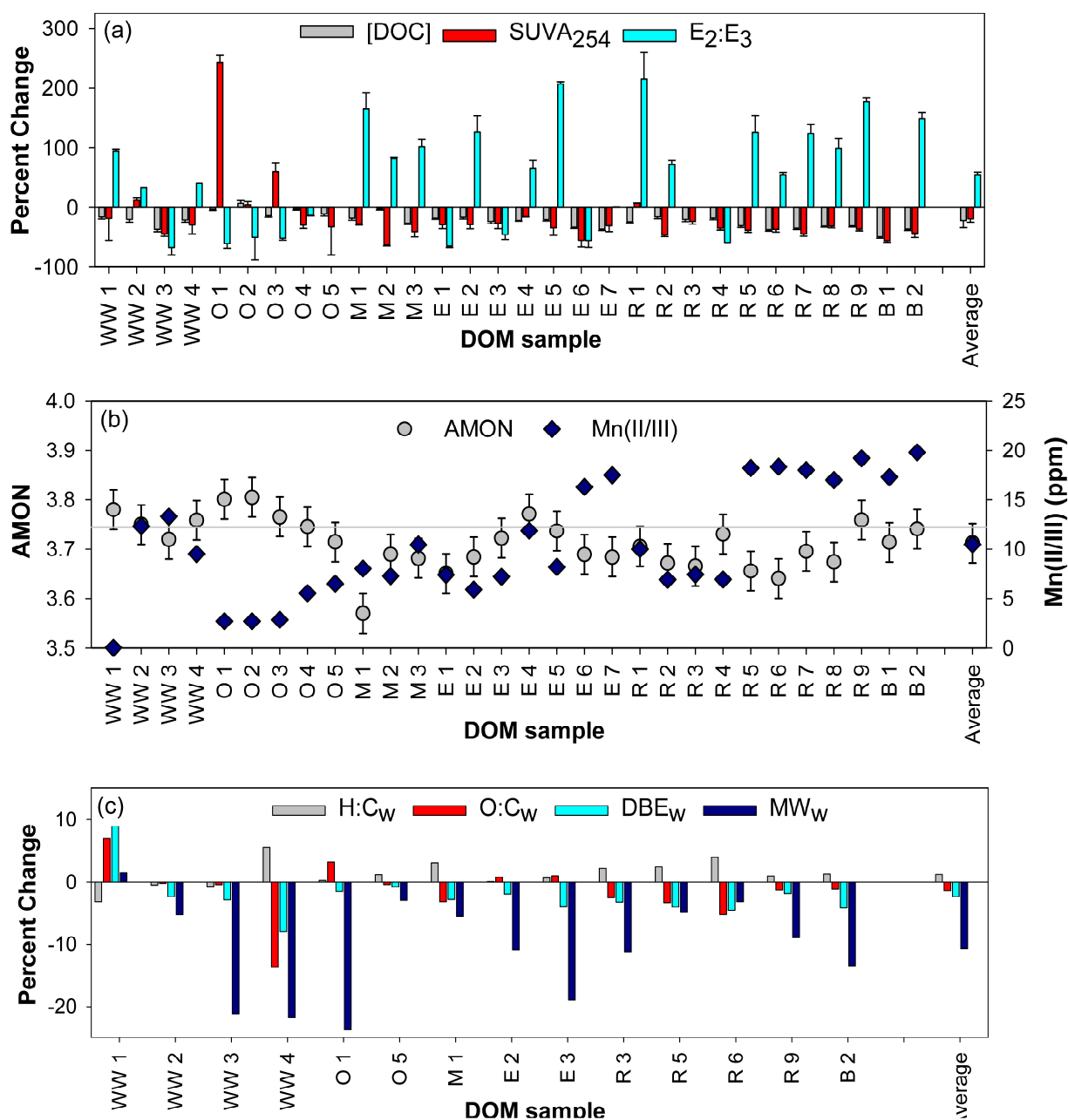


Figure 4.1. Percent changes in (a) [DOC], specific UV absorbance (SUVA₂₅₄), and E₂:E₃; (b) aqueous Mn(II/III) and average manganese oxidation number; and (c) weighted averages of H:C, O:C, DBE, and MW determined using high-resolution mass spectrometry following 50-hour reactions of DOM with acid birnessite (3:4 C:Mn molar ratio, pH 7). Average changes across all waters are included as the final point on each plot. Error bars represent (a) standard deviation of triplicate measurements and (b) standard deviation of triplicate Mn(II/III) measurements and AMON linear combination fitting method error described by Manceau et al.⁵³

Across all 30 waters, [DOC] decreases by an average of $22 \pm 12\%$ after 50 hours of reaction (**Figure 4.1a**). The average [DOC] loss is within the reported range of 5 to 40% loss in various DOM sources (e.g., forest leachates, commercial isolates, model organic acids) and Mn mineralogy (e.g., Mn-coated sands, birnessite).^{34-38,44} In this system, sorption to the mineral surface, mineralization to CO₂, or the formation of non-filter passing colloids with or without Mn(II/III) may all contribute to [DOC] loss. Determining the route(s) of [DOC] loss in these waters is beyond the scope of this analysis. However, sorption and colloid formation are the most likely mechanisms based on previous studies which use a combination of diffraction, X-ray photoelectron spectroscopy, electron microscopy, and XANES to confirm both sorption^{4,34,36-38,44} and colloid formation can occur.^{4,35,43,45}

The bulk composition of DOM measured using UV-vis spectroscopy changes over the course of 50 hours for all 30 waters (**Figure 4.1a**). In 25 waters, SUVA₂₅₄ decreases by an average of $1.1 \pm 0.5 \text{ L mg-C}^{-1} \text{ m}^{-1}$ ($36 \pm 11\%$), which indicates either transformation of aromatic formulas or their selective sorption to the Mn surface. Given observations that phenols, anilines, and other aromatic organic compounds are highly reactive with MnO₂^{13,20,27,30} and are present in DOM,¹⁴ both mechanisms are plausible explanations for the decreasing SUVA₂₅₄ values and likely coexist. Decreases in [DOC] across all samples support the possibility of sorption to the Mn surface, while evidence for oxidation at the molecular level is discussed below. SUVA₂₅₄ increases in five waters (O1, O2, O3, WW2, and R1) by an average of $0.9 \pm 1.2 \text{ L mg-C}^{-1} \text{ m}^{-1}$ ($65 \pm 102\%$) indicating an increase in the bulk aromaticity of DOM during reaction of these samples with MnO₂ (**Figure 4.1a**). The increases in SUVA₂₅₄ imply preferential removal of less aromatic fractions or non-oxidative transformations in these samples, contrary to previous reports and the other 25 waters.

$E_2:E_3$ values increase by an average of 4.7 ± 3.8 ($108 \pm 60\%$) in 21 of the 30 water samples, indicating a decrease in apparent molecular weight of DOM. In contrast, $E_2:E_3$ values decrease by an average of 2.1 ± 1.2 ($52 \pm 17\%$) in eight waters (O1, O2, O3, O4, E1, E3, E6, R4, and WW3), while $E_2:E_3$ in sample E7 does not change (**Figure 4.1a**). Previous studies generally note decreasing molecular weight after DOM reacts with Mn oxides, providing evidence for both molecular transformation (e.g., oxidation) and selective sorption of higher molecular weight compounds.^{34,36-38,44} For example, Fourier transform-infrared spectroscopy (FT-IR) analyses suggest low molecular weight carbonyls form during the reaction of a NOM isolate with sodium birnessite,⁴⁴ corresponding to an increase in $E_2:E_3$ and providing evidence of DOM transformation. Additionally, high molecular weight and aromatic DOM selectively sorbs to birnessite-coated sands and δ -MnO₂ based on high-pressure size exclusion chromatography analysis of three river DOM fractions.³⁴

Increases in aqueous Mn(II/III) and decreases in AMON are indirect indicators of DOM oxidation. In this study, filter-passing Mn concentrations after 50-hour reactions with acid birnessite are as high as 20 ppm, which suggests acid birnessite is reduced and forms dissolved Mn(II/III) (**Figure 4.1b**). However, visible particles form in all waters after filtration. After re-filtering the samples at 24 hours, dissolved Mn is below the detection limit (10 ppb) in all samples. The particles collected after 24 hours have an AMON of 2.64 ± 0.18 for selected waters analyzed by XANES (**Figure C.5**), which is consistent with Mn(II/III). Furthermore, modeling with Visual MINTEQ⁶² suggests that these particles are in fact colloidal forms of Mn(II/III) rather than rhodochrosite forming in the NaHCO₃ buffer as rhodochrosite is undersaturated in this system. Previous studies also observe colloidal organic matter-Mn(III) formation using a combination of diffraction, XANES, X-ray photoelectron spectroscopy, and electron

microscopy^{4,35,43,45,63} and note that Mn oxide AMON, aqueous cation content, and DOM aromaticity all increase colloid aggregation.^{4,22,35,45} Thus, the concentration and AMON of particles forming within 24 hours in the reaction filtrate provide evidence of manganese reduction and colloid formation in this system.

The AMON of the remaining solid Mn oxide decreases in four waters (E1, M1, R5, and R6) from the initial value of 3.74 ± 0.04 to 3.63 ± 0.04 . For these samples, the decrease in AMON is consistent with Mn reduction and concurrent DOM oxidation. For the other 26 waters, AMON does not change, with final values averaging 3.73 ± 0.04 . The slight AMON changes are not surprising given the low C:Mn ratio, as well as desorption of reduced Mn discussed above. The changes in AMON and the Mn(II/III) particle concentration are related; reactions with larger AMON decreases generally have more Mn(II/III) in the initial filtrate and more net reduction (**Figure C.6**) than waters with minimal AMON changes. These trends also cluster by water type; DOM from oligotrophic lakes results in minimal AMON reduction and Mn(II/III) formation, while DOM from rivers result in greater AMON reduction and higher dissolved Mn(II/III) concentrations (**Figure 4.1b**).

4.5.2 Impact of DOM composition and water chemistry on reactivity

While changes in bulk DOM composition and Mn oxide transformation are similar across most of the studied waters, the extent of change differs and a small number of samples diverge from the overall trends (**Table C.6**). In most cases we observe a slight decrease in [DOC], increase in E₂:E₃, decrease in SUVA₂₅₄, and little to no change in solid-phase AMON (**Figures 4.1a** and **4.1b**). These changes are observed in DOM from mesotrophic lakes, bogs, and rivers, as well as 4 of the 7 eutrophic lakes and 2 of the 4 wastewaters (i.e., 20 out of 30 waters). In

contrast, $E_2:E_3$ decreases in the five oligotrophic lakes and $SUVA_{254}$ increases in 3 of the 5 oligotrophic lakes. These five oligotrophic lakes, along with WW1, also have the lowest measured $[Mn(II/III)]$, suggesting minimal Mn reduction (**Figure C.6**). The trends among waters indicate that the reactivity of more aromatic DOM (e.g., from bogs) is consistent with DOM oxidation or preferential sorption of aromatic molecules, while DOM that is less aromatic and more microbially processed (e.g., oligotrophic lakes and wastewater effluents) may react through different mechanisms.

The changes in bulk DOM characteristics based on water source is supported by linear regression analysis (**Table C.7**). We compare changes in DOM and Mn bulk measurements with initial $SUVA_{254}$ and $E_2:E_3$ values to assess how aromaticity and apparent MW impact reactivity. Initial $SUVA_{254}$ values negatively correlate with percent changes in $SUVA_{254}$ ($p = 0.006$) and positively correlate with percent changes in both $E_2:E_3$ ($p = 0.004$) and reduced $Mn(II/III)$ concentrations ($p = 0.001$). These significant correlations suggest that DOM with greater initial $SUVA_{254}$ values will have larger decreases in $SUVA_{254}$ and increases in $E_2:E_3$ and aqueous $[Mn]$ during reaction with Mn oxides, supporting the observation that more aromatic DOM is more reactive. In contrast, initial $E_2:E_3$ values only significantly correlate with percent changes in $E_2:E_3$ ($p = 0.047$), indicating that the apparent molecular weight of DOM is not a major predictor of its reactivity. Furthermore, although sulfate and ionic strength may influence the reactivity of manganese oxides^{58,64-66} and DOM,^{15,19,22,46,47,67} they are not correlated with measured transformation parameters in these samples.

Changes in solid-phase AMON are also not significantly correlated with any of the tested bulk parameters (**Table C.7**), although this is not surprising given that many waters had final solid-phase AMON values within error of the starting material. However, the four waters with

AMON reduction have initial SUVA₂₅₄ values greater than 2.6 L mg-C⁻¹ m⁻¹. This provides further evidence of quantifiable Mn reduction and therefore DOM oxidation after reaction with aromatic DOM, as expected based on the high reactivity and oxidation potential of electron-rich phenolic moieties.^{13,14,20,34,36}

The decreases in [DOC], changes in optical parameters, and net Mn reduction observed in most DOM samples demonstrate that the concentration and composition of DOM changes due to reaction with acid birnessite. Although these trends may be attributable to DOM oxidation, bulk measurements alone cannot demonstrate that oxidation is the primary mechanism of transformation rather than selective sorption and colloid formation. Furthermore, a subset of waters do not follow the trends in bulk DOM and Mn changes exhibited by the majority of waters in this dataset (**Table C.6**). These opposing transformations demonstrate the complexity of DOM reactions with Mn oxides that can only be captured with a diverse set of samples and require further in-depth analysis of the molecular transformations.

4.5.3 Molecular transformations analyzed by FT-ICR MS

Fourteen waters which represent the range of 50-hour changes in apparent aromaticity, molecular weight, and Mn reduction (**Table C.6**) were analyzed with FT-ICR MS analysis to determine how reaction with acid birnessite alters DOM composition and to obtain evidence of DOM oxidation. FT-ICR MS data enables specific analyses of molecular changes in DOM. Some parameters (e.g., H:C_w, DBE_w) provide alternative methods to quantify changes in aromaticity, whereas other parameters (e.g., O:C_w) provide measurements of oxidation states that are not possible with bulk measurements. Additionally, the formulas assigned after FT-ICR MS

analysis can be used to identify products of specific reactions, notably oxidation of phenolic moieties.¹³

In the initial samples, $4,585 \pm 611$ formulas are identified by FT-ICR MS on average, which are visualized in van Krevelen diagrams (**Appendix C.7; Figure C.10**). Most of the identified formulas contain only C, H, and O ($52 \pm 7\%$), with variable amounts of N- ($35 \pm 3\%$) and S-containing formulas ($13 \pm 10\%$; **Table C.9**). The initial DOM composition varies widely among samples with H:C_w values ranging from 1.11 to 1.42, O:C_w from 0.41 to 0.54, and DBE_w from 6.81 to 10.09 (**Table C.10**).

The number of identified formulas decreases in all 14 samples after reaction with acid birnessite with an average loss of 268 CHO formulas (11%), 230 CHON formulas (14%), and 87 CHOS formulas (14%; **Table C.9**). The decrease in formulas corresponds to a decrease in chemodiversity of DOM after reaction. However, there is no preferential removal of heteroatom-containing formulas.

Principal component analysis using formula intensities in control and treated samples is used to differentiate between DOM composition at the molecular level. PCA reveals four clusters of samples: WW1, WW2-4, lakes, and rivers and bogs (**Figure C.8a**). These groupings suggest significant differences in the molecular composition of DOM in these samples both before and after reaction with acid birnessite. Notably, the reacted samples cluster near their controls (**Figure C.8b**), suggesting that differences among reacted samples are largely driven by initial DOM composition. The distances between control and treated samples are a proxy measure for the extent of reaction with acid birnessite⁶⁸ and, while PCA distance does not correlate significantly with other water characteristics (**Table C.8**), this metric suggests that WW2, WW3, and WW4 undergo the least change during reaction, natural waters undergo moderate changes,

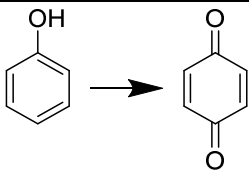
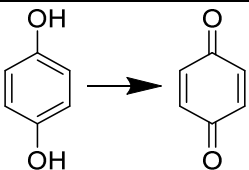
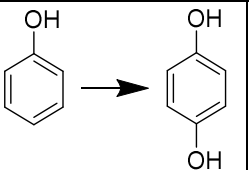
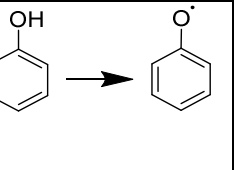
and WW1 has the greatest transformation with acid birnessite (**Figure C.9**). These PCA results confirm definitive delineations exist between water types as are observed in the bulk characteristics and support our hypothesis that reactivity in this system depends on DOM composition (**Figures 4.1** and **C.8**).

Changes in weighted averages derived from FT-ICR MS data provide additional insight into overall DOM reactivity with acid birnessite. $H:C_w$ increases by 1.2% and DBE_w decreases by 2.4% on average (**Figure 4.1c**), which is consistent with decreasing aromaticity and the observed average decrease in $SUVA_{254}$. MW_w decreases by 10.7% on average, in agreement with the general increase in $E_2:E_3$ (**Table C.6**). Inconsistent changes in MS-derived measures of aromaticity and apparent molecular weight are observed in WW1, WW2, and WW3, although the magnitude of decreases in $H:C_w$ or increases in DBE_w are small. The variable reactivity across DOM samples highlights the importance of using a wide range of whole waters to study DOM transformation. Additionally, the use of multiple techniques to investigate changes in these complex matrices and general agreement between UV-vis and FT-ICR MS measurements supports the conclusion that, on average, DOM becomes less aromatic and lower in molecular weight upon reaction with acid birnessite.

$O:C_w$ is a measure of the oxidation state of formulas detected by FT-ICR MS and does not align with any presented bulk measurements. Because MnO_2 reacts with phenolic compounds via O addition (**Table 4.1**)^{26-30,32} and phenols are important moieties in DOM,^{1,2,13,17,18,20,69-71} we expect that $O:C_w$ would increase in DOM after reaction. However, $O:C_w$ only increases in four of the 14 waters by an average of 2.1% and decreases in the remaining 10 samples by 1.9% on average (**Tables C.6** and **C.10**). This indicates that DOM remaining in solution is slightly reduced relative to the initial DOM, contradicting FT-IR

observations of reacted DOM,^{34,35,37} as well as measures of Mn reduction in this dataset and previous literature.^{4,24,34,35} However, weighted values encompass all transformations to the DOM pool including non-oxidative reactions and fractionation due to selective sorption and colloidal organic matter-Mn(II/III) formation. Fractionation by sorption and/or colloid formation is likely in these waters given the decreases in [DOC] and observed Mn(II/III) behavior (**Figure 4.1**). While decreases in O:C_w indicate reduction of C in the bulk DOM pool, this result does not negate other measures of aromaticity and molecular weight which suggest oxidation occurs. Rather, more specific evidence supporting the formation of oxidized product formulas is necessary.

Table 4.1. Schematic of tested phenol oxidation pathways and expected molecular changes for each reaction.

Pathway	Phenol → benzoquinone	Hydroquinone → benzoquinone	Phenol → hydroquinone	Hydrogen Abstraction
Change	+O, -2H	-2H	+O	-H
Reaction				
Δ H:C	-0.333	-0.333	0	-0.167
Δ O:C	0.167	0	0.167	0
Δ DBE	1	1	0	0.5
Δ MW	+13.9792645	-2.01565006	+15.9949146	-1.00782503

4.5.4 Oxidation product formulas

To determine whether oxidation occurs on a molecular level in the DOM samples despite contradictory O:C_w results, matched FT-ICR MS formulas are analyzed for potential oxidation products. Transformation of phenol to hydroquinone or benzoquinone (**Table 4.1**) is a common

oxidation pathway of reactive aromatic moieties in DOM^{13,19,20} and is likely to occur in this system as phenolic compounds are highly reactive with MnO₂.^{27,29,30} Three possible oxidation pathways are tested: phenol to hydroquinone (+O), hydroquinone to benzoquinone (-2H), and phenol to benzoquinone (+O and -2H), as well as hydrogen abstraction (-H) as an alternate rate-limiting pathway of phenol oxidation (**Table 4.1**).^{30,72,73} Formulas present after reaction are compared to potential oxidized products determined from the original control formula masses plus or minus the specific molecular weight corresponding to phenol oxidation. The resulting mass lists are compared to the matched control formulas to ensure any resulting product formulas are unique to the treated samples.

Predicted products based on phenol oxidation mechanisms are identified in all 14 samples (**Figure 4.2d**; **Table C.11**). These waters average 83 ± 48 phenol to hydroquinone, 88 ± 52 hydroquinone to benzoquinone, 78 ± 50 phenol to benzoquinone, and 6 ± 8 hydrogen abstraction products after reaction with acid birnessite. The limited number of hydrogen abstraction products suggests that this mechanism is possible but is less important for DOM transformation by acid birnessite in these waters. Sample WW1 has the most detected oxidation products (i.e., 687 in total; **Figure 4.2d**), which is notable as WW1 is a consistent outlier in DOM characteristic changes. Its increase in O:C_w (**Table C.6**) aligns with the large number of oxidized product formulas, while its trends of decreasing H:C_w and increasing MW_w are contrary to most other waters. The presence of oxidation products (**Figure C.11**) confirms that oxidation occurs at the molecular level in all samples, even those with decreasing O:C_w values over the course of reaction. This result agrees with the bulk and molecular trends for aromaticity (SUVA₂₅₄, DBE_w, H:C_w) and molecular weight (E₂:E₃, MW_w), which are consistent with DOM oxidation during reaction with MnO₂ (**Figure 4.1**).

The number of oxidation products formed across all waters correlates positively with percent changes in both DBE_w ($p = 7.6 \times 10^{-5}$) and MW_w ($p = 0.002$; **Table C.8**). These trends suggest that waters which form more DOM oxidation products also increase in both MW and DBE, which is counter-intuitive based on expected decreases in molecular weight and aromaticity of the entire DOM pool.^{8,13,18} However, these trends are consistent with known reactions of individual phenols or hydroquinones (**Table 4.1**). Notably, no bulk DOM properties or solid-phase Mn changes correlate with the number of phenolic oxidation products, indicating these measurements cannot be used as proxies for DOM oxidation.

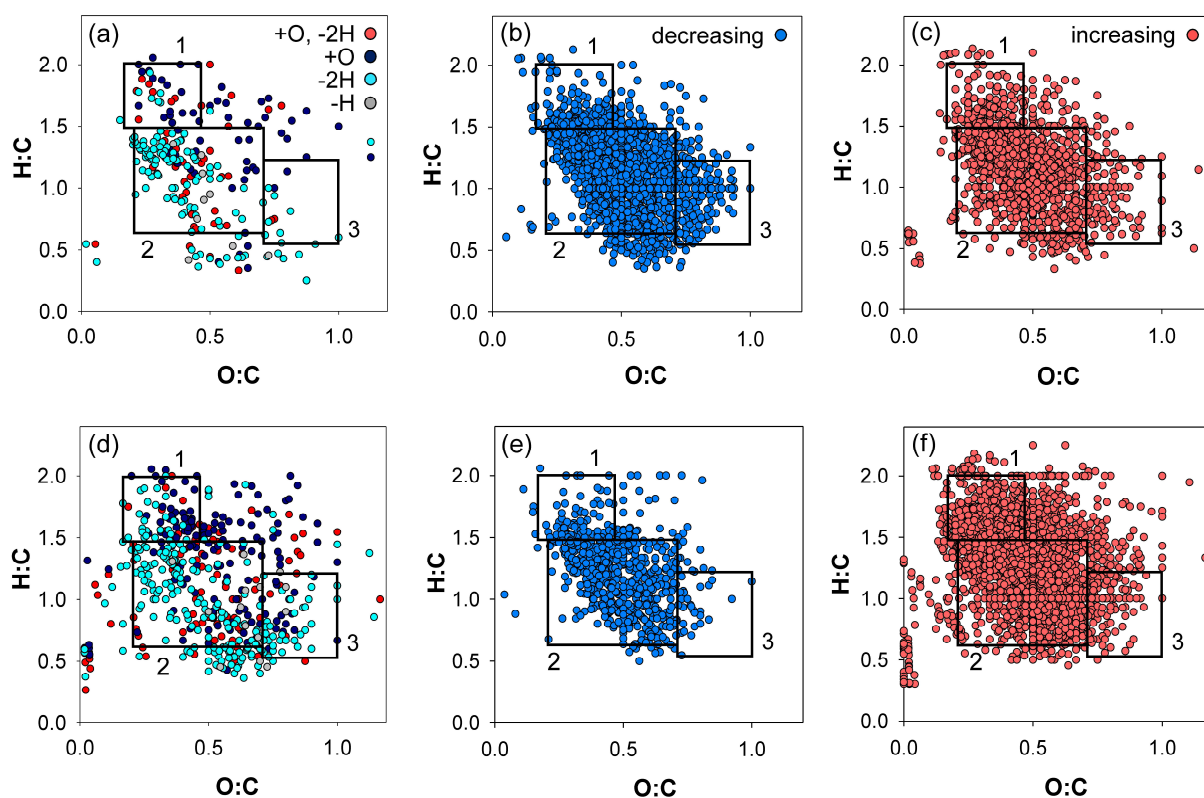


Figure 4.2. van Krevelen diagrams showing changes in St. Louis River (R6; a, b, and c) and Western Lake Superior Sanitary District effluent (WW1; d, e, and f) DOM formulas after 50-hour reactions with acid birnessite. Panels (a) and (d) show matched phenol oxidation and hydrogen abstraction products, panels (b) and (e) are formulas which decrease in intensity during reaction, and panels (c) and (f) show formulas which increase in intensity during reaction. The

overlaid boxes indicate (1) protein-like, (2) lignin-like, and (3) tannin-like formulas.¹ van Krevelen diagrams for the other 11 waters are in **Figures C.11 – C.14**.

This is the first, specific evidence of molecular oxidation products during the transformation of DOM by manganese oxides. The identified product formulas are not comprehensive as we match only phenolic oxidation pathways and other reactive DOM moieties may be oxidized in this system (e.g., anilines). Nonetheless, these results suggest that high-resolution formula identification can confirm specific oxidative transformations and provides conclusive evidence that oxidation occurs in the studied DOM samples.

4.5.5 Molecular reactivity trends

Despite the heterogeneous nature of the DOM in these waters, further analysis of FT-ICR MS data demonstrates that a common pool of formulas is most reactive with acid birnessite. We identify formulas that are unique to the control samples and treated waters (**Figure C.12**), which are designated as completely reacted and unique product formulas, respectively. Formulas that react completely with acid birnessite are primarily located in the lignin-like region, which is consistent with the oxidation of aromatic phenolic moieties,¹³ although protein-like formulas also react in some samples. Notably, most of the unique product formulas occupy similar regions on the van Krevelen diagram as the reacted formulas (**Figure C.12**), which agrees with the modest changes observed in the weighted averages in these waters (**Table C.6**).

Similar trends appear in van Krevelen diagrams of formulas which decrease in relative intensity during reaction and formulas which increase in relative intensity during reaction. As with the unique formulas, these plots are similar across all samples (**Figures 4.2, C.13, and C.14**). The reactive formulas fall in the same lignin-like region that contains aromatic, electron-

rich phenolic moieties and has been linked to DOM reactivity with other oxidants including ozone^{13, 21, 73-75} and hydroxyl radical.^{5,12,13,18,20,21,69,73,75} The formulas which increase in intensity during reaction are more widely distributed (**Figure C.14**), suggesting the possibility of different types of products and reaction mechanisms. Furthermore, the formulas that increase in relative intensity after reaction span a greater range of the van Krevelen diagram than the identified oxidation products, which are typically confined to the lignin-like region of the plots (**Figures 4.2 and C.11**). The scattered product formulas support the observed differences in aromaticity and molecular weight measures using both bulk measurements and FT-ICR MS analysis (**Table C.6**), as well as evidence of non-oxidative transformations occurring in the DOM pool. Although there are differences in bulk DOM compositional changes and a wide range of products are generated by the reaction of DOM and acid birnessite, these results demonstrate that MnO₂ reacts selectively with electron-rich, lignin-like formulas even in waters containing highly diverse DOM.

4.6 Environmental implications

Organic matter oxidation is considered a primary transformation pathway by Mn oxides and this study confirms, with molecular product identification, that oxidation selectively occurs with phenolic moieties in DOM regardless of the water source. We observe composition-dependent transformations to the bulk DOM pool, with oxidation products identified in all 14 waters analyzed by FT-ICR MS (**Figure 4.2; Table C.11**). DOM oxidation by Mn oxides is often assumed based on bulk results and theoretical reaction chemistry (e.g., Mn reduction),^{16,22,34-37,40,43,59,61,76-78} but was unsubstantiated with conclusive molecular evidence prior to this study. Furthermore, initial aromaticity, as measured by SUVA₂₅₄, H:C_w, and DBE_w,

is the greatest control on extent of DOM transformation and correlates significantly with the number of oxidation products detected after reaction with acid birnessite (**Table C.8**), suggesting aromaticity may be the best predictor of extent of oxidation among natural waters.

Bulk DOM measures suggest other transformation and organic matter removal pathways (e.g., sorption) occur alongside oxidation. [DOC] loss, reduced Mn colloid formation, and variability in bulk DOM transformation (e.g., apparent MW; **Figure 4.1**) indicate that oxidation is not the only mechanism altering DOM and Mn in this system. These competing mechanisms necessitate further research to identify other DOM transformation mechanisms and to elucidate influential environmental parameters on sorption and oxidation by manganese oxides.

The effects of these transformation mechanisms will impact our understanding and predictions of contaminant fate, bioavailability, and other dependent environmental processes. For example, organic matter was previously demonstrated to both enhance and inhibit contaminant degradation by MnO₂,^{22,23,27,36,38,40,78,79} although the mechanisms are unknown and may depend on DOM composition. Thus, this study provides the molecular framework and confirmation of oxidation necessary to investigate how DOM composition alters manganese oxide reactivity in complex environments.

4.7 Acknowledgements

Funding was provided by the National Science Foundation (CBET 1944464). We thank Stephanie Berg and Amber White for assistance with sample collection and Elizabeth Tomaszewski for collecting XANES spectra of 28-day reaction solids. X-ray absorption spectroscopy was conducted at Sector 10 of the Advanced Photon Source and Sector 4 at the National Synchrotron Light Source II. MRCAT operations are supported by the Department of

Energy and MRCAT member institutions. This research used resources of the Advanced Photon Source, a U.S. Department of Energy (DOE) Office of Science User Facility operated for the DOE Office of Science by Argonne National Laboratory under Contract No. DE-AC02-06CH11357 and the XFM Beamline of the National Synchrotron Light Source II, a U.S. Department of Energy (DOE) Office of Science User Facility operated for the DOE Office of Science by Brookhaven National Laboratory under Contract No. DE-SC0012704. The authors acknowledge the UW-Madison Human Proteomics Program Mass Spectrometry Facility (Wisconsin partnership funds; NIH S10OD018475) for support in obtaining FT-ICR MS data and Yanlong Zhu for assistance with the instrument. We also thank the Northern Temperate Lakes Long-Term Ecological Research Program (Continuing Grant 1440297), Madison Metropolitan Sewerage District, and Western Lake Superior Sanitary District for sampling resources.

4.8 Supporting information

Additional details pertaining to sample collection, water chemistry, formula matching, and DOM transformation can be found in Appendix C.

4.9 References

1. Minor, E. C.; Swenson, M. M.; Mattson, B. M.; Oyler, A. R., Structural characterization of dissolved organic matter: A review of current techniques for isolation and analysis. *Environ. Sci. Process. Impacts*. **2014**, *16*, (9), 2064-2079.
2. Nebbioso, A.; Piccolo, A., Molecular characterization of dissolved organic matter (DOM): a critical review. *Anal. Bioanal. Chem.* **2013**, *405*, (1), 109-124.
3. D'Andrilli, J.; Cooper, W. T.; Foreman, C. M.; Marshall, A. G., An ultrahigh-resolution mass spectrometry index to estimate natural organic matter lability. *Rapid Commun. Mass Spectrom.* **2015**, *29*, (24), 2385-2401.
4. Aiken, G. R.; Hsu-Kim, H.; Ryan, J. N., Influence of dissolved organic matter on the environmental fate of metals, nanoparticles, and colloids. *Environ. Sci. Technol.* **2011**, *45*, (8), 3196-3201.
5. Berg, S. M.; Whiting, Q. T.; Herrli, J. A.; Winkels, R.; Wammer, K. H.; Remucal, C. K., The role of dissolved organic matter composition in determining photochemical reactivity at the molecular level. *Environ. Sci. Technol.* **2019**, *53*, (20), 11725-11734.
6. Dittmar, T., Reasons behind the long-term stability of dissolved organic matter. In *Biogeochemistry of marine dissolved organic matter*, 2015; pp 369-388.
7. He, W.; Jung, H.; Lee, J. H.; Hur, J., Differences in spectroscopic characteristics between dissolved and particulate organic matters in sediments: insight into distribution behavior of sediment organic matter. *Sci. Total Environ.* **2016**, *547*, 1-8.
8. Maizel, A. C.; Remucal, C. K., Molecular composition and photochemical reactivity of size-fractionated dissolved organic matter. *Environ. Sci. Technol.* **2017**, *51*, (4), 2113-2123.
9. Wagner, S.; Riedel, T.; Niggemann, J.; Vahatalo, A. V.; Dittmar, T.; Jaffe, R., Linking the molecular signature of heteroatomic dissolved organic matter to watershed characteristics in world rivers. *Environ. Sci. Technol.* **2015**, *49*, (23), 13798-13806.
10. Bodhipaksha, L. C.; Sharpless, C. M.; Chin, Y. P.; Sander, M.; Langston, W. K.; MacKay, A. A., Triplet photochemistry of effluent and natural organic matter in whole water and isolates from effluent-receiving rivers. *Environ. Sci. Technol.* **2015**, *49*, (6), 3453-3463.
11. Chen, Y.; Hozalski, R. M.; Olmanson, L. G.; Page, B. P.; Finlay, J. C.; Brezonik, P. L.; Arnold, W. A., Prediction of photochemically produced reactive intermediates in surface waters via satellite remote sensing. *Environ. Sci. Technol.* **2020**, *54*, (11), 6671-6681.
12. Bulman, D. M.; Remucal, C. K., Role of reactive halogen species in disinfection byproduct formation during chlorine photolysis. *Environ. Sci. Technol.* **2020**, *54*, (15), 9629-9639.
13. Remucal, C. K.; Salhi, E.; Walpen, N.; von Gunten, U., Molecular-level transformation of dissolved organic matter during oxidation by ozone and hydroxyl radical. *Environ. Sci. Technol.* **2020**, *54*, (16), 10351-10360.
14. Fimmen, R. L.; Cory, R. M.; Chin, Y.P.; Trouts, T. D.; McKnight, D. M., Probing the oxidation-reduction properties of terrestrially and microbially derived dissolved organic matter. *Geochim. Cosmochim. Acta* **2007**, *71*, (12), 3003-3015.
15. Gucker, B.; Silva, R. C. S.; Graeber, D.; Monteiro, J. A. F.; Boechat, I. G., Urbanization and agriculture increase exports and differentially alter elemental stoichiometry of

- dissolved organic matter (DOM) from tropical catchments. *Sci. Total Environ.* **2016**, *550*, 785-792.
16. Polubesova, T.; Chefetz, B., DOM-affected transformation of contaminants on mineral surfaces: A review. *Environ. Sci. Technol.* **2014**, *44*, (3), 223-254.
 17. Subdiaga, E.; Orsetti, S.; Haderlein, S. B., Effects of sorption on redox properties of natural organic matter. *Environ. Sci. Technol.* **2019**, *53*, (24), 14319-14328.
 18. Maizel, A. C.; Li, J.; Remucal, C. K., Relationships between dissolved organic matter composition and photochemistry in lakes of diverse trophic status. *Environ. Sci. Technol.* **2017**, *51*, (17), 9624-9632.
 19. Wallace, G. C.; Sander, M.; Chin, Y. P.; Arnold, W. A., Quantifying the electron donating capacities of sulfide and dissolved organic matter in sediment pore waters of wetlands. *Environ. Sci. Process. Impacts* **2017**, *19*, (5), 758-767.
 20. Walpen, N.; Getzinger, G. J.; Schroth, M. H.; Sander, M., Electron-donating phenolic and electron-accepting quinone moieties in peat dissolved organic matter: quantities and redox transformations in the context of peat biogeochemistry. *Environ. Sci. Technol.* **2018**, *52*, (9), 5236-5245.
 21. Wenk, J.; Aeschbacher, M.; Salhi, E.; Canonica, S.; von Gunten, U.; Sander, M., Chemical oxidation of dissolved organic matter by chlorine dioxide, chlorine, and ozone: effects on its optical and antioxidant properties. *Environ. Sci. Technol.* **2013**, *47*, (19), 11147-11156.
 22. Zhang, S.; Gutierrez, L.; Niu, X. Z.; Qi, F.; Croue, J. P., The characteristics of organic matter influence its interfacial interactions with MnO₂ and catalytic oxidation processes. *Chemosphere* **2018**, *209*, 950-959.
 23. Borch, T.; Kretzschmar, R.; Kappler, A.; Van Cappellen, P.; Ginder-Vogel, M.; Voegelin, A.; Campbell, K., Biogeochemical redox processes and their impact on contaminant dynamics. *Environ. Sci. Technol.* **2010**, *44*, (1), 15-23.
 24. Pena, J.; Kwon, K. D.; Refson, K.; Bargar, J. R.; Sposito, G., Mechanisms of nickel sorption by a bacteriogenic birnessite. *Geochim. Cosmochim. Acta* **2010**, *74*, (11), 3076-3089.
 25. Wang, Z.; Giammar, D. E., Metal contaminant oxidation mediated by manganese redox cycling in subsurface environment. In *Advances in the environmental biogeochemistry of manganese oxides*, Feng, X.; Li, W.; Zhu, M.; Sparks, D. L., eds. American Chemical Society: Washington, D.C., 2015; Vol. 1197, pp 29-50.
 26. Balgooyen, S.; Alaimo, P. J.; Remucal, C. K.; Ginder-Vogel, M., Structural transformation of MnO₂ during the oxidation of bisphenol A. *Environ. Sci. Technol.* **2017**, *51*, (11), 6053-6062.
 27. Remucal, C. K.; Ginder-Vogel, M., A critical review of the reactivity of manganese oxides with organic contaminants. *Environ. Sci. Process. Impacts* **2014**, *16*, (6), 1247-1266.
 28. Shaikh, N.; Tadjale, S.; Zhang, H.; Artyushkova, K.; Ali, A. S.; Cerrato, J. M., Spectroscopic investigation of interfacial interaction of manganese oxide with triclosan, aniline, and phenol. *Environ. Sci. Technol.* **2016**, *50*, (20), 10978-10987.
 29. Stone, A. T., Reductive dissolution of manganese(III/IV) oxides by substituted phenols. *Environ. Sci. Technol.* **1987**, *21*, (10), 979-988.

30. Trainer, E. L.; Ginder-Vogel, M.; Remucal, C. K., Organic structure and solid characteristics determine reactivity of phenolic compounds with synthetic and reclaimed manganese oxides. *Environ. Sci. Water Res. Technol.* **2020**, *6*, (3), 540-553.
31. Wang, X.; Xiang, W.; Wang, S.; Ge, J.; Qu, R.; Wang, Z., Oxidative oligomerization of phenolic endocrine disrupting chemicals mediated by Mn(III)-L complexes and the role of phenoxyl radicals in the enhanced removal: Experimental and theoretical studies. *Environ. Sci. Technol.* **2020**, *54*, (3), 1573-1582.
32. Pavitt, A. S.; Bylaska, E. J.; Tratnyek, P. G., Oxidation potentials of phenols and anilines: Correlation analysis of electrochemical and theoretical values. *Environ. Sci. Process. Impacts* **2017**, *19*, (3), 339-349.
33. Salter-Blanc, A. J.; Bylaska, E. J.; Lyon, M. A.; Ness, S. C.; Tratnyek, P. G., Structure-activity relationships for rates of aromatic amine oxidation by manganese dioxide. *Environ. Sci. Technol.* **2016**, *50*, (10), 5094-5102.
34. Allard, S.; Gutierrez, L.; Fontaine, C.; Croue, J. P.; Gallard, H., Organic matter interactions with natural manganese oxide and synthetic birnessite. *Sci. Total Environ.* **2017**, *583*, 487-495.
35. Li, Q.; Xie, L.; Jiang, Y.; Fortner, J. D.; Yu, K.; Liao, P.; Liu, C., Formation and stability of NOM-Mn(III) colloids in aquatic environments. *Water Res.* **2019**, *149*, 190-201.
36. Ma, D.; Wu, J.; Yang, P.; Zhu, M., Coupled manganese redox cycling and organic carbon degradation on mineral surfaces. *Environ. Sci. Technol.* **2020**, *54*, (14), 8801-8810.
37. Stuckey, J. W.; Goodwin, C.; Wang, J.; Kaplan, L. A.; Vidal-Esquivel, P.; Beebe, T. P., Jr.; Sparks, D. L., Impacts of hydrous manganese oxide on the retention and lability of dissolved organic matter. *Geochim. Trans.* **2018**, *19*, (1), 6.
38. Taujale, S.; Baratta, L. R.; Huang, J.; Zhang, H., Interactions in ternary mixtures of MnO₂, Al₂O₃, and natural organic matter (NOM) and the impact on MnO₂ oxidative reactivity. *Environ. Sci. Technol.* **2016**, *50*, (5), 2345-2353.
39. Estes, E. R.; Andeer, P. F.; Nordlund, D.; Wankel, S. D.; Hansel, C. M., Biogenic manganese oxides as reservoirs of organic carbon and proteins in terrestrial and marine environments. *Geobiology* **2016**, *15*, (1), 158-172.
40. Li, C.; Zhang, B.; Ertunc, T.; Schaeffer, A.; Ji, R., Birnessite-induced binding of phenolic monomers to soil humic substances and nature of the bound residues. *Environ. Sci. Technol.* **2012**, *46*, (16), 8843-8850.
41. Schwarzenbach, R. P.; Gschwend, P. M.; Imboden, D. M. *Environmental organic chemistry*, 2nd ed.; John Wiley & Sons, Inc.: Hoboken, New Jersey, 2003.
42. Chen, M.; Hur, J., Pre-treatments, characteristics, and biogeochemical dynamics of dissolved organic matter in sediments: A review. *Water Res.* **2015**, *79*, 10-25.
43. Huangfu, X.; Jiang, J.; Ma, J.; Liu, Y.; Yang, J., Aggregation kinetics of manganese dioxide colloids in aqueous solution: Influence of humic substances and biomacromolecules. *Environ. Sci. Technol.* **2013**, *47*, (18), 10285-10292.
44. Chorover, J.; Amistadi, M. K., Reaction of forest floor organic matter at goethite, birnessite and smectite surfaces. *Geochim. Cosmochim. Acta* **2001**, *65*, (1), 95-109.
45. Graham, M. C.; Gavin, K. G.; Kirika, A.; Farmer, J. G., Processes controlling manganese distributions and associations in organic-rich freshwater aquatic systems: The example of Loch Bradan, Scotland. *Sci. Total Environ.* **2012**, *424*, 239-250.

46. Komada, T.; Burdige, D. J.; Li, H. L.; Magen, C.; Chanton, J. P.; Cada, A. K., Organic matter cycling across the sulfate-methane transition zone of the Santa Barbara basin, California borderland. *Geochim. Cosmochim. Acta* **2016**, *176*, 259-278.
47. Poulin, B. A.; Ryan, J. N.; Nagy, K. L.; Stubbins, A.; Dittmar, T.; Orem, W.; Krabbenhoft, D. P.; Aiken, G. R., Spatial dependence of reduced sulfur in Everglades dissolved organic matter controlled by sulfate enrichment. *Environ. Sci. Technol.* **2017**, *51*, (7), 3630-3639.
48. McKenzie, R. M., The synthesis of birnessite, cryptomelane, and some other oxides and hydroxides of manganese. *Mineral. Mag.* **1971**, *38*, 493-502.
49. Report on Superior Bay, St. Louis County, Minnesota, and Douglas County. Wisconsin E.P.A. Region V, **1975** No. 128.
50. Wisconsin Department of Natural Resources, Lake Water Quality Database. dnr.wi.gov/lakes/waterquality, **2021**.
51. Center for Limnology at Wisconsin-Madison, North Temperate Lakes U.S. Long-Term Ecological Research Network. National Science Foundation, lter.limnology.wisc.edu, **2021**.
52. Stumm, W.; Morgan, J. J., *Aquatic chemistry: Chemical equilibria and rates in natural waters*. 3rd ed.; John Wiley & Sons, Inc.: United States of America, 1996.
53. Manceau, A.; Marcus, M. A.; Grangeon, S., Determination of Mn valence states in mixed-valent manganates by XANES spectroscopy. *Am. Mineral.* **2012**, *97*, (5-6), 816-827.
54. Dittmar, T.; Koch, B.; Hertkorn, N.; Kattner, G., A simple and efficient method for the solid-phase extraction of dissolved organic matter (SPE-DOM) from seawater. *Limnol. Oceanogr. Methods* **2008**, *6*, (6), 230-235.
55. Koch, B. P.; Dittmar, T.; Witt, M.; Kattner, G., Fundamentals of molecular formula assignment to ultrahigh resolution mass data of natural organic matter. *Anal. Chem.* **2007**, *79*, (4), 1758-1763.
56. Maizel, A. C.; Remucal, C. K., The effect of advanced secondary municipal wastewater treatment on the molecular composition of dissolved organic matter. *Water Res.* **2017**, *122*, 42-52.
57. Maizel, A. C.; Remucal, C. K., The effect of probe choice and solution conditions on the apparent photoreactivity of dissolved organic matter. *Environ. Sci. Process. Impacts* **2017**, *19*, (8), 1040-1050.
58. Charbonnet, J. A.; Duan, Y.; Sedlak, D. L., The use of manganese oxide-coated sand for the removal of trace metal ions from stormwater. *Environ. Sci. Water Res. Technol.* **2020**, *6*, (3), 593-603.
59. Park, J. W.; Dec, J.; Kim, J. E.; Bollag, J. M., Effect of humic constituents on the transformation of chlorinated phenols and anilines in the presence of oxidoreductive enzymes or birnessite. *Environ. Sci. Technol.* **1999**, *33*, (12), 2028-2034.
60. Stone, A. T.; Morgan, J. J., Reduction and dissolution of manganese(III) and manganese(IV) oxides by organics: 2. Survey of the reactivity of organics. *Environ. Sci. Technol.* **1984**, *18*, (8), 617-624.
61. Wang, Y.; Stone, A. T., Reaction of Mn^{III,IV} (hydr)oxides with oxalic acid, glyoxylic acid, phosphonoformic acid, and structurally-related organic compounds. *Geochim. Cosmochim. Acta* **2006**, *70*, (17), 4477-4490.
62. Gustafsson, J. P. *Visual MINTEQ*, 3.1; KTH, Sweden, 2020.

63. Li, Z.; Shakiba, S.; Deng, N.; Chen, J.; Louie, S. M.; Hu, Y., Natural organic matter (NOM) imparts molecular-weight-dependent steric stabilization or electrostatic destabilization to ferrihydrite nanoparticles. *Environ. Sci. Technol.* **2020**, *54*, (11), 6761-6770.
64. Huang, J.; Zhong, S.; Dai, Y.; Liu, C. C.; Zhang, H., Effect of MnO₂ phase structure on the oxidative reactivity toward bisphenol A degradation. *Environ. Sci. Technol.* **2018**, *52*, (19), 11309-11318.
65. Tripathy, S. S.; Kanungo, S. B., Adsorption of Co²⁺, Ni²⁺, Cu²⁺ and Zn²⁺ from 0.5 m NaCl and major ion sea water on a mixture of delta-MnO₂ and amorphous FeOOH. *J. Colloid Interface Sci.* **2005**, *284*, (1), 30-38.
66. Balgooyen, S.; Remucal, C. K.; Ginder-Vogel, M., Identifying the mechanisms of cation inhibition of phenol oxidation by acid birnessite. *J. Environ. Qual.* **2020**, *49*, (6), 1644-1654.
67. Gomez-Saez, G. V.; Pohlabein, A. M.; Stubbins, A.; Marsay, C. M.; Dittmar, T., Photochemical alteration of dissolved organic sulfur from sulfidic porewater. *Environ. Sci. Technol.* **2017**, *51*, (24), 14144-14154.
68. Lever, J.; Krzywinski, M.; Altman, N., Principal component analysis. *Nature Methods* **2017**, *14*, (7), 641-642.
69. Arnold, W. A.; Oueis, Y.; O'Connor, M.; Rinaman, J. E.; Taggart, M. G.; McCarthy, R. E.; Foster, K. A.; Latch, D. E., QSARs for phenols and phenolates: Oxidation potential as a predictor of reaction rate constants with photochemically produced oxidants. *Environ. Sci. Process. Impacts* **2017**, *19*, (3), 324-338.
70. Davi, M. L.; Gnudi, F., Phenolic compounds in surface water. *Water Res.* **1999**, *33*, (14), 3213-3219.
71. McCabe, A. J.; Arnold, W. A., Reactivity of triplet excited states of dissolved natural organic matter in stormflow from mixed-use watersheds. *Environ. Sci. Technol.* **2017**, *51*, (17), 9718-9728.
72. Canonica, S.; Tratnyek, P. G., Quantitative structure-activity relationships for oxidation reactions of organic chemicals in water. *Environ. Toxicol. Chem.* **2003**, *22*, (8), 1743-1754.
73. Lee, Y.; von Gunten, U., Quantitative structure-activity relationships (QSARs) for the transformation of organic micropollutants during oxidative water treatment. *Water Res.* **2012**, *46*, (19), 6177-6195.
74. Bulman, D. M.; Mezyk, S. P.; Remucal, C. K., The impact of pH and irradiation wavelength on the production of reactive oxidants during chlorine photolysis. *Environ. Sci. Technol.* **2019**, *53*, (8), 4450-4459.
75. Tentscher, P. R.; Bourgin, M.; von Gunten, U., Ozonation of *para*-substituted phenolic compounds yields *p*-benzoquinones, other cyclic alpha,beta-unsaturated ketones, and substituted catechols. *Environ. Sci. Technol.* **2018**, *52*, (8), 4763-4773.
76. Li, Y.; Harir, M.; Uhl, J.; Kanawati, B.; Lucio, M.; Smirnov, K. S.; Koch, B. P.; Schmitt-Kopplin, P.; Hertkorn, N., How representative are dissolved organic matter (DOM) extracts? A comprehensive study of sorbent selectivity for DOM isolation. *Water Res.* **2017**, *116*, 316-323.
77. Wang, Q.; Yang, P.; Zhu, M., Structural transformation of birnessite by fulvic acid under anoxic conditions. *Environ. Sci. Technol.* **2018**, *52*, (4), 1844-1853.

78. Wang, Q.; Yang, P.; Zhu, M., Effects of metal cations on coupled birnessite structural transformation and natural organic matter adsorption and oxidation. *Geochim. Cosmochim. Acta* **2019**, *250*, 292-310.
79. Amiri, F.; Bornick, H.; Worch, E., Sorption of phenols onto sandy aquifer material: The effect of dissolved organic matter (DOM). *Water Res.* **2005**, *39*, (5), 933-941.

Chapter 5

Conclusions

5.1 Summary of findings

Understanding phenolic contaminant oxidation by manganese oxides is an important component to using manganese oxide media in stormwater runoff and wastewater reclamation systems. This dissertation provides a novel, mechanistic investigation into this process by combining aqueous kinetic data and mechanism determination with solid phase characterizations, QSAR modeling, and high-resolution mass spectrometry. We investigate the mechanism of phenol oxidation by first surveying the reactivity of a suite of diverse phenols with both synthetic and reclaimed oxides and relating their oxidation rates back to structural differences with QSARs. Second, we react mixtures of phenolic contaminants with manganese oxide and monitor individual phenol reactivity in each mixture in the absence or presence of *tert*-butanol. Finally, we use the mechanisms of phenol oxidation to assess the reactivity and transformation of whole water dissolved organic matter samples through a combination of solid phase characterization and high-resolution mass spectrometry. Together, this dissertation highlights the intricacies within the mechanism of phenol oxidation by manganese oxides and demonstrates the importance of exploring environmentally relevant complexities at the molecular, bench scale to better predict and explain *in situ* results.

Chapter 2 emphasizes the importance of incorporating both simple model compounds and complex contaminants in a single study to connect mechanistic differences to fundamental

properties of the reaction. We show that both electron transfer-limited and sorption-limited mechanisms are possible depending on both the phenol structure and manganese oxide phase and that this mechanism directly correlates with the pseudo-first-order oxidation rate. Through density functional theory modeling of each compound, we relate these reactive differences to specific functional groups and substituent placement. Traditional quantitative structure activity relationships cannot predict the reactivity of *ortho*-substituted or complex phenols and thus are not useful as a predictive tool in contaminated waters treated with manganese oxides. Furthermore, through in-depth solid phase characterizations, we determine that surface area, surface charge, and iron content are the most important factors in assessing the reactivity of reclaimed manganese oxides with phenols.

Chapter 3 expands on the results of Chapter 2 as we apply the fundamental mechanism differences between phenols to explore how mixtures affect oxidation of diverse phenols. In this study, we determined that electron transfer-limited phenols are inhibited by competitive intermolecular interactions, including electrostatic interactions, physical blocking, and intermolecular bonding. The extent of inhibition is not predicted by physiochemical properties of each compound, oxidation rates in isolate solutions, or extent of sorption in isolate solutions and these competitive interactions may cause these phenols to become rate-limited by formation of the precursor complex. We also determine that the oxidation of 4,4'-biphenol, a sorption-limited phenol, is enhanced in mixtures with other compounds and we attribute this increase in pseudo-first-order oxidation rates to indirect oxidation by phenoxy radical products of electron transfer-limited compounds in solution.

Chapter 4 moves beyond studying oxidation of individual phenols by employing both solid phase characterizations and high-resolution mass spectrometry to investigate the

transformation of dissolved organic matter by manganese oxides. Phenolic moieties are a reactive component of DOM that could potentially undergo oxidation by Mn oxides. Furthermore, DOM is present in all surface and wastewaters in which phenolic contaminants may be found, making DOM an important component to understanding phenol oxidation by manganese oxides. Bulk spectroscopy techniques suggest that the 29 studied waters transform uniquely in 50-hour reactions with acid birnessite and these results are confirmed by molecular analysis using high-resolution mass spectrometry. We use the molecular specificity of this technique to identify phenolic oxidation products which indicate that all waters are oxidized by manganese oxides and that other transformation processes account for the variety of reacted DOM characteristics.

This dissertation demonstrates that phenol oxidation cannot be studied through isolated reactions of simple model compounds alone. To fully elucidate details of the mechanism by which this reaction occurs, environmental intricacies such as complex phenol and manganese oxide structures, mixture effects, and the reactivity of dissolved organic matter must be better understood. Furthermore, transformations of both the organic and solid phases must be explored in tandem to identify the source of rate and mechanism changes, as is done in this dissertation. Our work expands upon initial mechanistic studies to further comprehensive knowledge of phenol oxidation by manganese oxides through novel combinations of kinetic studies, modeling, solid phase characterizations, and high-resolution mass spectrometry. Not only do our results help explain discrepancies between studies, we also provide foundational insights into phenol oxidation in engineered reclamation systems with manganese oxides which will be required to effectively treat these substituted contaminants in varying mixtures in the presence of DOM.

5.2 Directions for future research

This dissertation focuses on mechanisms of phenol oxidation by manganese oxides. However, manganese oxides can also oxidize anilines¹⁻¹¹ and other non-phenolic organic contaminants.⁸ The oxidation mechanisms and confounding factors of oxidation for these compounds are less understood than for phenols, but similar mechanistic studies should be carried out with these organic compounds as they will also interact and be degraded in passive *in situ* treatment systems. Furthermore, both phenolic contaminants and non-phenolic contaminants should be mechanistically investigated in non-batch reactions, ideally in stormwater treatment ponds or pilot plant setups which can mimic the conditions of passive *in situ* treatments. As described throughout the dissertation, there is a disconnect between controlled laboratory results and pilot treatment systems; monitoring the oxidation rates, manganese solid phase characterizations, or degradation mechanisms in such pilot systems will further help to bridge the results of this dissertation and other laboratory investigations with field results.

Another important component of this research is product identification. There are a number of studies which identify transformation products of single contaminants (i.e., triclosan, bisphenol A);^{1,12-21} however, there are many important contaminants which do not have identified oxidation products. As more products are identified, comprehensive reviews or databases will be necessary to organize these results by parent contaminant and reaction conditions (e.g., mineral phase, pH). In addition, product identification can help confirm our detailed mechanistic theories, especially the competitive interactions and indirect phenoxy radical oxidation pathways outlined in Chapter 3.

There is also a large knowledge gap in our understanding of dissolved organic matter interactions in this system. In Chapter 4, we demonstrate that manganese oxides can oxidize

DOM from a wide range of whole water sources, including wastewater effluent, but we also observe other reactions, in addition to oxidation, transform the DOM pool and likely alter the reactivity of DOM. In solutions with organic contaminants and DOM, such as stormwater runoff or wastewater effluent, phenolic moieties in the DOM pool may compete or indirectly oxidize the phenols, inhibiting or enhancing oxidation as we observe for phenolic mixtures in Chapter 3. Since DOM is a complex and diverse pool of potential reactive molecules, these interactions with phenolic contaminants and manganese oxides will depend not only on the manganese solid and phenolic structure, but also the specific whole water DOM pool. A few studies which have measured oxidation rates in the presence or absence of DOM report conflicting observations; pseudo-first-order oxidation rates of bisphenol A and other compounds both increase and decrease in the presence of DOM relative to controls.^{8,22,23} However, these studies use different DOM isolates or sources and do not explore the mechanistic interactions driving the observed oxidation changes. Thus, more fundamental studies exploring how DOM sources impact phenol oxidation by manganese oxides are necessary to better understand and predict oxidation in potential *in situ* treatment systems.

5.3 Implications for environmental justice

5.3.1 Environmental injustice in the United States

Topics in environmental chemistry are inherently linked to issues of environmental racism and environmental justice. Contaminants in the environment disproportionately affect minority and low-income communities across the United States and these same communities have lower access to education, health care, and other interventions which may help counteract exposure to environmental contaminants.²⁴⁻²⁸ These increased exposure levels among minority

and low-income communities are perpetuated by laws, environmental regulations, zoning regulations, and historical development practices which worsen environmental injustice by directing resources to higher-income and majority white communities or by developing low-income housing near industrial zones, active mining locations, or hazardous waste and municipal landfill sites.²⁷⁻³¹ A 1980s survey by the United States General Accounting Office found 40% of the country's landfill capacity is located within majority black zip codes in southern states and that race is the best predictor of hazardous waste site locations across the country.²⁷

More recently, the Flint, Michigan lead water crisis highlighted the impact of systematic structural racism on environmental pollution. Flint is the second poorest city in the United States and only 37% white according to the U.S. Census Bureau.³²⁻³⁴ The citizens of Flint suffered one of the worst modern U.S. environmental crises from 2014 to 2019 as their water supply was changed from the Detroit Water and Sewerage Department to the Flint River, causing a cascade of lead contamination and poisoning, *Legionella* outbreaks, and criminal indictments of public officials who mishandled or ignored the growing crisis.^{30,33} The Michigan Civil Rights Commission concluded that the crisis was a case of systematic, environmental racism based on the city's history of inadequate infrastructure and biased housing development, failure to act on citizen complaints about drinking water and health outcomes, and lack of adequate water treatment practices.³²⁻³⁴ Flint, Michigan is a well-documented case of environmental injustice which illuminates how quickly systemic flaws can become a nationally recognized crisis, although many cases of environmental injustice are the result of chronic contaminant exposure and thus are not represented or investigated as widely as the Flint crisis.

5.3.2 Manganese contamination

Manganese concentrations are regulated as a secondary drinking water standard by the Environmental Protection Agency at 0.05 mg/L.³⁵ Dissolved manganese in well and surface waters or distribution systems cause discoloration and taste in drinking waters.^{26,35-37} At high concentrations, manganese may cause infant mortality or neurodevelopmental defects, heart defects, or cancer.^{29,36-40} These exposures and impacts of manganese drinking water often affects families with shallow private wells³⁶ rather than populations served by municipal utilities. Among populations exposed through groundwater sourced from private wells, disadvantaged and less educated groups are significantly less likely to have their wells tested or treated for contaminants.^{25,26,36,38,39} Furthermore, while naturally occurring contaminants such as dissolved manganese affect all populations at similar rates, low socioeconomic groups are less likely to know about the potential risks or to take protective measures to reduce their exposure.^{25,26}

Another route of manganese contamination occurs through proximity to acid mine drainage-contaminated waters.^{28,41,42} Most acid mine drainage sites in the United States are surrounded by communities which rely on the contaminated stream or river for drinking, agriculture, or recreation.^{28,41} These communities are exposed through such activities but studies reveal that many rural communities near these mine sites have a disconnect between their perception of how the acid mine drainage affects their health and education or communication of health impacts. This disconnect stems from a lack of research into the invisible health effects of acid mine drainage as well as a loss of autonomy in these marginalized communities which are not included in mine planning and decision making by officials.^{28,41}

5.3.3 Phenol contamination

As discussed throughout this dissertation, phenolic contaminants are commonly found in natural waters and contaminated waste streams (e.g., wastewater effluents).^{8,43-53} These phenolic contaminants fall within a number of contaminant classes, including endocrine disruptors, antibacterial agents, surfactants, pharmaceuticals, and pesticides which negatively impact both natural environments (e.g., fish reproduction)⁵³⁻⁵⁹ and human health.^{28,31,48,51,53,60-62} Some of these contaminants and compound classes are covered by drinking or surface water standards;^{35,44} however, many organic contaminants remain unregulated and both regulated and unregulated organic contaminants disproportionately affect low income and minority communities as described above for aqueous manganese. Communities may be exposed through drinking water or contact with contaminated surface waters for work (e.g., agriculture) or recreation.^{25,29-31} Many of these phenolic contaminants are reagents, products, or intermediates of manufacturing processes,^{8,50,60} increasing exposure for low income manufacturing workers and low-income or minority neighborhoods located near industrial zones.^{31,53}

Additionally, communities are exposed to these organic contaminants through food as phenols may accumulate in both plants and seafood. For example, lettuce and radishes are two food products shown to accumulate triclosan and pesticides.⁵³ Phenols may also accumulate in sludge and biosolid products of wastewater treatment processes which are then commonly applied to agricultural fields to enhance crop yields.^{49,51,63-65} Over 1.1×10^5 kg/yr of triclosan is released into wastewater⁶⁴ and about 50% of the influent mass of triclosan is measured in sludge and biosolid products from wastewater treatment⁵⁶ at up to up to 40 $\mu\text{mol/kg}$ measured in survey studies.⁶⁶ Farmers are disproportionately exposed during application of these solids onto fields and all populations who consume food which has accumulated these contaminants through

biosolids, pesticide applications, contaminated irrigation waters, or other sources are exposed in consumption. Furthermore, these contaminants (e.g., BPA, triclosan) may be passed through breastmilk to infants who are then at risk of developmental and health effects,⁵³ especially within populations lacking education about these risks or the resources necessary to supplement or replace breastmilk with formula.

Native tribes in particular depend on seafood and native plants more than other communities and these foods are often tied to their culture, social interactions, and traditions.^{54,67-}
⁷¹ Fish make up 17% of the world's animal protein consumption in 2013,⁶⁹ and a 2016 EPA report noted that "tribal people suffer disproportionate exposure and risks associated with contaminants in fish [in the United States]" due to their higher fish consumption rates.⁶⁸ However, as with communities located near mining operations, Native Americans are frequently left out of regulatory and decision making processes which impact these food sources.^{68,70,71} Fish advisories are commonly implemented to curtail contaminant exposure through fish rather than implementing remediation techniques to reduce the contaminant load of this food source.⁶⁹ As a result, native populations lose their food autonomy and are forced to switch from their traditional food source, which is deeply tied to their culture and social connections, to more processed high-carbohydrate and high-fat foods which cause both cultural degradation⁷¹ and other health problems including heart disease.⁷² The increased exposure to contaminants from fish-based diets and/or the shift from fishing as a result of exclusionary regulations is observed for tribes across the United States including the Alaskan Iñupiat and Pacific Northwest tribes which have strong cultural ties with salmon,⁷⁰ the Houma and other nations of the Southeast which established their tribes on fishing crawfish from the bayous and canals,⁶⁷ and the Ho-Chunk and other Midwest tribes which extensively fish from the Great Lakes and Mississippi River

regions.⁷³ The effects of phenol contamination in surface waters and food sources disproportionately affect Tribal Nations as a result of the loss of autonomy and representation in regulatory decisions, continued systemic injustices which threaten their lands and natural resources, and the confounding factor of declining fish populations which result from contaminant-based fish deaths and reproductive effects.

5.3.4 Implications of this research

Manganese oxides included in Chapter 2 include reclaimed solids from both drinking water treatment of dissolved manganese through greensand filters (Well 29) and manganese oxides formed in passive acid mine drainage treatment systems. In Chapter 2, we explore whether these reclaimed solids degrade organic contaminants and have potential for reuse in phenolic contaminant treatment systems. Our results indicate that these solids can oxidize phenolic contaminants and thus should be considered for treatment systems as these materials are currently dumped on-site or in landfills where they add to the ongoing injustices faced by nearby communities.

Application of this research to inform such contaminant treatment systems is also a step towards addressing disproportionate contaminant exposures by degrading these contaminants in stormwater treatment ponds or wastewater and sewerage plants before they discharge to surface waters. If passive *in situ* treatments are implemented to reduce organic contaminant loads in natural waters, these systems must be equally implemented in low-income and minority dominated areas. The use of reclaimed manganese oxides and passive treatment systems, rather than resource intensive active systems, help lower barriers (e.g., cost, energy use) to building these systems, increasing accessibility for all communities.

5.4 References

1. Khatiwada, R.; Olivares, C.; Abrell, L.; Root, R. A.; Sierra-Alvarez, R.; Field, J. A.; Chorover, J., Oxidation of reduced daughter products from 2,4-dinitroanisole (DNAN) by Mn(IV) and Fe(III) oxides. *Chemosphere* **2018**, *201*, 790-798.
2. Klausen, J.; Haderlein, S. B.; Schwarzenbach, R. P., Oxidation of substituted anilines by aqueous MnO₂: Effect of co-solutes on initial and quasi-steady-state kinetics. *Environ. Sci. Technol.* **1997**, *31*, (9), 2642-2649.
3. Laha, S.; Luthy, R. G., Oxidation of aniline and other primary aromatic amines by manganese dioxide. *Environ. Sci. Technol.* **1990**, *24*, (3), 363-373.
4. Li, H.; Lee, L. S.; Schulze, D. G.; Guest, C. A., Role of soil manganese in the oxidation of aromatic amines. *Environ. Sci. Technol.* **2003**, *37*, (12), 2686-2693.
5. Luan, F.; Gorski, C. A.; Burgos, W. D., Linear free energy relationships for the biotic and abiotic reduction of nitroaromatic compounds. *Environ. Sci. Technol.* **2015**, *49*, (6), 3557-3565.
6. Park, J. W.; Dec, J.; Kim, J. E.; Bollag, J. M., Effect of humic constituents on the transformation of chlorinated phenols and anilines in the presence of oxidoreductive enzymes or birnessite. *Environ. Sci. Technol.* **1999**, *33*, (12), 2028-2034.
7. Pavitt, A. S.; Bylaska, E. J.; Tratnyek, P. G., Oxidation potentials of phenols and anilines: Correlation analysis of electrochemical and theoretical values. *Environ. Sci. Process. Impacts* **2017**, *19*, (3), 339-349.
8. Remucal, C. K.; Ginder-Vogel, M., A critical review of the reactivity of manganese oxides with organic contaminants. *Environ. Sci. Process. Impacts* **2014**, *16*, (6), 1247-1266.
9. Salter-Blanc, A. J.; Bylaska, E. J.; Lyon, M. A.; Ness, S. C.; Tratnyek, P. G., Structure-activity relationships for rates of aromatic amine oxidation by manganese dioxide. *Environ. Sci. Technol.* **2016**, *50*, (10), 5094-5102.
10. Shaikh, N.; Taujale, S.; Zhang, H.; Artyushkova, K.; Ali, A. S.; Cerrato, J. M., Spectroscopic investigation of interfacial interaction of manganese oxide with triclosan, aniline, and phenol. *Environ. Sci. Technol.* **2016**, *50*, (20), 10978-10987.
11. Tran, T. H.; Labanowski, J.; Gallard, H., Adsorption and transformation of the anthelmintic drug niclosamide by manganese oxide. *Chemosphere* **2018**, *201*, 425-431.
12. Im, J.; Prevatte, C. W.; Campagna, S. R.; Loffler, F. E., Identification of 4-hydroxycumyl alcohol as the major MnO₂-mediated bisphenol a transformation product and evaluation of its environmental fate. *Environ. Sci. Technol.* **2015**, *49*, (10), 6214-21.
13. Ding, J.; Su, M.; Wu, C.; Lin, K., Transformation of triclosan to 2,8-dichlorodibenzo-*p*-dioxin by iron and manganese oxides under near dry conditions. *Chemosphere* **2015**, *133*, 41-46.
14. Drewes, J. E.; Letzel, T., Chemicals of emerging concern and their transformation products in the aqueous environment. In *Assessing transformation products of chemicals by non-target and suspect screening – strategies and workflows volume 1*, **2016**; pp 3-9.
15. Gao, J.; Hedman, C.; Liu, C.; Guo, T.; Pedersen, J. A., Transformation of sulfamethazine by manganese oxide in aqueous solution. *Environ. Sci. Technol.* **2012**, *46*, (5), 2642-51.

16. Lin, K.; Liu, W.; Gan, J., Reaction of tetrabromobisphenol A (TBBPA) with manganese dioxide: Kinetics, products, and pathways. *Environ. Sci. Technol.* **2009**, *43*, (12), 4480-4486.
17. Lin, K.; Liu, W.; Gant, J., Oxidative removal of bisphenol A by manganese dioxide: Efficacy, products, and pathways. *Environ. Sci. Technol.* **2009**, *43*, (10), 3860-3864.
18. Liu, A.; Shi, J.; Qu, G.; Hu, L.; Ma, Q.; Song, M.; Jing, C.; Jiang, G., Identification of emerging brominated chemicals as the transformation products of tetrabromobisphenol A (TBBPA) derivatives in soil. *Environ. Sci. Technol.* **2017**, *51*, (10), 5434-5444.
19. Ukrainczyk, L.; McBride, M. B., Oxidation and dechlorination of chlorophenols in dilute aqueous suspensions of manganese oxides - reaction products. *Environ. Toxicol. Chem.* **1993**, *12*, (11), 2015-2022.
20. Zhang, H.; Huang, C. H., Oxidative transformation of triclosan and chlorophene by manganese oxides. *Environ. Sci. Technol.* **2003**, *37*, (11), 2421-2430.
21. Zhao, L.; Yu, Z.; Peng, P.; Huang, W.; Dong, Y., Oxidative transformation of tetrachlorophenols and trichlorophenols by manganese dioxide. *Environ. Toxicol. Chem.* **2009**, *28*, (6), 1120-9.
22. Lin, K.; Peng, Y.; Huang, X.; Ding, J., Transformation of bisphenol A by manganese oxide-coated sand. *Environ. Sci. Pollut. Res. Int.* **2013**, *20*, (3), 1461-7.
23. Zhang, T.; Zhang, X.; Yan, X.; Ng, J.; Wang, Y.; Sun, D. D., Removal of bisphenol A via a hybrid process combining oxidation on β -MnO₂ nanowires with microfiltration. *Colloids Surf. A: Physicochem. Eng. Aspects* **2011**, *392*, (1), 198-204.
24. Bullard, R. D., Anatomy of environmental racism and the environmental justice movement. In *Confronting environmental racism: voices from the grassroots*, South End Press: Boston, MA, 1993.
25. Flanagan, C. A.; Byington, R.; Gallay, E.; Sambo, A., Social justice and the environmental commons. *Adv. Child Dev. Behav.* **2016**, *51*, 203-30.
26. Flanagan, S. V.; Spayd, S. E.; Procopio, N. A.; Marvinney, R. G.; Smith, A. E.; Chillrud, S. N.; Braman, S.; Zheng, Y., Arsenic in private well water part 3 of 3: Socioeconomic vulnerability to exposure in Maine and New Jersey. *Sci. Total Environ.* **2016**, *562*, 1019-1030.
27. Bullard, R. D.; Wright, B. H., The quest for environmental equity: Mobilizing the African-American community for social change. *Soc. Natur. Resour.* **1990**, *3*, (4), 301-311.
28. Moeng, K., Community perceptions on the health risks of acid mine drainage: The environmental justice struggles of communities near mining fields. *Environ. Devel. Sustain.* **2018**, *21*, (6), 2619-2640.
29. Massey, R., Environmental justice: Income, race, and health. In Tufts University: Medford, MA, 2004.
30. Faber, D. R.; Krieg, E. J., Unequal exposure to ecological hazards: Environmental injustices in the Commonwealth of Massachusetts. *Environ. Just.* **2002**, *110*.
31. Johnston, J.; Cushing, L., Chemical exposures, health, and environmental justice in communities living on the fenceline of industry. *Curr. Environ. Health Rep.* **2020**, *7*, (1), 48-57.
32. Almasy, S.; Ly, L., Flint water crisis: Report says 'systemic racism' played role. *Cable News Network* 2017.

33. Commission, M. C. R. *The Flint water crisis: Systemic racism through the lens of Flint; Michigan*, 2017.
34. Ross, J., In Flint, bad tap water runs politically deep. *The Washington Post* 2016.
35. Environmental Protection Agency, National primary drinking water regulations. In National Service Center for Environmental Publications: 2021.
36. Gillispie, E. C.; Austin, R. E.; Rivera, N. A.; Bolich, R.; Duckworth, O. W.; Bradley, P.; Amoozegar, A.; Hesterberg, D.; Polizzotto, M. L., Soil weathering as an engine for manganese contamination of well water. *Environ. Sci. Technol.* **2016**, *50*, (18), 9963-71.
37. Schlenker, T.; Hausbeck, J.; Sorsa, K., Manganese in Madison's drinking water. *J. Environ. Health* **2008**, *71*, (5), 12-16.
38. Langley, R. L.; Kao, Y.; Mort, S. A.; Bateman, A.; Simpson, B. D.; Reich, B. J., Adverse neurodevelopmental effects and hearing loss in children associated with manganese in well water, North Carolina, USA. *J. Environ. Occup. Sci.* **2015**, *4*, (2), 62-69.
39. Sanders, A. P.; Desrosiers, T. A.; Warren, J. L.; Herring, A. H.; Enright, D.; Olshan, A. F.; Meyer, R. E.; Fry, R. C., Association between arsenic, cadmium, manganese, and lead levels in private wells and birth defects prevalence in North Carolina: A semi-ecologic study. *BMC Public Health* **2014**, *14*, 955-967.
40. Spangler, J. G.; Reid, J. C., Environmental manganese and cancer mortality rates by county in North Carolina: An ecological study. *Biol. Trace Elem. Res.* **2010**, *133*, (2), 128-35.
41. Bussiere, B., Acid mine drainage from abandoned mine sites: Problematic and reclamation approaches. In *Advances in environmental geotechnics*, 2010; pp 111-125.
42. Skousen, J.; Zipper, C. E.; Rose, A.; Ziemkiewicz, P. F.; Nairn, R.; McDonald, L. M.; Kleinmann, R. L., Review of passive systems for acid mine drainage treatment. *Mine Water Environ.* **2016**, *36*, (1), 133-153.
43. Charbonnet, J. A.; Duan, Y.; van Genuchten, C. M.; Sedlak, D. L., Chemical regeneration of manganese oxide-coated sand for oxidation of organic stormwater contaminants. *Environ. Sci. Technol.* **2018**, *52*, (18), 10728-10736.
44. Luthy, R.; Sedlak, D. L. *Enhanced removal of nutrients and trace organic contaminants in pilot-scale stormwater treatment systems*; Water Research Foundation; Water Environment & Reuse Foundation; U.S. Environmental Protection Agency: U.S.A., 2017.
45. Grebel, J. E.; Charbonnet, J. A.; Sedlak, D. L., Oxidation of organic contaminants by manganese oxide geomedia for passive urban stormwater treatment systems. *Water Res.* **2016**, *88*, 481-491.
46. Wang, X.; Xiang, W.; Wang, S.; Ge, J.; Qu, R.; Wang, Z., Oxidative oligomerization of phenolic endocrine disrupting chemicals mediated by Mn(III)-I complexes and the role of phenoxyl radicals in the enhanced removal: Experimental and theoretical studies. *Environ. Sci. Technol.* **2020**, *54*, (3), 1573-1582.
47. Zhang, Y.; Zhu, H.; Szewzyk, U.; Lübbecke, S.; Uwe Geissen, S., Removal of emerging organic contaminants with a pilot-scale biofilter packed with natural manganese oxides. *Chem. Eng. J.* **2017**, *317*, 454-460.
48. Lu, D.; Feng, C.; Wang, D.; Lin, Y.; Ip, H. S.; She, J.; Xu, Q.; Wu, C.; Wang, G.; Zhou, Z., Analysis of twenty phenolic compounds in human urine: Hydrochloric acid hydrolysis, solid-phase extraction based on K₂CO₃-treated silica, and gas chromatography tandem mass spectrometry. *Anal. Bioanal. Chem.* **2015**, *407*, (14), 4131-41.

49. Bina, B.; Mohammadi, F.; Amin, M. M.; Pourzamani, H. R.; Yavari, Z., Determination of 4-nonylphenol and 4-*tert*-octylphenol compounds in various types of wastewater and their removal rates in different treatment processes in nine wastewater treatment plants of Iran. *Chin. J. Chem. Eng.* **2018**, *26*, (1), 183-190.
50. Sim, W. J.; Lee, S. H.; Lee, I. S.; Choi, S. D.; Oh, J. E., Distribution and formation of chlorophenols and bromophenols in marine and riverine environments. *Chemosphere* **2009**, *77*, (4), 552-558.
51. Wu, Q.; Lam, J. C. W.; Kwok, K. Y.; Tsui, M. M. P.; Lam, P. K. S., Occurrence and fate of endogenous steroid hormones, alkylphenol ethoxylates, bisphenol A and phthalates in municipal sewage treatment systems. *J. Environ. Sci. (China)* **2017**, *61*, 49-58.
52. Bulloch, D. N.; Nelson, E. D.; Carr, S. A.; Wissman, C. R.; Armstrong, J. L.; Schlenk, D.; Larive, C. K., Occurrence of halogenated transformation products of selected pharmaceuticals and personal care products in secondary and tertiary treated wastewaters from southern California. *Environ. Sci. Technol.* **2015**, *49*, (4), 2044-51.
53. Olaniyan, L. W.; Mkwetshana, N.; Okoh, A. I., Triclosan in water, implications for human and environmental health. *Springerplus* **2016**, *5*, (1), 1639.
54. Ruczynska, W.; Szlinder-Richert, J.; Nermer, T., The occurrence and distribution of nonylphenols and nonylphenol ethoxylates in different species of fish. *Environ. Sci. Process. Impacts* **2020**, *22*, (4), 1057-1070.
55. Toft, G.; Baatrup, E., Sexual characteristics are altered by 4-*tert*-octylphenol and 17 β -estradiol in the adult male guppy (*Poecilia reticulata*). *Ecotoxicol. Environ. Saf.* **2001**, *48*, (1), 76-84.
56. Dann, A. B.; Hontela, A., Triclosan: Environmental exposure, toxicity and mechanisms of action. *J. Appl. Toxicol.* **2011**, *31*, (4), 285-311.
57. Wolfand, J. M.; Seller, C.; Bell, C. D.; Cho, Y. M.; Oetjen, K.; Hogue, T. S.; Luthy, R. G., Occurrence of urban-use pesticides and management with enhanced stormwater control measures at the watershed scale. *Environ. Sci. Technol.* **2019**.
58. Pollock, T.; Mantella, L.; Reali, V.; deCatanzaro, D., Influence of tetrabromobisphenol A, with or without concurrent triclosan, upon bisphenol A and estradiol concentrations in mice. *Environ. Health Perspect.* **2017**, *125*, (8).
59. Pollock, T.; Weaver, R. E.; Ghasemi, R.; deCatanzaro, D., A mixture of five endocrine-disrupting chemicals modulates concentrations of bisphenol A and estradiol in mice. *Chemosphere* **2018**, *193*, 321-328.
60. Bexfield, L. M.; Toccalino, P. L.; Belitz, K.; Foreman, W. T.; Furlong, E. T., Hormones and pharmaceuticals in groundwater used as a source of drinking water across the United States. *Environ. Sci. Technol.* **2019**, *53*, (6), 2950-2960.
61. Montes-Grajales, D.; Fennix-Agudelo, M.; Miranda-Castro, W., Occurrence of personal care products as emerging chemicals of concern in water resources: A review. *Sci. Total Environ.* **2017**, *595*, 601-614.
62. Thomaidis, N. S.; Gago-Ferrero, P.; Ort, C.; Maragou, N. C.; Alygizakis, N. A.; Borova, V. L.; Dasenaki, M. E., Reflection of socioeconomic changes in wastewater: Licit and illicit drug use patterns. *Environ. Sci. Technol.* **2016**, *50*, (18), 10065-10072.
63. Butler, E.; Whelan, M. J.; Sakrabani, R.; van Egmond, R., Fate of triclosan in field soils receiving sewage sludge. *Environ. Pollut.* **2012**, *167*, 101-109.
64. Heidler, J.; Halden, R. U., Mass balance assessment of triclosan removal during conventional sewage treatment. *Chemosphere* **2007**, *66*, (2), 362-369.

65. Oulton, R. L.; Kohn, T.; Cwiertny, D. M., Pharmaceuticals and personal care products in effluent matrices: A survey of transformation and removal during wastewater treatment and implications for wastewater management. *J. Environ. Monit.* **2010**, *12*, (11), 1956-1978.
66. Gottschall, N.; Topp, E.; Metcalfe, C.; Edwards, M.; Payne, M.; Kleywegt, S.; Russell, P.; Lapen, D. R., Pharmaceutical and personal care products in groundwater, subsurface drainage, soil, and wheat grain, following a high single application of municipal biosolids to a field. *Chemosphere* **2012**, *87*, (2), 194-203.
67. Smithsonian National Museum of the American Indian, Meet Native America: Lora Ann Chaisson, Vice Principal Chief of the United Houma Nation. In *Meet Native America*, Smithsonian Museum: 2015; Vol. 2021.
68. Polissar, N. L.; Salisbury, A.; Ridolfi, C.; Callahan, K.; Neradilek, M.; Hippe, D. S.; Beckley, W. H. *A fish consumption survey of the Nez Perce tribe*; 2016.
69. Food and Agricultural Organization of the United Nations, *The state of world fisheries and aquaculture*; Rome, 2016.
70. Columbia River Inter-Tribal Fish Commission,. Tribal Fishing Resources: Tribal salmon culture, CRITFC.org, accessed 2021.
71. Willette, M.; Norgaard, K.; Reed, R., You got to have fish: Families, environmental decline and cultural reproduction. *Families, Relationships and Societies* **2016**, *5*, (3), 375-392.
72. Alpert, J. S.; Goldberg, R.; Ockene, I. S.; Taylor, P., Heart disease in Native Americans. *Cardiology* **1991**, *78*, (1), 3-12.
73. Memorandum of understanding between the Ho-Chunk Nation and the State of Wisconsin. Kickapoo Reserve Management Board, ed. Wisconsin, 1997.

Appendix A

Supplementary Material for Chapter 2: Organic structure and solid characteristics determine reactivity of phenolic compounds with synthetic and reclaimed manganese oxides

A.1. Materials

All chemicals were commercially available and used as received. Details for all phenolic compounds are listed in **Table A.1**; structures are displayed in **Table A.2**.

Methanol (MeOH; HPLC grade), hydrochloric acid (HCl; Certified ACS Plus grade), sodium chloride (NaCl; Certified ACS grade), acetonitrile (HPLC grade), potassium permanganate (KMnO₄; Certified ACS grade), and sodium hydroxide (NaOH; Certified ACS grade) were purchased from Fisher Scientific. Sulfuric acid (H₂SO₄; 95.0 – 98.0 %), nitric acid (HNO₃; 70%), and L-ascorbic acid (BioXtra, ≥99%) were purchased from Sigma-Aldrich. Sodium oxalate (Na₂C₂O₄; 99%) and sodium acetate trihydrate (ACS grade, 99 – 100.5%) were purchased from Alfa Aesar. Formic acid (HCOOH; Reagent ACS grade, 88%) was purchased from Aqua Solution, Inc. Manganese nitrate tetrahydrate (Mn(NO₃)₂•4H₂O; analysis grade) was purchased from Acros Organics.

δ-MnO₂ was synthesized according to a modified Murray method.¹ By this method, Mn(NO₃)₂ was added at a rate of 1 mL per minute into a solution of KMnO₄ and NaOH at molar ratios of 3:2:4 Mn^{II}:Mn^{VII}:OH⁻ while stirring at 350 rpm. Following Mn(NO₃)₂ addition, the solid suspension was covered and stirred for 18 hours at 22 ± 2 °C. The suspension was rinsed and

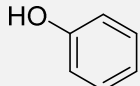
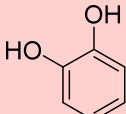
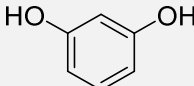
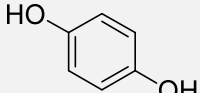
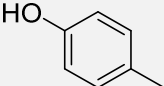
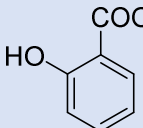
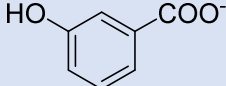
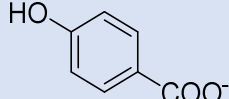
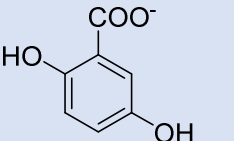
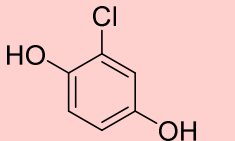
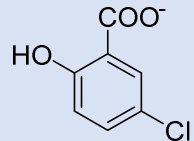
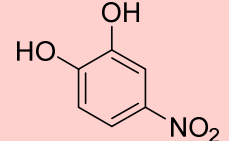
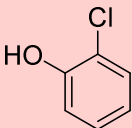
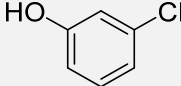
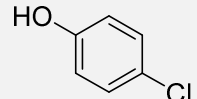
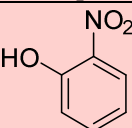
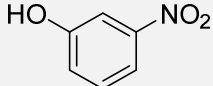
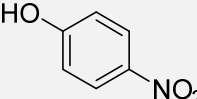
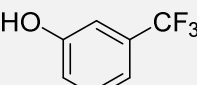
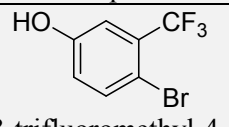
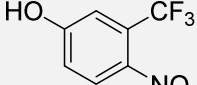
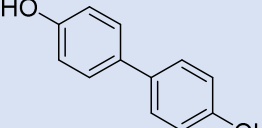
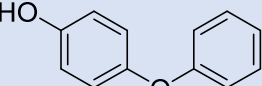
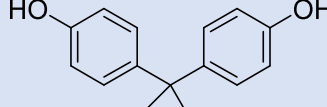
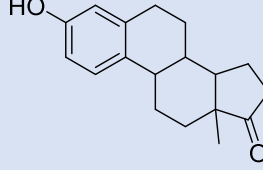
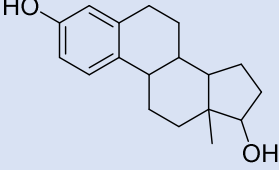
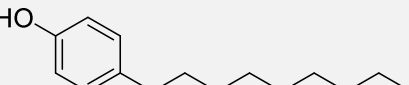
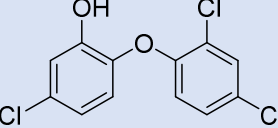
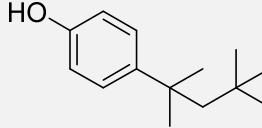
washed by centrifugation at 2500 rpm for 15 minutes in ultrapure water, decreasing the suspension volume over six sequential rinse cycles. For the two final centrifuge rinses, the solids were resuspended in pH 5.5 10 mM acetate buffer solution. The density of the slurry was determined by drying 1 mL of the suspension at 60 °C in triplicate and calculating the amount of dry Mn per volume.

The acid mine drainage remediation (AMD) solids were collected and dried by Hedin Environmental from the Glasgow treatment site in Pennsylvania.² The filtered drinking water treatment (DWT) solids were collected from Well 29 in Madison, WI. The DWT solids are the byproduct of a filter designed to remove aqueous manganese and iron that occur in the drinking water pumped at this well prior to disinfection and distribution. The solids were both rinsed with Milli-Q water (18.2 MΩ·cm) and equilibrated in 10 mM acetate buffer at 4 °C and adjusted to pH 5.5 until the pH remained stable.

Table A.1. Sources and purity of phenols.

Compound	Manufacturer	Purity
phenol	Sigma-Aldrich	molecular biology
1,2-dihydroxybenzene (catechol)	Sigma-Aldrich	>99%
resorcinol (3-hydroxyphenol)	Alfa Aesar	99-100.5%
hydroquinone (4-hydroxyphenol)	Sigma-Aldrich	>99%
<i>p</i> -cresol (4-methylphenol)	Sigma-Aldrich	99%
salicylic acid (2-hydroxybenzoic acid)	Sigma-Aldrich	>99%
3-hydroxybenzoic acid	Aldrich	99%
4-hydroxybenzoic acid	Aldrich	99%
2,5-dihydroxybenzoic acid	Aldrich	98%
5-chlorohydroquinone	Acros Organics	90%
5-chlorosalicylic acid	Aldrich	98%
4-nitrocatechol	Alfa Aesar	98+%
2-chlorophenol	Aldrich	>99%
3-chlorophenol	Aldrich	98%
4-chlorophenol	Aldrich	>99%
2-nitrophenol	Aldrich	98%
3-nitrophenol	Sigma-Aldrich	99%
4-nitrophenol	Aldrich	>99%
3-trifluoromethylphenol	Aldrich	99%
4-bromo-3-trifluoromethylphenol	Alfa Aesar	98%
4-nitro-3-trifluoromethylphenol	Acros Organics	99%
4,4'-dihydroxybiphenyl	Aldrich	97%
4-phenoxyphenol	Sigma-Aldrich	99%
bisphenol A	Aldrich	>99%
estrone (E1)	Acros Organics	99+%
17 β -estradiol (E2)	Sigma-Aldrich	>98%
4- <i>n</i> -nonylphenol	Alfa Aesar	98+%
triclosan	AccuStandard	N/A
4- <i>tert</i> -octylphenol	Sigma-Aldrich	97%

Table A.2. Structures of phenols shown at pH 5.5. Gray cells are simple (i.e., *meta*- and *para*-substituted phenols), red cells are *ortho*-substituted phenols, and blue cells are complex phenols.

 phenol	 catechol	 resorcinol	 hydroquinone
 4-cresol	 2-hydroxybenzoate	 3-hydroxybenzoate	 4-hydroxybenzoate
 2,5-dihydroxybenzoate	 5-chlorohydroquinone	 5-chlorosalicylate	 4-nitrocatechol
 2-chlorophenol	 3-chlorophenol	 4-chlorophenol	
 2-nitrophenol	 3-nitrophenol	 4-nitrophenol	
 3-trifluoromethylphenol	 3-trifluoromethyl-4-bromophenol	 3-trifluoromethyl-4-nitrophenol	
 4,4'-dihydroxybiphenyl	 4-phenoxyphenol	 bisphenol A	
 estrone		 estradiol	
 4- <i>n</i> -nonylphenol	 triclosan		 4- <i>tert</i> -octylphenol

A.2. Solid characterization

The average manganese oxidation numbers (AMON) determined by X-ray absorption near-edge spectroscopy (XANES) and the oxalate titration method were compared for δ -MnO₂.³⁻⁵ The oxalate titration determines the average oxidation state by dissolving the solid sample in excess sodium oxalate (0.5 g-Mn dissolved in 20 mL 100 mM Na₂C₂O₄ and 5 mL 6 M H₂SO₄), heating to 80 °C, and back titrating with 3 mM KMnO₄ (standardized against a Na₂C₂O₄ control sample prepared without Mn) until the solution begins to turn pink. The electron equivalents needed to fully oxidize the concentration of manganese in the sample are then converted to an average oxidation state based on the ratio of Mn^{III}:Mn^{IV}.⁵ The results agreed well between the XANES and oxalate titration methods (3.8 ± 0.2) and are within the expected range for δ -MnO₂.^{1,3,6-11} AMON values for the drinking water treatment and acid mine drainage remediation solids were also determined by XANES at the manganese edge (3.82 ± 0.04 and 3.79 ± 0.04 , respectively). This method has a reported error of 0.04 valence units for solids ranging in valence from +3 to +4.³

Scanning electron microscopy (SEM; LEO 1530, Schottky-type field-emission electron source; **Figure A.1**) was conducted to determine the general particle size, shape, and heterogeneity of these solids. The DWT solids are a heterogeneous mixture of particle size and shape, while the AMD solids have a more consistent particle size. SEM and transmission electron microscopy (TEM) images of δ -MnO₂ show the consistent, amorphous shape and generally small particle size.^{1,8,12} The δ -MnO₂ used in this study is consistent with these previously published images.

The bulk elemental composition of the solids was determined by inductively coupled plasma-optical emission spectroscopy (ICP-OES; Perkin Elmer 4300; **Table A.3**) of the material

dissolved in 6 M HCl. From these analyses, the AMD solids contain inorganic impurities (e.g., Mg, Na) with trace amounts of other metals (e.g., Fe, Al, Ni). Because other redox active metals are only present in relatively low concentrations (**Table A.3**), manganese is the primary redox active sorbent in this solid matrix. ICP-OES of the DWT solids indicate there are very few other trace metal species present (**Table A.3**). ICP-OES was also used to determine the sodium content of δ -MnO₂ dissolved in 6 M HCl (14.9 ± 0.9 % Na:Mn (mol:mol)).

The organic carbon content of each oxide was determined by weight loss on ignition. Pre-dried, finely ground solid (300 mg) was massed into a desiccated crucible. The samples were dried at 100° C for 16 hours then heated to 550° C for four hours to incinerate any organic carbon species.¹³ The three solids had low organic carbon content as expected; δ -MnO₂ had 0.7% organic carbon by weight, while the reclaimed drinking water treatment solids had 2.8% and the acid mine drainage remediation solids had 4.7% organic carbon by weight.

X-ray diffraction (XRD; Rigaku Rapid II, Mo K α source; $\lambda = 0.7093$ Å; **Figure 2.2**) spectra also indicate differences between the solids. The pattern for δ -MnO₂ is as expected for a poorly crystalline birnessite synthesized by the Murray method, with three characteristically broad peaks.^{1,6,7,10,12} The DWT solids have a similarly low crystallinity, with even less defined peaks than δ -MnO₂, while XRD of the AMD solids confirms the presence of crystalline phases identified by SEM and EDS (**Figure 2.2**).

The pH of zero charge (pH_{pzc}) was determined by rapid potentiometric titration performed with a Mettler Toledo G20 compact titrator and PNP sensor.^{14,15} To determine the pH at which the bulk surface is neutrally charged, 0.2 g of each solid were pre-equilibrated in solutions of 0.1 M, 0.01 M, and 0.001 M NaCl to control ionic strength for 24 hours. Following pre-equilibration, the solutions were adjusted to pH 11 with 1 M NaOH and allowed to shake

overnight, then readjusted as needed to maintain a pH of 11. Blank solutions of each ionic strength were prepared in the same manner. All solutions were titrated with 0.1 mL additions of 0.1 N H₂SO₄ to a final pH of 0.5. The data was blank subtracted, normalized to the sample mass, and plotted versus pH. The pH_{pzc} was identified as the intersect of the three ionic strength conditions for each solid. δ -MnO₂ and DWT data had multiple intersections; these values were averaged.

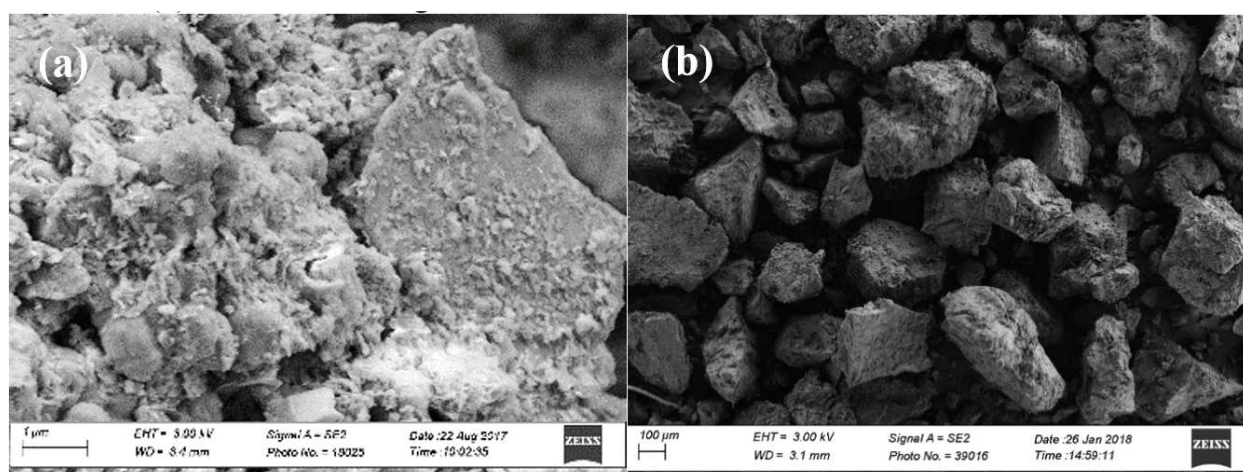


Figure A.1. Scanning electron microscopy images of (a) drinking water treatment solids and (b) acid mine drainage remediation solids.

Table A.3. Percent elemental composition (wt:wt) of metals and cations analyzed by ICP-OES for bulk solids extracted in 6 M HCl. N.D. indicates the element was below detection limits.

Solid	Mn	Fe	Zn	Al	Ni	Se	Ca	Mg	Na
δ -MnO ₂	63 ± 6	N.D.	N.D.	N.D.	N.D.	N.D.	N.D.	N.D.	15.0 ± 0.9
DWT	8.7 ± 0.8	43 ± 2	< 0.7	< 3	N.D.	0.8 ± 0.4	5.5 ± 0.1	0.4 ± 0.1	0.01 ± 0.02
AMD	42.8 ± 0.8	0.2 ± 0.2	0.98 ± 0.02	7.85 ± 0.01	0.61 ± 0.03	1 ± 7	-	0.63 ± 0.01	0.4 ± 0.8

A.3. Buffer selection and controls

A.3.1. Sodium acetate buffer

Sodium acetate buffer (pH 5.5) was selected because other buffers with buffering capacities in the range of pH 5 – 7 either interact with the manganese solids or, in the case of bicarbonate, do not adequately buffer these reactions under this experimental setup. Good's buffers (e.g., PIPES, MES) reduce manganese oxides and phosphate can strongly complex manganese sorption sites; previous studies using these buffers may be unreliable as these buffer interactions interfere with reported results.^{7,10,16-19} In control experiments, 10 mM pH 6.5 bicarbonate buffer did not adequately buffer the system in non-purged batch reactors, with final reaction pH values ranging from 6.8 to 8.1 (data not shown). In contrast, reactors with 10 mM pH 5.5 sodium acetate buffer had an average final pH at 5.59 ± 0.06 at the end of each reaction and showed no effects on the manganese structure or oxidation state.

A.3.2. Control reactions of solids and phenols

To test the effects that sodium acetate buffer may have on this system, control reactions were run for δ -MnO₂, DWT, and AMD solids in 10 mM pH 5.5 acetate buffer in the absence of phenolic compounds. AMON was determined by XANES for samples collected from the unreacted solids and after 10 days of equilibration in the buffer. There was no significant difference in AMON following the 10-day equilibrium period in pH 5.5 10 mM acetate buffer, indicating the sodium acetate buffer does not reduce these oxides over the maximum 10-day reaction period (**Table A.4**).

Table A.4. Average manganese oxidation number determined by XANES for manganese oxide starting materials and following 10-day equilibration in 10 mM pH 5.5 sodium acetate buffer without any organic reductants.

Manganese oxide	Initial AMON	Final AMON
δ -MnO ₂	3.84 ± 0.04	3.85 ± 0.04
DWT	3.82 ± 0.04	3.77 ± 0.04
AMD	3.79 ± 0.04	3.70 ± 0.04

A.4. Analytical Methods

A.4.1. Phenol quantification

An Agilent 1260 Infinity series high performance liquid chromatography instrument (HPLC; Agilent Technologies) was used to quantify the concentrations of all target phenolic compounds by an in-line diode array detector or fluorescence detector. Chromatography parameters are provided in **Table A.5**. The aqueous mobile phase was 10% volume:volume (v:v) acetonitrile and 0.1% v:v formic acid adjusted to pH 2.5 in ultrapure water. Acetonitrile was the organic mobile phase. All phenolic compounds were analyzed using an EC-C18 column (Agilent Poroshell-120; 3.0 x 50 mm, 2.7 μm) with an injection volume of 20 μL .

A.4.2. Observed rate constants

Experimental pseudo-first-order rate constants were determined for the quenched and filtered datasets collected for each phenol over the initial reaction period in triplicate (**Figure 2.1**; **Table A.6**). These values are the pseudo-first-order rate constants of oxidation (quenched rate constant) and total removal (i.e., oxidation and sorption; filtered rate constants).

Hydroquinone is re-reduced by the ascorbic acid during quenching, preventing quenched rate determinations,^{20,21} while 2,5-dihydroxybenzoic acid is unreactive in the 10-day reaction period. The reaction mechanism and kinetic model results are shown, but these compounds were excluded from quantitative structure-activity modeling. Similarly, quenched rate constants for 4-nitrophenol and 3-trifluoromethyl-4-nitrophenol show loss, but the filtered rate constants are unavailable as the error was greater than the loss of these phenols.

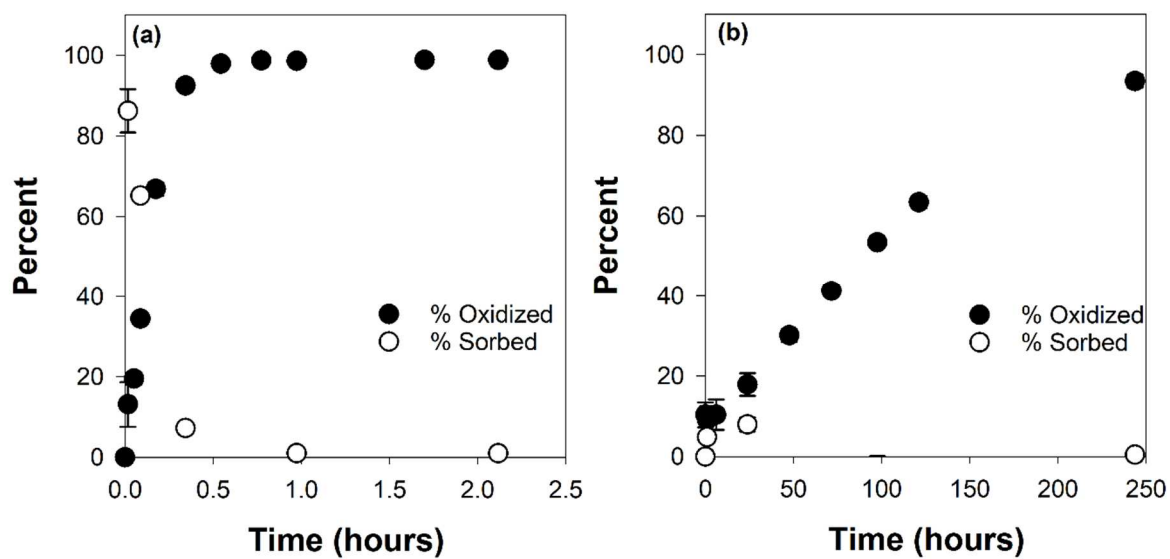


Figure A.2. Percent sorption and loss for (a) triclosan and (b) 4,4'-dihydroxybiphenyl. Error bars indicate standard deviation of triplicate data.

Table A.5. HPLC parameters for parent compound detection. The aqueous mobile phase was 10% v:v acetonitrile, 0.1% v:v formic acid at pH 2.5.

Compound	Aqueous mobile phase	Acetonitrile	Flow rate ($\mu\text{L}/\text{min}$)	Retention time (min)	Detection	
phenol	65%	35%	0.6	1	abs: 280 nm ref: 400 nm	
catechol	100%	0%		1.28		
resorcinol	40%	60%	1	0.4	Fluorescence: ex: 305 nm em: 290 nm	
hydroquinone	100%	0%	0.6	1.2	abs: 280 nm ref: 400 nm	
4-cresol	75%	25%		1.2	Fluorescence: ex: 305 nm em: 290 nm	
2-hydroxybenzoic acid	100%	0%		1.4	abs: 280 nm ref: 400 nm	
3-hydroxybenzoic acid				2.05		
4-hydroxybenzoic acid				1.5		
2,5-dihydroxybenzoic acid				1.8		
5-chlorohydroquinone				1.8		
5-chlorosalicylic acid				1.8		
4-nitrocatechol	100%	0%		2.5		
2-chlorophenol	75%	25%		3		
3-chlorophenol				3.5		
4-chlorophenol				3.5		
2-nitrophenol				3.5		
3-nitrophenol				2		
4-nitrophenol				1.5		
3-trifluoromethylphenol	65%	35%		2		
3-trifluoromethyl-4-bromophenol				3.5		
3-trifluoromethyl-4-nitrophenol				2		
4,4'-dihydroxybiphenyl	75%	25%		0.9		Fluorescence: ex: 305 nm em: 290 nm
bisphenol A	65%	35%		1		1.8
4-phenoxyphenol			2.8			
estrone			0.6	0.6		
17 β -estradiol	40%	60%	0.6	3	Fluorescence: ex: 305 nm em: 290 nm	
4- <i>tert</i> -octylphenol			1	0.7		
triclosan			1	1.45	abs: 280 nm ref: 400 nm	
4- <i>n</i> -nonylphenol	30%	70%	3.1			

Table A.6. Quenched and filtered pseudo-first-order rate constants for 29 phenolic compounds reacted with δ -MnO₂ and 15 phenols reacted with AMD and DWT reclaimed solids. The time for which the initial pseudo-first-order rate constants were determined and the observed rate-limiting step (RLS) for each reaction are included.

Compound	Quenched k (hr ⁻¹)	Filtered k (hr ⁻¹)	Analyzed reaction time (hr)	RLS
<i>δ-MnO₂</i>				
phenol	0.12 ± 0.03	0.20 ± 0.16	1.9	electron transfer
catechol	0.20 ± 0.07	0.18 ± 0.06	6.1	electron transfer
resorcinol	10.0 ± 0.6	25 ± 2	0.13	electron transfer
hydroquinone	-	35 ± 10	-	electron transfer
4-cresol	16 ± 11	47 ± 35	0.10	electron transfer
2-hydroxybenzoate	0.036 ± 0.009	0.006 ± 0.005	0.61	sorption
3-hydroxybenzoate	0.10 ± 0.04	1.2 ± 1.6	2.1	sorption
4-hydroxybenzoate	0.08 ± 0.02	0.9 ± 1.4	2.0	sorption
2,5-dihydroxybenzoate	0.079 ± 0.009	38.9 ± 0.5	14	electron transfer
5-chlorohydroquinone	0.033 ± 0.003	54.4 ± 0.5	48	electron transfer
5-chlorosalicylic acid	2.5 ± 2.3	0.21 ± 0.02	0.50	sorption
4-nitrocatechol	112 ± 6	355 ± 7	0.02	electron transfer
2-chlorophenol	1.2 ± 0.4	31 ± 18	0.56	electron transfer
3-chlorophenol	0.44 ± 0.09	0.51 ± 0.46	0.25	sorption
4-chlorophenol	2.8 ± 0.8	23 ± 16	0.13	electron transfer
2-nitrophenol	0.171 ± 0.002	0.11 ± 0.09	3.8	sorption
3-nitrophenol	0.01 ± 0.01	0.0003 ± 0.0007	3.8	sorption
4-nitrophenol	0.004 ± 0.002	-	6.1	sorption
3-trifluoromethylphenol	0.06 ± 0.03	0.08 ± 0.06	3.5	sorption
3-trifluoromethyl-4-bromophenol	0.11 ± 0.03	0.15 ± 0.13	3.4	sorption
3-trifluoromethyl-4-nitrophenol	0.001 ± 0.01	-	5.7	sorption
4,4'-dihydroxybiphenyl	0.009 ± 0.002	0.06 ± 0.07	182	sorption
4-phenoxyphenol	26 ± 1	82 ± 45	0.07	electron transfer
bisphenol A	8.5 ± 0.7	139 ± 84	0.20	electron transfer
Compound	Quenched k (hr ⁻¹)	Filtered k (hr ⁻¹)	Analyzed reaction	RLS

			time (hr)	
<i>δ-MnO₂ continued</i>				
estrone	6.0 ± 0.5	53 ± 37	0.38	electron transfer
17β-estradiol	19 ± 10	90 ± 49	0.13	electron transfer
4- <i>n</i> -nonylphenol	1.5 ± 0.7	74 ± 10	0.26	electron transfer
triclosan	7.6 ± 0.2	126 ± 61	0.44	electron transfer
4- <i>tert</i> -octylphenol	149 ± 24	114 ± 33	0.04	sorption
<i>Drinking water treatment solids</i>				
phenol	0.02 ± 0.01	0.014 ± 0.007	25	sorption
resorcinol	0.08 ± 0.05	0.012 ± 0.007	9.6	sorption
4-cresol	0.12 ± 0.02	0.21 ± 0.16	4.5	electron transfer
4-nitrocatechol	0.8 ± 0.3	1.7 ± 1.1	1.6	electron transfer
2-chlorophenol	0.003 ± 0.001	0.0019 ± 0.0008	191	sorption
3-chlorophenol	0.003 ± 0.004	0.001 ± 0.003	67	electron transfer
4-chlorophenol	0.019 ± 0.005	0.03 ± 0.02	14	electron transfer
2-nitrophenol	0.001 ± 0.001	0.0003 ± 0.0007	87	sorption
3-nitrophenol	0.001 ± 0.002	0.003 ± 0.002	92	electron transfer
4,4'-dihydroxybiphenyl	0.026 ± 0.004	0.038 ± 0.003	107	electron transfer
4-phenoxyphenol	2.6 ± 2.9	11 ± 14	0.88	electron transfer
bisphenol A	0.10 ± 0.02	0.7 ± 0.4	2.6	electron transfer
estrone	0.09 ± 0.04	0.2 ± 0.1	7.1	electron transfer
triclosan	0.07 ± 0.10	0.03 ± 0.03	0.52	sorption
4- <i>tert</i> -octylphenol	0.54 ± 0.48	0.8 ± 1	33	electron transfer
<i>Acid mine drainage remediation solids</i>				
phenol	0.05 ± 0.03	0.001 ± 0.009	64	sorption
resorcinol	0.04 ± 0.04	0.06 ± 0.06	7.7	sorption
4-cresol	0.01 ± 0.01	0.01 ± 0.01	8.4	sorption

Compound	Quenched <i>k</i>	Filtered <i>k</i>	Analyzed	RLS
-----------------	--------------------------	--------------------------	-----------------	------------

	(hr ⁻¹)	(hr ⁻¹)	reaction time (hr)	
<i>Acid mine drainage remediation solids continued</i>				
4-nitrocatechol	1.1 ± 0.3	1.4 ± 0.5	1.5	electron transfer
2-chlorophenol	0.001 ± 0.001	0.002 ± 0.003	165	sorption
3-chlorophenol	0.001 ± 0.003	0.007 ± 0.015	32	electron transfer
4-chlorophenol	0.005 ± 0.004	0.8 ± 0.7	19	electron transfer
2-nitrophenol	0.0003 ± 0.002	0.003 ± 0.005	276	sorption
3-nitrophenol	-	-	-	electron transfer
4,4'-dihydroxybiphenyl	0.017 ± 0.004	0.018 ± 0.003	193	electron transfer
4-phenoxyphenol	0.09 ± 0.02	0.09 ± 0.02	7.9	sorption
bisphenol A	0.01 ± 0.03	0.008 ± 0.005	13	sorption
estrone	0.010 ± 0.008	0.02 ± 0.01	48	sorption
triclosan	0.03 ± 0.01	0.05 ± 0.03	0.14	sorption
4- <i>tert</i> -octylphenol	0.07 ± 0.03	0.2 ± 1.2	9.9	electron transfer

A.5. Sorption validation

Previous literature identified the two potential rate limiting steps of phenol oxidation by manganese oxides as (1) the sorption process of the phenolate ion to the manganese reaction site, and (2) the first electron transfer between the sorbed phenolate and manganese center.^{7,8} If the reaction between the phenol and Mn oxide is sorption-limited, the sorption of the phenolate ion to the manganese surface site is the rate-limiting step of the reaction, indicating that after sorption occurs, the first electron transfer occurs relatively quickly. As a result, the phenol does not accumulate on the mineral surface and only low levels of the unreacted parent phenol are measured. The concentration of sorbed phenol was measured as the difference between the total phenol concentration (measured from the quenched aliquot) and the phenol concentration in the filtered aliquot (e.g., 4,4'-dihydroxybiphenyl in **Figure 2.1b**).

Alternatively, electron transfer-limited reactions are characterized by measurable phenol concentrations on the manganese surface. Because the rate of the first one-electron transfer is rate-limiting in this mechanism, the sorption of the phenol to the manganese surface is relatively fast. Therefore, phenol sorbs to the mineral surface and accumulates faster than electron transfer occurs. When this occurs, the quenched (i.e., total) phenol aliquot has a greater concentration than that of the filtered (i.e., dissolved) phenol aliquot taken at the same reaction timepoint. The difference represents the concentration of phenol sorbed to the manganese surface at that timepoint (e.g., triclosan in **Figure 2.1a**).

A maximum observed percent sorption of 10% was chosen to delineate electron transfer-limited versus sorption-limited mechanisms as a proxy for sorption rates compared to electron transfer rates. The maximum percent sorption is observed during the initial reaction period (in the first or second collected timepoint, **Figure A.2**). This defined cutoff value was applied to the

error interval; compounds with high error for which one standard deviation from the reported percent sorption fell below the 10% cutoff were considered sorption-limited. Previous studies examining mechanistic differences between organic compounds^{8,21-23} or synthetic manganese oxides²⁴ do not outline a standard method for mechanism determination based on kinetic data.

We chose this 10% cutoff based on observed trends in the data, as most phenols fell well above or below this cutoff amount, and a theoretical cutoff of 0% measured sorption does not account for instrumental and sampling error. Of the 27 phenols determined as sorption-limited (<10% sorption) with any solid oxidant, only two had greater than 5% sorption, with 7-8% observed sorption (4,4'-dihydroxybiphenyl reacted with δ -MnO₂ and resorcinol reacted with DWT). On the other side of the defined 10% value, only 1 of the 22 phenols defined to be electron transfer-limited (3-nitrophenol reacted with DWT) had sorption values between 10-17%, at $13 \pm 2\%$. The results of kinetic modeling (**Section A.6**) and rate constant trends in QSARs support the choice of a 10% maximum percent sorption cutoff for mechanism determination. The mechanism determined using the kinetic model agreed with experimental results using the 10% maximum sorption cutoff for 23 of 29 phenols reacted with δ -MnO₂. At a 5% cutoff, as explored above, only 19 of the 29 phenols would be predicted correctly.

A.6. Kinetic modeling

We used the kinetic model developed by Zhang et al.²² to test whether the oxidation mechanism-dependent modeled rate constants agree with the mechanisms determined by the measured sorption for reactions between δ -MnO₂ and a suite of 29 phenols. This model fits the experimental time data to theoretical equations for electron transfer-limited (**Equation A.1**) and sorption-limited mechanisms (**Equation A.2**) by least squares regression.

$$C = (C_0 - S_{\text{rxn}}) + S_{\text{rxn}}e^{-k't} \quad \text{Equation A.1}$$

$$C = \frac{S_{\text{rxn}} - C_0}{\frac{S_{\text{rxn}}}{C_0}e^{k''(S_{\text{rxn}} - C_0)t} - 1} \quad \text{Equation A.2}$$

$$S_{\text{rxn}} = C_0 - C_e \quad \text{Equation A.3}$$

k' and k'' are the calculated first- and second-order rate constants, respectively. C_0 and C_e are the initial and equilibrium concentrations of the phenol, t is time, and S_{rxn} is the number of available surface sites on the solid. This value may be either fit to the data as a second variable or calculated as the difference between the initial and steady state concentrations of the compound (**Equation A.3**). The latter was used here. After determining k'' (units of M⁻¹ time⁻¹), the value was multiplied by the initial concentration (C_0 ; in M) to find the pseudo-first-order rate constant for this reaction mechanism (i.e., $k''*C_0$).

The values of the two theoretical pseudo-first-order rate constants, k' and $k''*C_0$, were compared using R² and root mean square error (RMSE) values for the fit of the modeled rate constant equation to the experimental loss data (**Figure A.3**). The modeled rate constant giving the higher R² fit to the experimental loss data was selected as the modeled mechanism (e.g., k' ,

the electron transfer-limited rate constant, when k' gave a higher R^2 fit). The values for k' , k'' , $k''*C_0$, R^2 fits, and the determined mechanistic rate-limiting step are given in **Table A.7**.

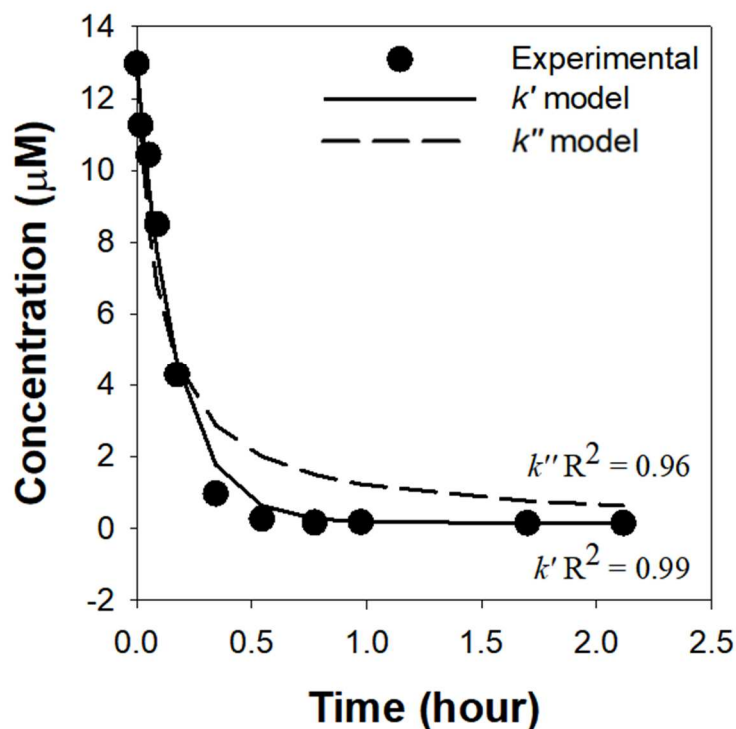


Figure A.3. Experimental and modeled concentrations of triclosan versus time. The kinetic model fit for k' and k'' determination is shown.

Table A.7. Modeled k' and k'' , respective R^2 values, and pseudo-first-order $k''*C_0$ values for 29 phenols reacted with δ -MnO₂.

Compound	k' (hr ⁻¹)	$k' R^2$	k'' (M ⁻¹ hr ⁻¹)	$k'' R^2$	$k''*C_0$ (hr ⁻¹)	Model rate-limiting step
phenol	0.87	0.994	0.08	0.991	0.97	electron transfer
catechol	0.22	0.99	0.03	0.95	0.32	electron transfer
resorcinol	11.4	0.999	2.51	0.98	18.8	electron transfer
hydroquinone	0.05	0.87	1.94	0.60	17.5	electron transfer
4-cresol	11.7	0.98	2.11	0.999	21.1	sorption
2-hydroxybenzoate	0.14	0.988	0.01	0.990	0.12	sorption
3-hydroxybenzoate	0.13	0.98	0.02	0.99	0.15	sorption
4-hydroxybenzoate	0.11	0.993	0.01	0.998	0.13	sorption
2,5-dihydroxybenzoate	0.11	0.99	0.01	0.96	0.16	electron transfer
5-chlorohydroquinone	0.12	0.89	0.02	0.88	0.17	electron transfer
5-chlorosalicylic acid	34.3	0.962	3.05	0.963	37.7	sorption
4-nitrocatechol	109.3	0.9997	23.1	0.98	220.6	electron transfer
2-chlorophenol	1.09	0.995	0.18	0.997	1.93	sorption
3-chlorophenol	0.63	0.996	0.10	0.997	0.85	sorption
4-chlorophenol	2.47	0.998	0.48	0.994	4.48	electron transfer
2-nitrophenol	0.47	0.998	0.06	0.997	0.48	electron transfer
3-nitrophenol	0.01	0.429	0.001	0.430	0.01	sorption
4-nitrophenol	0.01	0.687	0.001	0.690	0.01	sorption
3-trifluoromethylphenol	0.28	0.985	0.04	0.988	0.33	sorption
3-trifluoromethyl-4-bromophenol	0.29	0.995	0.04	0.996	0.37	sorption
3-trifluoromethyl-4-nitrophenol	0.04	0.995	0.004	0.996	0.04	sorption
4,4'-dihydroxybiphenyl	0.01	0.97	0.001	0.92	0.01	electron transfer
4-phenoxyphenol	25.6	0.999	5.32	0.97	47.7	electron transfer
bisphenol A	7.47	0.98	1.23	0.94	10.6	electron transfer
estrone	7.96	0.990	1.22	0.988	14.2	electron transfer
17 β -estradiol	23.8	0.976	64.1	0.975	44.7	electron transfer
4- <i>n</i> -nonylphenol	2.78	0.960	21.2	0.964	3.27	sorption
triclosan	6.02	0.99	0.81	0.96	10.6	electron transfer
4- <i>tert</i> -octylphenol	158.63	0.9998	95.45	0.9999	1010	sorption

A.7. Quantitative structure activity relationship data

The NWChem ESML API was used to model the specific QSAR descriptors energy of the highest occupied molecular orbital (E_{HOMO}) and oxidation energy of the first electron (E_{ox}). This resource was chosen as it represents the most user-friendly and widely available platform for calculating these specific molecular descriptors, and thus is a valuable tool to assess for the development of QSARs that rely on the availability of these calculations. E_{HOMO} was determined for the parent phenol or phenolate compound at pH 5.5, and values were used as given in the output.²⁵ E_{ox} values were determined for the half reaction of the loss of the first electron from the parent phenolate ion.²⁵⁻²⁷ This modeled reaction output gives the $\Delta G_{\text{rxn(aq)}}$ in units of kcal mol⁻¹, which was converted to an oxidation potential (E_{ox}) via the Nernst equation, including a factor to convert to units of volts versus standard hydrogen electrode (V vs. SHE).²⁵⁻²⁹

$$E_{\text{ox}} = \frac{-G_{\text{rxn(aq)}}}{23.061} + 4.28 \quad \text{Equation A.4}$$

After E_{ox} values were calculated from the Nernst equation, they were standardized to values reported by Pavitt et al.²⁶ by linear regression for compounds included in both studies ($n = 15$; **Figure A.4**). The resulting linear equation was applied to phenols in this study for which E_{ox} values are available (23 phenols) to give $E_{\text{ox,corr.}}$ values.²⁵ QSAR plots and validation measurements for literature data (**Figure 2.6**; **Figure A.5**) use E_{ox} values rather than $E_{\text{ox,corr.}}$ to facilitate comparison.

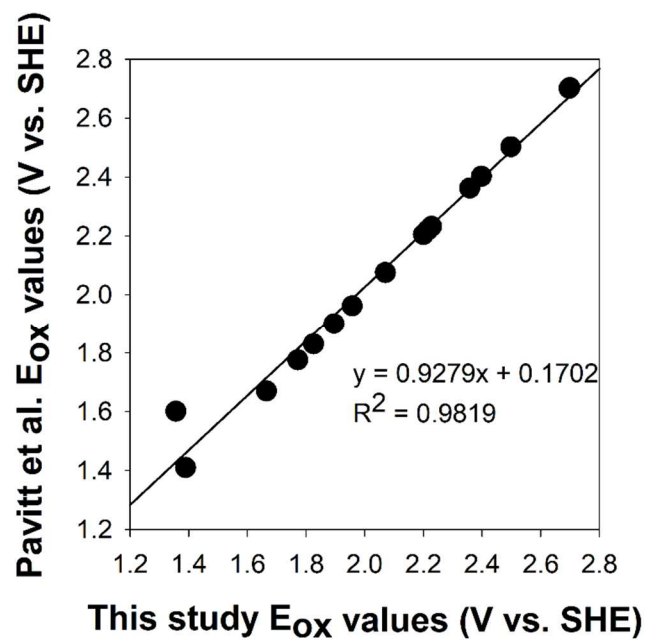


Figure A.4. E_{ox} values versus oxidation potentials reported by Pavitt et al.²⁶ for phenolic compounds (n = 15) calculated using the M06-2x theory. The linear regression shown was used to calculate E_{ox,corr.} values.

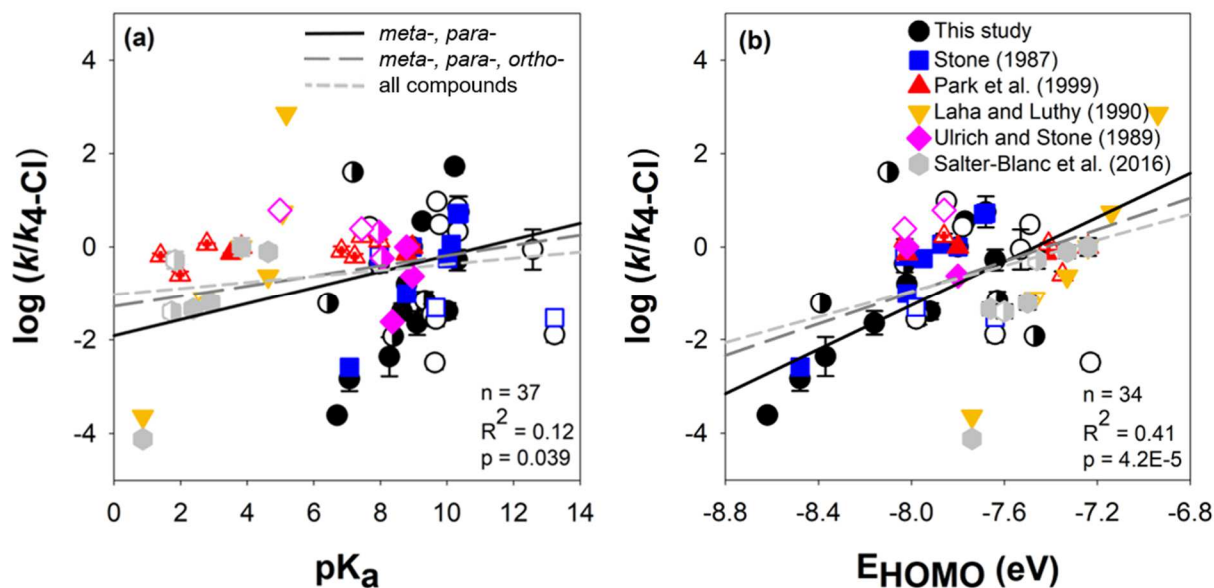


Figure A.5. QSAR plots of normalized pseudo-first-order rate constants from literature^{8,9,27,29,30} and δ -MnO₂ reactions in this study versus (a) pK_a values of the speciated (e.g., phenol versus phenolate) compounds and (b) energy of the highest occupied molecular. Filled data points indicate *meta*- or *para*-substitution, *ortho*-substituted compounds are partially filled, and complex compounds are indicated by hollow points. Error bars indicate the standard deviation of triplicate measurements. Given regression values are for the simple *meta*- and *para*-compounds; regressions values for all lines are given in **Table A.10**.

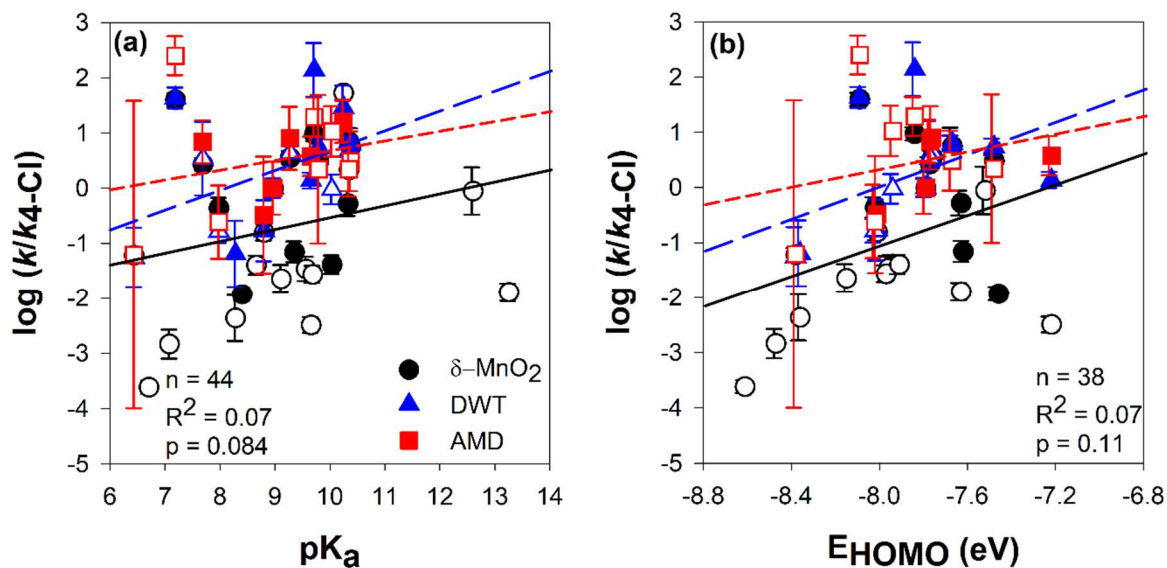


Figure A.6. Quantitative structure-activity relationships for 15 phenols reacted with drinking water treatment and acid mine drainage remediation reclaimed solids and 29 phenols reacted with δ -MnO₂, all normalized to 15 mg-Mn L⁻¹. Plots show the log of the average observed quenched rate constant normalized to the rate constant of 4-chlorophenol versus (a) first phenolic pK_a and (b) energy of the highest occupied molecular orbital. Error bars indicate the standard deviation of triplicate measurements. Filled data points indicate electron transfer-limited mechanisms and hollow data points indicate sorption-limited reaction mechanism. Lines indicate regression fits for all 15 phenols reacted with each manganese oxide; regressions values are given in **Table A.11**.

Table A.8. Calculated phenol descriptor data including QSAR Hammett constants (σ),³¹⁻³³ predicted pK_a values,³⁴ E_{HOMO} , and $E_{ox,corr.}$,³⁵ as well as the pK_a corrected distribution ratio for the compound in octanol versus water ($\log D_{ow}$),³⁴ and partitioning coefficients for soil organic carbon to water ($\log K_{oc}$) and octanol to water ($\log K_{ow}$).³⁶

Compound	$\log (k/k_{4-cl})$ $\delta\text{-MnO}_2$	σ	pK_a	E_{HOMO} (eV)	$E_{ox,corr.}$ (V vs. SHE)	$\log D_{ow}$ pH 5.5	$\log K_{oc}$ (L/kg)	$\log K_{ow}$
<i>Simple (meta-, para-) compounds</i>								
phenol	-1.38 ± 0.17	0	10.02	-7.95	1.92	1.67	2.27	1.46
resorcinol	0.55 ± 0.12	0.1	9.26	-7.77	1.86	1.37	2.38	0.93
hydroquinone	-	-0.36	9.68	-7.41	1.44	1.37	2.38	0.59
4-cresol	0.75 ± 0.33	-0.16	10.36	-7.68	1.70	2.18	2.48	1.94
3-chlorophenol	-0.80 ± 0.15	0.37	8.79	-8.02	2.24	2.27	2.48	2.5
4-chlorophenol	0.00 ± 0.17	0.22	8.96	-7.8	1.80	2.27	2.48	2.39
3-nitrophenol	-2.36 ± 0.42	0.73	8.27	-8.37	2.36	1.61	2.46	2
4-nitrophenol	-2.84 ± 0.26	1.25	7.07	-8.48	2.50	1.60	2.46	1.91
3-trifluoromethylphenol	-1.64 ± 0.25	0.44	9.1	-8.16	2.06	2.55	3.10	2.95
3-trifluoromethyl-4-bromophenol	-1.39 ± 0.17	0.67	8.65	-7.92	2.51	3.32	-	-
3-trifluoromethyl-4-nitrophenol	-3.61 ± 0.12	1.69	6.7	-8.62	2.70	2.46	3.31	2.87
4- <i>n</i> -nonylphenol	-0.28 ± 0.22	-0.16	10.31	-7.64	1.83	5.74	4.58	5.76
4- <i>tert</i> -octylphenol	1.73 ± 0.14	-0.1	10.23	-	-	4.69	4.00	4.93
<i>ortho-substituted compounds</i>								
catechol	-1.15 ± 0.19	-	9.34	-7.63	1.41	1.37	2.39	0.88
5-chlorohydroquinone	-1.93 ± 0.12	-	8.39	-7.47	-	1.97	2.60	1.4
4-nitrocatechol	1.60 ± 0.12	-	7.18	-8.1	2.12	1.30	2.58	1.66
2-chlorophenol	-0.36 ± 0.18	-	7.97	-8.03	1.98	2.27	2.50	2.15
2-nitrophenol	-1.21 ± 0.12	-	6.43	-8.39	2.40	1.59	2.47	1.79
<i>Complex compounds</i>								
2-hydroxybenzoic acid	-1.89 ± 0.16	-	13.23	-7.64	2.69	-0.72	1.34	2.26
3-hydroxybenzoic acid	-1.46 ± 0.22	-	9.55	-7.97	2.21	-0.38	1.33	1.5
4-hydroxybenzoic acid	-1.56 ± 0.15	-	9.67	-7.98	2.69	0.13	1.33	1.58
2,5-dihydroxybenzoic acid	-	-	10.02	-7.25	1.71	-1.23	1.45	1.74
5-chlorosalicylic acid	-0.05 ± 0.43	-	12.58	-7.53	2.21	-0.28	1.54	3.09
4,4'-dihydroxybiphenyl	-2.49 ± 0.14	0.01	9.64	-7.23	1.85	3.01	3.93	2.8
4-phenoxyphenol	0.97 ± 0.12	-	9.7	-7.85	1.53	3.17	3.39	3.35
bisphenol A	0.48 ± 0.12	-	9.78	-7.49	2.23	4.05	4.58	3.32
estrone	0.33 ± 0.12	-	10.33	-	-	4.31	4.38	3.13
17 β -estradiol	0.84 ± 0.25	-	10.33	-	-	3.75	4.19	4.01
triclosan	0.43 ± 0.12	-	7.68	-7.78	2.09	4.98	4.37	4.76

Table A.9. Regression statistics for QSAR descriptors versus normalized observed initial rate constants of 29 phenols reacted with δ -MnO₂ (**Figure 2.4**) calculated for 95% confidence interval. Gray values indicate $p < 0.005$; bold values are $p < 0.05$.

Substitution		Simple	Simple + <i>ortho</i>	All substituents
Hammett Constant	n	12	15	16
	R²	0.76	0.6	0.46
	p	2.20E-04	6.80E-04	4.20E-03
pK_a	n	12	17	27
	R²	0.69	0.55	0.16
	p	8.50E-04	6.90E-04	0.04
E_{HOMO}	n	11	16	24
	R²	0.89	0.29	0.13
	p	1.30E-05	0.032	0.084
E_{ox,corr.}	n	11	15	23
	R²	0.77	0.37	0.29
	p	3.90E-04	0.016	8.20E-03

Table A.10. Regression statistics for QSAR descriptors versus normalized literature rate constants and reactions of 29 phenols with δ -MnO₂ (**Figure 2.6**; **Figure A.5**) calculated for 95% confidence interval. Literature data available in **Table A.12**. Gray values indicate $p < 0.005$; bold values are $p < 0.05$.

Substitution		Simple	Simple + <i>ortho</i>	All substituents
Hammett Constant	n	37	53	55
	R²	0.74	0.25	0.16
	p	1.20E-11	1.30E-04	2.50E-03
pK_a	n	37	54	69
	R²	0.12	0.06	0.02
	p	0.039	0.069	0.21
pK_a phenols	n	25	37	51
	R²	0.68	0.16	0
	p	3.70E-07	0.014	0.75
pK_a anilines	n	12	17	18
	R²	0.84	0.57	0.57
	p	2.40E-05	4.30E-04	2.70E-04
E_{HOMO}	n	34	48	60
	R²	0.41	0.23	0.14
	p	4.20E-05	5.90E-04	2.90E-03
E_{ox,corr.}	n	34	47	59
	R²	0.35	0.21	0.17
	p	2.30E-04	1.10E-03	1.20E-03

Table A.11. Regression statistics for QSAR descriptors versus normalized observed initial rate constants of 15 phenols reacted with δ -MnO₂, drinking water treatment solids, and acid mine drainage remediation solids (**Figure 2.5**; **Figure A.6**) calculated for 95% confidence interval. Gray values indicate $p < 0.005$; bold values are $p < 0.05$.

Solid phases		δ -MnO ₂	DWT	AMD	All solids
Hammett Constant	n	10	10	9	29
	R²	0.18	0.75	0.81	0.41
	p	2.20E-01	1.20E-03	1.00E-03	2.00E-04
pK _a	n	15	15	14	44
	R²	0.03	0.19	0.06	0.07
	p	5.60E-01	1.10E-01	4.00E-01	8.30E-02
E _{HOMO}	n	13	13	12	38
	R²	0.01	0.02	0.06	0.07
	p	7.30E-01	1.20E-01	4.40E-01	1.10E-01
E _{ox,corr.}	n	13	13	12	38
	R²	0.13	0.4	0.16	0.2
	p	2.30E-01	2.00E-02	2.00E-01	4.50E-03

Table A.12. Literature data sources and reported reaction conditions.

Compound	Reported loss	Reported loss method	log (k/k_{4-Cl})	buffer	[Organic] (μM)
<i>Park, 1999³⁰</i>					
2-chlorophenol	62 ± 0.6	Quenched; % loss in 24 hr	0.14 ± 0.04	pH 5.6; 200 mM acetate	300
3-chlorophenol	32.8 ± 5.6		-0.14 ± 0.08		
4-chlorophenol	45.4 ± 3.8		0 ± 0.05		
2,4-dichlorophenol	77.6 ± 6.4		0.23 ± 0.05		
2,5-dichlorophenol	28.4 ± 3.1		-0.20 ± 0.06		
2,4,5-trichlorophenol	37.6 ± 7.9		-.08 ± 0.10		
2-chloroaniline	99.6 ± 0.8		0.07 ± 0.02		
3-chloroaniline	63.7 ± 0.5		-0.1288 ± 0.0001		
4-chloroaniline	85.7 ± 4.2		0 ± 0.03		
2,4-dichloroaniline	22 ± 3.4		-0.59 ± 0.07		
2,4,5-trichloroaniline	56.1 ± 6		-0.18 ± 0.05		
<i>Laha and Luthy, 1990²⁹</i>					
aniline	10.4	Filtered; second-order rate constant ($\text{M}^{-1} \text{min}^{-1}$)	-0.626	pH 4 or 4.4; acetate	2500
4-chloroaniline	44		0		5000
4-methoxyaniline	32000		2.86		62
4-methylaniline	240		0.737		2000
4-nitroaniline	0.01		-3.643		2000
4-aminobenzoic acid	3.44		-1.107		5000
<i>Ulrich and Stone, 1989⁹</i>					
2-chlorophenol	0.11	Filtered, then quenched; first-order rate constant (min^{-1})	-0.237	pH 4.2 or 4.84 2.5 mM acetate	150
3-chlorophenol	0.018		-1.023		140
4-chlorophenol	0.19		0		
2,4-dichlorophenol	0.4		0.323		110
3,4-dichlorophenol	0.045		-0.626		120
3,5-dichlorophenol	0.0046		-1.616		120
2,4,6-trichlorophenol	1.17		0.789		140
pentachlorophenol	0.47		0.393		11
<i>Stone, 1987⁸</i>					
phenol	2.22E-07	Filtered; zero-order rate constant (M min^{-1})	-0.244	pH 4.4; 1 mM acetate	100
2-hydroxybenzoate	1.15E-08		-1.529		
4-hydroxybenzoate	1.93E-08		-1.304		
2-chlorophenol	2.48E-07		-0.195		
3-chlorophenol	3.84E-08		-1.006		
4-chlorophenol	3.89E-07		0		
4-nitrophenol	1.00E-09		-2.590		
3-methylphenol	4.48E-07		0.061		
4-methylphenol	2.06E-06		0.724		
4-ethylphenol	1.97E-06		0.705		
Compound	Reported loss	Reported	log (k/k_{4-Cl})	buffer	[Organic]

		loss method		(μM)
<i>Salter-Blanc et al., 2016²⁷</i>				
aniline	0.0216 \pm 0.0012	Filtered or quenched; first-order rate constant (sec ⁻¹)	-0.10 \pm 0.14	pH 6; 10 mM bicarbonate 10
4-chloroaniline	0.0272 \pm 0.0085		0 \pm 0.2	
3-nitroaniline	0.00125 \pm 5.69e-5		-1.3 \pm 0.1	
4-nitroaniline	2.06E-06		-4.121	
4-methyl-3-nitroaniline	0.0017 \pm 0.0003		-1.2 \pm 0.2	
2-methoxy-5-nitroaniline	0.0143 \pm 0.0041		-0.28 \pm 0.18	
2-methyl-5-nitroaniline	0.00109 \pm 1.55e-4		-1.4 \pm 0.1	
Compound	[Mn]	Ionic strength	AMON; Surface Area	Mn synthesis method
<i>Park, 1999³⁰</i>				
2-chlorophenol	0.5 g/L	Not reported	Not reported	McKenzie
3-chlorophenol				
4-chlorophenol				
2,4-dichlorophenol				
2,5-dichlorophenol				
2,4,5-trichlorophenol				
2-chloroaniline				
3-chloroaniline				
4-chloroaniline				
2,4-dichloroaniline				
2,4,5-trichloroaniline				
<i>Laha and Luthy, 1990²⁹</i>				
aniline	5 mM	0.1 M NaNO ₃	Not reported	Murray
4-chloroaniline	5 mM			
4-methoxyaniline	33 μM			
4-methylaniline	2.5 mM			
4-nitroaniline	5 mM			
4-aminobenzoic acid	5 mM			

Compound	[Mn]	Ionic strength	AMON; Surface Area	Mn synthesis method
<i>Ulrich and Stone, 1989⁹</i>				

2-chlorophenol	0.16 mM	50 mM NaCl	3.93; S.A. not reported	Boiling, purged, 1.98 mM Mn(ClO ₄) ₂ + 10.3 mM NaOH + 10.4 mM NaOCl
3-chlorophenol				
4-chlorophenol				
2,4-dichlorophenol				
3,4-dichlorophenol				
3,5-dichlorophenol				
2,4,6-trichlorophenol				
pentachlorophenol				
<i>Stone, 1987⁸</i>				
phenol	48 μM	50 mM NaCl	3.81; 25 m ² g ⁻¹	MnSO ₄ + 2 mM NaMnO ₄ in pH 6.6, 50 mM phosphate buffer
2-hydroxybenzoate				
4-hydroxybenzoate				
2-chlorophenol				
3-chlorophenol				
4-chlorophenol				
4-nitrophenol				
3-methylphenol				
4-methylphenol				
4-ethylphenol				
<i>Salter-Blanc et al., 2016²⁷</i>				
aniline	Not reported	0.1 M NaCl	Not reported	Murray and Villalobos
4-chloroaniline				
3-nitroaniline				
4-nitroaniline				
4-methyl-3-nitroaniline				
2-methoxy-5-nitroaniline				
2-methyl-5-nitroaniline				

Table A.13. Literature QSAR descriptors. Log (k/k_{4-Cl}) values calculated based on reported loss rates (Table A.12). Hammett constants (σ), pK_a values, E_{HOMO} and E_{ox} values determined in this study.

Compound	Category	log (k/k_{4-Cl})	σ	pK _a	E _{HOMO} (eV)	E _{ox} (V vs. SHE)
<i>Park, 1999³⁰</i>						
2-chlorophenol	ortho	0.14 ± 0.04	0.68	7.97	-8.03	1.96
3-chlorophenol	simple	-0.14 ± 0.08	0.37	8.79	-8.02	2.23
4-chlorophenol	simple	0 ± 0.05	0.22	8.96	-7.8	1.77
2,4-dichlorophenol	ortho	0.23 ± 0.05	0.9	7.44	-7.86	2.08
2,5-dichlorophenol	ortho	-0.20 ± 0.06	1.05	7.23	-	-
2,4,5-trichlorophenol	ortho	-0.08 ± 0.10	1.27	6.83	-	-
2-chloroaniline	ortho	0.07 ± 0.02	0.67	2.79	-7.41	1.38
3-chloroaniline	simple	-0.1288 ± 0.0001	0.37	3.52	-7.42	1.37
4-chloroaniline	simple	0 ± 0.03	0.22	3.83	-7.24	1.26
2,4-dichloroaniline	ortho	-0.59 ± 0.07	0.89	1.98	-7.35	1.50
2,4,5-trichloroaniline	ortho	-0.18 ± 0.05	1.26	1.4	-	-
<i>Laha and Luthy, 1990²⁹</i>						
aniline	simple	-0.63	0	4.63	-7.33	1.21
4-chloroaniline	simple	0	0.22	3.83	-7.24	1.26
4-methoxyaniline	simple	2.86	0.12	5.17	-6.94	0.83
4-methylaniline	simple	0.74	-0.16	5.06	-7.14	1.01
4-nitroaniline	simple	-3.64	1.25	0.87	-7.74	1.71
4-aminobenzoate	complex	-1.11	-	2.69	-7.47	1.75
<i>Ulrich and Stone, 1989⁹</i>						
2-chlorophenol	ortho	-0.24	0.68	7.97	-8.03	1.96
3-chlorophenol	simple	-1.02	0.37	8.79	-8.02	2.23
4-chlorophenol	simple	0	0.22	8.96	-7.8	1.77
2,4-dichlorophenol	ortho	0.32	0.9	7.44	-7.86	2.08
3,4-dichlorophenol	simple	-0.63	0.59	8.36	-	-
3,5-dichlorophenol	simple	-1.62	0.74	8.06	-	-
2,4,6-trichlorophenol	ortho	0.79	1.58	5.99	-8.02	2.14
pentachlorophenol	complex	0.39	2.32	4.98	-	-
<i>Stone, 1987⁸</i>						
phenol	simple	-0.24	0	10.02	-7.95	1.90
2-hydroxybenzoate	complex	-1.53	-	13.23	-7.64	1.37
4-hydroxybenzoate	complex	-1.3	-	9.67	-7.98	2.27
2-chlorophenol	ortho	-0.19	0.68	7.97	-8.03	1.96
3-chlorophenol	simple	-1.01	0.37	8.79	-8.02	2.23
4-chlorophenol	simple	0	0.22	8.96	-7.8	1.77

Compound	Category	$\log(k/k_{4cl})$	σ	pK _a	E _{HOMO} (eV)	E _{ox} (V vs. SHE)
<i>Stone, 1987⁸ continued</i>						
4-nitrophenol	simple	-2.59	1.25	7.07	-8.48	2.50
3-methylphenol	simple	0.06	-0.06	10.13	-7.87	1.90
4-methylphenol	simple	0.72	-0.16	10.36	-7.68	1.67
4-ethylphenol	simple	0.70	-0.15	10.32	-7.69	1.71
<i>Salter-Blanc et al., 2016²⁷</i>						
aniline	simple	-0.10 ± 0.14	0	4.63	-7.33	1.21
4-chloroaniline	simple	0 ± 0.2	0.22	3.83	-7.24	1.26
3-nitroaniline	simple	-1.3 ± 0.1	0.73	2.38	-7.66	1.58
4-nitroaniline	simple	-4.12	1.25	0.87	-7.74	1.71
4-methyl-3-nitroaniline	simple	-1.2 ± 0.2	0.57	2.90	-7.5	1.39
2-methoxy-5-nitroaniline	ortho	-0.28 ± 0.18	0.75	1.83	-7.46	1.38
2-methyl-5-nitroaniline	ortho	-1.4 ± 0.1	0.83	1.73	-7.60	1.52

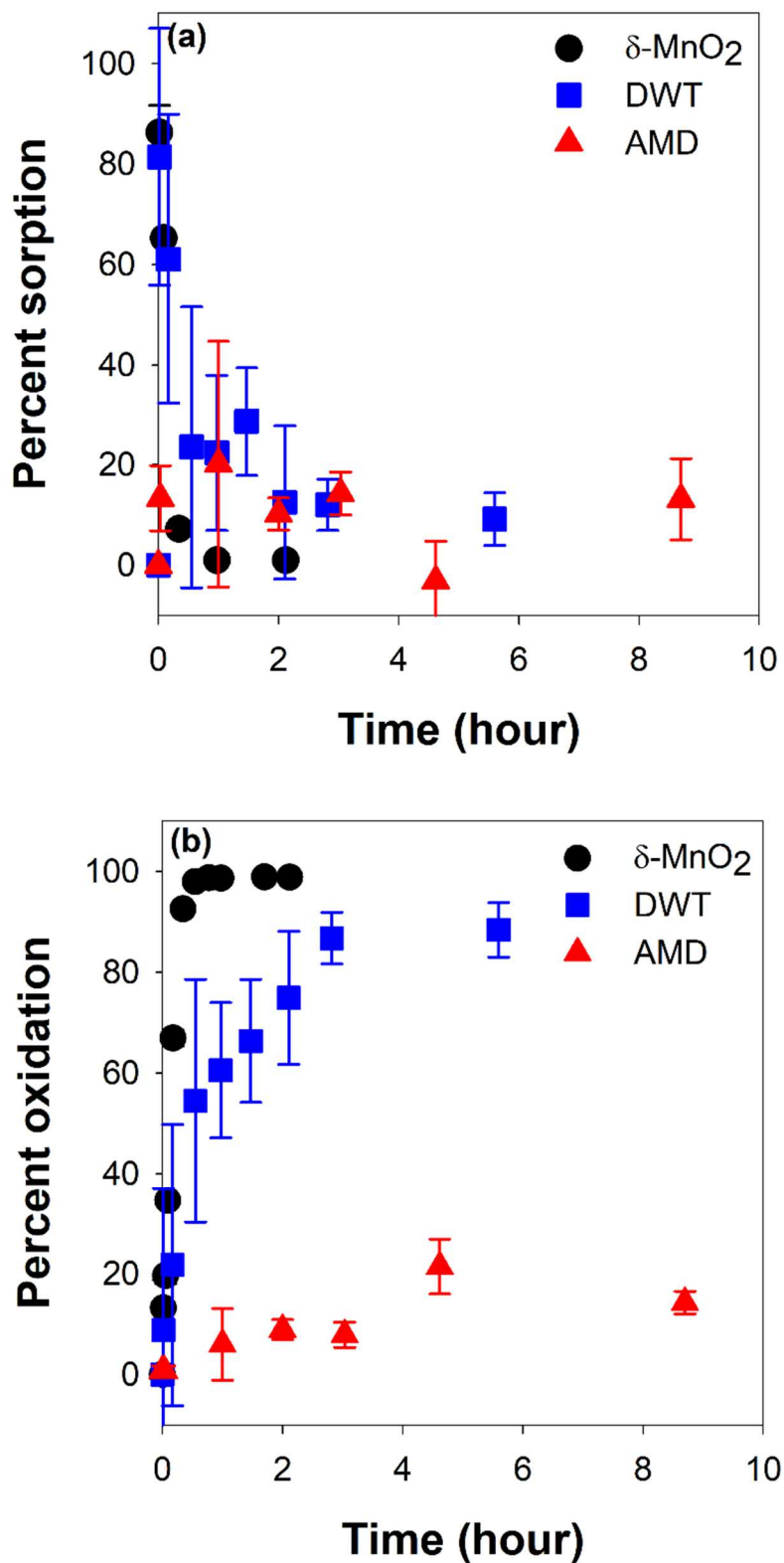


Figure A.7. Percent of initial triclosan concentration (a) sorbed to solid surface and (b) oxidized over the first 10 hours of reaction with δ -MnO₂, DWT solids, and AMD solids. Error bars represent the standard deviation of triplicate measurements.

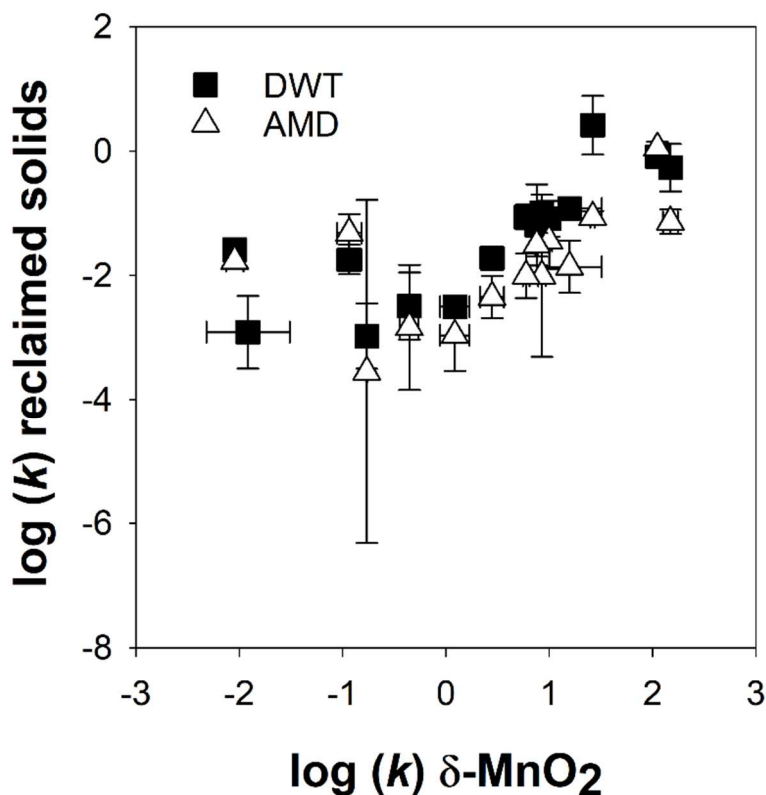


Figure A.8. Comparison of $\log k$ for DWT and AMD solids with $\delta\text{-MnO}_2$ reacted with 15 phenols. Error bars indicate the standard deviation of triplicate measurements.

Table A.14. Observed oxidation rate-limiting step for phenols reacted with $\delta\text{-MnO}_2$, DWT, and AMD solids.

Compound	$\delta\text{-MnO}_2$	DWT	AMD
phenol	electron transfer	sorption	sorption
resorcinol	electron transfer	sorption	sorption
estrone	electron transfer	electron transfer	sorption
4-cresol	electron transfer	electron transfer	sorption
4- <i>tert</i> -octylphenol	sorption	electron transfer	electron transfer
bisphenol A	electron transfer	electron transfer	sorption
4-phenoxyphenol	electron transfer	electron transfer	sorption
4-nitrocatechol	electron transfer	electron transfer	electron transfer
triclosan	electron transfer	sorption	sorption
2-chlorophenol	electron transfer	sorption	sorption
3-chlorophenol	sorption	electron transfer	electron transfer
4-chlorophenol	electron transfer	electron transfer	electron transfer
2-nitrophenol	sorption	sorption	sorption
3-nitrophenol	sorption	electron transfer	electron transfer
4,4'-dihydroxybiphenyl	sorption	electron transfer	electron transfer

A.8. QSAR residuals and validation

The residuals of each developed quantitative structure-activity relationships were analyzed to determine the normality of the data to the linear fit. Residuals were calculated from the data from this study (**Figures 2.4** and **2.5** in the manuscript) and literature rates (**Figure 2.6**) for the QSAR lines developed with only the simple *meta*- and *para*-substituted compounds, as well as the QSAR relationships developed with all plotted compounds to consider both the simplest and most all-encompassing linear relationships. In the case of the QSARs developed using the data from the three studied manganese oxides, the linear models including data from individual solids and all three solids combined were used for the simple and all-encompassing cases, respectively. From the linear QSAR relationships, we calculated predicted values of normalized $\log(k/k_{4-Cl})$ from the QSAR descriptors (e.g., Hammett constants), then this predicted y term was subtracted from the experimental value to ascertain each residual value (**Tables A.15 – A.17**). Positive values indicate the experimental value was larger than the predicted (i.e., the model underpredicts the normalized rate constant) and negative values indicate the model overpredicted the observed rate constant terms.

The calculated residuals were plotted against the independent QSAR descriptor values to test for random distribution (**Figures A.9** and **A.10**). If the developed linear model is a good fit for the data, the residuals should fall in a random manner around the x -axis across the range of the independent variable.³⁷ As some of the resulting plots show non-random behavior (i.e., linear or funnel-like trends) while in other the randomness is ambiguous, we also plotted the residuals against the probability of each residual. To do this, the residuals were ranked in ascending order and the rank of each residual (i) and the total sample size (N) were used to predict the probability, P , for that value.

$$P = \frac{i}{(N+1)}$$

Equation A.5

The resulting plots should lay along a clear line if the data is distributed normally. Bimodal, or ‘s’ shaped, data trends indicate the residuals are not normally distributed. As a result, bimodal distributions suggest the data used to develop the linear model should be transformed to achieve a better fit, or that the relationship is better fit by another power of relationship.³⁷

The predictive strength of the developed QSAR was also tested using external validation strategies. External validation separates data into test and training data sets. A training QSAR is built from the training data set and the linear regression from that data is used to predict reactivity values for the test set. The predicted and experimental values are compared statistically to determine the predictive strength of the overall QSAR. Typically, the independent variables of the QSAR are first internally validated to determine which predictive descriptors best correlate with reactivity; however, since we are interested in evaluating literature QSAR models, the same independent variables were used as in those studies.^{26,27,29,38}

To test the predictive strength of the QSARs included in this study, validation statistics were adopted from bioinformatics QSAR validation studies.³⁹⁻⁴² R^2 is the common squared correlation coefficient determined between the predicted and experimental values for the test set. r_0^2 is the squared correlation coefficient between predicted and experimental values with an intercept set to (0,0). r_m^2 , calculated from R^2 and r_0^2 (**Equation A.6**), is a value for external validation that is advantageous for small test sets. This value determines whether the range of predicted values falls near that of observed values. In **Table A.18**, this value is accompanied by

the equivalent measurements for reversed axes (r_m^2 ; i.e., predicted versus experimental values and experimental versus predicted values).

R_{pred}^2 is also an external validation comparing the test set predicted and experimental values, as well as the average training set dependent variable (i.e., $\log k/k_{4-Cl}$), as shown in **Equation A.7**. The shown minimum value of 0.5 is less conservative, as some sources argue 0.6 is a better minimum value.⁴¹ R_p^2 (**Equation A.8**) corrects for the differences between randomized and non-randomized test sets, to determine whether the other statistics are true indicators of the QSAR's robust nature, rather than chance.

$$r_m^2 = R^2(1 - \sqrt{R^2 - r_0^2}) \quad \text{Equation A.6}$$

$$R_{\text{pred}}^2 = 1 - \frac{\sum_1^{\text{test}}(\log(\frac{k}{k_{4-Cl}})_{\text{exp}} - \log(\frac{k}{k_{4-Cl}})_{\text{pred}})^2}{\sum_1^{\text{test}}(\log(\frac{k}{k_{4-Cl}})_{\text{exp}} - \log(\frac{k}{k_{4-Cl}})_{\text{training}})^2} \quad \text{Equation A.7}$$

$$R_p^2 = R^2(1 - \sqrt{|R^2 - R_f^2|}) \quad \text{Equation A.8}$$

The range of accepted values for comparing the experimental and predicted $\log(k/k_{4-Cl})$ values for each defined test set based on the correlating training set are included in **Table A.18** and summarized in Veerasamy et al.⁴¹

These validation measurements include 27 phenols reacted with $\delta\text{-MnO}_2$ in this study as well as all literature data analyzed in this study. The total maximum sample size was 69 points, excluding any phenols for which experimental $\log(k/k_{4-Cl})$ values are not available (hydroquinone and 2,5-dihydroxybenzoate). The total sample size is smaller in conditions for which QSAR descriptors are not available for all included compounds (e.g., a lack of tabulated Hammett constants). The overall data set is small for QSAR development but demonstrates

whether the current state of the literature allows for accurate reactivity predictions for phenolic contaminants as previous studies have suggested. The data set is also large enough to support trends outlined in the manuscript by clarifying the relationship between compound structure and QSAR predictability.

To determine the ability of commonly studied *meta*- and *para*-substituted phenols to predict the behavior of *ortho*- and complex compounds, the data was dividing into test and training sets for all four QSAR parameters (i.e., Hammett constants, pK_a , E_{HOMO} , and E_{ox}) based on substituent placement. This non-random division of data was chosen to investigate whether the linear relationships developed based on simple, well-studied phenols can accurately predict the pseudo-first-order rate constants for *ortho*-substituted or complex phenolic contaminants of environmental concern. The QSARs developed for four independent descriptors were also probed by separating test and training sets based on this study (δ -MnO₂ data) versus literature data (**Table A.18**) and by using δ -MnO₂ data to predict $\log(k/k_{4-Cl})$ values for reclaimed solids (**Table A.19**). This division was chosen to scrutinize whether normalized, pseudo-first-order $\log k$ values follow the same trend across reaction conditions. Specifically, we tested whether a historic data set collected across studies with varying reaction conditions is able to predict the normalized trends in a specific study and whether a synthetic manganese oxide data set (e.g., δ -MnO₂) can predict normalized $\log k$ values for reclaimed solids with varying solid composition and characteristics. Both overall data sets (i.e., synthetic manganese oxides with data from this study and literature, and this study's data for δ -MnO₂ and reclaimed solids) were also tested using randomized training and test sets (about 70% and 30% of the overall data sets, respectively; one randomization per QSAR descriptor).

To be validated, multiple measures should fall within the respective acceptable ranges for the QSAR in question. Where the analyzed QSAR relationships do fall within the accepted range of a validation measurement (e.g., R^2_{pred} , r_m^2), it is only for one validation test variable, indicating the regression is useful under the conditions tested by that variable (e.g., linearity, non-random correlation) but the QSARs are not predictive across all analyzed validity conditions. Only the literature training set, δ -MnO₂ test set division of data fell within the accepted ranges for multiple measures (R^2_{pred} and p). This indicates the included literature data was potentially predictive towards the normalized pseudo-first-order rate constants of the compounds included in this study, but only with necessarily structurally selective Hammett constants as the independent descriptor. That scenario is also not necessarily applicable for other compounds or reaction (or environmental) conditions, even using Hammett constants as a descriptor, as the division of data was non-random.

Table A.15. Residual values calculated against the *meta*- and *para*-substituted and all compound QSARs developed with data from this study. QSAR linear regressions provided in **Table A.9**.

	Simple substituents				All substituents			
	$\Sigma\sigma$	pK _a	E _{HOMO}	E _{ox,corr.}	$\Sigma\sigma$	pK _a	E _{HOMO}	E _{ox,corr.}
phenol	-1.1	-0.9	-0.4	-0.9	-1.4	-1.6	-0.5	-1.0
catechol		-0.4	-0.6	-1.7		-0.6	-1.6	-2.6
resorcinol	1.0	1.3	1.3	0.9	0.7	1.2	0.7	0.7
hydroquinone								
4-cresol	0.8	1.1	1.4	0.8	0.3	0.2	0.5	0.4
2-hydroxybenzoate		-2.6	-1.3	0.08		-5.6	-2.3	1.3
3-hydroxybenzoate		-0.8	-0.5	-0.4		-1.1	-0.5	-0.002
4-hydroxybenzoate		-1	-0.5	0.4		-1.4	-0.6	1.6
2,5-dihydroxybenzoate								
5-chlorohydroquinone		-0.9	-1.6			-0.4	-3.0	
5-chlorosalicylic acid		-0.5	0.3	1.0		-3.0	-0.9	1.4
4-nitrocatechol		3.1	2.8	2.5		4.5	3.0	2.7
2-chlorophenol		0.8	0.7	0.2		1.7	0.8	0.3
3-chlorophenol	0.1	0.1	0.3	0.3	0.02	0.3	0.3	0.8
4-chlorophenol	0.7	0.8	0.8	0.2	0.5	1.0	0.2	0.001
2-nitrophenol		0.5	0.4	0.2		2.5	1.4	0.9
3-nitrophenol	-0.8	-1.3	-0.8	-1.0	-0.6	-0.7	0.1	-0.4
4-nitrophenol	-0.4	-1.3	-1.1	-1.2	0.07	0.2	0.1	-0.4
3-trifluoromethylphenol	-0.6	-0.9	-0.4	-0.9	-0.7	-0.8	0.03	-0.7
3-trifluoromethyl-4-bromophenol	0.06	-0.4	-0.5	0.2	0.1	-0.1	-0.7	1.1
3-trifluoromethyl-4-nitrophenol	-0.4	-2	-1.7	-1.6	0.3	-0.2	-0.1	-0.4
4,4'-dihydroxybiphenyl	-2.2	-1.9	-2.5	-2.2	-2.5	-2.3	-4.5	-2.3
4-phenoxyphenol		1.6	1.8	0.7		1.1	1.4	0.004
bisphenol A		1.0	0.8	1.5		0.6	-0.5	2.0
estrone		0.7				-0.2		
17 β -estradiol		1.2				0.3		
4- <i>n</i> -nonylphenol	-0.3	0.08	0.3	-0.01	-0.7	-0.8	-0.7	-0.2
triclosan		2.8	0.6	1.5		1.7	1.2	1.2
4- <i>tert</i> -octylphenol	1.4	1.3			1.8	2.1		

Table A.16. Residual values calculated against the *meta*- and *para*-substituted and all compound QSARs developed with data from this study and compiled from literature. QSAR linear regressions provided in **Table A.10**.

	Simple substituents				All substituents			
	$\Sigma\sigma$	pK _a	E _{HOMO}	E _{ox}	$\Sigma\sigma$	pK _a	E _{HOMO}	E _{ox}
<i>This study</i>								
phenol	-1.7	-1.2	-0.2	-0.5	-1.3	-1.0	-0.5	-0.7
catechol		-1.5	-0.8	-1.3		-1.5	-0.7	-1.1
resorcinol	0.5	0.9	1.3	1.3	0.7	1.0	1.2	1.1
hydroquinone								
4-cresol	0.002	0.9	1.3	1.2	0.7	1.1	1.3	1.1
2-hydroxybenzoate		-2.3	-1.5	0.5		-1.7	-1.4	-0.3
3-hydroxybenzoate		-1.2	-0.3	0.02		-1.1	-0.5	-0.4
4-hydroxybenzoate		-1.3	-0.3	0.9		-1.2	-0.6	0.07
2,5-dihydroxybenzoate								
5-chlorohydroquinone	-1.4	2.3	-1.9		-1.6	2.2	-1.7	
5-chlorosalicylic acid		-0.3	0.1	1.4		0.2	0.3	1.0
4-nitrocatechol		0.2	3.1	2.9		0.1	2.7	2.5
2-chlorophenol	1.1	-0.4	1.0	0.7	0.3	-0.6	0.6	0.4
3-chlorophenol	-0.1	-0.4	0.5	0.7	-0.4	-0.4	0.2	0.3
4-chlorophenol	0.3	0.4	0.8	0.7	0.3	0.4	0.7	0.5
2-nitrophenol	1.7	1.4	1.0	0.6	0.01	1.1	0.3	0.05
3-nitrophenol	-0.7	-1.9	-0.2	-0.6	-1.6	-1.9	-0.9	-1.1
4-nitrophenol	0.2	-2.1	-0.4	-0.8	-1.6	-2.3	-1.2	-1.5
3-trifluoromethylphenol	-0.8	-1.3	-0.002	-0.5	-1.2	-1.2	-0.5	-0.8
3-trifluoromethyl-4-bromophenol	0.06	-1.0	-0.3	0.7	-0.7	-0.9	-0.5	0.01
3-trifluoromethyl-4-nitrophenol	0.5	-2.9	-0.9	-1.2	-2.0	-3.0	-1.8	-2.0
4,4'-dihydroxybiphenyl	-2.8	-2.2	-3.1	-1.7	-2.4	-2.1	-2.6	-1.9
4-phenoxyphenol		1.2	1.9	1.1		1.4	1.7	1.1
bisphenol A		0.7	0.5	2.0		0.9	0.7	1.5
estrone		0.5				0.7		
17 β -estradiol		1.0				1.2		
4- <i>n</i> -nonylphenol	-1.0	-0.2	0.1	0.5	-0.4	0.07	0.2	0.3
triclosan		1.0	1.1	1.7		1.0	1.1	1.3
4- <i>tert</i> -octylphenol	1.1	1.9			1.7	2.1		
<i>Park, 1999³⁰</i>								
2-chlorophenol	1.6	0.6	1.5	1.2	0.8	0.5	1.1	0.9
3-chlorophenol	0.5	0.3	1.2	1.4	0.3	0.3	0.8	0.9
4-chlorophenol	0.3	0.4	0.8	0.7	0.3	0.4	0.7	0.5
2,4-dichlorophenol	2.3	0.5	1.2	1.5	1.1	0.3	1.0	1.1
	Simple substituents				All substituents			
	$\Sigma\sigma$	pK _a	E _{HOMO}	E _{ox}	$\Sigma\sigma$	pK _a	E _{HOMO}	E _{ox}

<i>Park, 1999³⁰ continued</i>								
2,5-dichlorophenol	2.3	1.5			0.8	0.7		
2,4,5-trichlorophenol	3.0	0.9			1.2	0.8		
2-chloroaniline	1.5	-0.9	-0.07	0.009	0.8	-0.7	0.2	0.1
3-chloroaniline	0.5	1.2	-0.2	-0.2	0.3	0.7	0.02	-0.1
4-chloroaniline	0.3	1.3	-0.5	-0.3	0.3	0.8	-0.1	-0.1
2,4-dichloroaniline	1.4	1.5	-0.9	-0.4	0.3	0.9	-0.5	-0.4
2,4,5-trichloroaniline	2.8	1.0			1.1	0.3		
<i>Laha and Luthy, 1990²⁹</i>								
aniline	-1.0	0.5	-1.0	-1.0	-0.6	0.08	-0.6	-0.8
4-chloroaniline	0.3	1.3	-0.5	-0.3	0.3	0.8	-0.1	-0.1
4-methoxyaniline	2.9	3.9	1.6	1.8	3.0	3.5	2.3	2.2
4-methylaniline	-0.01	1.8	-0.04	0.001	0.6	1.4	0.5	0.3
4-nitroaniline	-0.7	-1.9	-3.0	-3.1	-2.4	-2.7	-3.0	-3.2
4-aminobenzoic acid		0.3	-1.1	-0.5		-0.3	-0.9	-0.6
<i>Ulrich and Stone, 1989⁹</i>								
2-chlorophenol	1.2	0.9	1.1	0.8	0.5	0.9	0.8	0.5
3-chlorophenol	-0.4	-0.6	0.3	0.5	-0.6	-0.6	-0.04	0.04
4-chlorophenol	0.3	0.4	0.8	0.7	0.3	0.4	0.7	0.5
2,4-dichlorophenol	2.4	0.3	1.3	1.6	1.2	0.3	1.1	1.2
3,4-dichlorophenol	0.6	-0.2			-0.01	-0.1		
3,5-dichlorophenol	0.02	-1.1			-0.8	-1.1		
2,4,6-trichlorophenol	4.7	1.7	2.1	2.2	2.3	1.4	1.8	1.7
pentachlorophenol	6.2	0.3			2.6	0.3		
<i>Stone, 1987⁸</i>								
phenol	-0.6	-0.06	0.9	0.7	-0.2	0.1	0.6	0.4
2-hydroxybenzoate		-1.9	-1.1	-1.6		-1.4	-1.1	-1.5
4-hydroxybenzoate		-1.1	-0.09	0.3		-0.9	-0.4	-0.2
2-chlorophenol	1.3	1.3	1.1	0.8	0.5	0.6	0.8	0.5
3-chlorophenol	-0.4	-0.6	0.3	0.5	-0.6	-0.6	-0.02	0.05
4-chlorophenol	0.3	0.4	0.8	0.7	0.3	0.4	0.7	0.5
4-nitrophenol	0.4	-1.9	-0.2	-0.6	-1.4	-2.0	-1.0	-1.2
3-methylphenol	-0.4	0.2	1.0	1.0	0.06	0.4	0.8	0.7
4-methylphenol	-0.03	0.8	1.2	1.2	0.6	1.1	1.2	1.1
4-ethylphenol	-0.02	0.8	1.2	1.3	0.6	1.1	1.2	1.1
<i>Salter-Blanc et al., 2016²⁷</i>								
aniline	-0.4	1.0	-0.4	-0.5	-0.05	0.6	-0.07	-0.3
4-chloroaniline	0.3	1.3	-0.5	-0.3	0.3	0.8	-0.1	-0.1
	Simple substituents				All substituents			
	$\Sigma\sigma$	pK _a	E _{HOMO}	E _{ox}	$\Sigma\sigma$	pK _a	E _{HOMO}	E _{ox}

<i>Salter-Blanc et al., 2016²⁷ continued</i>								
3-nitroaniline	0.3	0.2	-0.9	-1.0	-0.6	-0.5	-0.9	-1.1
4-nitroaniline	-1.1	-2.4	-3.5	-3.6	-2.9	-3.2	-3.5	-3.7
4-methyl-3-nitroaniline	-0.02	0.2	-1.1	-1.2	-0.6	-0.4	-0.9	-1.1
2-methoxy-5-nitroaniline	1.4	0.2	-0.3	-0.3	0.5	-0.5	-0.07	-0.2
2-methyl-5-nitroaniline	0.5	0.7	-1.1	-1.2	-0.6	0.6	-1.0	-1.2

Table A.17. Residual values calculated against the individual solid and all three solids QSARs, developed with data from this study. QSAR linear regressions provided in **Table A.11**.

	Simple substituents				All substituents			
	$\Sigma\sigma$	pK _a	E _{HOMO}	E _{ox,corr.}	$\Sigma\sigma$	pK _a	E _{HOMO}	E _{ox,corr.}
<i>Drinking water treatment solids</i>								
phenol	-0.5	-0.7	-0.1	-0.4	-0.3	-0.5	-0.06	-0.3
resorcinol	0.4	0.2	0.3	0.05	0.5	0.3	0.4	0.2
estrone		-0.1				0.1		
4-cresol	0.09	-0.01	0.3	-0.2	0.2	0.2	0.5	0.09
4- <i>tert</i> -octylphenol	0.9	0.7			1.0	0.9		
bisphenol A		0.1	-0.04	1.1		0.3	0.3	1.1
4-phenoxyphenol		1.6	1.9	0.8		1.7	2.0	1.1
4-nitrocatechol		2.0	1.8	1.7		1.8	1.7	1.8
triclosan		0.7	0.2	0.5		0.6	0.3	0.6
2-chlorophenol	-0.04	-0.7	-0.8	-1.1	-0.01	-0.8	-0.7	-0.9
3-chlorophenol	-0.6	-1.0	-0.8	-0.4	-0.5	-1.0	-0.7	-0.4
4-chlorophenol	-0.05	-0.3	-0.3	-0.7	0.04	-0.2	-0.2	-0.5
2-nitrophenol	0.5	-0.7	-0.7	-0.5	0.4	-0.9	-0.9	-0.6
3-nitrophenol	-0.4	-1.3	-0.7	-0.5	-0.3	-1.3	-0.8	-0.6
4,4'-dihydroxybiphenyl	-0.3	-0.4	-1.0	-0.5	-0.2	-0.3	-0.6	-0.3
<i>Acid mine drainage solids</i>								
phenol	0.4	0.3	0.7	0.5	0.7	0.6	1.0	0.8
resorcinol	0.4	0.5	0.4	0.3	0.8	0.6	0.7	0.5
estrone		-0.5				-0.2		
4-cresol	-0.4	-0.3	-0.1	-0.4	-0.07	-0.07	0.2	-0.2
4- <i>tert</i> -octylphenol	0.4	0.4			0.8	0.7		
bisphenol A		-0.3	-0.4	0.3		-0.08	-0.1	0.7
4-phenoxyphenol		0.7	0.8	0.1		0.9	1.2	0.2
4-nitrocatechol		2.7	2.1	2.2		2.6	2.5	2.5
triclosan		1.0	0.3	0.6		0.9	0.6	0.9
2-chlorophenol	-0.1	-0.6	-0.9	-1.1	0.2	-0.6	-0.6	-0.8
3-chlorophenol	-0.5	-0.7	-0.8	-0.6	-0.2	-0.7	-0.5	-0.1
4-chlorophenol	-0.3	-0.3	-0.5	-0.7	0.04	-0.2	-0.2	-0.5
2-nitrophenol	0.2	-0.6	-1.2	-1.0	0.5	-0.8	-0.8	-0.5
3-nitrophenol								
4,4'-dihydroxybiphenyl	-0.05	0.02	-0.4	-0.08	0.3	0.2	-0.1	0.2

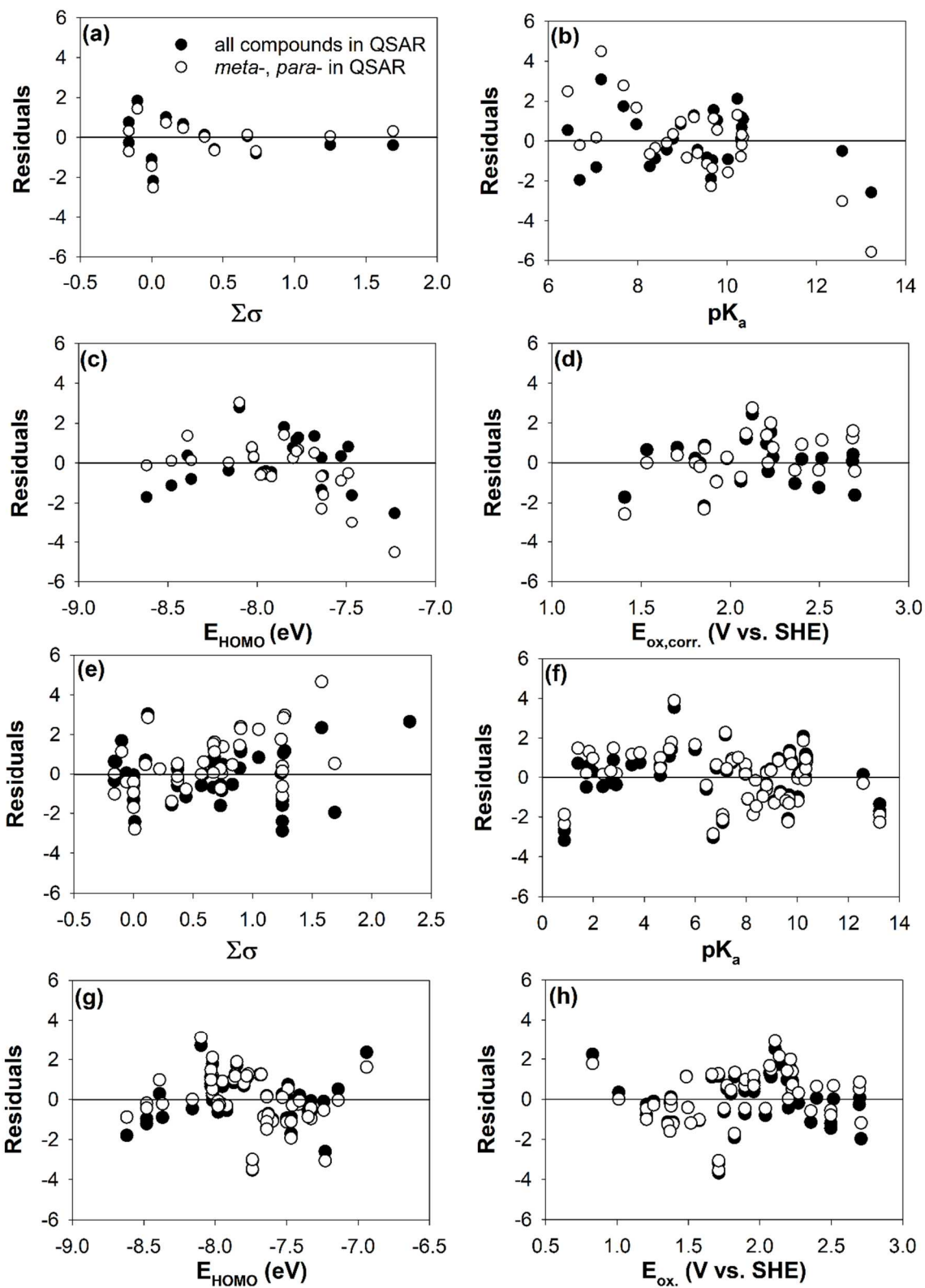


Figure A.9. Plots of residuals versus independent QSAR descriptors for this study (a through d) and literature data (e through h). Residuals were calculated for QSAR relationships including either the simple (*meta-*, *para-*) or all compounds.

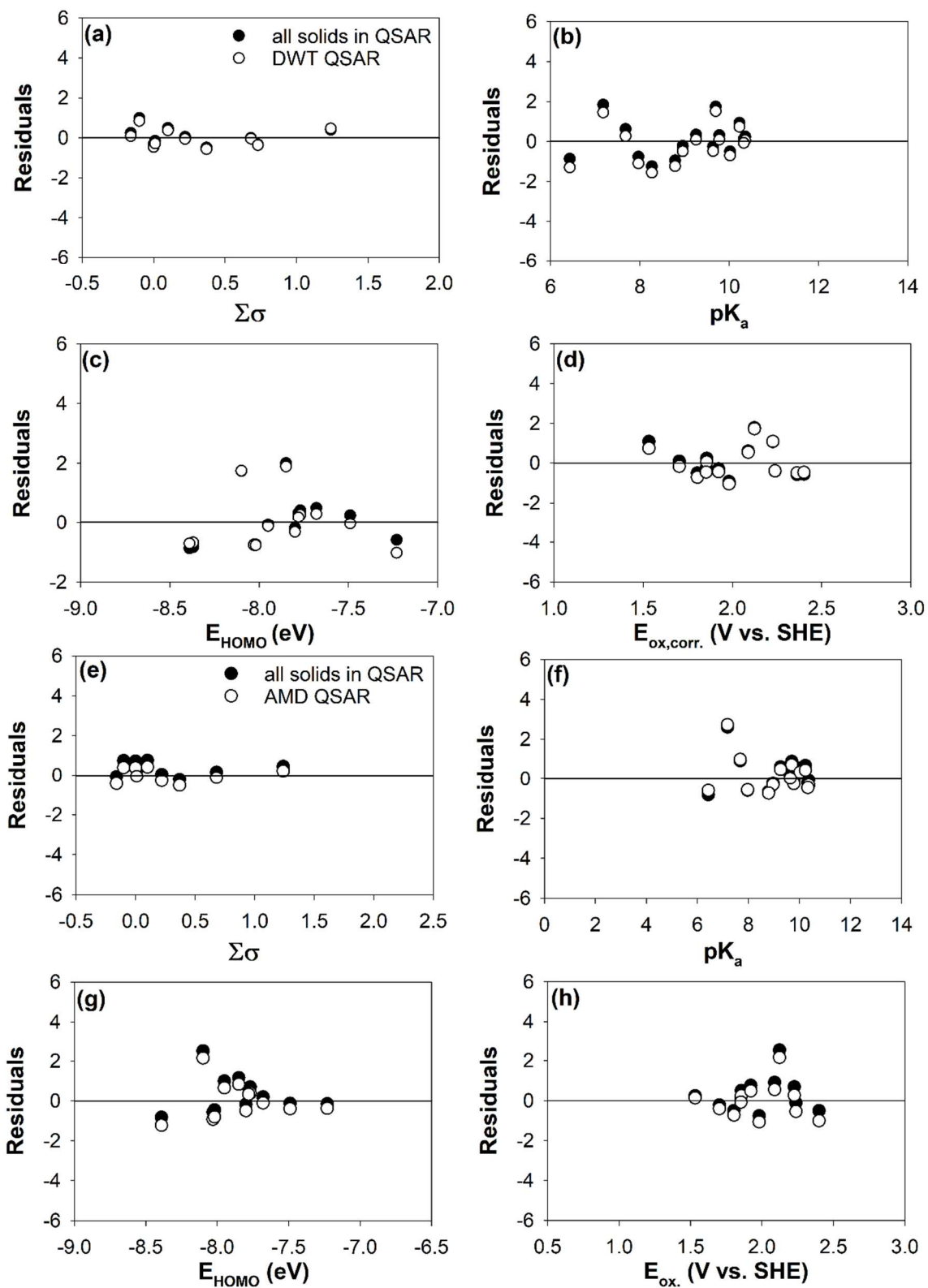


Figure A.10. Plots of residuals versus independent QSAR descriptors for drinking water treatment (DWT) and acid mine drainage (AMD) solids. Residuals were calculated for QSAR relationships calculated for both the individual solids and all solids.

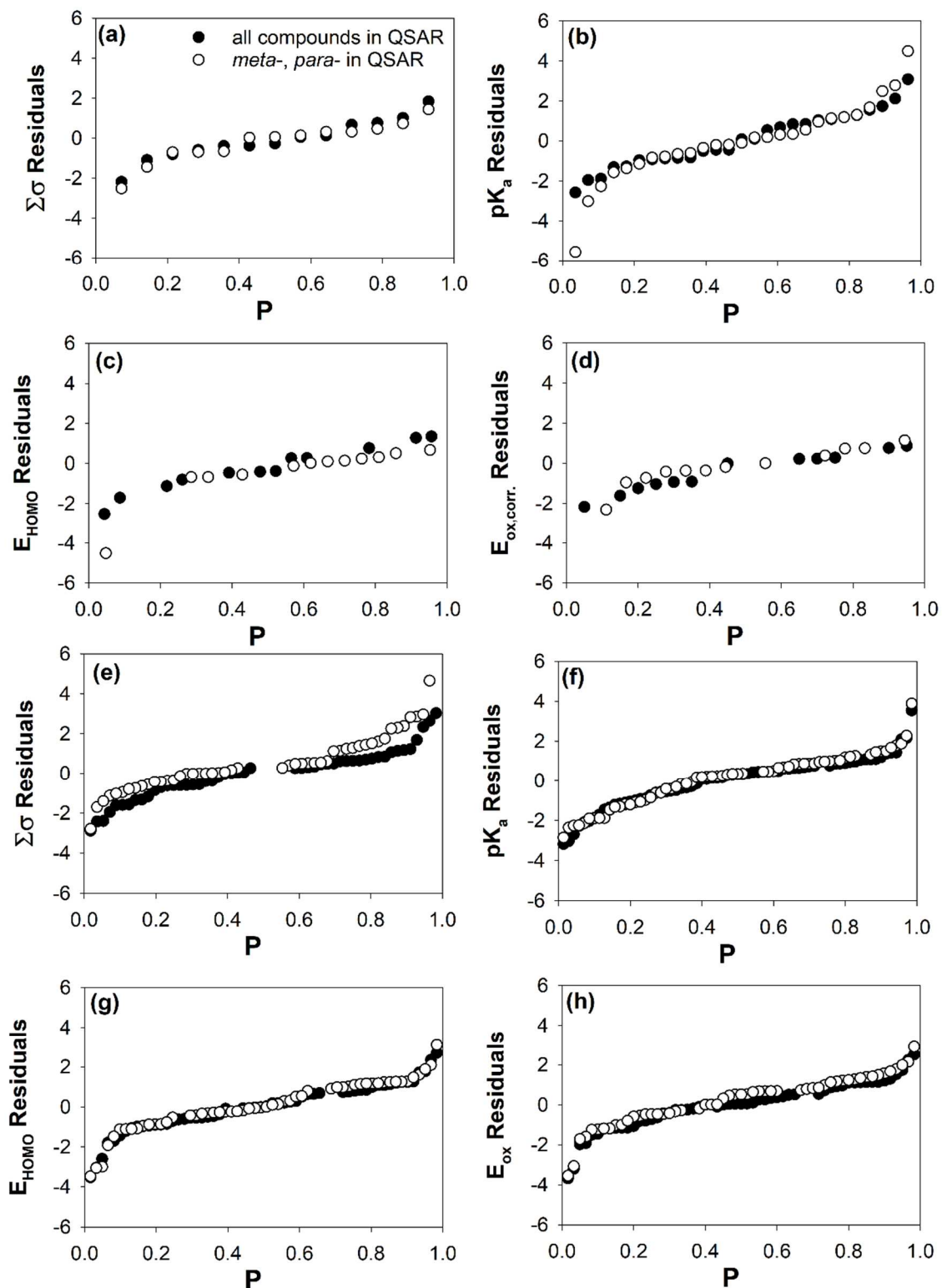


Figure A.11. Residual normality plots of the calculated residuals versus probability (P) of each residual for QSAR relationships including using only simple *meta*- and *para*-substituted compounds or all compounds. Plots (a) through (d) show data from only this study and plots (e) through (h) show the data for the larger literature data set.

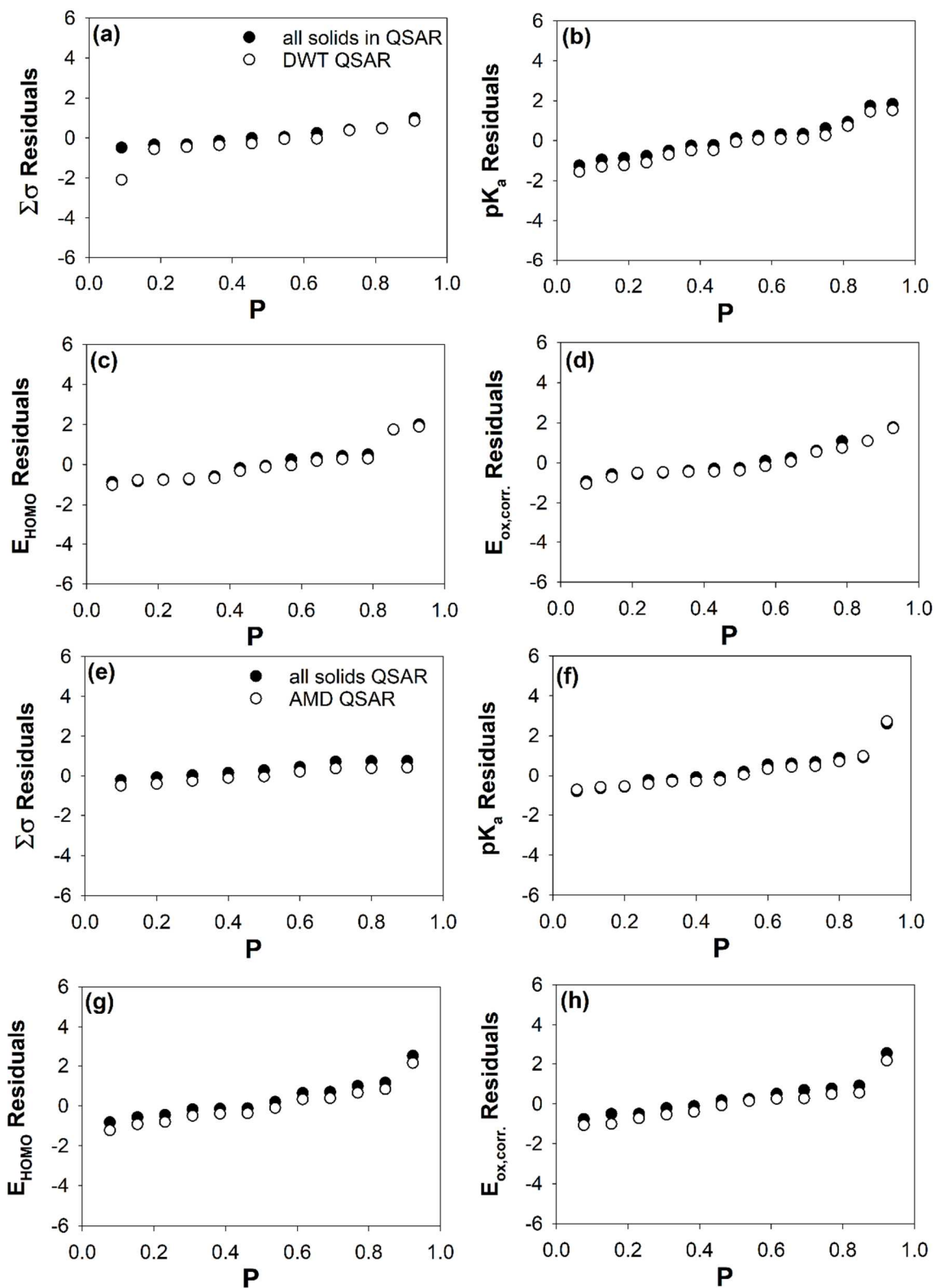


Figure A.12. Residual normality plots of the calculated residuals versus probability of each residual for QSAR relationships including using only a single manganese oxide or all solids. Plots (a) through (d) show data for drinking water treatment (DWT) solids and plots (e) through (h) show the data for the acid mine drainage (AMD) solids data.

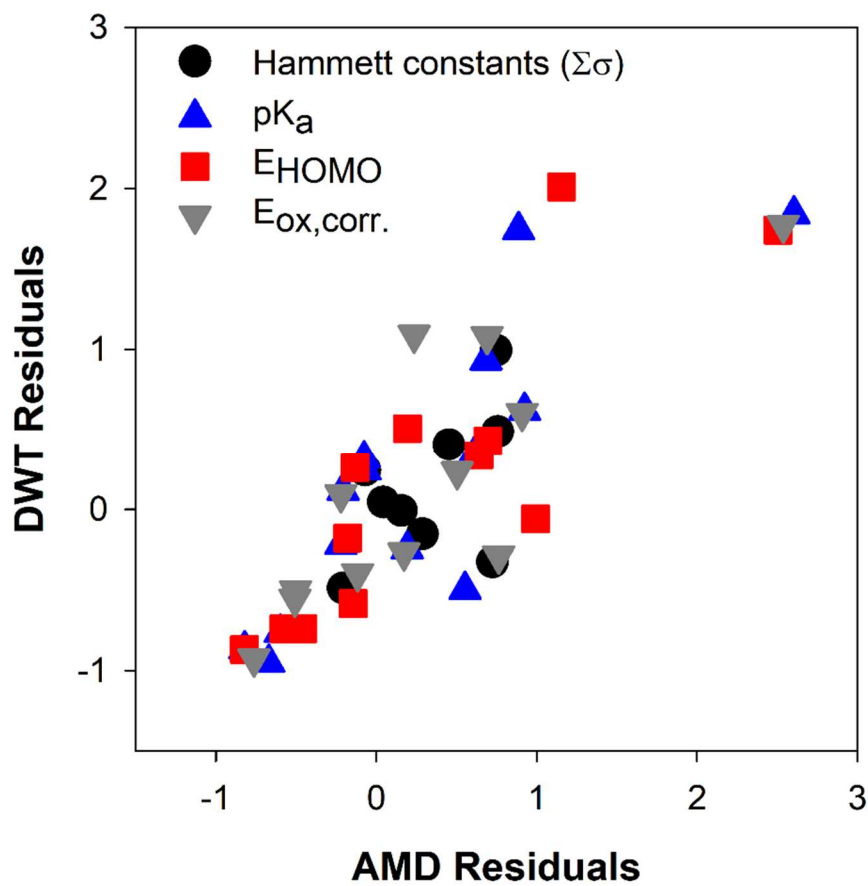


Figure A.13. Residuals of each QSAR for phenols reacted with drinking water treatment solids (DWT) versus the residuals for phenols reacted with acid mine drainage solids (AMD).

Table A.18. QSAR validation based on structural substitutions using data from this study (with δ -MnO₂) and literature. Gray values fall within the accepted ranges for that measure.

	Training set	Test set	Training set			Test set: Comparing predicted and experimental $\log(k/k_{4-C1})$ values					
	n	n	Slope	R ²	p	r ²	r _m ²	r _m ' ²	R ² _{pred}	p	R ² _p
Accepted values	-	-	-	>0.6	<0.05	-	>0.5	>0.5	>0.5	<0.05	>0.5
<i>meta-, para-, ortho- training set, complex compounds test set</i>											
Hammett constant	53	2	1.43	0.21	0.001	1.00	0.06	0.03	0.54	-	0.07
pK _a	55	14	0.18	0.09	0.01	0.03	0.01	0.02	0.28	0.58	0.03
E _{HOMO}	48	12	1.48	0.10	0.03	0.02	-0.01	0.01	0.46	0.63	0.02
E _{ox}	47	12	-1.19	0.08	0.20	0.07	-0.07	0.07	0.49	0.40	0.04
<i>meta-, para- training set, ortho- test set</i>											
Hammett constant	37	18	3.25	0.61	1.3E-8	0.37	0.08	0.29	-3.33	0.01	0.19
pK _a	37	32	0.31	0.21	0.005	0.03	0.01	0.02	-0.01	0.34	0.03
E _{HOMO}	34	26	2.11	0.17	0.01	0.06	-0.03	0.03	0.33	0.24	0.05
E _{ox}	34	25	-1.61	0.14	0.03	0.01	-0.01	0.01	0.30	0.61	0.01
<i>meta-, para- training set, ortho-, complex test set</i>											
Hammett constant	37	16	3.25	0.61	1.3E-8	0.15	0.06	0.13	-3.66	0.15	0.14
pK _a	37	18	0.31	0.21	0.005	0.02	-0.01	0.02	-0.22	0.54	0.02
E _{HOMO}	34	14	2.11	0.17	0.01	0.09	-0.05	0.05	0.15	0.29	0.08
E _{ox}	34	13	-1.61	0.14	0.03	0.10	-0.09	0.06	0.07	0.29	0.06
<i>Literature data training set, This study test set</i>											
Hammett constant	39	16	-1.02	0.10	0.054	0.45	0.37	0.36	0.65	0.004	0.20
pK _a	42	27	0.16	0.09	0.052	0.09	0.07	0.05	0.39	0.14	0.06
E _{HOMO}	36	24	1.17	0.04	0.22	0.13	-0.08	0.12	0.62	0.08	0.10
E _{ox}	36	23	-0.70	0.02	0.39	0.29	-0.48	0.19	0.36	0.008	0.23
<i>This study training set, Literature data test set</i>											
Hammett constant	16	39	-1.74	0.46	0.004	0.10	-0.02	0.09	0.25	0.054	0.08
pK _a	27	42	0.26	0.09	0.04	0.09	-0.06	0.08	0.21	0.052	0.06
E _{HOMO}	24	36	1.39	0.13	0.08	0.04	-0.01	0.04	0.37	0.22	0.03
E _{ox}	23	36	-1.89	0.29	0.01	0.02	0.02	0.01	0.25	0.39	0.01
<i>Randomized training set, Randomized test set</i>											
Hammett constant	39	16	-1.20	0.14	0.02	0.14	0.13	0.03	0.60	0.15	-
pK _a	50	19	0.16	0.09	0.03	0.00	0.00	0.00	0.47	0.87	-
E _{HOMO}	45	15	1.39	0.07	0.07	0.07	-0.02	0.06	0.57	0.34	-
E _{ox}	45	14	-0.88	0.05	0.14	0.25	-0.19	0.19	0.61	0.07	-

Table A.19. QSAR validation measures using data from this study with three manganese oxides (i.e., δ -MnO₂ and two reclaimed solids). Gray values fall within the accepted ranges for that measure.

	Training set	Test set	Training set			Test set: Comparing predicted and experimental $\log(k/k_{4-CI})$ values					
Accepted values	n	n	Slope	R ²	p	r ²	r _m ²	r _m ' ²	r ² _{pred}	p	R ² _p
	-	-	-	>0.6	<0.05	-	>0.5	>0.5	>0.5	<0.05	>0.5
<i>δ-MnO₂ training set, Reclaimed solids test set</i>											
Hammett constant	16	19	0.43	0.45	0.004	0.76	0.25	-0.09	0.36	1.0E-6	0.31
pK _a	27	29	-0.35	0.06	0.22	0.12	0.06	-2.15	-0.02	0.07	0.09
E _{HOMO}	24	25	-0.14	0.13	0.08	0.14	0.07	-0.15	-0.12	0.07	0.11
E _{ox}	23	25	0.10	0.29	0.01	0.28	0.11	-0.09	0.23	0.01	0.22
<i>Randomized training set Randomized test set</i>											
Hammett constant	27	8	1.30	0.53	1.5E-5	0.41	0.28	0.20	0.32	0.09	-
pK _a	38	18	-0.40	0.19	0.01	0.07	0.07	0.06	-0.70	0.28	-
E _{HOMO}	34	15	0.62	0.13	0.04	0.08	0.07	0.01	0.05	0.31	-
E _{ox}	33	15	0.61	0.38	1.5E-4	0.24	0.17	0.003	0.10	0.06	-

A.9. References

1. J. W. Murray, The surface chemistry of hydrous manganese dioxide, *J. Colloid Interface Sci.*, **1974**, *46*, 357-371.
2. R. Hedin, T. Weaver, N. Wolfe and G. Watzlaf, presented in part at the 35th Annual National Association of Abandoned Mine Land Programs Conference, Daniels, West Virginia, **2013**.
3. A. Manceau, M. A. Marcus and S. Grangeon, Determination of Mn valence states in mixed-valent manganates by XANES spectroscopy, *Am. Mineral.*, **2012**, *97*, 816-827.
4. O. A. Ohlweiler and A. M. H. Schneider, Standardization of potassium permanganate by titration of sodium oxalate in presence of perchloric acid and manganese(II) sulfate, *Anal. Chim. Acta*, **1972**, *58*, 477-480.
5. R. M. Fowler and H. A. Bright, Standardization of permanganate solutions with sodium oxalate, *J. Res. Natl. Bur. Stand.s*, **1935**, *15*, 493-501.
6. J. E. Post, Manganese oxide minerals: Crystal structures and economic and environmental significance, *Proc. Natl. Acad. Sci. U.S.A.*, **1999**, *96*, 3447-3454.
7. C. K. Remucal and M. Ginder-Vogel, A critical review of the reactivity of manganese oxides with organic contaminants, *Environ. Sci. Processes Impacts*, **2014**, *16*, 1247-1266.
8. A. T. Stone, Reductive dissolution of manganese(III/IV) oxides by substituted phenols, *Environ. Sci. Technol.*, **1987**, *21*, 979-988.
9. H. J. Ulrich and A. T. Stone, Oxidation of chlorophenols adsorbed to manganese oxide surfaces, *Environ. Sci. Technol.*, **1989**, *23*, 421-428.
10. S. Balgooyen, P. J. Alaimo, C. K. Remucal and M. Ginder-Vogel, Structural transformation of MnO₂ during the oxidation of bisphenol A, *Environ. Sci. Technol.*, **2017**, *51*, 6053-6062.
11. S. Balgooyen, G. Campagnola, C. K. Remucal and M. Ginder-Vogel, Impact of bisphenol A influent concentration and reaction time on MnO₂ transformation in a stirred flow reactor, *Environ. Sci. Processes Impacts*, **2019**, *21*, 19-27.
12. M. Villalobos, B. Toner, J. Bargar and G. Sposito, Characterization of the manganese oxide produced by *Pseudomonas putida* strain MnB1, *Geochim. Cosmochim. Acta*, **2003**, *67*, 2649-2662.
13. E. E. Schulte and B. G. Hopkins, Estimation of organic matter by weight loss-on-ignition, **1996**, *SSSA Special Publication Number 46*, 21-31.
14. M. Kosmulski, Isoelectric points and points of zero charge of metal (hydr)oxides: 50 years after Parks' review, *Adv. Colloid Interface Sci.*, **2016**, *238*, 1-61.
15. T. Mahmood, M. T. Saddique, A. Naeem, P. Westerhoff, S. Mustafa and A. Alum, Comparison of different methods for the point of zero charge determination of NiO, *Ind. Eng. Chem. Res.*, **2011**, *50*, 10017-10023.
16. J. Klausen, S. B. Haderlein and R. P. Schwarzenbach, Oxidation of substituted anilines by aqueous MnO₂: Effect of co-solutes on initial and quasi-steady-state kinetics, *Environ. Sci. Technol.*, **1997**, *31*, 2642-2649.
17. K. Rubert and J. A. Pedersen, Kinetics of oxytetracycline reaction with a hydrous manganese oxide, *Environ. Sci. Technol.*, **2006**, *40*, 7216-7221.
18. S. C. Ying, B. D. Kocar, S. D. Griffis and S. Fendorf, Competitive microbially and Mn oxide mediated redox processes controlling arsenic speciation and partitioning, *Environ. Sci. Technol.*, **2011**, *45*, 5572-5579.

19. W. S. Yao and F. J. Millero, Adsorption of phosphate on manganese dioxide in seawater, *Environ. Sci. Technol.*, **1996**, *30*, 536-541.
20. Z. Moldovan, D. E. Popa, I. G. David, M. Buleandra and I. A. Badea, A derivative spectrometric method for hydroquinone determination in the presence of kojic acid, glycolic acid, and ascorbic acid, *J. Spectrosc.*, **2017**, 1-9.
21. A. T. Stone and J. J. Morgan, Reduction and dissolution of manganese(III) and manganese(IV) oxides by organics. 1. Reaction with hydroquinone, *Environ. Sci. Technol.*, **1984**, *18*, 450-456.
22. H. Zhang, W. R. Chen and C. H. Huang, Kinetic modeling of oxidation of antibacterial agents by manganese oxide, *Environ. Sci. Technol.*, **2008**, *42*, 5548-5554.
23. A. T. Stone and J. J. Morgan, Reduction and dissolution of manganese(III) and manganese(IV) oxides by organics: 2. Survey of the reactivity of organics, *Environ. Sci. Technol.*, **1984**, *18*, 617-624.
24. N. Shaikh, H. Zhang, K. Rasamani, K. Artyushkova, A. S. Ali and J. M. Cerrato, Reaction of bisphenol A with synthetic and commercial $MnO_{x(s)}$: Spectroscopic and kinetic study, *Environ. Sci. Processes Impacts*, **2018**, *20*, 1046-1055.
25. W. A. Arnold, Y. Oueis, M. O'Connor, J. E. Rinaman, M. G. Taggart, R. E. McCarthy, K. A. Foster and D. E. Latch, QSARs for phenols and phenolates: Oxidation potential as a predictor of reaction rate constants with photochemically produced oxidants, *Environ. Sci. Processes Impacts*, **2017**, *19*, 324-338.
26. A. S. Pavitt, E. J. Bylaska and P. G. Tratnyek, Oxidation potentials of phenols and anilines: Correlation analysis of electrochemical and theoretical values, *Environ. Sci. Processes Impacts*, **2017**, *19*, 339-349.
27. A. J. Salter-Blanc, E. J. Bylaska, M. A. Lyon, S. C. Ness and P. G. Tratnyek, Structure-activity relationships for rates of aromatic amine oxidation by manganese dioxide, *Environ. Sci. Technol.*, **2016**, *50*, 5094-5102.
28. J. C. Suatoni, R. E. Snyder and R. O. Clark, Voltammetric studies of phenol and aniline ring substitution, *Anal. Chem.*, **1961**, *33*, 1894-&.
29. S. Laha and R. G. Luthy, Oxidation of aniline and other primary aromatic amines by manganese dioxide, *Environ. Sci. Technol.*, **1990**, *24*, 363-373.
30. J. W. Park, J. Dec, J. E. Kim and J. M. Bollag, Effect of humic constituents on the transformation of chlorinated phenols and anilines in the presence of oxidoreductive enzymes or birnessite, *Environ. Sci. Technol.*, **1999**, *33*, 2028-2034.
31. G. B. Barlin and D. D. Perrin, Prediction of the strengths of organic acids, *Quarterly Reviews, Chemical Society*, **1966**, 75-101.
32. J. Clark and D. D. Perrin, Prediction of the strengths of organic bases, *Quarterly Reviews, Chemical Society*, **1964**, 295-320.
33. C. Hansch, A. Leo and R. W. Taft, A survey of Hammett substituent constants and resonance and field parameters, *Chem. Review*, **1991**, *91*, 165-195.
34. M. Swain, Chemicalize.org, *J. Chem. Inf. Model.*, **2012**, *52*, 613-615.
35. M. Valiev, E. J. Bylaska, N. Govind, K. Kowalski, T. P. Straatsma, H. J. J. Van Dam, D. Wang, J. Nieplocha, E. Apra, T. L. Windus and W. de Jong, NWChem: A comprehensive and scalable open-source solution for large scale molecular simulations, *Comp. Phys. Commun.*, **2010**, *181*, 1477-1489.
36. U.S. Environmental Protection Agency, Estimation Programs Interface Suite™ for Microsoft® Windows, 2012.

37. J. L. Devore, *Probability & Statistics for Engineering and the Sciences*, Brooks/Cole, Boston, MA, 8th edn., **2012**.
38. P. G. Tratnyek, E. J. Weber and R. P. Schwarzenbach, Quantitative structure-activity relationships for chemical reductions of organic contaminants, *Environ. Toxicol. Chem.*, **2003**, *22*, 1733-1742.
39. N. Frimayanti, M. L. Yam, H. B. Lee, R. Othman, S. M. Zain and N. A. Rahman, Validation of quantitative structure-activity relationship (QSAR) model for photosensitizer activity prediction, *Int. J. Mol. Sci.*, **2011**, *12*, 8626-8644.
40. P. Gramatica, On the development and validation of QSAR models, *Methods Mol. Biol.*, **2013**, *930*, 499-526.
41. R. Veerasamy, H. Rajak, A. Jain, S. Sivadasan, C. P. Varghese and R. K. Agrawal, Validation of QSAR models - strategies and importance, *Int. J. Drug Des. Discov.*, **2011**, *2*, 511-519.
42. A. Cherkasov, E. N. Muratov, D. Fourches, A. Varnek, Baskin, II, M. Cronin, J. Dearden, P. Gramatica, Y. C. Martin, R. Todeschini, V. Consonni, V. E. Kuz'min, R. Cramer, R. Benigni, C. Yang, J. Rathman, L. Terfloth, J. Gasteiger, A. Richard and A. Tropsha, QSAR modeling: Where have you been? Where are you going to?, *J. Med. Chem.*, **2014**, *57*, 4977-5010.

Appendix B

Supplementary Material for Chapter 3: Enhancement and inhibition of oxidation rates in mixtures of phenolic compounds reacted with manganese oxides

B.1. Materials

Methanol (HPLC grade), hydrochloric acid (Certified ACS Plus grade), sodium chloride (Certified ACS grade), acetonitrile (HPLC grade), potassium permanganate (Certified ACS grade; KMnO_4), and sodium hydroxide (Certified ACS grade; NaOH) were purchased from Fisher Scientific. Sulfuric acid (95.0-98.0 %), nitric acid (70%), L-ascorbic acid (BioXtra, $\geq 99\%$), 4,4'-biphenol (97%), and bisphenol A (BPA, $>99\%$) were purchased from Sigma-Aldrich. Sodium oxalate (99%), sodium acetate trihydrate (ACS grade, 99-100.5%), and resorcinol (99-100.5%) were purchased from Alfa Aesar. Formic acid (Reagent ACS grade, 88%) was purchased from Aqua Solution, Inc. Manganese nitrate tetrahydrate (for analysis; $\text{Mn}(\text{NO}_3)_2$) was purchased from Acros Organics. Triclosan (certified reference material) was purchased from AccuStandard. Tert-butanol was purchased from Honeywell (ACS reagent; $> 99.7\%$). All commercially available chemicals were used as received.

B.2. Manganese oxide composition

δ -MnO₂ was synthesized according to a modified Murray method.¹ By this method, Mn(NO₃)₂ was added at a rate of 1 mL per minute into a solution of KMnO₄ and NaOH at molar ratios of 3:2:4 Mn^{II}:Mn^{VII}:OH⁻ while stirring at 350 rpm. The suspension was covered and stirred for 20 hours at 22 ± 2 °C and rinsed and washed by centrifugation at 2500 rpm for 12 minutes in ultrapure water, decreasing the suspension volume each rinse cycle. During the two final centrifuge rinses, solids were resuspended in pH 5.5 10 mM acetate buffer solution. The slurry was dried at 60 °C in triplicate to calculate the slurry density for reactions.

The initial δ -MnO₂ starting material and subsequent δ -MnO₂ controls were characterized for average manganese oxidation number using an oxalate-permanganate titration method described previously.²⁻⁴ The oxidation number of the initial solid was also confirmed by X-ray absorption near edge structure spectroscopy (XANES) with resulting values of 3.92 ± 0.05 and 3.86 ± 0.04 for the titration and XANES methods, respectively. All solids were also characterized by their Brunauer-Emmett-Teller surface area (Quantachrome Autosorb-1, nitrogen adsorbate; 30 °C) and X-ray diffraction spectra (Rigaku Rapid II, Mo K α source; λ = 0.7093 Å; **Figure B.1**). Concentration of released aqueous Mn into solution were quantified by inductively coupled plasma-optical emission spectroscopy (ICP-OES; Agilent 5110 VDV). All δ -MnO₂ controls in 10 mM sodium acetate buffer with and without *tert*-butanol had less than 10 ppb aqueous Mn release. The relative ratio of sodium (Na) incorporated in the δ -MnO₂ layer structure was also determined by ICP-OES; the starting material had 11.9% Na:Mn. Other characteristic values for the starting material and δ -MnO₂ reacted in the presence of 10 mM pH 5.5 sodium acetate buffer with or without 2 mM *tert*-butanol are given in **Table B.1**.

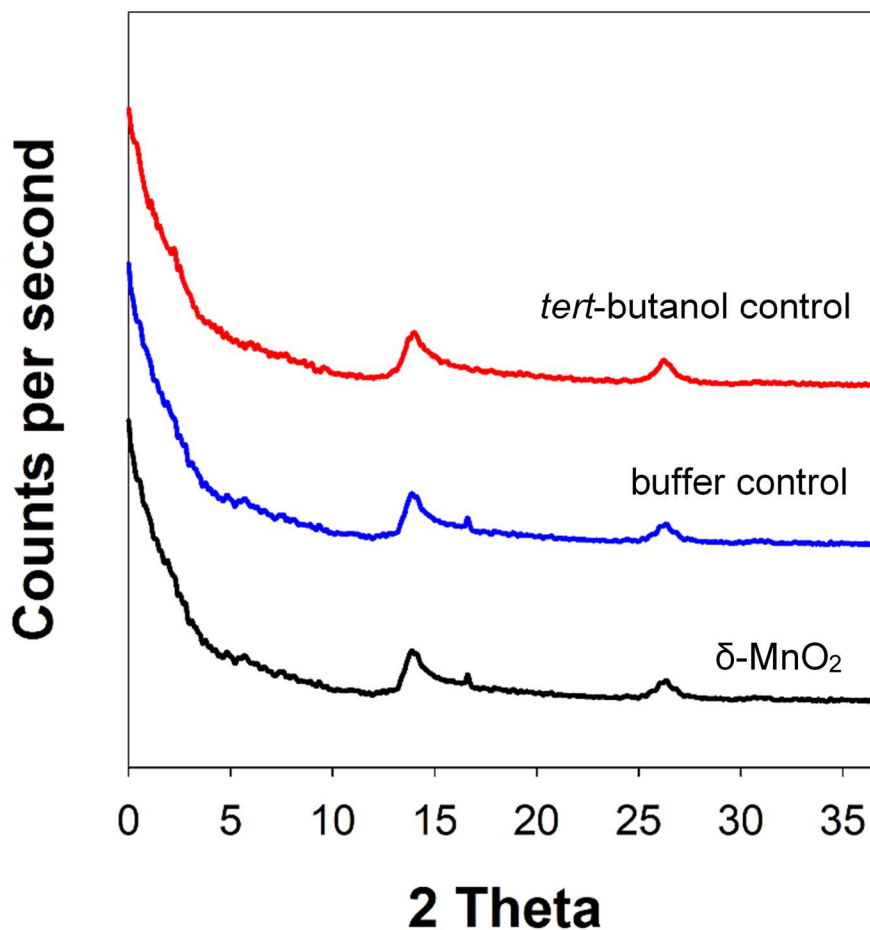


Figure B.1. X-ray diffraction spectra of synthesized δ -MnO₂ starting material, buffered control reacted for 14 days in 10 mM pH 5.5 sodium acetate, and *tert*-butanol control reacted for 14 days in 2 mM *tert*-butanol and 10 mM pH 5.5 sodium acetate.

Table B.1. Average manganese oxidation number (AMON) and Brunauer-Emmett-Teller N₂ surface area of Mn reacted in sodium acetate buffered control solutions with and without varying concentrations of *tert*-butanol in solution. Reported error is the standard deviation of replicate measurements.

	AMON	Surface area (m ² /g)
Starting material	3.92 ± 0.05	169.41
Buffer only control	3.93 ± 0.30	180.07
1 mM <i>tert</i> -butanol control	3.88 ± 0.10	N/A
2 mM <i>tert</i> -butanol control	3.97 ± 0.18	154.01
4 mM <i>tert</i> -butanol control	4.00 ± 0.22	N/A

B.3. Phenol concentration quantification

Phenol concentrations and loss were quantified using an Agilent 1260 Infinity series high performance liquid chromatography instrument (HPLC; Agilent Technologies) by an in-line diode array (UV-vis) or fluorescence detector. Chromatography parameters are provided in **Table B.2**. For all phenols, the aqueous mobile phase was 10% acetonitrile and 0.1% v:v formic acid adjusted to pH 2.5 in ultrapure water. The organic mobile phase was acetonitrile. All analyses were done with an EC-C18 column (Agilent Poroshell-120; 3.0 x 50 mm, 2.7 μm) with an injection volume of 20 μL .

Table B.2. HPLC Parameters for compound detection for individual phenols and mixtures. The aqueous mobile phase A was 10% acetonitrile, and 0.1% formic acid at pH 2.5. Acetonitrile was the organic mobile phase.

Compound	Aqueous mobile phase	Flow rate ($\mu\text{L}/\text{min}$)	Retention time (min)	Detection
<i>Individual compounds</i>				
resorcinol	40% A	1	0.5	Fluorescence: ex: 305 nm em: 290 nm
4,4'-biphenol	75% A	0.6	0.9	
bisphenol A	65% A	1	1.8	
triclosan	40% A	1	1.5	Absorbance: abs: 280 nm ref: 400 nm
<i>Mixtures of compounds</i>				
resorcinol	40% A	1	0.5	Fluorescence: ex: 305 nm em: 290 nm
4,4'-biphenol			4.1	
bisphenol A			2.7	
triclosan			1.5	Absorbance abs: 280 nm ref: 400 nm

B.4. Observed rate constants

Experimental pseudo-first-order rate constants were determined for each phenol from quenched concentrations plotted versus time. Each reported pseudo-first-order rate constant is the average of at least 3 rate constants determined from different reaction time ranges based on the linear regions of each phenol degradation curve (e.g., average of $k_{0-3 \text{ min}}$, $k_{0-5 \text{ min}}$, and $k_{0-7 \text{ min}}$). These values are the pseudo-first-order rate constants of oxidation (quenched rate constant); only oxidation rates are analyzed in this study while filtered concentrations are used to determine sorption and rate-limiting steps of oxidation (**Section B.5**). Quenched pseudo-first-order constants are reported in **Tables B.3 – B.5**.

Table B.3. Average pseudo-first-order rate constants (hr^{-1}) for each phenol at initial concentrations of 10, 20 and 40 μM with no competing phenolic compounds in solution. Rate constants are the average of multiple time ranges and triplicate solutions; error is ± 1 standard deviation.

	10 μM	20 μM	40 μM
resorcinol	11.2 ± 1	11.5 ± 0.9	9.0 ± 1.8
bisphenol A	8.4 ± 0.8	9.7 ± 1.4	7.2 ± 1.6
triclosan	6.2 ± 0.9	5.4 ± 0.6	6.1 ± 1.5
4,4'-biphenol	$3.1 \pm 1.7 \times 10^{-3}$	$5.1 \pm 0.9 \times 10^{-3}$	$7.2 \pm 0.2 \times 10^{-3}$

Table B.4. Average pseudo-first-order rate constants (hr^{-1}) for each phenol with competing phenolic compounds in solution, listed at the top of each column. Rate constants are the average of multiple time ranges and triplicate solutions; error is ± 1 standard deviation.

	Resorcinol in solution	Bisphenol A in solution	Triclosan in solution	4,4'- Biphenol in solution	All phenols in solution
resorcinol		$2.1 \pm 0.6 \times 10^{-2}$	1.0 ± 0.4	0.23 ± 0.02	0.4 ± 0.09
bisphenol A	2.2 ± 0.5		3.6 ± 0.8	2.2 ± 0.5	3.3 ± 0.6
triclosan	0.15 ± 0.02	1.3 ± 0.2		0.9 ± 0.3	3.3 ± 0.6
4,4'-biphenol	0.47 ± 0.04	0.17 ± 0.03	0.13 ± 0.06		0.83 ± 0.04

Table B.5. *Tert*-butanol quenched average pseudo-first-order rate constants (hr^{-1}) for each phenol with competing phenolic compounds in solution, listed at the top of each column. Rate constants are the average of multiple time ranges and triplicate solutions; error is ± 1 standard deviation.

	10 μM	Resorcinol in solution	Bisphenol A in solution	Triclosan in solution	4,4'- Biphenol in solution	All phenols in solution
resorcinol	5.3 ± 0.8		6.0 ± 0.9	6.2 ± 1.1	4.0 ± 0.6	9.9 ± 2.1
bisphenol A	9.3 ± 0.9	8.0 ± 1.5		9.5 ± 0.9	4.6 ± 0.4	4.2 ± 0.8
triclosan	4.9 ± 1.2	3.6 ± 1.1	4.5 ± 0.6		2.3 ± 0.4	0.41 ± 0.07
4,4'-biphenol	3.7 ± 0.2 $\times 10^{-3}$	0.12 ± 0.03	0.13 ± 0.05	5.6 ± 0.8 $\times 10^{-2}$		0.14 ± 0.03

B.5. Sorption and mechanism determination

In addition to total phenolic compound concentrations, quantified by dissolving $\delta\text{-MnO}_2$ with ascorbic acid at each kinetic timepoint and used to determine pseudo-first-order rate constants, reactions were filtered at each timepoint to determine the sorbed concentration of each compound. The maximum percent of each phenol which sorbs to the Mn surface is used to determine the rate-controlling mechanism for each compound in any given solution. As previously demonstrated,² phenols with low pseudo-first-order rates and $< 10\%$ sorption can be classified as having sorption-limited oxidation rates while phenols with greater observed pseudo-first-order rate constants and $>10\%$ sorption are electron transfer-limited. The maximum percent sorption for each studied contaminant in each reaction matrix are provided in **Tables B.6 – B.8**.

Table B.6. Average maximum percent sorption for each phenol at initial concentrations of 10, 20 and 40 μM with no competing compounds in solution. Percent sorption values are the average of triplicate reactions; error is ± 1 standard deviation. Cells with no fill are electron transfer-limited; gray cells indicate reactions are sorption-limited.

	10 μM	20 μM	40 μM
resorcinol	49 ± 4	86 ± 19	45 ± 10
bisphenol A	100 ± 10	99 ± 9	96 ± 26
triclosan	92 ± 28	93 ± 19	84 ± 16
4,4'-biphenol	28 ± 29	19 ± 22	56 ± 32

Table B.7. Average maximum percent sorption for each phenol with competing phenolic compounds in solution, listed at the top of each column. Percent sorption values are the average of triplicate reactions; error is ± 1 standard deviation. Cells with no fill are electron transfer-limited; gray cells indicate reactions are sorption-limited.

	Resorcinol in solution	Bisphenol A in solution	Triclosan in solution	4,4'-Biphenol in solution	All phenols in solution
resorcinol	-	7 \pm 16	29 \pm 3	22 \pm 4	21 \pm 2
bisphenol A	8 \pm 20	-	74 \pm 11	74 \pm 3	80 \pm 35
triclosan	49 \pm 5	65 \pm 15	-	85 \pm 16	100 \pm 7
4,4'-biphenol	52 \pm 7	39 \pm 11	77 \pm 4	-	17 \pm 15

Table B.8. *Tert*-butanol quenched average maximum percent sorption for each phenol with competing phenolic compounds in solution, listed at the top of each column. Percent sorption values are the average of triplicate reactions; error is ± 1 standard deviation. Cells with no fill are electron transfer-limited; gray cells indicate reactions are sorption-limited.

	10 μM	Resorcinol in solution	Bisphenol A in solution	Triclosan in solution	4,4'-Biphenol in solution	All phenols in solution
resorcinol	47 \pm 13	-	48 \pm 15	49 \pm 9	68 \pm 19	100 \pm 15
bisphenol A	99 \pm 6	68 \pm 28	-	83 \pm 5	88 \pm 27	78 \pm 6
triclosan	92 \pm 13	38 \pm 7	82 \pm 4	-	93 \pm 15	97 \pm 3
4,4'-biphenol	81 \pm 6	89 \pm 4	87 \pm 11	70 \pm 11	-	56 \pm 4

Table B.9. Structure-activity and partitioning constants for resorcinol, bisphenol A, triclosan, and 4,4'-biphenol. Constants include the acid dissociation constant (pK_a), energy of the highest occupied molecular orbital (E_{HOMO}), oxidation potential (E_{ox}), log of the octanol:water partitioning coefficient ($\log K_{ow}$) and the pH adjusted value ($\log D_{ow}$), and the log of the organic carbon:water partitioning coefficient ($\log K_{oc}$). Sources for each constant are given in subscript following the column heading.

	pK_a⁵	E_{HOMO} (eV)²	E_{ox} (V vs. SHE)²	$\log K_{ow}$⁵	$\log D_{ow}$⁵	$\log K_{oc}$⁵
resorcinol	9.26	-7.77	1.83	0.93	1.37	2.38
bisphenol A	9.78	-7.49	2.22	3.32	4.05	4.58
triclosan	7.68	-7.78	2.07	4.76	4.98	4.37
4,4'-biphenol	9.64	-7.23	1.82	2.80	3.01	3.93

B.6. Effect of *tert*-butanol

In the presence of *tert*-butanol, triclosan, BPA, and resorcinol all oxidize in a similar manner to the non-quenched 10 μM controls regardless of mixture effects (**Figure 3.3**). Triclosan oxidation rates are only reduced by half with 4,4'-biphenol and an order of magnitude with all four phenols in solution, with no changes in sorption compared to the control. Bisphenol A similarly has no large changes in either pseudo-first-order oxidation rates or sorption compared to the unquenched 10 μM control, including in solution with resorcinol which causes large competition effects in the non-quenched reaction. Resorcinol undergoes more change in reactivity than either triclosan or bisphenol A in the presence of *tert*-butanol with 50% reductions in pseudo-first-order oxidation rates in isolated controls as well as solutions with BPA, triclosan, and 4,4'-biphenol compared to the non-quenched control. There is no change in sorption to the Mn surface in these paired reactions and in solution with all three other contaminants, resorcinol has no change in the pseudo-first-order oxidation rates but an increase in sorption from 47 to 100%.

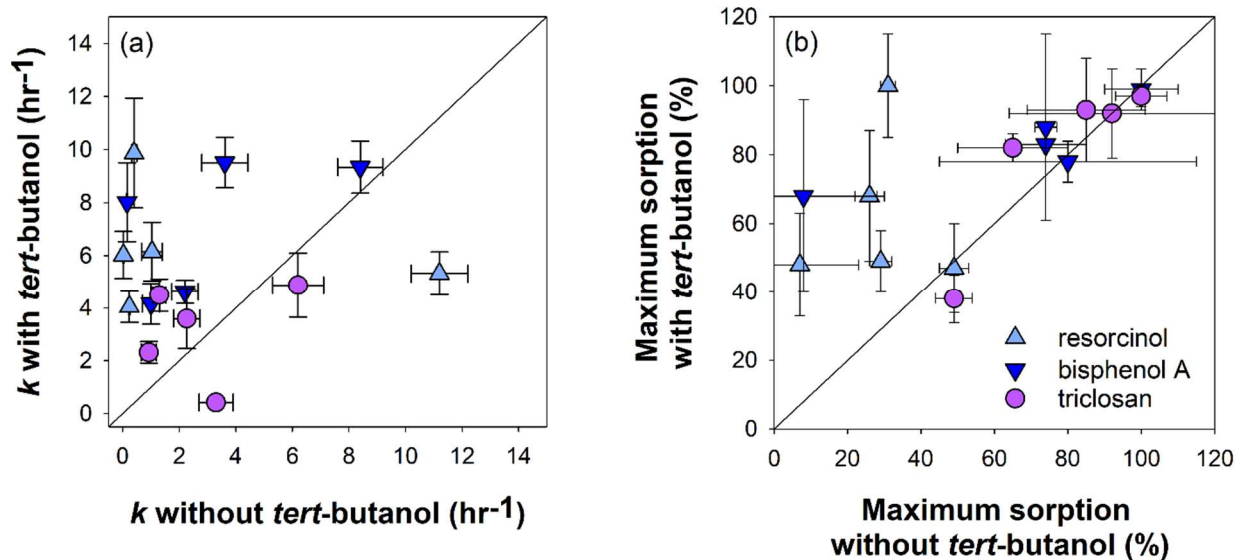


Figure B.2. Plots of (a) pseudo-first-order oxidation rates and (b) maximum percent sorption of triclosan, bisphenol A, and resorcinol reacted with δ - MnO_2 with 2 mM *tert*-butanol in solution versus without *tert*-butanol. Each point is either an isolated reaction or mixture with one or three other phenols in solution. Error bars are ± 1 standard deviation of triplicate reactors.

B.7. References

1. Murray, J. W., The surface chemistry of hydrous manganese dioxide. *J. Colloid Interf. Sci.* **1974**, *46*, (3), 357-371.
2. Trainer, E. L.; Ginder-Vogel, M.; Remucal, C. K., Organic structure and solid characteristics determine reactivity of phenolic compounds with synthetic and reclaimed manganese oxides. *Environ. Sci.: Water Res. Technol.* **2020**, *6*, (3), 540-553.
3. Fowler, R. M.; Bright, H. A., Standardization of permanganate solutions with sodium oxalate. *J. Res. Natl. Bur. Stand.* **1935**, *15*, 493-501.
4. Ohlweiler, O. A.; Schneider, A. M. H., Standardization of potassium permanganate by titration of sodium oxalate in presence of perchloric acid and manganese(II) sulfate. *Anal. Chim. Acta* **1972**, *58*, 477-480.
5. U.S. Environmental Protection Agency, Estimation Programs Interface Suite™ for Microsoft® Windows, V. 4.11; United States Environmental Protection Agency: Washington DC, USA, 2012.

Appendix C

Supplementary Material for Chapter 4: Selective reactivity and oxidation of dissolved organic matter by manganese oxides

C1. Materials

All chemicals were commercially available and used as received. Methanol (HPLC grade), hydrochloric acid (Certified ACS Plus grade), sodium chloride (Certified ACS grade), acetonitrile (HPLC grade), potassium permanganate (Certified ACS grade; KMnO_4), sodium bicarbonate (Certified ACS grade; NaHCO_3), and sodium hydroxide (Certified ACS grade; NaOH) were purchased from Fisher Scientific. Nitric acid (70%) was purchased from Sigma-Aldrich. Solid-phase extraction (SPE) cartridges were purchased from Agilent Technologies (500 mg BondElut PPL).

Acid birnessite (MnO_2) was synthesized according to McKenzie.¹ A 6M HCl solution was added dropwise (<1 mL/min) to a boiling 0.67 M KMnO_4 solution while stirred vigorously in a 3:20 HCl: KMnO_4 volume ratio. The solution remained boiling for 60 minutes before cooling to room temperature and reheating to 60 °C, all while continuously stirring. The 60 °C solution was covered and allowed to react for ~18 hours then cooled to room temperature. The manganese oxide particles were filtered by vacuum filtration through a 0.22 μm nylon filter,

rinsed thoroughly with MQ to remove any remaining reactants and freeze dried. The dried solids were stored dark at room temperature until reaction.

All glassware was combusted for 8 hours at 450 °C prior to use. Ultrapure water was supplied by a Milli-Q water purification system maintained at 18.2 MΩ·cm.

C.2. Sampling and water chemistry

C.3.1. Sampling

Sampling locations are shown in **Figure C.1**. One wastewater effluent sample was collected from the Western Lake Superior Sanitary District (WLSSD) treatment plant in Duluth, MN following seasonal disinfection by sodium hypochlorite and dechlorination using sodium bisulfite (WW1). Final wastewater effluent was also collected from the Madison Metropolitan Sewerage District (MMSD) in Madison, WI both before (WW2) and after UV disinfection (WW3). The WLSSD wastewater plant treats both municipal and industrial wastewater while MMSD primarily treats municipal wastewater.

The Blatnik Bridge and Badfish Creek samples were collected downstream of the WLSSD and MMSD effluent releases, respectively. The water in the St. Louis River at Blatnik Bridge is < 5% wastewater effluent by a conservative mixing model,² while Badfish Creek downstream is composed primarily of effluent at that point. Due to these differences, as well as statistical cluster analyses (**Figure C.8**), Blatnik Bridge is designated as a river sample (R9) while the downstream Badfish Creek sample is designated as a wastewater (WW4).

Madison, WI collection sites from the Yahara River and Badfish Creek chain include R1, collected from the upstream Yahara River surrounded by conserved wetlands, lakes E1-E3 collected from the middle of the respective lakes in the urbanized Madison area, and R2

collected downstream of the urban Madison area. R3 was collected immediately upstream MMSD wastewater effluent release point (WW4) in an agricultural area with forested lands buffering the agricultural fields from the creek. R4 was collected where Badfish Creek (R3) feeds the Yahara River and is the most downstream site sampled from the Yahara watershed.

Samples O1-O4, B1-B2, and M3 are well-studied waterbodies in the North Temperate Lakes-Long Term Ecological Research (NTL-LTER) network.³ Sites M1 and M2 are south of the NTL-LTER sites but have similar surrounding land use, while lake E4 is in southern Wisconsin. All of these lakes are surrounded by a mixture of forested and agricultural lands but are different sizes and represent a range of trophic statuses as designated by their acronyms.

St. Louis River collection sites include R5, collected from a tributary feeding the main branch of the river, and sites R6-R8 which were each sampled directly from the river. Samples E5, E6, and E7 were collected from the barrier peninsula between Lake Superior and Superior Bay and have been previously categorized as eutrophic,⁴ while O5 was collected from the shore of Lake Superior near the St. Louis River estuary. These samples from the St. Louis River into Lake Superior range in land use and composition from terrestrial wetlands (R5) to urban industrial surroundings in Duluth, MN to the large microbially processed Lake Superior.

C.2.2 Water chemistry

All water samples were analyzed for initial water chemistry within two weeks of sample collection and filtration. Some of the waters included in this study from the St. Louis River Estuary were also included in a previous study from Berg et al.² and the same initial water chemistry values are reported here, with the exception of cations as the waters were reanalyzed on an upgraded instrument with better detection limits. The concentration of dissolved organic

carbon ([DOC]) was measured with a Shimadzu total organic carbon analyzer and calibrated to a standard of potassium hydrogen phthalate. Alkalinity was measured using a Mettler Toledo G20 autotitrator calibrated with pH 4, 7, and 10 standards (Aqua Solutions). Samples were titrated to an endpoint of pH 4.5 and reported with units of mg of $\text{CaCO}_3 \text{ L}^{-1}$ (**Table C.2**).

A Shimadzu 2401PC Spectrophotometer was used to measure ultraviolet-visible (UV-vis) absorbances of whole water samples. Spectra were collected from 200-800 nm in 1 nm intervals and corrected by blank subtraction (Milli-Q water reference), as well as subtraction of the average absorbance from 700-800 nm to account for light scattering. From the corrected spectra, we characterized the bulk natural organic matter by specific ultraviolet absorbance at 254 nm (SUVA_{254}), which is equivalent to the absorbance at 254 nm divided by the dissolved organic carbon concentration in mg-C/L. We also calculated the $E_2:E_3$ spectral ratio from the corrected spectra, which is equal to the absorbance at 250 nm divided by the absorbance at 365 nm. Initial values are reported in **Table C.2**.

Anion concentrations were measured using anion exchange chromatography on a Dionex ICS-2100 with a Dionex IonPac AS11-HC RFIC 4 x 250 mm column. Chloride, nitrate, nitrite, sulfate, and phosphate were all measured with an isocratic method using 30 mM sodium hydroxide at 1.0 mL per minute flow rate over 20 minutes. Phosphate was not detected in any samples (< 0.3 ppm) and is not included in the following water chemistry tables; all other values are shown in **Table C.3**.

Cations were measured using an Agilent 5110 VDV inductively coupled plasma-optical emission spectrometer (ICP-OES) and calibrated using commercially available standards. Typical water cations (calcium, magnesium, potassium, and sodium) were analyzed in addition

to aqueous iron and manganese. Aqueous manganese concentrations were below the limit of detection (0.1 ppm) in all waters. Concentrations are listed in **Table C.4**.

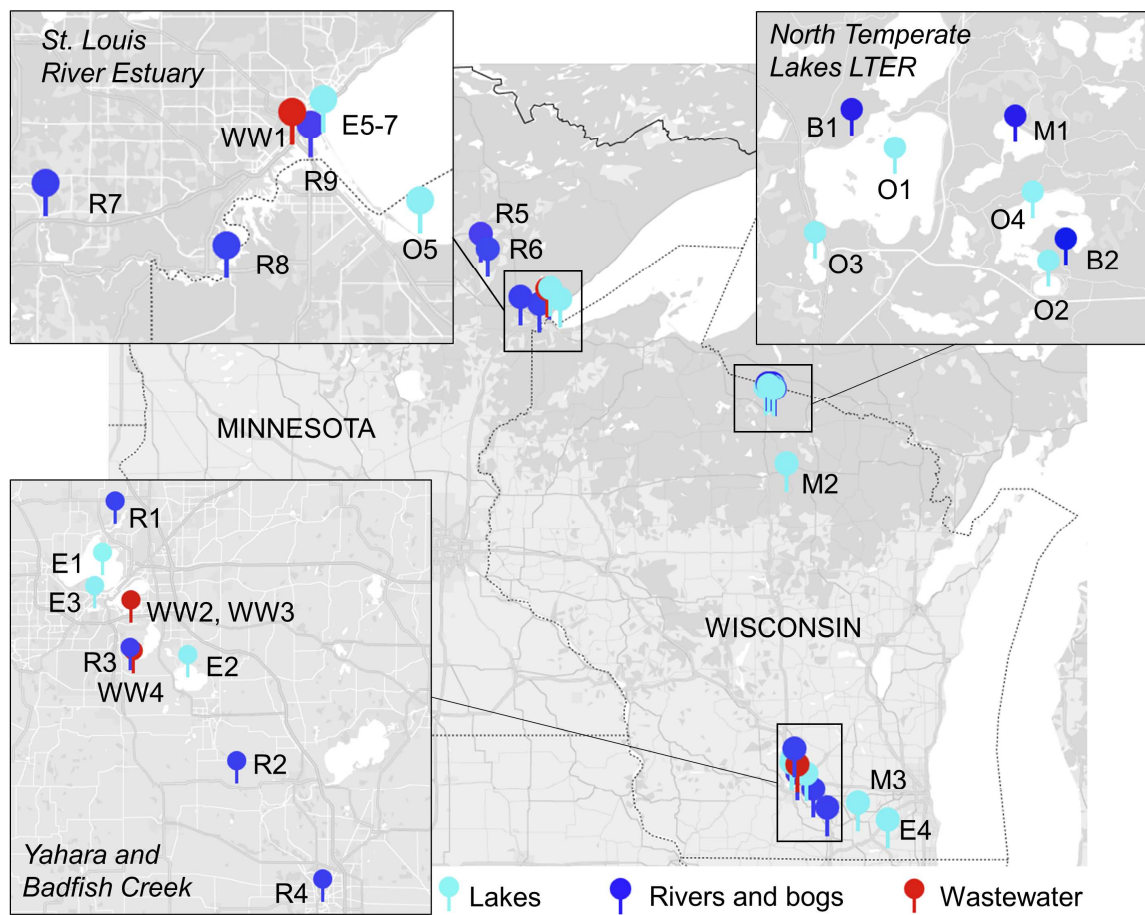


Figure C.1. Maps of sampling locations, color coded by water type. **Table C.1** lists the full name and coordinates for each sampling site.

Table C.1. Sampling site coordinates and sample collection dates. Abbreviations correspond to bogs (B), eutrophic lakes (E), mesotrophic lakes (M), oligotrophic lakes (O), rivers (R), and wastewater effluent or wastewater-impacted sites (WW).

Sample Name	Abbreviation	Coordinates	Year
<i>St. Louis River Estuary</i>			
Blatnik Bridge	R9	46.751031, -92.102092	2017
East Detroit	R7	46.651824, -92.203205	2017
Park Point West	E5	46.771889, -92.087935	2017
Park Point 2	E6	46.731359, -92.055793	2017
Park Point 3	E7	46.743405, -92.064993	2017
River Inn	R8	46.702892, -92.418854	2017
Sand Creek	R5	47.185510, -92.853331	2017
Meadowlands	R6	47.068966, -92.775002	2017
WLSSD Effluent	WW1	46.761325, -92.124443	2019
Wisconsin Point	O5	46.688643, -91.972299	2017
<i>Yahara and Badfish Creek</i>			
Badfish Creek CE	WW4	42.970995, -89.352258	2019
Badfish Creek DB	R3	42.922992, -89.355636	2019
Confluence	R4	42.832167, -89.171484	2019
Lake Kegonsa	E2	42.966112, -89.256442	2019
Lake Mendota	E1	43.096011, -89.404760	2019
Lake Wingra	E3	43.05348, -89.418864	2019
MMSD Effluent Pre-UV Treatment	WW2	43.035321, -89.356284	2019
MMSD Effluent Post-UV Treatment	WW3	43.035321, -89.356284	2019
North Yahara	R1	43.091840, -89.222930	2019
South Yahara	R2	42.530390, 89.124700	2019
<i>North Temperate Lakes LTER</i>			
Allequash Lake	M1	46.039309, -89.625009	2016
Big Muskellunge Lake	O4	46.019528, -89.618579	2016
Crystal Bog	B2	46.007501, -89.606100	2019
Crystal Lake	O2	46.001836, -89.612853	2016
Sparkling Lake	O3	46.009051, -89.700026	2016
Trout Bog	B1	46.041069, -89.686305	2016
Trout Lake	O1	46.030988, -89.670097	2016
<i>Other sites in WI</i>			
Lake Ivanhoe	E4	42.582945, -88.348455	2019
Seven Island Lake	M2	45.423813, -89.472031	2019
Turtle Lake	M3	42.726021, -88.685101	2019

Table C.2. [DOC], alkalinity, SUVA₂₅₄, and E₂:E₃ of filtered samples. Reported error is the standard deviation of triplicate measurements. N/A indicates data that is unavailable.

Sample Name	[DOC] (mg-C L ⁻¹)	Alkalinity (mg-CaCO ₃ L ⁻¹)	SUVA ₂₅₄ (L mg-C ⁻¹ m ⁻¹)	E ₂ :E ₃
<i>St. Louis River Estuary</i>				
R9	17.4 ± 0.3	12.7 ± 0.1	3.8 ± 0.1	5.0 ± 0.1
R7	20.7 ± 0.2	10.8 ± 0.1	4.0 ± 0.2	4.7 ± 0.1
E5	5.2 ± 0.1	10.4 ± 0.1	3.0 ± 0.1	5.2 ± 0.1
E6	17.0 ± 0.1	11.2 ± 0.1	4.1 ± 0.1	4.7 ± 0.1
E7	17.5 ± 0.2	10.7 ± 0.1	4.1 ± 0.1	4.8 ± 0.1
R8	22.3 ± 0.2	10.7 ± 0.1	4.1 ± 0.1	4.7 ± 0.1
R5	26.9 ± 0.2	5.9 ± 0.1	4.2 ± 0.1	5.0 ± 0.2
R6	24.7 ± 0.4	13.7 ± 0.1	4.1 ± 0.2	4.7 ± 0.1
WW1	18.7 ± 0.3	56.8 ± 0.9	2.6 ± 0.1	6.3 ± 0.1
O5	6.9 ± 0.1	12.6 ± 0.2	2.5 ± 0.1	5.8 ± 0.1
<i>Yahara and Badfish Creek</i>				
WW4	6.6 ± 0.1	N/A	4.8 ± 0.6	3.8 ± 0.1
R3	5.5 ± 0.1	64.6 ± 0.1	3.4 ± 0.3	5.6 ± 0.1
R4	6.8 ± 0.2	55.4 ± 0.1	2.1 ± 0.1	6.8 ± 0.1
E2	7.7 ± 0.1	40.6 ± 0.2	1.8 ± 0.1	8.4 ± 0.2
E1	6.34 ± 0.1	37.6 ± 0.1	1.6 ± 0.2	8 ± 2
E3	6.2 ± 0.2	40.8 ± 0.1	2.0 ± 0.1	6.8 ± 0.3
WW2	8.2 ± 0.1	279 ± 1	2.6 ± 0.1	4.4 ± 0.2
WW3	8.3 ± 0.8	285 ± 1	2.7 ± 0.2	4.0 ± 0.1
R1	7.3 ± 0.1	65.8 ± 0.2	2.5 ± 0.1	7.3 ± 0.1
R2	7.1 ± 0.3	44.2 ± 0.1	1.8 ± 0.1	6.4 ± 0.1
<i>North Temperate Lakes LTER</i>				
M1	6.0 ± 0.1	10.3 ± 0.1	2.6 ± 0.1	6.1 ± 0.1
O4	4.3 ± 0.1	5.8 ± 0.1	0.9 ± 0.1	8.2 ± 0.1
B2	10.4 ± 0.1	1.3 ± 0.1	3.5 ± 0.1	4.6 ± 0.1
O2	2.1 ± 0.1	0.7 ± 0.1	0.5 ± 0.1	14.7 ± 0.5
O3	3.4 ± 0.1	8.2 ± 0.1	1.2 ± 0.1	9.8 ± 0.1
B1	24.8 ± 0.3	1.0 ± 0.1	3.9 ± 0.1	4.4 ± 0.1
O1	2.7 ± 0.1	10.7 ± 0.2	1.4 ± 0.1	9.3 ± 0.2
<i>Other sites in WI</i>				
E4	13.7 ± 0.2	52.0 ± 0.1	3.7 ± 0.2	5.4 ± 0.1
M2	6.1 ± 0.1	N/A	1.7 ± 0.1	7.9 ± 0.1
M3	9.3 ± 0.2	45.8 ± 0.1	2.2 ± 0.1	7.9 ± 0.1

Table C.3. Initial anion concentrations of filtered grab samples measured by ion chromatography. St. Louis River Estuary values (R5-R9, E5-E7, WW1, O5) include those reported by Berg et al.² Reported error is standard deviation of triplicate measurements.

Sample	[Cl ⁻] (ppm)	[NO ₂ ⁻] (ppm)	[NO ₃ ⁻] (ppm)	[SO ₄ ²⁻] (ppm)
<i>St. Louis River Estuary</i>				
R9 ²	16.2 ± 0.2	< 1	0.4 ± 0.1	30.3 ± 5.9
R7 ²	5.0 ± 0.1	< 1	0.7 ± 0.1	9.9 ± 1.8
E5 ²	3 ± 1	< 1	1.1 ± 0.8	< 1
E6 ²	8 ± 3	< 1	0.2 ± 0.1	< 1
E7 ²	8 ± 3	< 1	1.8 ± 0.1	9.1 ± 2.0
R8 ²	4.4 ± 0.6	< 1	1.9 ± 0.1	5.3 ± 0.7
R5 ²	2.1 ± 0.1	< 1	0.9 ± 0.1	9.7 ± 1.8
R6 ²	6.4 ± 2.5	< 1	1.1 ± 0.1	13.1 ± 2.4
WW1 ²	371 ± 1	3.3 ± 0.2	86.2 ± 0.5	267.4 ± 0.9
O5 ²	2.3 ± 0.1	< 1	0.3 ± 0.1	3.7 ± 0.9
<i>Yahara and Badfish Creek</i>				
WW4	460 ± 5	2.4 ± 0.1	72.5 ± 0.5	35.9 ± 2.0
R3	95.7 ± 0.9	4.6 ± 0.2	14.1 ± 0.1	13.6 ± 0.2
R4	72.3 ± 0.3	2.2 ± 0.1	10.2 ± 0.1	18.1 ± 0.2
E2	63.9 ± 0.2	1.9 ± 0.1	< 0.3	11.5 ± 0.2
E1	52.3 ± 0.2	1.8 ± 0.1	< 0.3	14.5 ± 0.2
E3	81.2 ± 0.2	1.9 ± 0.1	< 0.3	11.8 ± 0.4
WW2	357 ± 1	4.5 ± 0.2	74.6 ± 0.5	46.4 ± 0.6
WW3	462 ± 3	4.7 ± 0.2	77.9 ± 0.5	47.5 ± 0.6
R1	45.9 ± 0.2	2.51 ± 0.6	11.3 ± 0.5	15.0 ± 0.2
R2	66.5 ± 0.3	2.0 ± 0.1	0.8 ± 0.5	13.0 ± 0.2
<i>North Temperate Lakes LTER</i>				
M1	0.5 ± 0.2	0.7 ± 0.1	< 0.3	2.9 ± 0.2
O4	0.8 ± 0.2	0.5 ± 0.1	< 0.3	2.4 ± 0.2
B2	1.1 ± 0.2	< 0.3	< 0.3	1.7 ± 0.2
O2	0.6 ± 0.2	< 0.3	< 0.3	2.0 ± 0.2
O3	29.6 ± 0.2	0.8 ± 0.1	< 0.3	3.5 ± 0.2
B1	0.8 ± 0.2	< 0.3	< 0.3	1.9 ± 0.2
O1	2.3 ± 0.2	< 0.3	< 0.3	2.7 ± 0.2
<i>Other sites in WI</i>				
E4	33.2 ± 0.2	< 0.3	< 0.2	3.9 ± 0.2
M2	1.4 ± 0.1	< 0.3	< 0.2	1.2 ± 0.2
M3	33.1 ± 0.1	0.3 ± 0.1	0.3 ± 0.1	16.4 ± 0.2

Table C.4. Initial cation concentrations of filtered grab samples measured by ICP-OES. St. Louis River Estuary values include those reported by Berg et al.² using the same samples. Reported error is the standard deviation of triplicate measurements.

Sample	[Fe] (ppm)	[Na ⁺] (ppm)	[K ⁺] (ppm)	[Ca ²⁺] (ppm)	[Mg ²⁺] (ppm)
<i>St. Louis River Estuary</i>					
R9 ²	< 0.1	23 ± 0.3	8.1 ± 0.9	23.3 ± 0.3	9.7 ± 0.2
R7 ²	< 0.1	5.1 ± 0.1	8.2 ± 0.7	18.4 ± 0.2	10.1 ± 0.1
E5 ²	< 0.1	5.2 ± 0.2	0.9 ± 0.1	10.2 ± 0.1	4.3 ± 0.1
E6 ²	0.37 ± 0.01	2.7 ± 0.1	1.1 ± 0.1	13.4 ± 0.1	6.0 ± 0.1
E7 ²	0.39 ± 0.01	2.8 ± 0.1	1.1 ± 0.1	14.2 ± 0.1	6.4 ± 0.1
R8 ²	0.12 ± 0.01	4.8 ± 0.1	10.5 ± 0.4	17.0 ± 0.3	9.9 ± 0.1
R5 ²	0.63 ± 0.05	1.9 ± 0.1	12.7 ± 0.7	14.8 ± 0.2	4.0 ± 0.1
R6 ²	0.25 ± 0.02	4.8 ± 0.2	1.0 ± 0.1	9.8 ± 0.2	7.9 ± 0.2
WW1 ²	< 0.1	202.1 ± 2.8	4.3 ± 0.6	58.2 ± 1.4	10.2 ± 0.2
O5 ²	< 0.1	2.2 ± 0.1	6.0 ± 0.2	15.2 ± 0.2	3.5 ± 0.1
<i>Yahara and Badfish Creek</i>					
WW4	0.09 ± 0.01	60.7 ± 0.4	10.5 ± 0.1	84.4 ± 0.1	41.3 ± 2.8
R3	< 0.1	17.1 ± 0.4	5.3 ± 0.1	64.8 ± 0.2	30.1 ± 2.2
R4	< 0.1	36.4 ± 0.2	2.8 ± 0.1	37.23 ± 0.3	30.5 ± 0.9
E2	< 0.1	10.4 ± 0.4	2.2 ± 0.2	27.1 ± 0.1	8.4 ± 0.6
E1	< 0.1	13.8 ± 0.1	2.9 ± 0.1	15.7 ± 0.3	3.3 ± 0.1
E3	< 0.1	8.1 ± 0.3	1.9 ± 0.1	43.9 ± 0.2	25.1 ± 0.9
WW2	< 0.1	71.0 ± 6.2	11.4 ± 0.4	84.7 ± 1.1	45.7 ± 0.6
WW3	< 0.1	71.2 ± 0.3	12.1 ± 0.2	85.2 ± 0.3	45.3 ± 0.2
R1	< 0.1	23.5 ± 0.3	2.1 ± 0.2	61.3 ± 0.3	35.9 ± 0.6
R2	< 0.1	42.4 ± 2.9	3.2 ± 0.1	51.9 ± 0.3	33.8 ± 0.9
<i>North Temperate Lakes LTER</i>					
M1	< 0.1	3.6 ± 0.2	0.4 ± 0.1	7.6 ± 0.4	5.6 ± 0.1
O4	< 0.1	1.7 ± 0.2	0.6 ± 0.2	4.3 ± 0.2	3.4 ± 0.3
B2	0.14 ± 0.01	2.9 ± 0.3	0.8 ± 0.3	0.7 ± 0.1	0.2 ± 0.1
O2	< 0.1	0.4 ± 0.1	0.8 ± 0.2	1.0 ± 0.1	0.2 ± 0.2
O3	< 0.1	3.4 ± 0.2	0.5 ± 0.1	11.8 ± 0.3	3.4 ± 0.2
B1	0.18 ± 0.02	0.7 ± 0.2	0.3 ± 0.1	3.0 ± 0.2	0.5 ± 0.1
O1	< 0.1	6.4 ± 0.5	0.4 ± 0.2	7.4 ± 0.2	6.0 ± 0.7
<i>Other sites in WI</i>					
E4	0.24 ± 0.02	16.1 ± 0.3	1.5 ± 0.1	55.2 ± 0.3	22.9 ± 0.6
M2	< 0.1	1.1 ± 0.2	0.5 ± 0.2	3.7 ± 0.2	1.4 ± 0.2
M3	< 0.1	13.4 ± 0.1	1.8 ± 0.3	38.2 ± 0.1	30.4 ± 0.1

Table C.5. Samples included in each phase of this study as marked by an X.

Reaction	Short-term kinetic	50-hour bulk	28-day bulk	FT-ICR MS
Number	1	30	30	14
<i>St. Louis River Estuary</i>				
R9		X	X	X
R7		X	X	
E5		X	X	
E6		X	X	
E7		X	X	
R8		X	X	
R5		X	X	X
R6		X	X	X
WW1	X	X	X	X
O5		X	X	X
<i>Yahara and Badfish Creek</i>				
WW4		X	X	X
R3		X	X	X
R4		X	X	
E2		X	X	X
E1		X	X	
E3		X	X	X
WW2		X	X	X
WW3		X	X	X
R1		X	X	
R2		X	X	
<i>North Temperate Lakes LTER</i>				
M1		X	X	X
O4		X	X	
B2		X	X	
O2		X	X	
O3		X	X	
B1		X	X	X
O1		X	X	X
<i>Other sites in WI</i>				
E4		X	X	
M2		X	X	
M3		X	X	

C.3. 50-hour kinetic transformations

To identify kinetic trends in the initial interactions between DOM and Mn oxides and to determine how long reactions must proceed to generate quantifiable results, we analyze kinetic timepoints for acid birnessite reacted with a chlorinated wastewater effluent (WW1). This wastewater sample has low aromaticity and should be less susceptible to oxidation by acid birnessite as wastewaters generally have fewer phenolic moieties than natural waters.² Therefore, we expect this DOM to transform either on the same time scale, or slower, than more aromatic natural waters.

The WW1 sample was analyzed for time resolved changes in bulk DOM, aqueous Mn, and average manganese oxidation number (AMON) at the Advanced Photon Source at line 10-BM. Following reaction, acid birnessite-coated filter papers were immediately folded to increase the amount of Mn in the beam path, Kapton taped, and analyzed by quick X-ray absorption near edge spectroscopy (Q-XANES). Q-XANES samples were measured in triplicate at 4 spots on each prepared filter to elucidate AMON changes from either beam damage or delayed redox reactions with sorbed organic matter. This procedure was repeated for each kinetic timepoint, ranging from 1 minute to 50 hours, and filtrates were preserved for characterization.

Changes in the AMON, aqueous Mn concentration, dissolved organic carbon concentration, and bulk DOM characteristics $SUVA_{254}$ and $E_2:E_3$ are analyzed for each timepoint over the first 50 hours of reaction. Current knowledge of the oxidation of organic compounds by Mn oxides suggests sorption must occur for oxidation followed by possible desorption of the oxidized organic products.⁵⁻⁸ From this theory, we expect to see no change or a slight decrease in [DOC] over time resulting from sorption to the Mn surface. Based on previous reports of DOM isolates or model compound oxidation by Mn oxides, we hypothesize $SUVA_{254}$ values will

decrease as aromatic formulas specifically sorb or transform. Similarly, $E_2:E_3$ values should increase as the average molecular weight decreases with the transformation and degradation of organic matter, although specific oxidation products may have larger molecular weights than their reduced precursors. For acid birnessite, we hypothesize small decreases in AMON, reflecting Mn reduction, accompanies DOM oxidation; alternatively, aqueous Mn(II/III) cations may desorb from reactive surface sites resulting in greater aqueous Mn concentrations and less change within the bulk AMON.

Reactions with WW1 DOM support these hypothesized changes after 50 hours of reaction for [DOC], which decreases from 8.8 to 7.4 mg-C/L, and $E_2:E_3$, which increases from 5.43 to 9.8 (**Figure C.2**). $SUVA_{254}$ values increase from 2.13 to 2.31 L mg-C⁻¹ m⁻¹. The changes in UV-vis parameters indicate that the wastewater DOM decreases in average molecular weight, while increasing in aromaticity over 50 hours. This may be the result of direct transformation to smaller, lower molecular weight compounds and/or selective sorption of large molecular weight compounds to the Mn surface lowering both the average molecular weight of the remaining aqueous DOM pool and the DOC concentration.

The acid birnessite oxidation state also changes over this 50-hour reaction by dropping from an initial AMON of 3.74 to a final value of 3.65, indicating a slight reduction of the bulk Mn solid compared to the carbonate control which increases slightly. However, the AMON initially increases unexpectedly by 0.1-0.2 units over the first 30 minutes of reaction (similar to the control; **Figure C.2d**). These increases are likely due to the release of any low oxidation state Mn present from surface or vacancy sites into solution as the solid mixes into the reaction matrix and the subsequent reduction of the WW1 sample can then be attributed to the presence of DOM in solution.

As with AMON values, $SUVA_{254}$ and $E_2:E_3$ also peak over the first 30 minutes of reaction. $SUVA_{254}$ values increase from 2.13 to 3.09 $L\ mg-C^{-1}\ m^{-1}$ and $E_2:E_3$ increases from 5.43 to 6.91 initially (**Figures C.2b** and **C.2c**), indicating immediate sorption or transformation of the bulk DOM pool decreases the average molecular weight while increasing aromaticity. These initial transformations which occur within the first 30 minutes and are not sustained over 50 hours agree with other studies reporting fast, then slow, sorption kinetics by time resolved dynamic light scattering⁵ and the formation of chromophoric DOM intermediates which are no longer observed after sustained reactions.⁹ Since each bulk DOM characteristic appears to undergo these intermediary reactions for the first 30 minutes to 1 hour of reaction then transform more consistently through 50-hour timepoints, 50 hours is used for our subsequent reactions comparing the reactivity of diverse DOM sources.

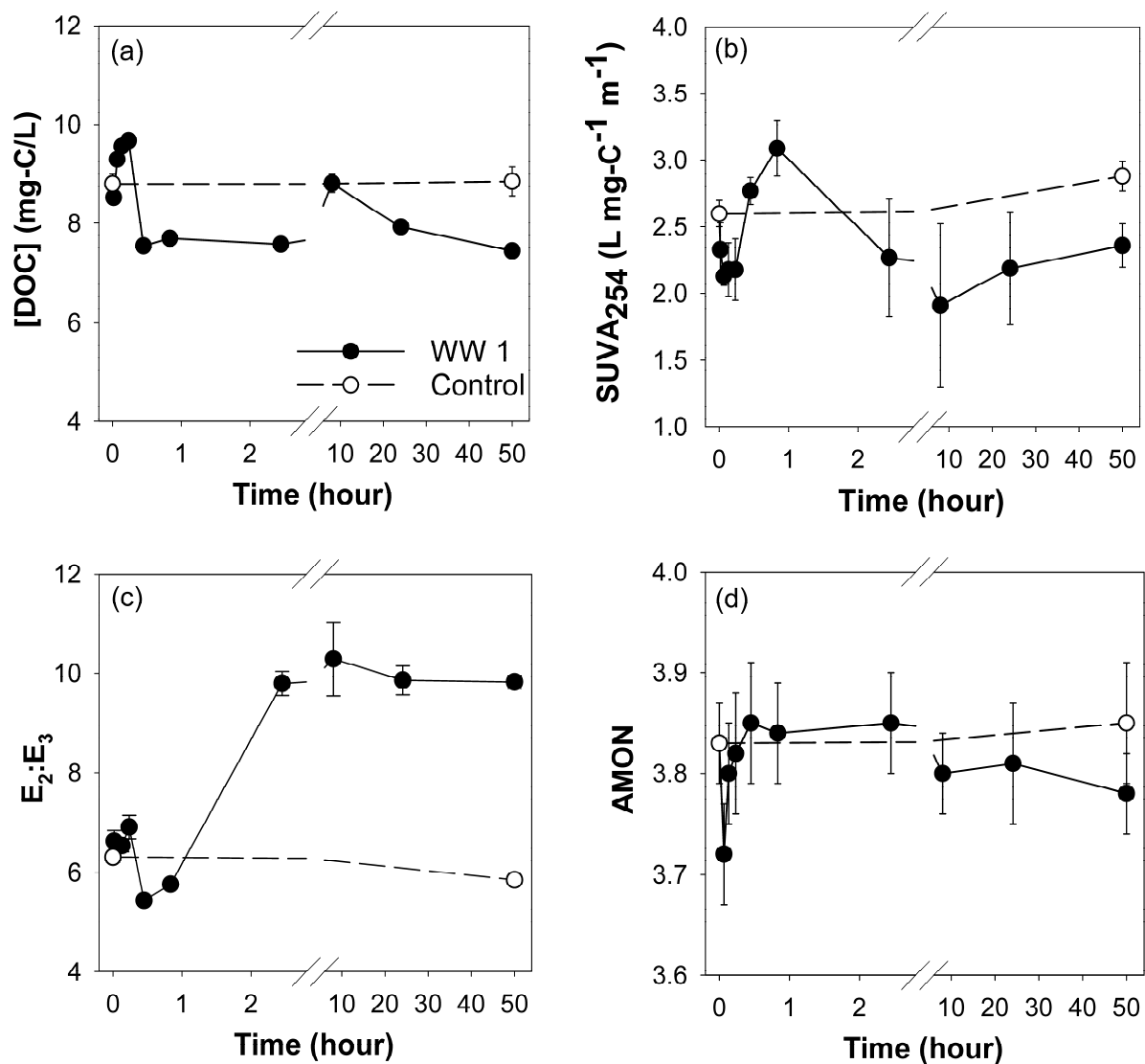


figure C.2. Time series plots of bulk changes in (a) DOC, (b) SUVA₂₅₄, (c) E₂:E₃, and (d) AMON. Error bars represent (a-c) standard deviation of triplicate measurements and (d) XANES and linear combination fitting method error as determined by Manceau et al.¹⁰

C.4. 28-day bulk transformations

All 50-hour bulk reactions were repeated for 28 days with the same 30 DOM samples to determine if the observed 50-hour changes are indicative of longer-term processes. While some waters change considerably between the 50-hour and 28-day timepoints, the majority do not change appreciably and any changes that occur are generally within error of the 50-hour sample or represent further transformation in the same direction.

For bulk organic matter characterization, no more [DOC] is appreciably lost after 28 days compared to 50 hours for any of the 30 DOM samples, suggesting [DOC] removal by sorption and/or colloid formation is a relatively fast process in the transformation of DOM by MnO_2 . Seven waters have positive SUVA_{254} changes indicating increasing aromaticity of the dissolved DOM pool. These 7 waters have low initial SUVA_{254} values, with the exception of E5 which has the greatest control SUVA_{254} value yet also increases in aromaticity. Fourteen samples have lower $E_2:E_3$ values than the controls, indicating an increasing average molecular weight, although these samples do not follow any trends with initial water characteristics. The remaining 23 and 16 waters, respectively, follow the same trends with initial SUVA_{254} as described for 50 hour reactions although the trend for $E_2:E_3$ is much weaker than after 50 hours ($R^2 = 0.053$; **Figure C.3**).

Large bulk AMON differences are measured for 9 waters following 28-day reactions. Seven samples (O3, E2, E5, R1, R5, R6, and B1) have final AMON values of 3.38 – 3.68, which fall within the expected range following Mn reduction by DOM, while O1 and O4 have final AMON values of 2.25 and 2.43, respectively, which are lower than expected. It is worth noting that samples O1 and O4 (i.e., the two waters with AMON values near 2) also have the least filter-passing Mn. The MnO_2 in these samples may have been reduced; however, instead of being

released or stabilized in solution as is observed in other waters, the reduced Mn may remain sorbed to the surface or ingrained within the bulk solid matrix, lowering both the AMON and measured aqueous Mn concentrations compared to the other 28 waters. These two waters also have very low initial SUVA₂₅₄ values of 1.24 and 1.31 L mg-C⁻¹ m⁻¹ which may contribute to this observed transformation of Mn (**Figure C.3**).

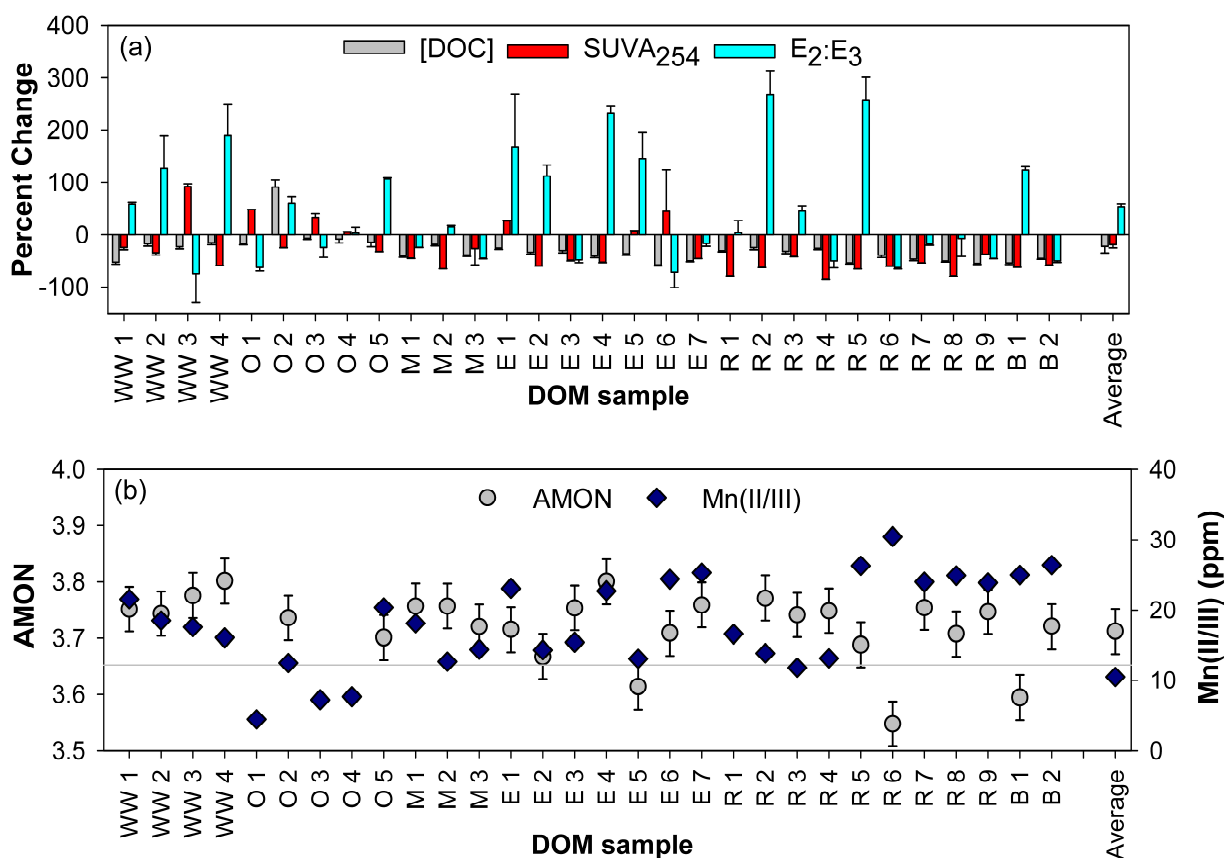


Figure C.3. Percent changes in (a) DOC, SUVA₂₅₄, and E₂:E₃; and (b) aqueous Mn(II/III) and AMON after 28-day reactions. Error bars represent (a) standard deviation of triplicate measurements and (b) standard deviation of triplicate Mn(II/III) measurements and AMON linear combination fitting method error as determined by Manceau et al.¹⁰

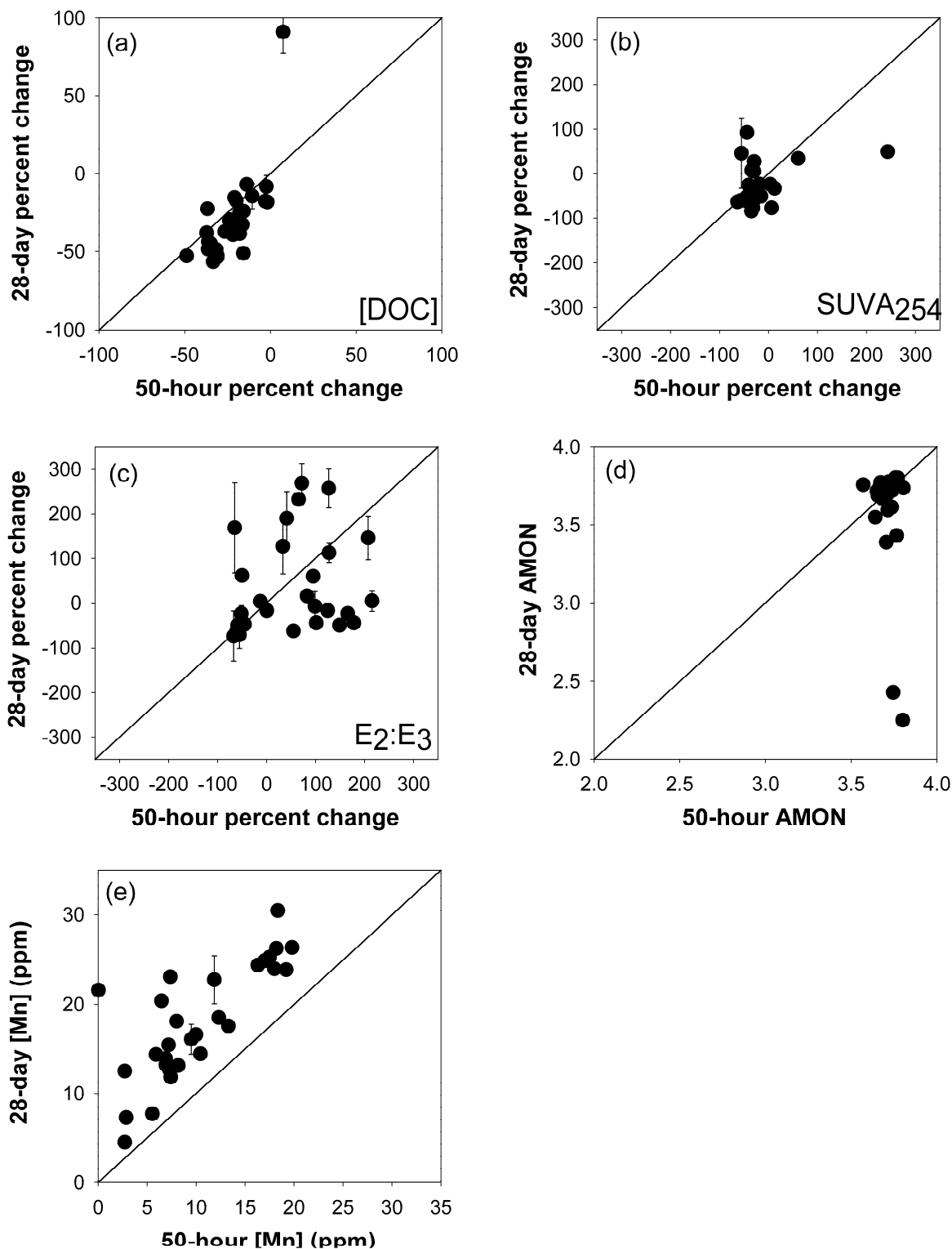


Figure C.4. Comparisons in percent change of (a) [DOC], (b) E₂:E₃, and (c) SUVA₂₅₄ between 50-hour reactions and 28-day reactions. Comparisons of absolute measured values of (d) AMON and (e) Mn(II/III) for 50-hour and 28-day reactions. Error is ± 1 standard deviation of triplicate measurements in plots (a), (b), (c), and (e). Error in plot (d) is the linear combination fitting error determined by Manceau et al.¹⁰

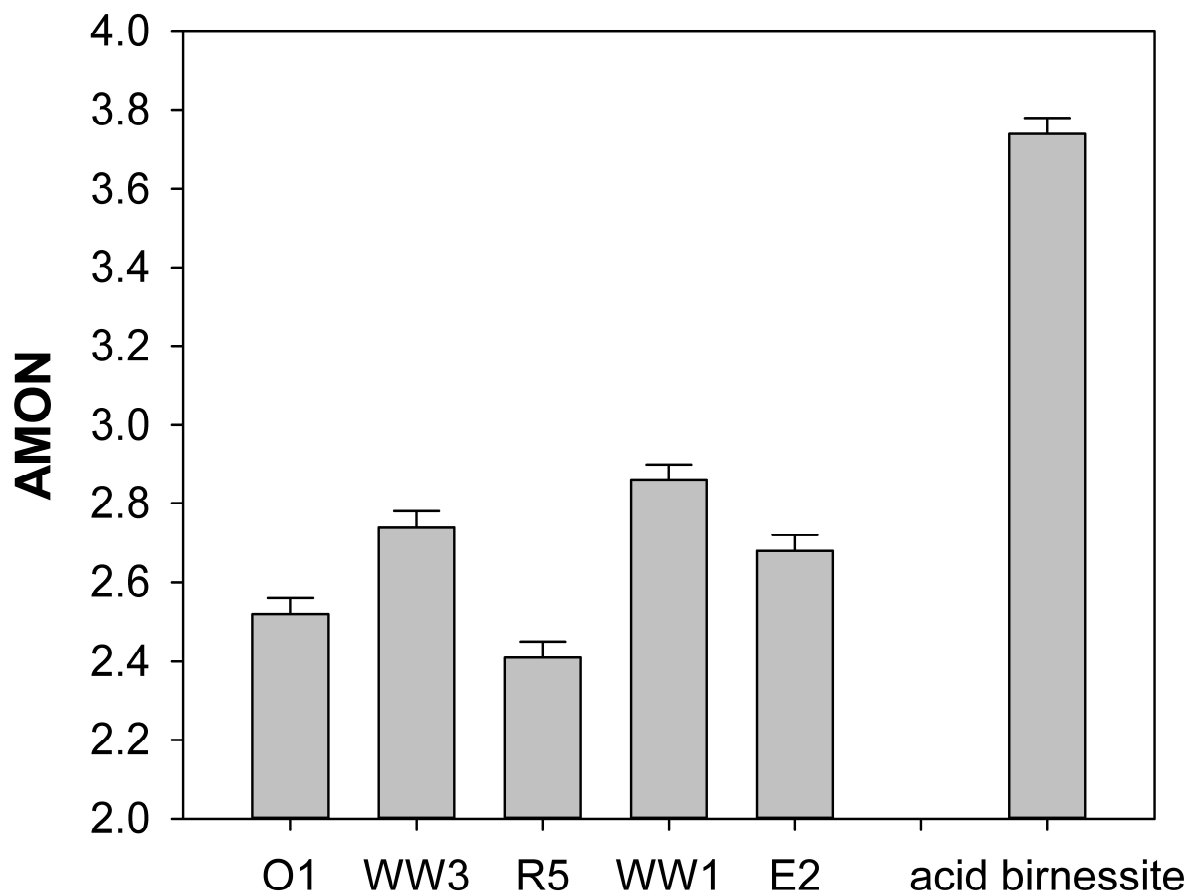


Figure C.5. Average manganese oxidation number of particles formed after reactions of MnO_2 in the initial filtrate. AMON values and error are calculated by linear combination fitting.¹⁰

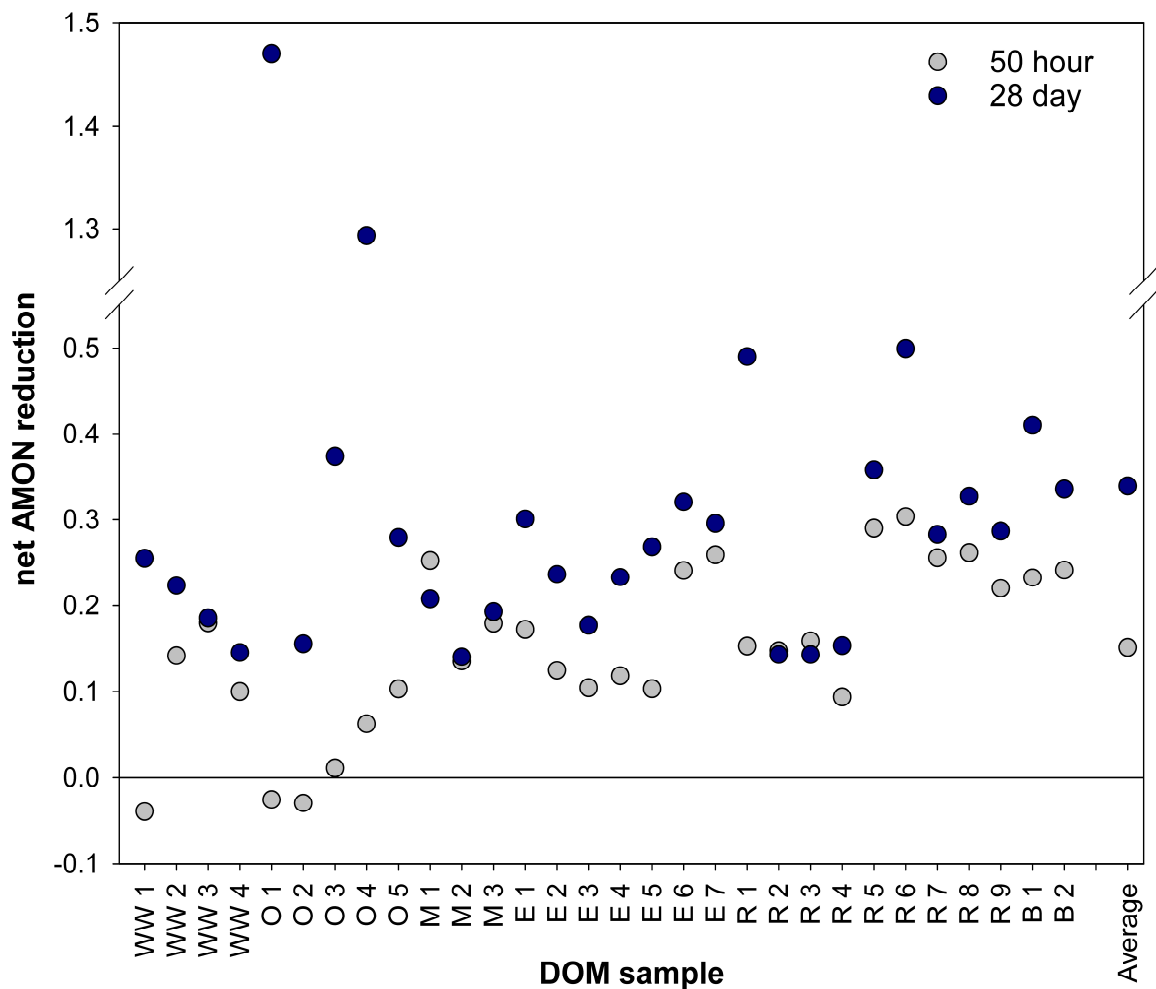


Figure C.6. Net Mn reduction of acid birnessite after 50-hour or 28-day reactions with DOM. Net Mn reduction is calculated as the difference between the starting AMON (3.74) and a mass balance after reaction, using the measured solid AMON and the concentrations and average AMON (2.64) of filtrate Mn(II/III). AMON values and Mn(II/III) concentrations are given in **Figure 3.1** and **Figure C.3**.

Table C.6. Percent change in measured DOM characteristics during reaction with MnO₂. Values which increase during reaction are shaded green while decreases are shaded red; lighter colors indicate changes less than 2% in either direction. Gray boxes mark unavailable data.

	[DOC]	E ₂ :E ₃	SUVA ₂₅₄	H:C _w	DBE _w	MW _w	O:C _w
Hypothesized Changes	Decrease	Increase	Decrease	Increase	Increase	Decrease	Increase
Average change	-22.0	54.5	-18.9	1.2	-2.4	-10.7	-1.4
WW 1	-15.8	95.0	-18.1	-3.2	8.9	1.5	6.9
WW 2	-19.9	33.2	12.6	-0.5	-2.4	-5.2	-0.2
WW 3	-36.8	-67.4	-43.9	-0.7	-2.9	-21.2	-0.4
WW 4	-21.0	41.2	-29.6	5.5	-8.0	-21.9	-13.6
O 1	-3.1	-60.8	243.5	0.2	-1.5	-23.7	3.2
O 2	7.4	-50.0	3.5				
O 3	-13.9	-51.5	60.8				
O 4	-2.3	-12.9	-29.8				
O 5	-10.7		-32.5	1.2	-0.7	-3.0	-0.4
M 1	-18.0	165.8	-27.6	3.1	-2.8	-5.5	-3.2
M 2	-1.8	82.6	-63.2				
M 3	-26.6	101.4	-40.4				
E 1	-17.9	-65.3	-29.3				
E 2	-16.3	127.3	-29.1	0.1	-1.9	-10.9	0.8
E 3	-23.7	-45.0	-26.6	0.7	-3.9	-19.0	1.0
E 4	-21.9	65.5	-15.2				
E 5	-20.2	207.4	-34.3				
E 6	-33.4	-55.5	-55.1				
E 7	-36.4	0.4	-30.9				
R 1	-24.0	215.1	6.4				
R 2	-15.7	71.8	-45.8				
R 3	-19.9		-23.6	2.2	-3.2	-11.2	-2.5
R 4	-17.8	-59.1	-34.8				
R 5	-31.0	126.9	-38.1	2.5	-3.9	-4.8	-3.3
R 6	-37.2	54.8	-36.7	4.0	-4.6	-3.2	-5.2
R 7	-34.9	124.8	-44.0				
R 8	-31.6	98.9	-31.6				
R 9	-31.1	178.1	-36.5	1.0	-1.8	-9.0	-1.3
B 1	-48.9		-56.0				
B 2	-36.2	149.2	-42.9	1.3	-4.2	-13.4	-1.1

C.5. Mass spectrometry

C.5.1. Sample preparation

Organic matter was extracted from both control and treated whole water samples in a matrix of pH 7.0 ± 0.5 10 mM NaHCO₃ buffer. Treated samples were filtered prior to extraction with 0.22 μ m nylon filters. Solid phase extraction was conducted using 500 mg Agilent PPL cartridges as described previously.^{2,11,12} Control waters and filtered treated waters (250 mL) were acidified with hydrochloric acid to pH 2 and extracted through pre-wetted SPE cartridges. Hydrochloric acid (1 mL, 0.01 M) was then passed through the filters to rinse any salts retained on the cartridge material and cartridges were dried for 5 minutes. DOM extracts were eluted in 2.5 mL of methanol and stored in the dark in combusted amber vials at 4°C.

C.5.2 FT-ICR MS Analysis

SPE extracts were diluted 100x in a 50:50 acetonitrile:Milli-Q water solution and directly injected into a Bruker Solarix XR 12T Fourier transform-ion cyclotron resonance mass spectrometer (FT-ICR MS). Samples were ionized by electrospray ionization in negative mode at -1.4 kV with 0.3 psi gas pressure. Accumulation time was either 0.5 or 1.0 seconds, chosen for each sample to record approximately 10^8 counts per scan, and 350 scans were collected per sample from 202 to 1000 m/z . Peaks with signal to noise ratios > 3 with an absolute intensity threshold of 1,000,000 were exported for analysis.

Exported results were analyzed in R using code developed by the Remucal group and reported previously.^{2,12-16} Specifically, exported m/z peaks were converted to neutral masses and linearly calibrated with known formulas found in DOM samples.¹⁷ Potential masses for formula matching included C₁₋₁₈₀¹³C₀₋₁H₁₋₁₄₀O₀₋₈₀N₀₋₁S₀₋₁P₀₋₁. Mass error cutoffs of 0.5 ppm were applied

to individual samples to minimize error away from calibrated m/z values. Potential masses were also required to fall within a homologous series (CH_4 v. O or $+\text{CH}_2$) with at least three members.¹⁷

The number of formulas identified in each water sample and the breakdown of CHO, CHON, CHOS, and CHOP formulas are shown in **Table C.9**. Cl was excluded from formula matching due to the potential of Cl adduct formation in waters acidified with HCl. The intensity of each matched formula m/z peak was used to calculate the relative intensities, equal to the intensity of any individual peak divided by the total intensity across all m/z peaks.

The formulas matched for each control and treatment sample are visualized on van Krevelen diagrams which allow for comparison of structurally similar compounds (e.g., lignin-like, tannin-like) and molecular formula characteristics (e.g., double bond equivalents (DBE)) across waters. Following formula matching procedures, relative intensities were calculated for each m/z peak by dividing the absolute intensity of the peak by the total intensity of all identified formulas within the sample. Similarly, we determined weighted H:C, O:C, molecular weights, and double bond equivalents (H:C_w , O:C_w , MW_w , and DBE_w) values for each sample by averaging the products of each formula's relative intensity and H:C, O:C, MW, or DBE, respectively.

Principal component analysis (PCA) was conducted in R using `prcomp` to determine water clustering patterns and classify samples for comparative analysis. The resulting PCA plots using the relative intensities of matched formulas in control samples and treated samples, as well as the change in relative intensities between control and treated samples, are shown in **Figure C.8**. Finally, we calculated the linear distance between control and treated samples in **Figure C.9** as a proxy for the extent of transformation by MnO_2 .¹⁸

C.6. Linear correlations

Table C.7. Linear correlation statistics between various initial bulk characteristics, absolute changes in AMON and Mn(II/III), and percent changes in bulk characteristics from 50-hour reactions with MnO₂. Both absolute delta values and percent changes were calculated as the final value minus the initial value. Slope (m) and intercept (b) are reported for a line of the form $y = mx + b$. p-values from 2-tailed t-tests are reported and cells are shaded for significant results ($p < 0.05$). X-variables are listed in first row and y-variables in first column of table.

	[DOC] control	E ₂ :E ₃ control	SUVA ₂₅₄ control	Ionic Strength	[SO ₄ ²⁻]
% [DOC]	n = 30 m = -4.90 b = 4.09 R ² = 0.596 p = 5.01E-7	n = 29 m = 0.24 b = -23.82 R ² = 5.87E-4 p = 0.901	n = 30 m = -6.41 b = -2.80 R ² = 0.215 p = 0.010	n = 30 m = -7.15E-6 b = -21.88 R ² = 7.00E-4 p = 0.900	n = 28 m = 0.16 b = -22.00 R ² = 0.004 p = 0.788
Delta SUVA ₂₅₄	n = 27 m = -0.26 b = 0.57 R ² = 0.250 p = 0.005	n = 27 m = -0.08 b = -0.33 R ² = 0.011 p = 0.590	n = 27 m = -0.77 b = 1.51 R ² = 0.472 p = 1.33E-5	n = 27 m = 2.85E-6 b = -0.86 R ² = 0.017 p = 0.478	n = 27 m = 9.38E-4 b = -0.75 R ² = 0.002 p = 0.798
% SUVA ₂₅₄	n = 30 m = -11.80 b = 43.67 R ² = 0.178 p = 0.020	n = 29 m = -7.87 b = 27.00 R ² = 0.031 p = 0.359	n = 30 m = -29.90 b = 70.68 R ² = 0.242 p = 0.006	n = 30 m = -3.14E-5 b = -18.32 R ² = 7.01E-4 p = 0.900	n = 28 m = -0.18 b = -16.75 R ² = 2.63E-4 p = 0.944
Delta E ₂ :E ₃	n = 29 m = 1.06 b = -2.13 R ² = 0.142 p = 0.040	n = 29 m = 2.19 b = -9.16 R ² = 0.248 P = 0.005	n = 29 m = 2.74 b = -4.63 R ² = 0.188 p = 0.016	n = 29 m = -1.39E-5 b = 3.92 R ² = 0.014 p = 0.529	n = 29 m = 0.01 b = 3.49 R ² = 0.006 p = 0.689
% E ₂ :E ₃	n = 27 m = 19.90 b = -52.92 R ² = 0.191 p = 0.022	n = 27 m = 27.33 b = -104.7 R ² = 0.148 p = 0.047	n = 27 m = 54.40 b = -108.8 R ² = 0.285 p = 0.004	n = 27 m = -1.91E-4 b = 58.72 R ² = 0.010 p = 0.28	n = 27 m = 0.19 b = 48.72 R ² = 0.013 p = 0.623
Aqueous [Mn]	n = 30 m = 1.98 b = -0.07 R ² = 0.463 p = 3.20E-5	n = 29 m = -0.37 b = 12.77 R ² = 0.006 p = 0.677	n = 30 m = 3.53 b = -0.09 R ² = 0.309 p = 0.001	n = 30 m = -2.50E-5 b = 10.99 R ² = 0.041 p = 0.334	n = 28 m = -0.04 b = 11.08 R ² = 0.095 p = 0.173
AMON	n = 30 m = -7.61E-3 b = 3.75 R ² = 0.084 p = 0.120	n = 29 m = -0.01 b = 3.78 R ² = 0.067 p = 0.176	n = 30 m = -0.016 b = 3.76 R ² = 0.082 p = 0.125	n = 30 m = 3.48E-7 b = 3.71 R ² = 0.969 p = 0.129	n = 28 m = 2.90E-4 b = 3.71 R ² = 0.073 p = 0.235
Extent of reaction	n = 14 m = -1.52E-3 b = 0.03	n = 14 m = -1.60E-3 b = 0.031	n = 14 m = -4.22E-3 b = 0.03	n = 14 m = 2.23E-8 b = 0.02	n = 14 m = -9.25E-7 b = 0.02

	[DOC] control	E₂:E₃ control	SUVA₂₅₄ control	Ionic Strength	[SO₄²⁻]
	R ² = 0.039 p = 0.495	R ² = 0.015 p = 0.674	R ² = 0.067 p = 0.370	R ² = 0.009 p = 0.742	R ² = 1.92E-5 p = 0.988
Delta H:C_w	n = 14 m = -1.41E-3 b = -9.04E-3 R ² = 0.009 p = 0.747	n = 14 m = -2.04E-3 b = 0.81 R ² = 0.007 p = 0.782	n = 14 m = 8.22E-3 b = 0.026 R ² = 0.068 p = 0.368	n = 14 m = -1.56E-7 b = -0.175 R ² = 0.121 p = 0.221	n = 14 m = -2.49E-4 b = 0.024 R ² = 0.369 p = 0.060
% H:C_w	n = 14 m = -0.04 b = 1.45 R ² = 9.82E-4 p = 0.915	n = 14 m = -0.20 b = 2.40 R ² = 0.011 p = 0.724	n = 14 m = 0.72 b = -0.73 R ² = 0.089 p = 0.300	n = 14 m = -1.21E-5 b = 1.74 R ² = 0.124 p = 0.214	n = 14 m = -0.18 b = 1.82 R ² = 0.316 p = 0.035
Delta O:C_w	n = 14 m = -2.77E-3 b = 0.013 R ² = 0.063 p = 0.387	n = 14 m = 1.59E-3 b = -0.373 R ² = 0.007 p = 0.771	n = 14 m = -6.87E-3 b = -0.015 R ² = 0.085 p = 0.311	n = 14 m = -2.21E-8 b = 0.076 R ² = 0.004 p = 0.822	n = 14 m = 8.63E-5 b = -8.45E-3 R ² = 0.080 p = 0.326
% O:C_w	n = 14 m = -0.17 b = -0.38 R ² = 5.13E-3 p = 0.807	n = 14 m = 0.13 b = -2.22 R ² = 0.001 p = 0.913	n = 14 m = -1.06 b = 1.54 R ² = 0.042 p = 0.481	n = 14 m = 2.24E-6 b = -1.47 R ² = 9.36E-4 p = 0.917	n = 14 m = 0.03 b = -2.35 R ² = 0.195 p = 0.112
Delta DBE_w	n = 14 m = 0.02 b = -3.84E-2 R ² = 0.023 p = 0.607	n = 14 m = 0.04 b = -6.08 R ² = 0.022 p = 0.611	n = 14 m = -0.06 b = -0.44 R ² = 0.041 p = 0.486	n = 14 m = 1.98E-6 b = 2.18 R ² = 0.199 p = 0.108	n = 14 m = 3.34E-3 b = -0.35 R ² = 0.678 p = 2.33E-4
% DBE_w	n = 14 m = 0.46 b = -4.99 R ² = 0.056 p = 0.414	n = 14 m = 0.43 b = -4.99 R ² = 0.018 p = 0.647	n = 14 m = -0.36 b = -1.37 R ² = 0.008 p = 0.766	n = 14 m = 2.25E-5 b = -3.26 R ² = 0.148 p = 0.172	n = 14 m = 0.04 b = -3.82 R ² = 0.697 p = 1.56E-4
Delta MW_w	n = 14 m = 9.59 b = -88.0 R ² = 0.301 p = 0.041	n = 14 m = 10.3 b = 62.9 R ² = 0.132 p = 0.201	n = 14 m = 15.7 b = -10.7 R ² = 0.178 p = 0.132	n = 14 m = 1.24E-5 b = -6.79 R ² = 5.50E-4 p = 0.936	n = 14 m = 0.218 b = -50.7 R ² = 0.205 p = 0.102

% MW_w	n = 14 m = 2.21 b = -23.4 R ² = 0.271 p = 0.055	n = 14 m = 2.47 b = -25.6 R ² = 0.129 p = 0.205	n = 14 m = 4.07 b = -21.96 R ² = 0.204 p = 0.103	n = 14 m = -4.05E-6 b = -10.59 R ² = 0.001 p = 0.914	n = 14 m = 0.05 b = -12.4 R ² = 0.193 p = 0.114
Number of oxidation products	n = 14 m = 29.7 b = 86.9 R ² = 0.137	n = 14 m = 18.5 b = 135.6 R ² = 0.022	n = 14 m = 6.44 b = 239.6 R ² = 0.001	n = 14 m = 9.05E-4 b = 220.9 R ² = 0.140	n = 14 m = 1.81 b = 197.9 R ² = 0.673

	[DOC] control	E₂:E₃ control	SUVA₂₅₄ control	Ionic Strength	[SO₄²⁻]
	p = 0.191	p = 0.615	p = 0.898	p = 0.186	p = 2.55E-4

Table C.8. Linear correlation statistics based on control molecular dissolved organic matter characteristics or extent of reaction values with absolute changes (delta) or percent changes measured after 50-hour reactions with MnO₂. Both absolute delta values and percent changes were calculated as the final value minus the initial value. Slope (m) and intercept (b) are reported for a line of the form $y = mx + b$. p-values from 2-tailed t-tests are reported and cells are shaded for significant results ($p < 0.05$). X-variables are listed in first row and y-variables in first column of table.

	H:C_w control	O:C_w control	MW_w control	DBE_w control	Extent of reaction	Oxidation products
Extent of reaction	n = 14 m = 4.88E-4 b = 0.02 R ² = 1.07E-5 p = 0.991	n = 14 m = -0.06 b = 0.05 R ² = 0.023 p = 0.607	n = 14 m = -4.43E-5 b = 0.04 R ² = 0.007 p = 0.774	n = 14 m = -8.37E-4 b = 0.03 R ² = 0.005 p = 0.811		n = 14 m = -5.80E-6 b = 0.02 R ² = 0.004 p = 0.836
Delta H:C_w	n = 14 m = -0.17 b = -0.21 R ² = 0.362 p = 0.022	n = 14 m = 0.45 b = -0.07 R ² = 0.314 p = 0.036	n = 14 m = -2.9E-4 b = 6.1E-5 R ² = 0.226 p = 0.191	n = 14 m = 9.95E-3 b = 0.13 R ² = 0.186 p = 0.122	n = 14 m = 0.61 b = -2.52E-3 R ² = 0.099 p = 0.272	n = 14 m = 0.0 b = 0.1 R ² = 0.30 p = 0.051
% H:C_w	n = 14 m = -14.1 b = 18.3 R ² = 0.405 p = 0.013	n = 14 m = 32.9 b = -15.6 R ² = 0.292 p = 0.044	n = 14 m = -0.02 b = 8.91 R ² = 0.054 p = 0.422	n = 14 m = 0.87 b = -6.20 R ² = 0.243 p = 0.072	n = 14 m = 53.0 b = 0.07 R ² = 0.128 p = 0.208	n = 14 m = -6.7E-3 b = 2.98 R ² = 0.227 p = 0.083
Delta O:C_w	n = 14 m = 0.07 b = 0.09 R ² = 0.114 p = 0.236	n = 14 m = -0.19 b = 0.03 R ² = 0.105 p = 0.258	n = 14 m = 2.79E-4 b = 4.57E-3 R ² = 0.135 p = 0.195	n = 14 m = -4.16E-3 b = -0.12 R ² = 0.058 p = 0.404	n = 14 m = -0.46 b = 4.98E-3 R ² = 0.103 p = 0.262	n = 14 m = 4.40E-5 b = -0.02 R ² = 0.102 p = 0.265
% O:C_w	n = 14 m = 18.1 b = -23.3 R ² = 0.146 p = 0.175	n = 14 m = -55.0 b = 26.8 R ² = 0.179 p = 0.130	n = 14 m = 0.06 b = -28.7 R ² = 0.151 p = 0.168	n = 14 m = -0.86 b = 5.99 R ² = 0.052 p = 0.432	n = 14 m = -119.0 b = 1.25 R ² = 0.140 p = 0.185	n = 14 m = 0.01 b = -5.03 R ² = 0.220 p = 0.891
Delta DBE_w	n = 14 m = 1.73 b = 2.62 R ² = 0.366 p = 0.021	n = 14 m = -5.54 b = 0.59 R ² = 0.494 p = 0.005	n = 14 m = 4.57E-3 b = -0.14 R ² = 0.205 p = 0.102	n = 14 m = -0.09 b = -2.15 R ² = 0.169 p = 0.142	n = 14 m = -3.21 b = -0.08 R ² = 0.028 p = 0.568	n = 14 m = 1.51E-3 b = -0.60 R ² = 0.676 p = 2.43E-4
% DBE_w	n = 14 m = 19.5 b = -26.1 R ² = 0.269 p = 0.056	n = 14 m = -70.0 b = 33.5 R ² = 0.457 p = 0.007	n = 14 m = 0.07 b = -29.9 R ² = 0.242 p = 0.072	n = 14 m = -0.90 b = 5.36 R ² = 0.090 p = 0.297	n = 14 m = -50.1 b = -1.25 R ² = 0.039 p = 0.496	n = 14 m = 0.02 b = -7.66 R ² = 0.729 p = 7.61E-5
Delta MW_w	n = 14 m = -37.8 b = -45.1 R ² = 0.012 p = 0.705	n = 14 m = 0.69 b = -112 R ² = 5.44E-7 p = 0.998	n = 14 m = 0.30 b = -22.8 R ² = 0.064 p = 0.384	n = 14 m = 7.84 b = -172 R ² = 0.083 p = 0.316	n = 14 m = -991 b = -41.7 R ² = 0.188 p = 0.119	n = 14 m = 0.16 b = -86.4 R ² = 0.551 p = 0.002

	H:C _w control	O:C _w control	MW _w control	DBE _w control	Extent of reaction	Oxidation products
% MW _w	n = 14 m = -11.8 b = 3.59 R ² = 0.021 p = 0.625	n = 14 m = 0.32 b = -10.9 R ² = 1.99E-6 p = 0.996	n = 14 m = 0.10 b = -51.2 R ² = 0.109 p = 0.248	n = 14 m = 2.11 b = -28.8 R ² = 0.103 p = 0.262	n = 14 m = -251.0 b = -5.18 R ² = 0.206 p = 0.101	n = 14 m = 0.04 b = -20.8 R ² = 0.543 p = 0.002
Number of oxidation products	n = 14 m = 516.3 b = -369.7 R ² = 0.109 p = 0.247	n = 14 m = -2311 b = 1441 R ² = 0.290 p = 0.056	n = 14 m = 2.74 b = -900.8 R ² = 0.248 p = 0.068	n = 14 m = -14.1 b = 378.4 R ² = 0.013 p = 0.699	n = 14 m = -637.3 b = 271.5 R ² = 0.004 p = 0.829	

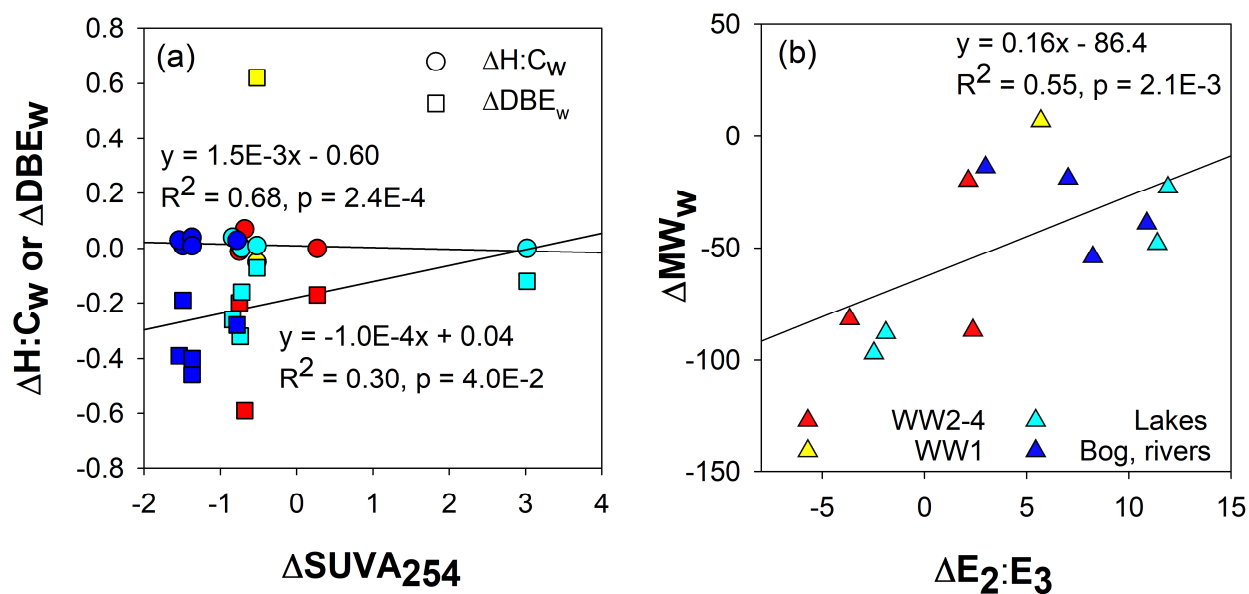


Figure C.7. Changes in bulk UV-vis measurements versus molecular FT-ICR measurements which represent changes in organic matter (a) aromaticity, H:C_w and DBE_w versus SUVA₂₅₄, and (b) molecular weight, MW_w versus E₂:E₃.

C.7. Molecular transformations

Table C.9. Number of matched formulas and percent of total formulas for control and treated waters reacted with acid birnessite for 50 hours.

Sample	Total formulas	CHO	CHON	CHOS	% CHO	% CHON	% CHOS
<i>Control samples</i>							
M1	4155	2447	1500	208	58.9	36.1	5.0
WW4	4659	2060	1578	1021	44.2	33.9	21.9
R3	5067	2507	1914	646	49.5	37.8	12.7
R9	4141	2435	1544	162	58.8	37.3	3.9
B2	3883	2128	1562	193	54.8	40.2	5.0
E2	4997	2441	1802	754	48.8	36.1	15.1
E3	5751	2785	1965	1001	48.4	34.2	17.4
WW3	4481	1953	1475	1053	43.6	32.9	23.5
WW2	4398	1932	1461	1005	43.9	33.2	22.9
R5	3713	2246	1394	73	60.5	37.5	2.0
R6	4223	2527	1546	150	59.8	36.6	3.6
O1	4485	2629	1545	311	58.6	34.4	6.9
O5	4534	2740	1590	204	60.4	35.1	4.5
WW1	5705	2288	1613	1804	40.1	28.3	31.6
<i>Treated samples</i>							
M1	3878	2334	1343	201	60.2	34.6	5.2
WW4	3591	1519	1241	831	42.3	34.6	23.1
R3	4054	2045	1556	453	50.4	38.4	11.2
R9	3771	2322	1312	137	61.6	34.8	3.6
B2	3438	1970	1306	162	57.3	38.0	4.7
E2	4211	2096	1543	572	49.8	36.6	13.6
E3	3999	1924	1477	598	48.1	36.9	15.0
WW3	3481	1561	1162	758	44.8	33.4	21.8
WW2	4079	1797	1359	923	44.1	33.3	22.6
R5	3597	2237	1303	57	62.2	36.2	1.6
R6	4504	2480	1437	587	55.1	31.9	13.0
O1	3317	1892	1226	199	57.0	37.0	6.0
O5	4145	2669	1317	159	64.4	31.8	3.8
WW1	5937	2525	1681	1731	42.5	28.3	29.2
Average	585	268	230	87	45.8	39.3	14.9

Table C.10. Average weighted values for control and treated waters after reaction with acid birnessite for 50 hours.

Sample	H:C_w	O:C_w	DBE_w	MW_w
<i>Control samples</i>				
M1	1.13	0.53	9.42	418
WW4	1.27	0.49	7.45	398
R3	1.19	0.51	8.77	445
R9	1.11	0.54	10.07	435
B2	1.14	0.53	9.78	402
E2	1.23	0.51	8.21	440
E3	1.22	0.49	8.34	463
WW3	1.34	0.51	6.81	387
WW2	1.33	0.52	6.90	384
R5	1.11	0.54	10.09	394
R6	1.11	0.54	10.01	440
O1	1.25	0.50	7.90	409
O5	1.17	0.54	9.10	440
WW1	1.42	0.41	7.01	467
<i>Treated samples</i>				
M1	1.17	0.52	9.16	395
WW4	1.34	0.43	6.86	311
R3	1.22	0.50	8.49	395
R9	1.12	0.54	9.88	396
B2	1.15	0.52	9.38	348
E2	1.23	0.52	8.05	392
E3	1.23	0.50	8.02	375
WW3	1.33	0.51	6.61	305
WW2	1.33	0.52	6.73	364
R5	1.14	0.52	9.70	375
R6	1.15	0.51	9.55	426
O1	1.25	0.52	7.78	312
O5	1.18	0.54	9.03	427
WW1	1.37	0.43	7.63	474

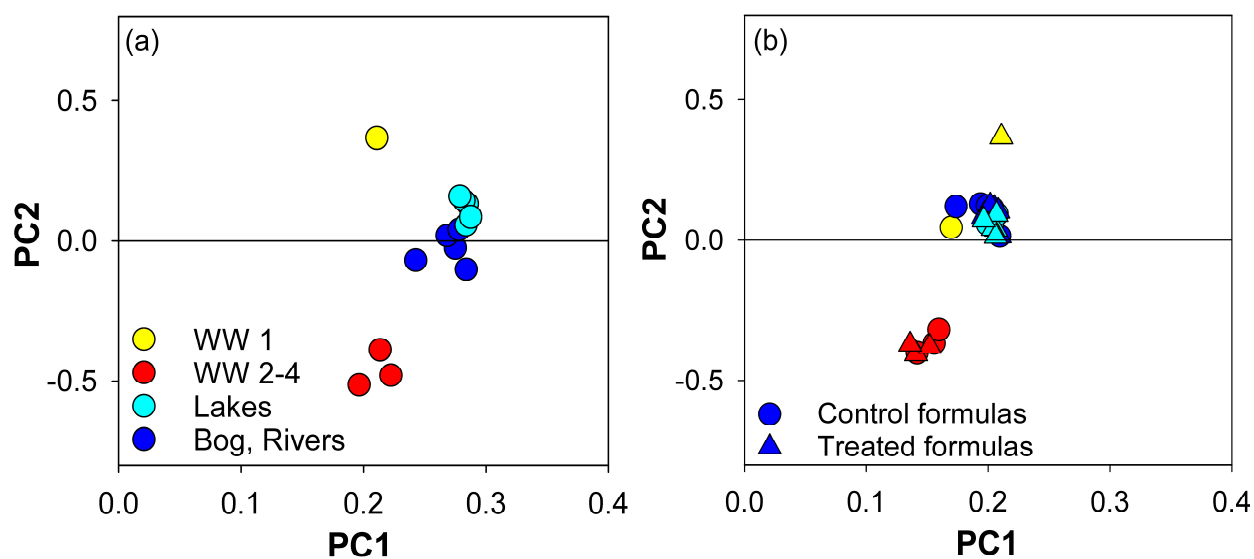


Figure C.8. Principal component analysis (PCA) plots of (a) control relative formula intensities and (b) relative formula intensities of both control and treated waters. The variance explained by PC1 and PC2, respectively, is (a) 77.6% and 11.4% and (b) 77.6% and 11.7%.

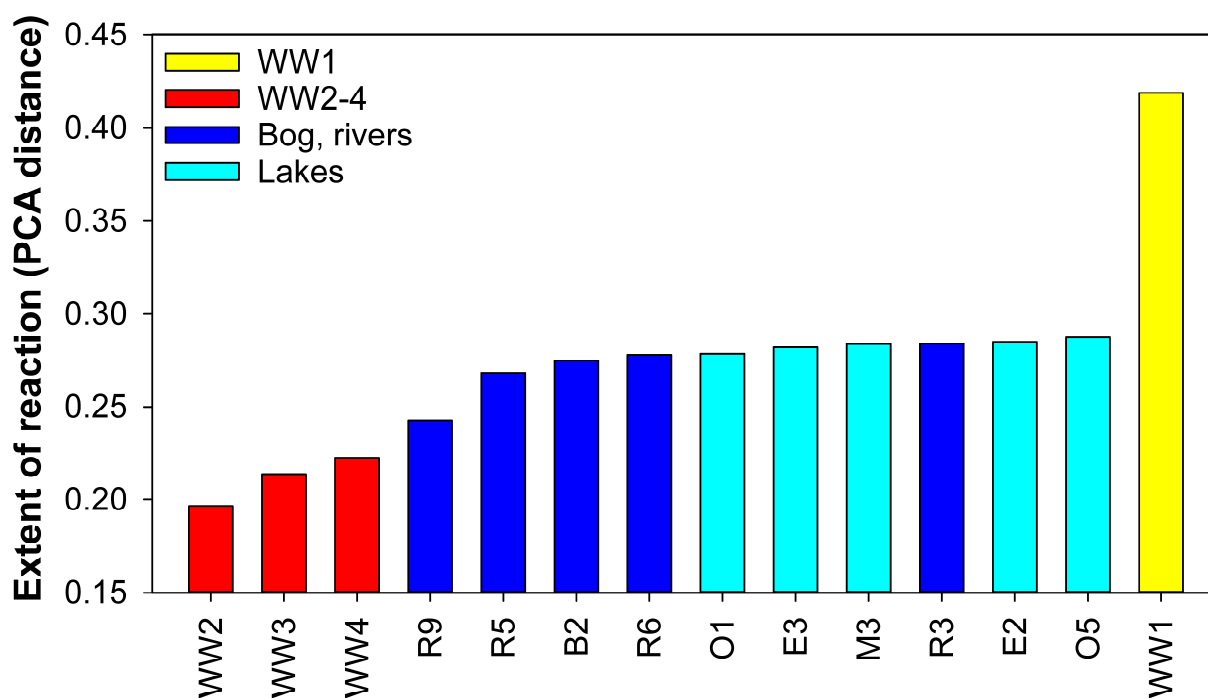


Figure C.9. Linear distances between control and treated waters on PCA plot (Figure C.8b). Distances are a proxy for extent of reaction.

Table C.11. Number of matched oxidized product formulas in each sample.

	Phenol to hydroquinone	Hydroquinone to benzoquinone	Phenol to benzoquinone	Hydrogen abstraction	Total
Sample	+O	-2H	+O, -2H	-H	
M1	92	76	74	8	250
WW4	45	70	43	1	159
R3	54	53	45	1	153
R9	79	91	69	28	267
B2	53	56	49	7	165
E2	70	75	69	1	215
E3	64	47	52	1	164
WW3	34	50	48	0	132
WW2	79	95	83	0	257
R5	86	80	61	16	243
R6	75	121	72	9	277
O1	64	43	56	0	163
O5	156	144	155	2	457
WW1	220	241	226	14	701

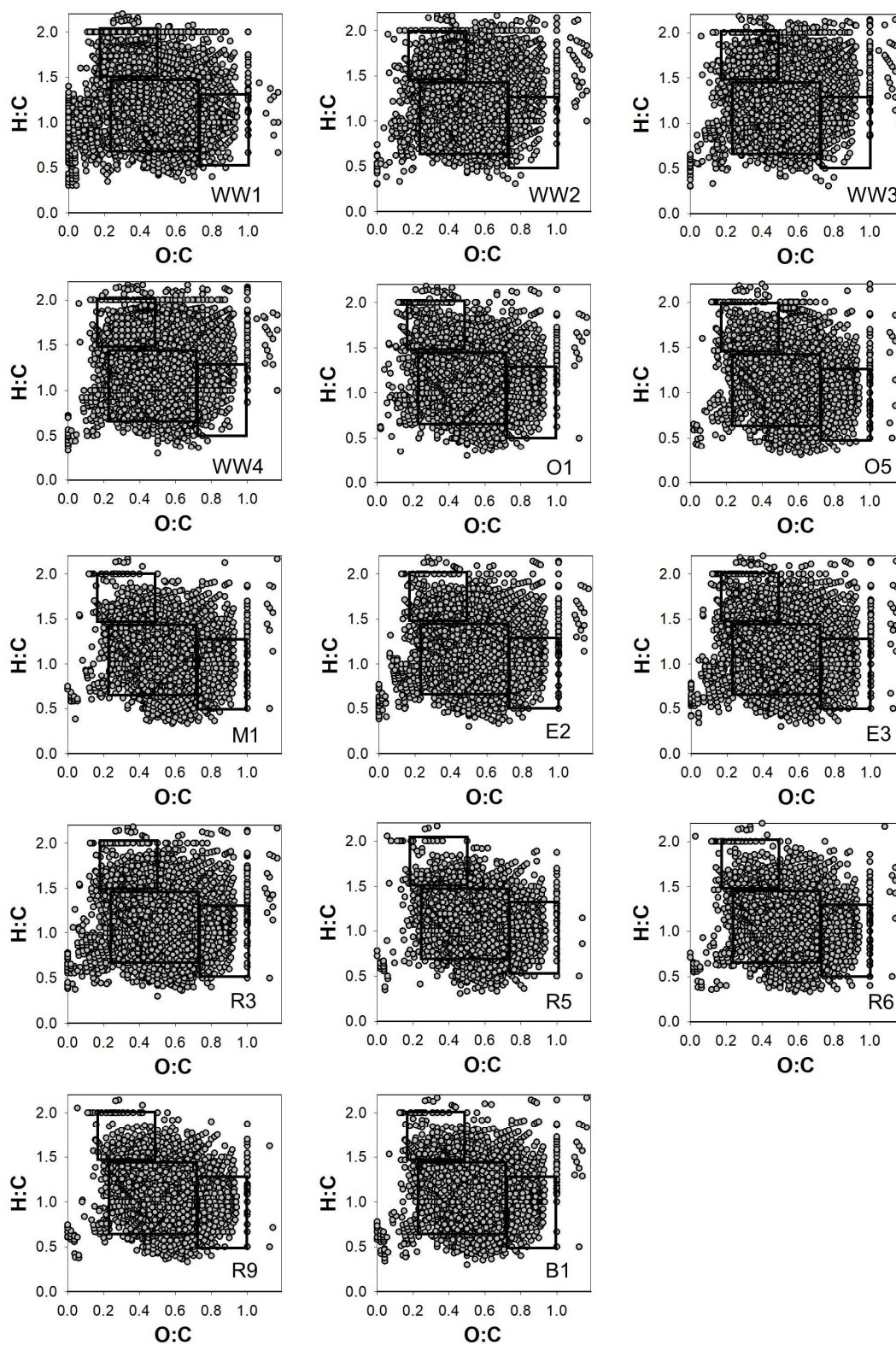


Figure C.10. H:C versus O:C van Krevelen plots of matched CHO formulas in control waters. Overlaid boxes indicate (1) protein-like, (2) lignin-like, and (3) tannin-like formulas.¹⁹ Sample name is indicated in each panel.

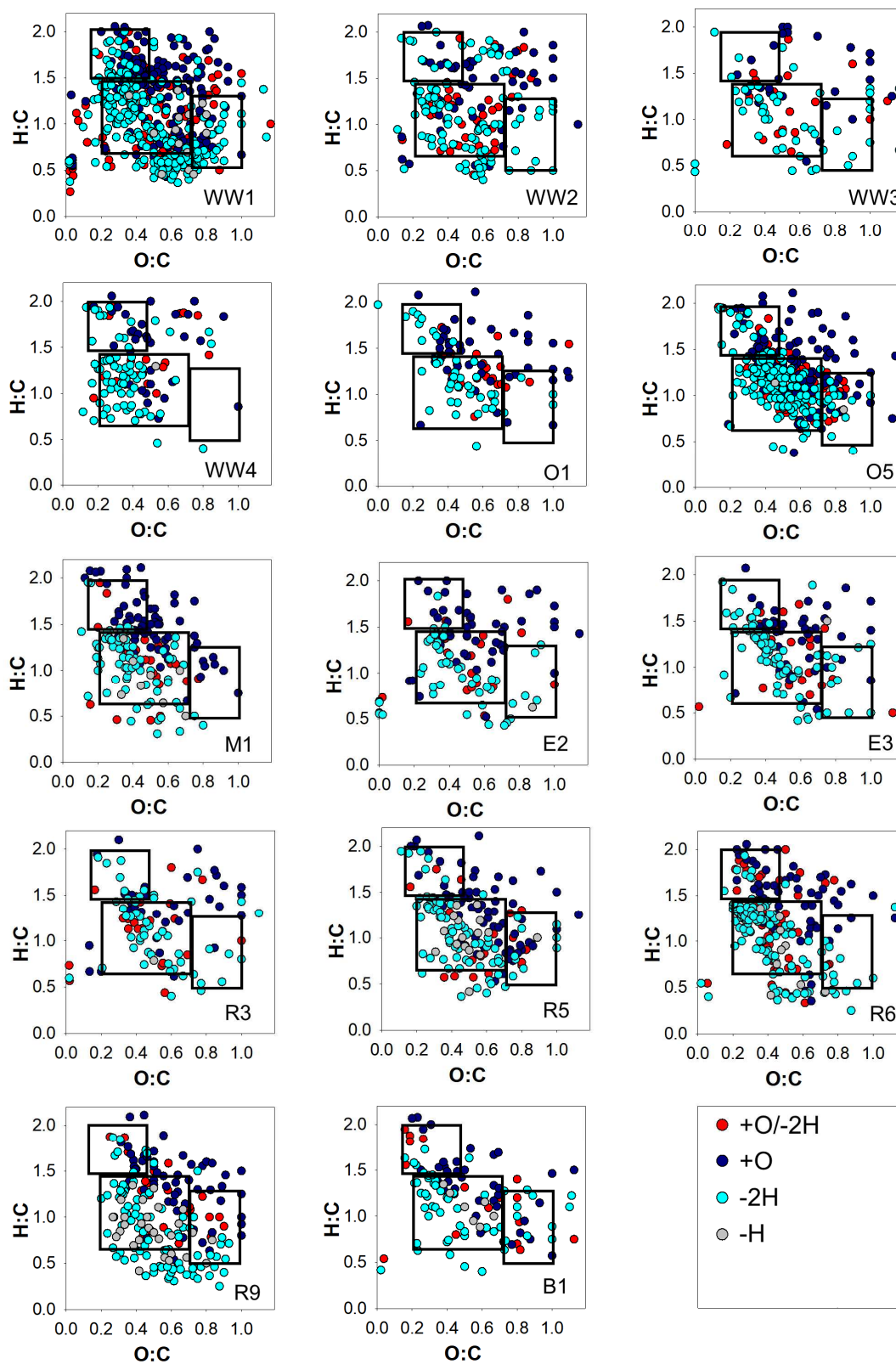


Figure C.11. H:C versus O:C van Krevelen plots of oxidation product formulas formed from 50-hour reactions with acid birnessite. Overlaid boxes indicate (1) protein-like, (2) lignin-like, and (3) tannin-like formulas.¹⁹ Sample name is indicated in each panel.

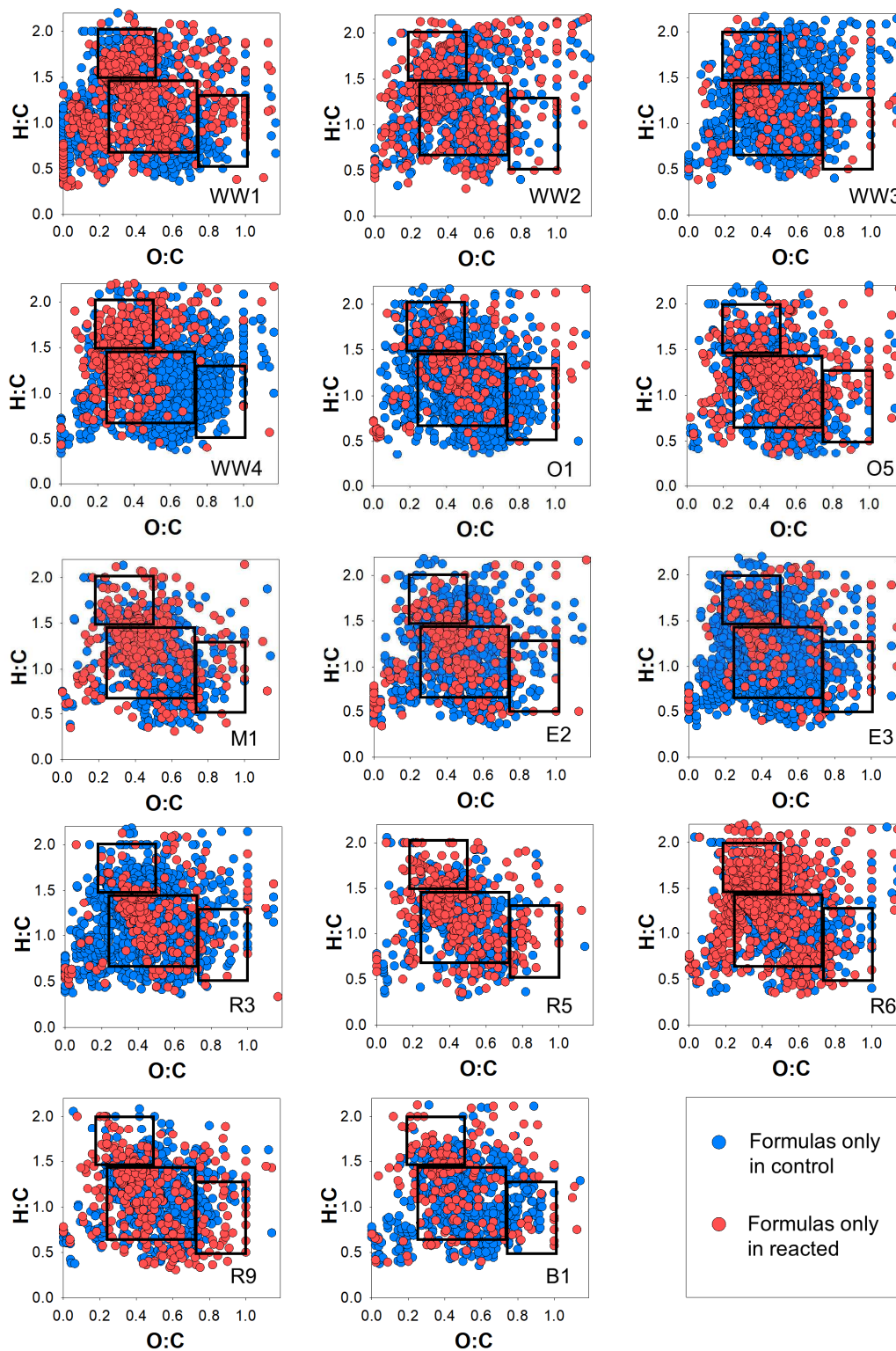


Figure C.12. H:C versus O:C van Krevelen plots of formulas present only in the control samples or only in the reacted samples. Overlaid boxes indicate (1) protein-like, (2) lignin-like, and (3) tannin-like formulas.¹⁹ Sample name is indicated in each panel.

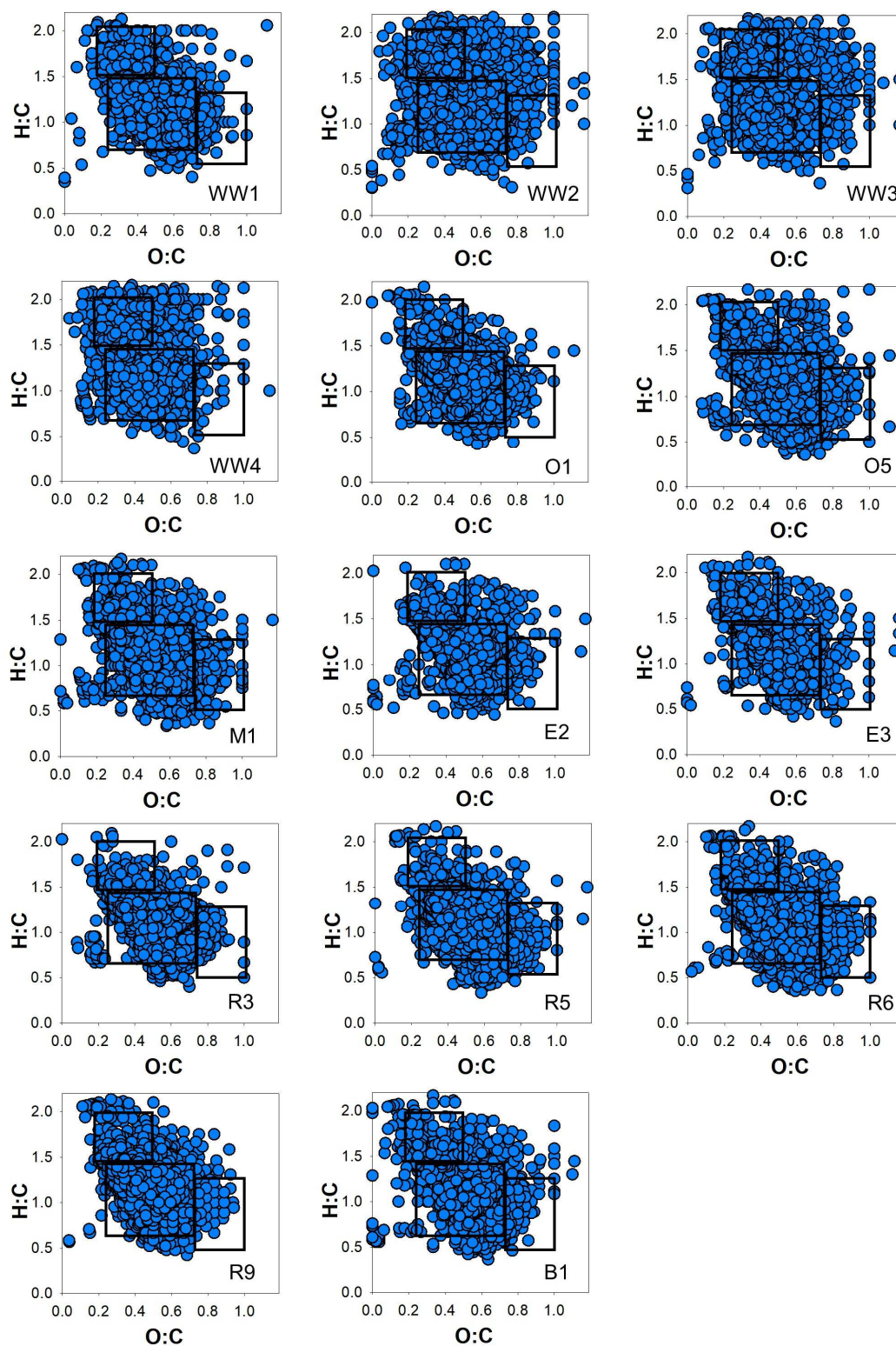


Figure C.13. H:C versus O:C van Krevelen plots of formulas matched in both control and treated samples which decrease in intensity after reacting 50 hours with acid birnessite. Overlaid boxes indicate (1) protein-like, (2) lignin-like, and (3) tannin-like formulas.¹⁹ Sample name is indicated in each panel.

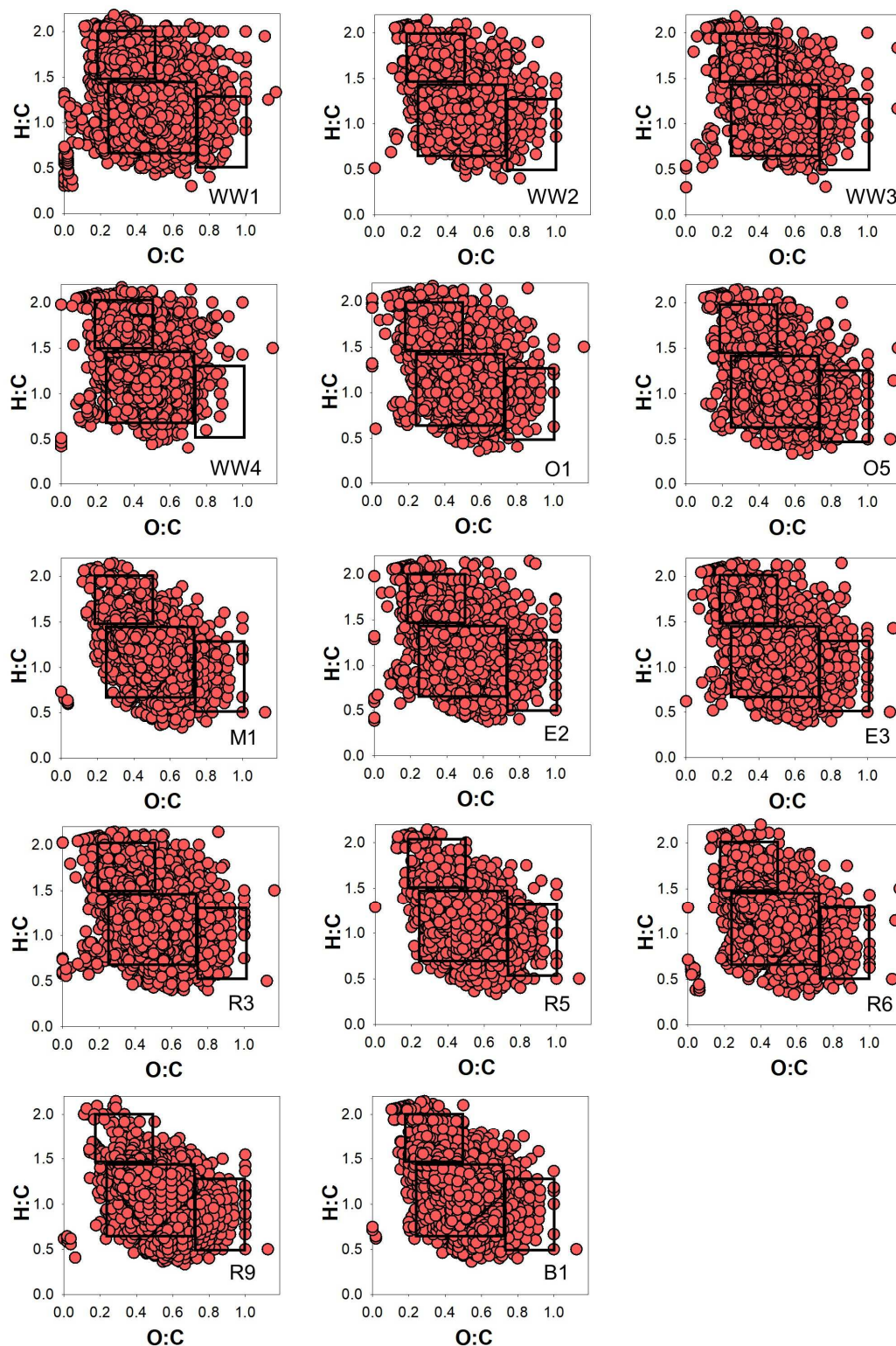


Figure C.14. H:C versus O:C van Krevelen plots of formulas matched in both control and treated samples which increase in intensity after reacting 50 hours with acid birnessite. Overlaid boxes indicate (1) protein-like, (2) lignin-like, and (3) tannin-like formulas.¹⁹ Sample name is indicated in each panel.

C.8. References

1. McKenzie, R. M., The synthesis of birnessite, cryptomelane, and some other oxides and hydroxides of manganese. *Mineral. Mag.* **1971**, *38*, 493-502.
2. Berg, S. M.; Whiting, Q. T.; Herrli, J. A.; Winkels, R.; Wammer, K. H.; Remucal, C. K., The role of dissolved organic matter composition in determining photochemical reactivity at the molecular level. *Environ. Sci. Technol.* **2019**, *53*, (20), 11725-11734.
3. Center for Limnology at Wisconsin-Madison, North Temperate Lakes U.S. Long-Term Ecological Research Network. National Science Foundation, ter.limnology.wisc.edu, **2021**.
4. Report on Superior Bay, St. Louis County, Minnesota, and Douglas County. Wisconsin E.P.A. Region V, **1975**, No. 128.
5. Allard, S.; Gutierrez, L.; Fontaine, C.; Croue, J. P.; Gallard, H., Organic matter interactions with natural manganese oxide and synthetic birnessite. *Sci. Total Environ.* **2017**, *583*, 487-495.
6. Remucal, C. K.; Ginder-Vogel, M., A critical review of the reactivity of manganese oxides with organic contaminants. *Environ. Sci. Process. Impacts* **2014**, *16*, (6), 1247-1266.
7. Stone, A. T.; Morgan, J. J., Reduction and dissolution of manganese(III) and manganese(IV) oxides by organics 1. Reaction with hydroquinone. *Environ. Sci. Technol.* **1984**, *18*, (6), 450-456.
8. Trainer, E. L.; Ginder-Vogel, M.; Remucal, C. K., Organic structure and solid characteristics determine reactivity of phenolic compounds with synthetic and reclaimed manganese oxides. *Environ. Sci.: Water Res. & Technol.* **2020**, *6*, (3), 540-553.
9. Chorover, J.; Amistadi, M. K., Reaction of forest floor organic matter at goethite, birnessite and smectite surfaces. *Geochim. Cosmochim. Acta* **2001**, *65*, (1), 95-109.
10. Manceau, A.; Marcus, M. A.; Grangeon, S., Determination of Mn valence states in mixed-valent manganates by XANES spectroscopy. *Am. Mineral.* **2012**, *97*, (5-6), 816-827.
11. Dittmar, T.; Koch, B.; Hertkorn, N.; Kattner, G., A simple and efficient method for the solid-phase extraction of dissolved organic matter (SPE-DOM) from seawater. *Limnol. Oceanogr.: Methods* **2008**, *6*, (6), 230-235.
12. Bulman, D. M.; Remucal, C. K., Role of reactive halogen species in disinfection byproduct formation during chlorine photolysis. *Environ. Sci. Technol.* **2020**, *54*, (15), 9629-9639.
13. Maizel, A. C.; Remucal, C. K., The effect of probe choice and solution conditions on the apparent photoreactivity of dissolved organic matter. *Environ. Sci. Process. Impacts* **2017**, *19*, (8), 1040-1050.
14. Maizel, A. C.; Remucal, C. K., Molecular composition and photochemical reactivity of size-fractionated dissolved organic matter. *Environ. Sci. Technol.* **2017**, *51*, (4), 2113-2123.
15. Maizel, A. C.; Remucal, C. K., The effect of advanced secondary municipal wastewater treatment on the molecular composition of dissolved organic matter. *Water Res.* **2017**, *122*, 42-52.

16. Remucal, C. K.; Salhi, E.; Walpen, N.; von Gunten, U., Molecular-level transformation of dissolved organic matter during oxidation by ozone and hydroxyl radical. *Environ. Sci. Technol.* **2020**, *54*, (16), 10351-10360.
17. Koch, B. P.; Dittmar, T.; Witt, M.; Kattner, G., Fundamentals of molecular formula assignment to ultrahigh resolution mass data of natural organic matter. *Anal. Chem.* **2007**, *79*, (4), 1758-1763.
18. Lever, J.; Krzywinski, M.; Altman, N., Principal component analysis. *Nature Methods* **2017**, *14*, (7), 641-642.
19. Minor, E. C.; Swenson, M. M.; Mattson, B. M.; Oyler, A. R., Structural characterization of dissolved organic matter: A review of current techniques for isolation and analysis. *Environ. Sci. Process. Impacts.* **2014**, *16*, (9), 2064-2079.